



Michigan Technological University
Create the Future Digital Commons @ Michigan Tech

Dissertations, Master's Theses and Master's
Reports - Open

Dissertations, Master's Theses and Master's
Reports

2013

COMPARATIVE ANALYSIS OF EFFICIENCY AND OPERATING CHARACTERISTICS OF AUTOMOTIVE POWERTRAIN ARCHITECTURES THROUGH CHASSIS DYNAMOMETER TESTING

Jeremy J. Anderson
Michigan Technological University

Follow this and additional works at: <https://digitalcommons.mtu.edu/etds>



Part of the [Energy Systems Commons](#)

Copyright 2013 Jeremy J. Anderson

Recommended Citation

Anderson, Jeremy J., "COMPARATIVE ANALYSIS OF EFFICIENCY AND OPERATING CHARACTERISTICS OF AUTOMOTIVE POWERTRAIN ARCHITECTURES THROUGH CHASSIS DYNAMOMETER TESTING", Master's Thesis, Michigan Technological University, 2013.
<https://doi.org/10.37099/mtu.dc.etds/671>

Follow this and additional works at: <https://digitalcommons.mtu.edu/etds>



Part of the [Energy Systems Commons](#)

COMPARATIVE ANALYSIS OF EFFICIENCY AND OPERATING CHARACTERISTICS OF
AUTOMOTIVE POWERTRAIN ARCHITECTURES THROUGH CHASSIS DYNAMOMETER
TESTING

By

Jeremy J. Anderson

A THESIS

Submitted in partial fulfillment of the requirements for the degree of

MASTER OF SCIENCE

In Mechanical Engineering

MICHIGAN TECHNOLOGICAL UNIVERSITY

2013

COPYRIGHT © JEREMY J. ANDERSON 2013

This thesis has been approved in partial fulfillment of the requirements for the Degree of MASTER OF SCIENCE in Mechanical Engineering.

Department of Mechanical Engineering- Engineering Mechanics

Thesis Advisor: *Dr. Scott A. Miers*

Committee Member: *Dr. Henning R.A. Lohse-Busch*

Committee Member: *Dr. David D. Wanless*

Department Chair: *Dr. William W. Predebon*

Table of Contents

List of Figures.....	6
List of Tables	11
Acknowledgements	13
Nomenclature	14
Abstract.....	15
Chapter 1 Introduction.....	16
1.1 Project Origins and Motivation.....	16
1.2 Project Objectives	17
1.3 Summary	18
Chapter 2 Project Background.....	19
2.1 Vehicle Testing Facilities and Practices	19
2.1.1 Advanced Powertrain Research Facility (APRF)	19
2.1.2 Instrumentation and Measurement Specifications	19
2.1.3 Vehicle Road Load Determination	21
2.1.4 Dynamometer Testing Cycles.....	22
2.1.5 Vehicle Analysis Metrics and Equations	26
2.2 Modern Passenger Vehicle Powertrain Technology & Architecture.....	32
2.2.1 Modern Conventional Gasoline	36
2.2.2 Modern Conventional Turbodiesel	36
2.2.3 Downsized, Forced-Induction Gasoline Conventional	37
2.2.4 Gasoline-Electric Hybrid	38
Chapter 3 MY2012 Ford Fusion 2.5.....	39

3.1 Relevant Vehicle Features	39
3.2 Instrumentation Specifics.....	42
3.3 Drive Cycle Performance.....	44
3.4 Cycle-Based Heat Loss Proportions	57
3.5 Cycle-Based Emissions Measurements	60
3.6 Engine Indicating System Measurements	63
Chapter 4 MY2009 Volkswagen Jetta TDI 2.0	68
4.1 Relevant Vehicle Features	68
4.2 Instrumentation Specifics.....	71
4.3 Drive Cycle Performance.....	74
4.4 Cycle-Based Heat Loss Proportions	85
4.5 Cycle-Based Emissions Measurements	88
4.6 Engine Indicating System Measurements	91
Chapter 5 MY2010 Volkswagen Jetta TSI 1.4	98
5.1 Relevant Vehicle Features	98
5.2 Instrumentation Specifics.....	100
5.3 Drive Cycle Performance.....	102
5.4 Cycle-Based Heat Loss Proportions	112
5.5 Cycle-Based Emissions.....	116
5.6 Engine Indicating System Measurements	118
Chapter 6 MY2010 Toyota Prius 1.8.....	124
6.1 Relevant Vehicle Features	124
6.2 Instrumentation Specifics.....	127

6.3 Drive Cycle Performance.....	130
6.4 Cycle-Based Heat Loss Proportions	145
6.5 Cycle-Based Emissions Measurements	148
6.6 Engine Indicating System Measurements	150
Chapter 7 Data Synthesis and Comparative Analysis.....	156
7.1 Vehicle Parameters and Performance Envelopes	156
7.2 Drive Cycle Performance.....	161
7.3 Cold Start Mileage Penalties & Emissions Behavior	164
7.4 Powertrain Utilization.....	168
7.5 Cycle Based Heat Losses	174
7.6 WOT Combustion Behavior	178
Chapter 8 Conclusions and Future Work	181
8.1 Conclusions.....	181
8.2 Reccomendatons for Future Work	183
Bibliography	186
Appendix A.....	188
A.1 Additional Figures	188
A.2 Matlab Analysis Code.....	189
A.3 Permissions	242

List of Figures

Figure 2.1.1: Urban Dynamometer Driving Schedule (UDDS)	24
Figure 2.1.2: Highway Fuel Economy Driving Schedule (HWFET)	25
Figure 2.1.3: US06 Driving Schedule.....	25
Figure 2.1.4: 0-80-0 Steady State Speed Driving Schedule.....	26
Figure 2.1.5: Vehicle Efficiency Metrics.....	29
Figure 3.1.1: 2012 Ford Fusion.....	42
Figure 3.2.1: Ford Fusion Engine Bay.....	44
Figure 3.3.1: Ford Fusion Idle Fuel Use	47
Figure 3.3.2: Ford Fusion Deceleration Fuel Cutoff (DFCO), UDDS HS	48
Figure 3.3.3: Ford Fusion Deceleration Fuel Cutoff (DFCO), US06 HS	49
Figure 3.3.4: Ford Fusion Deceleration Fuel Cutoff (DFCO) Map	49
Figure 3.3.5: Ford Fusion Indicated Engine Efficiency and Vehicle Efficiency.....	51
Figure 3.3.6: Ford Fusion Oil and Coolant Temperatures, US06 Cycles	52
Figure 3.3.7: Ford Fusion Engine Utilization, UDDS HS Cycle.....	53
Figure 3.3.8: Ford Fusion Engine Utilization, US06 HS Cycle.....	54
Figure 3.3.9: Ford Fusion Engine Utilization, HWFET HS Cycle.....	55
Figure 3.3.10: Ford Fusion Steady State Performance	56
Figure 3.4.1: Ford Fusion Cycle-Based Fuel Energy Usage	58
Figure 3.4.2: Ford Fusion Coolant Enthalpy Change by Source	59
Figure 3.5.1: Ford Fusion US06 Cold Start Integrated NOx and THC	61
Figure 3.5.2: Ford Fusion US06 Hot Start Integrated NOx and THC	61
Figure 3.5.3: Ford Fusion US06 Hot and Cold Start Emissions.....	62

Figure 3.6.1: Ford Fusion P-V Diagram, Point 1	64
Figure 3.6.2: Ford Fusion P-V Diagram, Point 2.....	65
Figure 3.6.3: Ford Fusion P-V Diagram, Point 3.....	67
Figure 4.1.1: Volkswagen Jetta TDI Exhaust Aftertreatment System Schematic	69
Figure 4.1.2. 2009 Volkswagen Jetta TDI	69
Figure 4.2.1: Volkswagen Jetta TDI TDC Adapter & Fuel Injector	73
Figure 4.2.2: Volkswagen Jetta TDI TDC Determination.....	74
Figure 4.3.1: Volkswagen Jetta TDI Oil and Coolant Temperatures, US06 Cycles	76
Figure 4.3.2: Volkswagen Jetta TDI Idle Fuel Use	77
Figure 4.3.3: Volkswagen Jetta TDI Deceleration Fuel Cutoff (DFCO), UDDS HS.....	78
Figure 4.3.4: Volkswagen Jetta TDI Deceleration Fuel Cutoff (DFCO), US06 HS	79
Figure 4.3.5: Volkswagen Jetta TDI Deceleration Fuel Cutoff (DFCO) Map	80
Figure 4.3.6: Volkswagen Jetta TDI Engine Utilization, UDDS HS Cycle	81
Figure 4.3.7: Volkswagen Jetta TDI Engine Utilization, US06 HS Cycle	82
Figure 4.3.8: Volkswagen Jetta TDI Engine Utilization, HWFET Cycle	83
Figure 4.3.9: Volkswagen Jetta TDI Steady State Performance.....	84
Figure 4.4.1: Volkswagen Jetta TDI Cycle-Based Fuel Energy Usage.....	86
Figure 4.4.2: Volkswagen Jetta TDI Coolant Enthalpy Change by Source.....	87
Figure 4.5.1 Volkswagen Jetta TDI US06 Cold Start Integrated NOx and THC.....	90
Figure 4.5.2 Volkswagen Jetta TDI US06 Hot Start Integrated NOx and THC.....	90
Figure 4.6.1: Volkswagen Jetta TDI P-V Diagram, Point 1	93
Figure 4.6.2: Volkswagen Jetta TDI P-V Diagram, Point 2	95
Figure 4.6.3: Volkswagen Jetta TDI P-v Diagram, Point 3	97

Figure 5.1.1: 2010 Volkswagen Jetta TSI.....	100
Figure 5.2.1: Volkswagen Jetta TSI Flow Sensor & Thermocouple Installation in Coolant Hose	102
Figure 5.3.1: Volkswagen Jetta TSI Oil and Coolant Temperatures, US06 Cycles	104
Figure 5.3.2: Volkswagen Jetta TSI Fuel Mixture Enrichment During Aggressive Operation, US06 Cycle	105
Figure 5.3.3: Volkswagen Jetta TSI Idle Fuel Use	106
Figure 5.3.4: Volkswagen Jetta TSI Deceleration Fuel Cutoff (DFCO), UDDS HS	107
Figure 5.3.5: Volkswagen Jetta TSI Deceleration Fuel Cutoff (DFCO) Map	108
Figure 5.3.6: Volkswagen Jetta TSI Engine Utilization, UDDS HS Cycle	109
Figure 5.3.7: Volkswagen Jetta TSI Engine Utilization, US06 HS Cycle	110
Figure 5.3.8: Volkswagen Jetta TSI Engine Utilization, HWFET Cycle	111
Figure 5.3.9: Volkswagen Jetta TSI Steady State Performance	112
Figure 5.4.1: Volkswagen Jetta TSI Cycle-Based Fuel Energy Usage	114
Figure 5.4.2: Volkswagen Jetta TSI Coolant Enthalpy Change by Source	115
Figure 5.5.1: Volkswagen Jetta TSI US06 Cold Start Integrated NOx and THC	117
Figure 5.5.2: Volkswagen Jetta TSI US06 Hot Start Integrated NOx and THC	118
Figure 5.6.1: Volkswagen Jetta TSI P-V Diagram, Point 1	120
Figure 5.6.2: Volkswagen Jetta TSI P-V Diagram, Point 2	121
Figure 5.6.3: Volkswagen Jetta TSI P-V Diagram, Point 3	122
Figure 6.1.1: Toyota Hybrid System Architecture. Reprinted with permission from SAE Paper 2009-01-1061 © 2009 SAE International. Further use or distribution is not permitted without permission from SAE.	125
Figure 6.1.2: Toyota Prius on Chassis Dynamometer	127

Figure 6.2.1: Toyota Prius Engine Output Torque Sensor.....	129
Figure 6.2.2: Toyota Prius Transaxle with Spacer Plate.....	129
Figure 6.3.1: Toyota Prius Battery Net Energy Change, UDDS Hot Start Cycle	132
Figure 6.3.2: Toyota Prius EV Operation, UDDS Hot Start Cycle	134
Figure 6.3.3: Toyota Prius EV Operation, UDDS, HWFET and US06 Cycles.....	134
Figure 6.3.4: Toyota Prius Idle Fuel Use.....	136
Figure 6.3.5: Toyota Prius Engine Utilization, UDDS HS Cycle.....	137
Figure 6.3.6: Toyota Prius Engine Utilization, US06 HS Cycle	138
Figure 6.3.7: Toyota Prius Engine Utilization, HWFET Cycle.....	138
Figure 6.3.8: Toyota Prius Engine Operating Line.....	140
Figure 6.3.9: Toyota Prius Measured Energy Proportions, US06 Hot Start Cycle	141
Figure 6.3.10: Toyota Prius Cold Start Behavior, UDDS Cycles.....	143
Figure 6.3.11: Toyota Prius Oil and Coolant Temperatures, US06 Cycles.....	144
Figure 6.3.12: Toyota Prius Steady State Performance	145
Figure 6.4.1: Toyota Prius Cycle-Based Fuel Energy Use	146
Figure 6.4.2: Toyota Prius Coolant Enthalpy Change by Source	147
Figure 6.5.1: Toyota Prius US06 Cold Start Integrated NOx and THC	149
Figure 6.5.2: Toyota Prius US06 Hot Start Integrated NOx and THC	149
Figure 6.6.1: Toyota Prius P-V Diagram, Point 1.....	153
Figure 6.6.2: Toyota Prius P-V Diagram, Point 2.....	154
Figure 6.6.3: Toyota Prius P-V Diagram, Point 3.....	155
Figure 7.1.1: Road Load Power vs. Speed.....	158
Figure 7.1.2: Vehicle Tractive Effort Capability	160

Figure 7.2.1: Vehicle Efficiency by Cycle.....	163
Figure 7.3.1: Cold Start Fuel Mileage Penalty by Vehicle	165
Figure 7.3.2: Normalized Modal NOx Emissions by Vehicle, UDDS CS Cycle.....	167
Figure 7.3.3: Normalized Modal THC Emissions by Vehicle, UDDS CS Cycle.....	167
Figure 7.4.1: Engine Utilization Maps by Vehicle, UDDS, HWFET & US06 Cycles ..	169
Figure 7.4.2: Engine Speed vs. Vehicle Speed, UDDS, HWFET & US06 Cycles	171
Figure 7.4.3: Deceleration Fuel Cutoff (DFCO) Maps by Vehicle	172
Figure 7.5.1: Fuel Energy Utilization by Vehicle, US06 HS Cycle	174
Figure 7.5.2 Fuel Energy Utilization by Vehicle, HWFET Cycle.....	175
Figure 7.5.3: Fuel Energy Utilization by Vehicle, UDDS Cycle.....	177
Figure 7.6.1: Pressure Traces at WOT Conditions	178
Figure A.1.1 – Vehicle Dynamometer Test Plan Document	188

List of Tables

Table 3.1.1: Ford Fusion Vehicle Metrics	41
Table 3.1.2: Ford Fusion Fuel Specifications	41
Table 3.3.1: Ford Fusion Drive Cycle Economy and Vehicle Efficiency	44
Table 3.3.2: Ford Fusion Cycle Indicated Engine Efficiency	50
Table 1.5.1: Ford Fusion Total Emissions by Cycle	60
Table 3.6.1: Ford Fusion Engine Operating Points	63
Table 4.1.1: Volkswagen Jetta TDI Vehicle Metrics	70
Table 4.1.2: Volkswagen Jetta TDI Fuel Specifications	70
Table 4.3.1: Volkswagen Jetta TDI Drive Cycle Economy and Vehicle Efficiency	75
Table 4.5.1: Volkswagen Jetta TDI Total Emissions by Cycle	88
Table 4.6.1: Volkswagen TDI Engine Operating Points	93
Table 5.1.1: Volkswagen Jetta TSI Vehicle Metrics	99
Table 5.1.2: Volkswagen Jetta TSI Fuel Properties	100
Table 5.3.1: Volkswagen Jetta TSI Drive Cycle Economy and Vehicle Efficiency	103
Table 5.5.1: Volkswagen Jetta TSI Total Emissions by Cycle	116
Table 5.6.1: Volkswagen Jetta TSI Engine Operating Points	119
Table 6.1.1: Toyota Prius Vehicle Metrics	126
Table 6.1.2: Toyota Prius Fuel Properties	126
Table 6.3.1: Toyota Prius Drive Cycle Economy and Vehicle Efficiency	131
Table 6.3.2: Toyota Prius Cycle-Based Efficiencies	141
Table 6.5.1: Toyota Prius Total Emissions by Cycle	148
Table 6.6.1: Toyota Prius Engine Operating Points	152

Table 7.1.1: Selected Vehicle Parameters.....	157
Table 7.3.3: Vehicle Road Load Relative to Fusion, 80 mph.....	158
Table 7.1.3: Vehicle Acceleration Performance	159
Table 7.2.1: Cycle Fuel Economy (mpg) by Test Vehicle	161
Table 7.2.2: Cycle Vehicle Efficiency by Test Vehicle.....	162
Table 7.6.1: WOT Combustion Characteristics	179

Acknowledgements

The work found in this thesis was made possible in large part by the guidance and assistance of the author's advisor at Michigan Technological University and colleagues at Argonne National Laboratory.

Thanks are due to Dr. Scott Miers for his unwavering optimism and guidance in matters spanning the breadth of this work, from the initial scoping of the project to the development of this thesis document. Without his foresight, the collaboration at Argonne would not have been possible.

Mr. Eric Rask made important contributions to the data analysis required for this thesis, and has served as an invaluable mentor to the author as well as an excellent sounding board for instrumentation and analysis ideas. His experience and insight as an analyst helped to add depth and usefulness to the project.

A debt of gratitude is owed to Dr. Henning Lohse-Busch for lending the perspective he has gained over many years of vehicle testing, and for making the initial project connections on the Argonne side.

Mr. Zachary Stauber was similarly integral to the project, supporting many hours of vehicle testing and contributing significantly to test vehicle instrumentation. Zach was able to provide excellent troubleshooting skills for finicky instrumentation and innovative solutions to mechanical issues that helped to keep the project on track.

Finally, thanks are due to the colleagues, friends and family of the author who continue to provide support as well as much needed distractions and diversions along the way.

Nomenclature

ATDC – After Top Dead Center

Battery NEC – (Battery Net Energy Change)

Battery SOC – (Battery State of Charge)

BDC – Bottom Dead Center

BTDC – Before Top Dead Center

CVT – Continuously Variable Transmission

DFCO – Deceleration Fuel Cutoff

ECU – Engine Control Unit

GDI – Gasoline Direct Injection

HEV – Hybrid Electric Vehicle

IC Engine – Internal Combustion Engine

IMEP – Indicated Mean Effective Pressure

MPG – Miles Per Gallon

MY201X – Model Year 201X

NO_x – Oxides of Nitrogen

PFI – Port Fuel Injection

TDC – Top Dead Center

THC – Total Hydrocarbons

Abstract

The thesis “COMPARATIVE ANALYSIS OF EFFICIENCY AND OPERATING CHARACTERISTICS OF AUTOMOTIVE POWERTRAIN ARCHITECTURES THROUGH CHASSIS DYNAMOMETER TESTING” was completed through a collaborative partnership between Michigan Technological University and Argonne National Laboratory under a contractual agreement titled “Advanced Vehicle Characterization at Argonne National Laboratory”. The goal of this project was to investigate, understand and document the performance and operational strategy of several modern passenger vehicles of various architectures. The vehicles were chosen to represent several popular engine and transmission architectures and were instrumented to allow for data collection to facilitate comparative analysis. In order to ensure repeatability and reliability during testing, each vehicle was tested over a series of identical drive cycles in a controlled environment utilizing a vehicle chassis dynamometer. Where possible, instrumentation was preserved between vehicles to ensure robust data collection. The efficiency and fuel economy performance of the vehicles was studied. In addition, the powertrain utilization strategies, significant energy loss sources, tailpipe emissions, combustion characteristics, and cold start behavior were also explored in detail. It was concluded that each vehicle realizes different strengths and suffers from different limitations in the course of their attempts to maximize efficiency and fuel economy. In addition, it was observed that each vehicle regardless of architecture exhibits significant energy losses and difficulties in cold start operation that can be further improved with advancing technology. It is clear that advanced engine technologies and driveline technologies are complimentary aspects of vehicle design that must be utilized together for best efficiency improvements. Finally, it was concluded that advanced technology vehicles do not come without associated cost; the complexity of the powertrains and lifecycle costs must be considered to understand the full impact of advanced vehicle technology.

Chapter 1 Introduction

1.1 Project Origins and Motivation

In March of 2012, talks were begun between Michigan Technological University and Argonne National Laboratory to discuss conducting collaborative research pertaining to advanced technology passenger vehicles. In June of the same year, a contract was established between Michigan Tech and the Argonne Center for Transportation Research titled “Advanced Vehicle Characterization at Argonne National Laboratory” which detailed the scope of work and research timeline that led to the definition of this thesis project. The primary participants at Argonne National Laboratory were Dr. Henning Lohse-Busch and Mr. Eric Rask, who provided technical guidance throughout the course of the project. Dr. Scott Miers was the primary representative at Michigan Technological University and provided further direction while I, Jeremy J. Anderson, was the project architect and graduate research assistant.

The project was focused on a multi-architectural advanced technology vehicle comparison, incorporating several of the most popular technologies available today in the light-duty passenger vehicle market. Four vehicles were selected for study. One of these served as a baseline of sorts, while the others represented different strategies to obtain high efficiency and superior fuel economy. The vehicles were studied in detail to understand the details of their operational strategy.

This work was largely inspired by the lack of publicly available technical comparative data between advanced technology vehicles. Benchmarking studies similar in nature to this project are conducted by commercial automakers, but the results are not made available for consumption by those outside the automotive industry. The creation of this thesis work was motivated by a desire to provide a detailed investigation of popular vehicle architectures available in the light duty market with a technical audience in mind.

1.2 Project Objectives

The purpose of this project was to investigate and understand the operational characteristics and behavior of four modern passenger vehicles of varying architectures with the intent of providing publicly available data and prose explaining the results. Primary objectives of the project are listed below:

- Determine research vehicles representing popular modern vehicle architectures, including downsized gasoline conventional vehicles, turbodiesel vehicles, and hybrid electric vehicles. Further determine a legacy technology conventional vehicle to serve as the baseline against which to compare the advanced technology vehicles.
- Obtain the research vehicles for participation in the study.
- Instrument the research vehicles to facilitate observation of the following:
 - Fuel Consumption
 - Tractive Power Output
 - Engine Utilization
 - Transmission Utilization
 - Coolant and Exhaust Heat Loss
 - Tailpipe Emissions
 - Cylinder Pressure Indication
- Determine a selection of chassis dynamometer test cycles to illuminate vehicle performance under varying driving conditions as well as steady-state operation.
- Analyze data to determine vehicle operational strategies and to quantify the results for comparative purposes.
- Determine study conclusions as well as recommendations for future work.

Extensive instrumentation and testing was conducted to satisfy these objectives and is catalogued in this thesis.

1.3 Summary

The purpose of this thesis was to understand and document the operational strategy and performance of a set of advanced technology passenger vehicles.

In order to accomplish this goal, several research vehicles were chosen that represent different powertrain architectures available in the passenger vehicle market, including a modern turbodiesel vehicle, a vehicle utilizing a downsized and boosted gasoline engine, and a gasoline-electric hybrid vehicle. A fourth vehicle was chosen to represent baseline legacy powertrain architecture. These research vehicles were equipped with extensive instrumentation to allow for the collection of signals to illuminate and understand the behavioral strategy and resulting performance of each of the vehicles. In order to ensure repeatable and reliable data collection, all testing efforts were conducted at the Argonne National Laboratory Advanced Powertrain Research Facility, utilizing a vehicle chassis dynamometer and EPA drive cycles. The drive cycles were chosen to provide several different vehicle usage profiles, including urban driving, highway driving, and aggressive vehicle operation. Additionally, steady-state testing was conducted to capture vehicle performance at a range of speeds.

The observed performance and operation of each vehicle is first discussed individually in chapters dedicated to each research vehicle. The results are then compared to one another where appropriate in order to investigate the relative advantages and limitations of each platform, and are explained in detail in an additional chapter reserved for comparative analysis.

Chapter 2 Project Background

2.1 Vehicle Testing Facilities and Practices

2.1.1 Advanced Powertrain Research Facility (APRF)

The experimental work discussed in this thesis was performed at the Advanced Powertrain Research Facility (APRF) at Argonne National Laboratory in Argonne, IL. The APRF exists to further the available knowledge base regarding modern transportation vehicles and their powertrains in a setting largely independent of the constraints of for-profit research. Research conducted in the APRF spans a litany of powertrain related topics including conventional, hybrid, and alternative fuel vehicle research and is primarily funded by the United States Department of Energy and its subsidiaries. The APRF facilities allows Argonne engineers to explore vehicle powertrains and ancillary components in order to determine which technologies provide the best balance of maximizing fuel economy while lowering environmental impact.

2.1.2 Instrumentation and Measurement Specifications

The majority of the testing performed to support the vehicle-centric research performed at the APRF is conducted in a pair of vehicle chassis dynamometer test cells. The research conducted for this thesis took place in APRF Test Cell #7.

Cell 7 is constructed around a Burke E. Porter 2WD electric chassis dynamometer. The dynamometer allows APRF engineers to perform road load simulation and measure vehicle tractive effort for front or rear-wheel-drive vehicles. It also allows for vehicle loss determinations in order to match the vehicle road load terms provided by the Environmental Protection Agency (EPA) for passenger vehicles. This dynamometer uses 48" O.D. rollers and is fitted with a 300 horsepower electric motor that provides a simulated vehicle inertia range of 1,000 to 14,000 lbf with accuracy of $\pm 1\%$. The inertial response time of 60-70 ms allows rapid emulation of real world conditions.

Environmental conditions in the cell are controlled by a dedicated HVAC system. Test cell temperature is nominally 72°F. Vehicle cooling during testing is provided by a

24" 0.25 horsepower constant-speed electric fan placed in front of the vehicle radiator. The test vehicle's OEM cooling fans provide additional airflow when needed.

In order to measure the fuel consumption of vehicles tested in the APRF, Cell 7 is equipped with a Re-Sol RS840-060 fuel measurement system. This device is suitable for all vehicles with return-less style fuel delivery systems. It is installed in-line with the vehicle's fuel supply and makes use of a positive displacement flow meter to measure the volumetric flow rate of fuel consumed by the engine. The meter is able to measure flow rates between 0.3 and 60 liters per hour with accuracy of $\pm 0.5\%$ of reading.

Batch emissions measurements are facilitated by the use of a Semtech unit by Sensors, Inc. The Semtech continuously samples the vehicle exhaust gas and passes it through several analysis modules. These analyzers use techniques such as flame ionization and spectroscopy in order to determine the concentrations of the exhaust gas constituents. This is combined with a total exhaust volumetric flow measurement to determine the total vehicle emissions of CO, NO_x, and total hydrocarbons (THC). Measurements from the Semtech can be used with fuel stoichiometry calculations to calculate the real time fuel flow rate in cases where a more responsive fuel cart measurement is not available. The Semtech is used with an AVL Direct Volume Exhaust (DVE) system which provides real time measurements of the exhaust gas flow while maintaining atmospheric pressure at the tailpipe so as not to influence engine backpressure.

Pertinent electrical measurements such as battery current and voltage are collected using a Hioki 3390 power analyzer. Inductive current clamps are used in conjunction with voltage measurements to determine component-level power consumption and the energy expenditure of high voltage batteries. The accuracy of the power analyzer is cited as $\pm 0.1\%$ of reading with a sampling rate of 20 Hz.

Cell 7 also has the capability to use optical character recognition to interface with manufacturer provided vehicle diagnostic tools in order to record signals provided by the

CAN bus. The CAN bus can be instrumented directly when appropriate which can improve the data sampling rate. The test cell is also equipped with a thermocouple bus which allows research vehicles to be instrumented with a number of temperature measurements.

In addition, the vehicles used in this study were instrumented with Omega FTB series turbine-style flow meters in their cooling systems. These were used in conjunction with fluid temperature measurements to determine the enthalpy change of the engine coolant as it absorbed or rejected thermal energy to regulate the temperature of the engine.

Finally, each of the test vehicles was instrumented with an AVL InidModul to facilitate real-time measurements of in-cylinder pressures on a crank-angle basis. This allows for the calculation of pertinent engine work parameters such as indicated mean effective pressure (IMEP).

Data collected by each of these measurement systems is fed into a custom LabView construct that samples each channel at a rate of 10 Hz. The data are time aligned and assembled into a .TDMS file for later analysis. The LabView construct also provides a user interface that allows for customization of the test cell channels and allows the test cell operator to monitor signals in real time. Together these systems facilitate the collection of a multitude of signals for each test vehicle that are used to support the research goals of the APRF.

2.1.3 Vehicle Road Load Determination

When a vehicle is operated on a chassis dynamometer, it is important that the force provided to resist the vehicle's accelerations accurately reflects the forces experienced by the vehicle when operating on the road. Coast down tests are conducted by the Environmental Protection Agency (EPA) for commercially available passenger vehicles where the vehicle's deceleration rate on level ground is observed with the vehicle transmission in neutral gear. The deceleration profile is used for the calculation of

the summation of the forces experienced by the vehicle at a given speed, often referred to as the vehicle road load. A second order polynomial is then fit to the road load profile, the coefficients of which are reported as the vehicle road load coefficients. These coefficients then allow for the calculation and replication of the vehicle road load at any speed.

It is important to note that the external forces and deceleration rate are affected by many factors, including aerodynamic drag and driveline losses. By nature, operation on a chassis dynamometer is not subject to all of the same losses as open road operation. For example, aerodynamic drag is almost completely non-existent in a test cell setting. To determine which proportion of the losses is still physically present, a similar coast down test is performed on the chassis dynamometer. Again a second order polynomial is fit to the resulting road load. These coefficients are termed the vehicle loss coefficients. The dynamometer controller then determines an applicable force determined by the difference between the road load coefficients and vehicle loss coefficient. If vehicle speed is changing, an additional calculation to determine the force resulting from vehicle inertia is applied. The sum of these forces is applied to the vehicle in order to influence the amount of work that must be done to accelerate and decelerate during testing, closely replicating the real-world vehicle road load. This ensures that the vehicle behavior on the dynamometer is consistent with on-road operation.

2.1.4 Dynamometer Testing Cycles

To facilitate research continuity in vehicle testing at the APRF, most research is conducted using dynamometer drive cycles. Drive cycles are defined on a speed vs. time basis. During a dynamometer test, the test driver will operate the vehicle in a best-effort manner to attempt to match the vehicle speed to the drive cycle speed at all times, ensuring that the work performed by the vehicle on a given drive cycle is consistent from test to test.

The drive cycle-based work discussed in this thesis is limited to three separate EPA drive cycles: the Urban Dynamometer Driving Schedule (UDDS), the Highway Fuel Economy Driving Schedule (HWFET), and the US06 cycle.

The UDDS test is designed to simulate city driving. It is 7.45 miles long and takes 1369 seconds to complete, with an average speed of 19.6 mph. The HWFET test simulates highway driving. It lasts 765 seconds and covers 10.26 miles with an average speed of 48.3 mph. The US06 is a more aggressive cycle that encompasses both city and highway type driving. It covers 8.01 miles with an average speed of 48.4 mph and takes 596 seconds to complete.

These drive cycles are typically performed when the vehicle is in a quasi-steady thermal state, with lubricants at operating temperature. This is often accomplished by repeating a given cycle several times until stable temperatures are reached. In addition, the UDDS and US06 cycles were repeated for each vehicle under cold start conditions after a twelve hour soak at ambient test cell temperatures. This allows for an understanding of the fuel economy penalties involved when the vehicle begins a test at ambient temperature.

Additionally, the vehicles were subjected to a steady state speed tests in order to illuminate their performance under constant load conditions. In this test, the vehicle is held at constant speed in ten mile per hour increments for thirty seconds at a time. The cycle climbs from ten to eighty miles per hour, and then descends again through the speeds allowing each constant speed portion to be performed twice. This can help to illuminate inconsistencies due to transmission hysteresis.

It should be noted that some drive cycles are divided into multiple phases, sometimes referred to as ‘bags’. This is not only done for data analysis purposes, but also is used to denote which part of a given cycle is being used for analysis or discussion. The UDDS and HWFET tests are both single phase drive cycles. The US06 cycle is divided into two phases. The beginning and ending sections of the drive cycle are both included

in the first test phase. The second phase contains the higher speed portion of the cycle. The first phase is often referred to as the ‘city’ portion of the US06 cycle, while the second phase is referred to as the ‘highway’ portion. The drive cycles are illustrated in Figures 2.1.1 – 2.1.4.

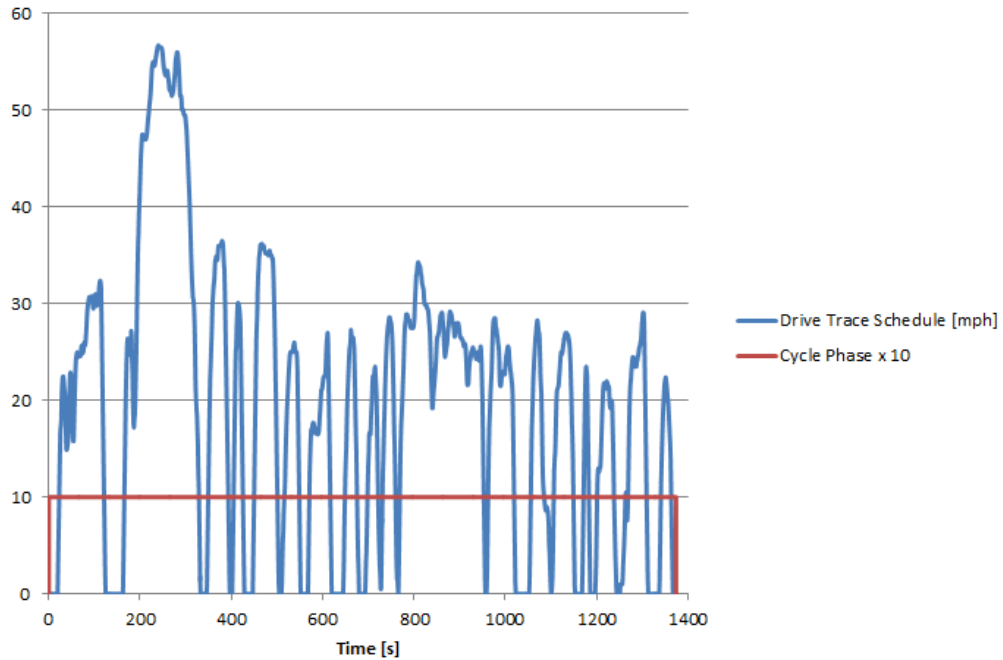


Figure 2.1.1: Urban Dynamometer Driving Schedule (UDDS)

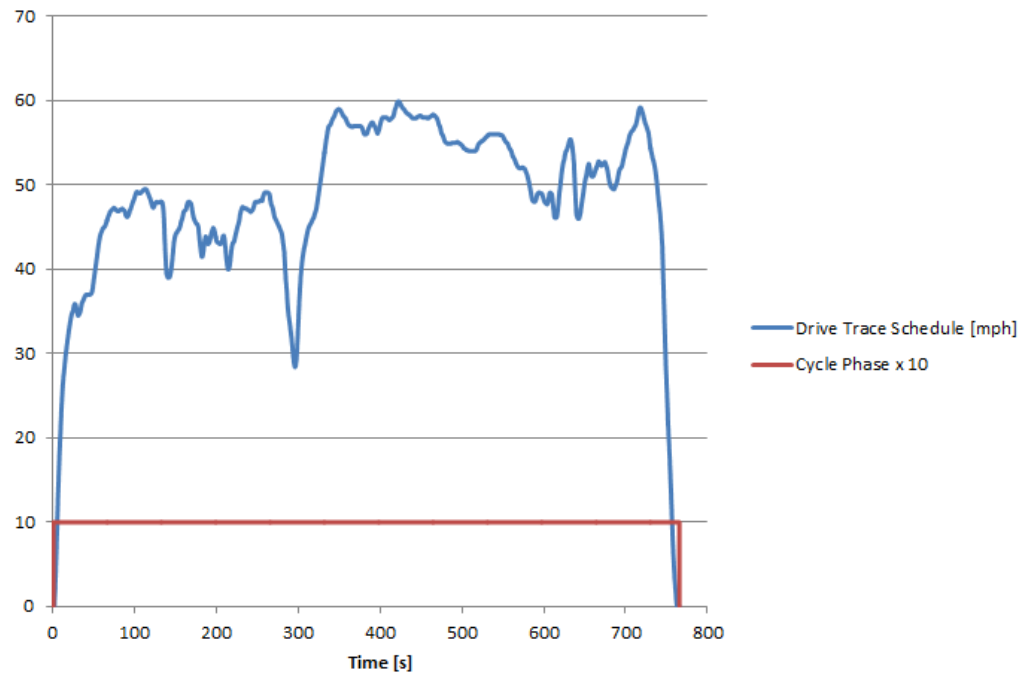


Figure 2.1.2: Highway Fuel Economy Driving Schedule (HWFET)

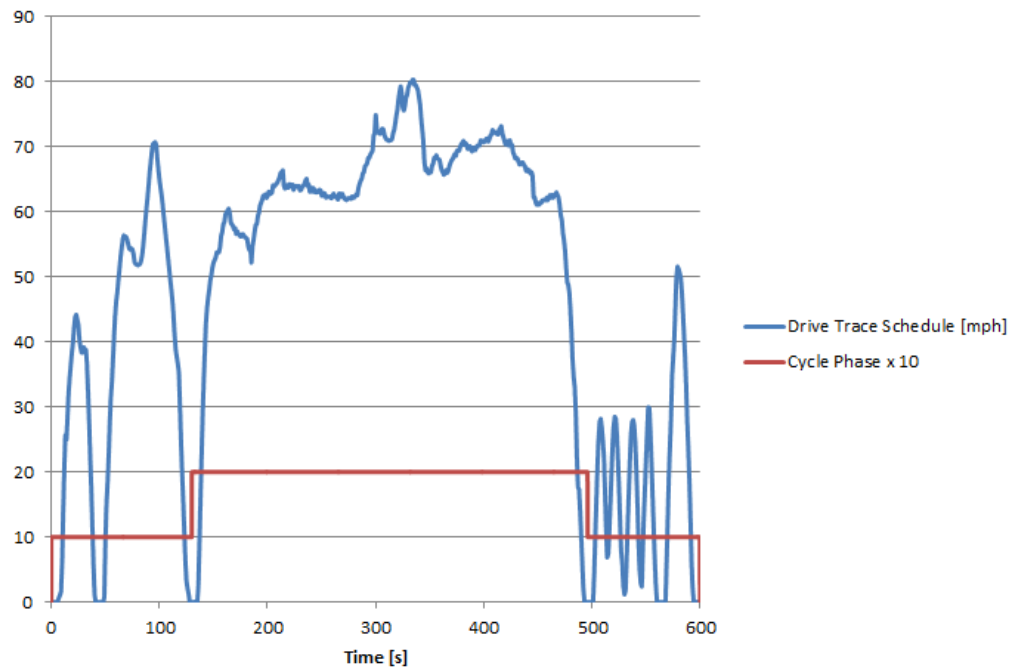


Figure 2.1.3: US06 Driving Schedule

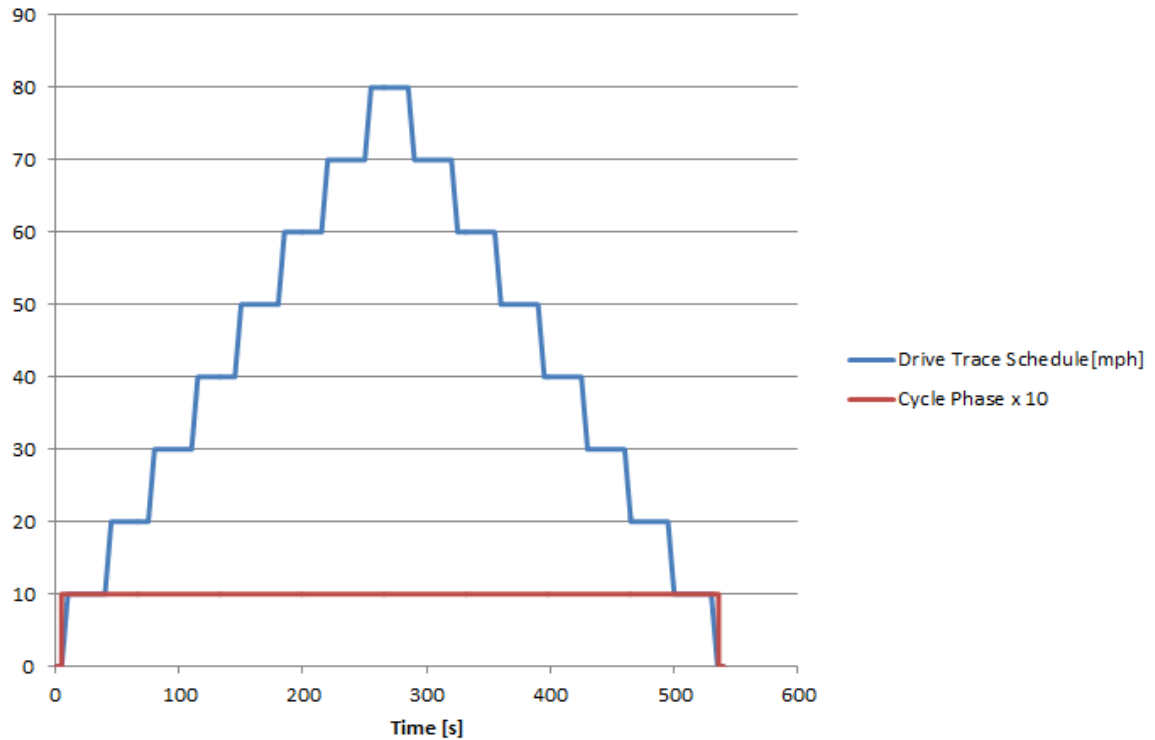


Figure 2.1.4: 0-80-0 Steady State Speed Driving Schedule

2.1.5 Vehicle Analysis Metrics and Equations

In order to compare and contrast the merits of the research vehicles included in this project, a number of different metrics were calculated to quantify the performance and efficiencies of the respective vehicles. In the case of a vehicle-centric research project, the term ‘efficiency’ must be further qualified to be of proper descriptive use. Several different measurement points were used on each vehicle to compute relevant efficiency metrics.

An important quantity used to calculate several different efficiency metrics is the rate at which fuel energy is delivered to the vehicle’s engine. This fuel power is calculated by multiplying the mass flow rate of fuel delivered by the lower heating value of the fuel, as shown by Equation 2.1. It represents the total rate of energy available to the vehicle for conversion to mechanical work.

$$\text{Fuel Power (W)} = \text{Fuel Mass Flow Rate} \left(\frac{g}{s} \right) * \text{Fuel LHV} \left(\frac{J}{g} \right)$$

■ Equation 2.1

Vehicle wheel power is also important to the calculation of efficiency metrics. This quantity is the tractive work done by the vehicle's tires on the dynamometer, and represents the work the vehicle does in order to move down the road. It is calculated by multiplying the tractive force by the linear speed of the vehicle, as shown by Equation 2.2

$$\text{Vehicle Wheel Power (W)} = \text{Tractive Effort (N)} * \text{Vehicle Speed} \left(\frac{m}{s} \right)$$

■ Equation 2.2

A third parameter of importance is the indicated engine power. This quantity represents the work done on the engine's pistons by the combustion events taking place in-cylinder. It is calculated as shown by Equation 2.3, where IMEP is the indicated mean effective pressure, V_d is the engine displacement volume, and n_r denotes the number of revolutions per engine cycle.

$$\text{Indicated Engine Power (W)} = \frac{\text{IMEP (Pa)} * V_d \left(\frac{m^3}{rev} \right) * \text{Engine Speed} \left(\frac{rev}{s} \right)}{n_r}$$

■ Equation 2.3

If the vehicle's engine output shaft is fitted with a torque sensor, the engine brake work can also be calculated. This represents the mechanical work done by the engine on the vehicle drivetrain, and is calculated using Equation 2.4. It should be noted that due to the cost and complexity inherent in fitting a crankshaft torque sensor, this measurement is only available for the Toyota Prius.

$$\text{Brake Engine Power (W)} = \text{Brake Engine Torque (Nm)} * \text{Engine Speed} \left(\frac{rad}{s} \right)$$

■ Equation 2.4

These parameters can be used to calculate several efficiency parameters that can illustrate the performance of the test vehicles. The first of these is the engine indicated efficiency. It is defined as the indicated engine power divided by the fuel power shown in Equation 2.5. This represents the proportion of the fuel energy that is converted to work on the piston crown. This includes losses such as blow-by past the piston rings and heat transfer from the combustion charge to the cylinder walls, but is unaffected by engine mechanical friction.

$$\text{Indicated Efficiency (\%)} = \frac{\text{Indicated Engine Power (W)}}{\text{Fuel Power (W)}} * 100$$

■ Equation 2.5

The engine mechanical efficiency (known also as engine brake thermal efficiency) can be calculated when both the engine brake power and incoming fuel power are available. This is computed by the use of Equation 2.6. The losses involved in indicated efficiency are included in this metric as well as additional losses inherent to the engine rotating assembly such as bearing friction and friction between the cylinder wall and piston rings. The proportion of these losses attributable to the rotating assembly is defined as the engine friction power. In cases where the engine brake power and indicated power are both available, engine friction power can be computed by Equation 2.7

$$\text{Engine Efficiency (\%)} = \frac{\text{Brake Engine Power (W)}}{\text{Fuel Power (W)}} * 100$$

■ Equation 2.6

$$\begin{aligned} \text{Engine Friction Power (W)} \\ = \text{Indicated Engine Power (W)} - \text{Brake Engine Power (W)} \end{aligned}$$

■ Equation 2.7

The drivetrain mechanical efficiency can be calculated using Equation 2.8. This metric requires the presence of a crankshaft torque sensor. This represents the efficiency of the transmission and driveline through to the vehicle's tires.

$$\text{Drivetrain Efficiency (\%)} = \frac{\text{Positive Wheel Power (W)}}{\text{Brake Engine Power (W)}} * 100$$

■ Equation 2.8

Finally, we can calculate the overall vehicle efficiency using Equation 2.9. This includes all of the losses inherent in the vehicle powertrain from the fuel to the tires.

$$\text{Vehicle Efficiency (\%)} = \frac{\text{Positive Wheel Power (W)}}{\text{Fuel Power (W)}} * 100$$

■ Equation 2.9

Figure 2.1.5 provides a schematic representation of a typical vehicle powertrain. The measurement points discussed in the preceding equations are labeled as points A-D, and the efficiency parameters discussed in this section are shown according to their corresponding measurements.

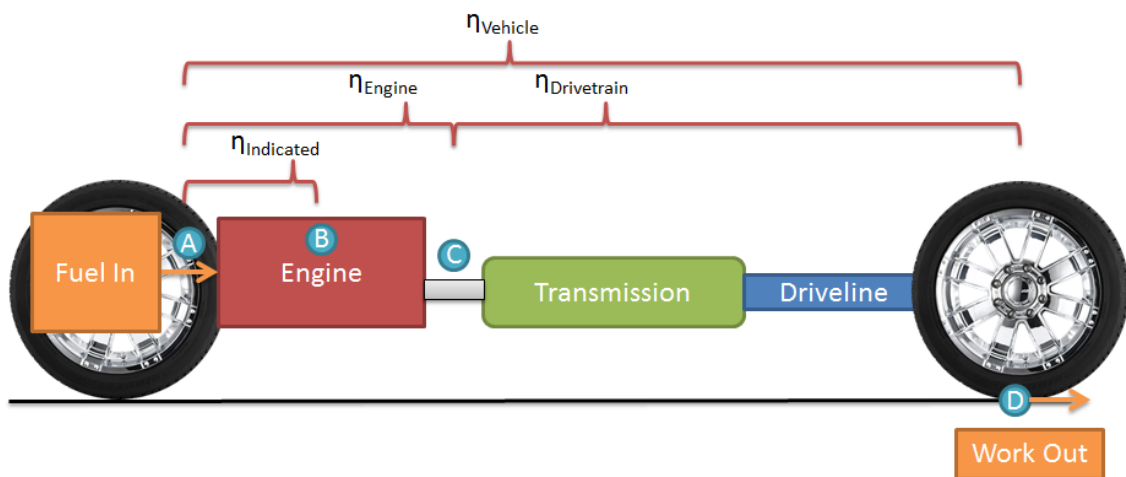


Figure 2.1.5: Vehicle Efficiency Metrics

In order to quantify the energy lost to the surroundings through coolant and exhaust heat transfer, the enthalpy changes of these fluid streams between the exit and ambient conditions were calculated. In general, the rate of enthalpy change of a fluid is given by Equation 2.10 [14].

$$\Delta h(W) = \dot{m}_{fluid} \left(\frac{g}{s} \right) * cp_{fluid} \left(\frac{J}{g * K} \right) * \Delta T(K)$$

■ Equation 2.10

For the purposes of this study, the specific heat of the engine coolant was determined by fitting a linear curve to temperature-dependent specific heat data for a 50/50 by volume mixture of ethylene glycol and water, which is the commonly accepted mixture for passenger vehicle cooling systems. This resulted in Equation 2.11, which was used with the real-time fluid temperature to calculate the specific heat at any given time. For the engine coolant, mass flow rate and the temperature differential are both easily measurable quantities. Equation 2.10 can then be used to calculate the enthalpy change.

$$cp_{coolant} \left(\frac{J}{kg * K} \right) = 3.2675 * T_{coolant}(K) + 2429.1$$

■ Equation 2.11

In order to calculate the exhaust flow enthalpy drop, combustion stoichiometry calculations must be performed to understand the mass fractions of the combustion products in order to calculate the exhaust stream specific heat. For the purposes of this project, operation at the stoichiometric air-fuel ratio (AFR) was assumed for gasoline vehicles. This ratio is found by via stoichiometry calculations for one mole of fuel combusted with atmospheric oxygen. AFR_{stoich} is calculated for each vehicle on an individual basis to accommodate for the difference in carbon-to-hydrogen ratios between fuel batches used in the test vehicles. Once AFR_{stoich} and the mass fractions of the products are known, the exhaust gas specific heat can be calculated using Equation 2.12.

$$cp_{exhaust} = \sum_{i=1}^{n_{products}} mfrac_i * cp_i$$

■ Equation 2.12

Once the exhaust gas specific heat is known, the mass flow rate of the exhaust is calculated using the measured fuel flow rate and the air-fuel ratio. For gasoline vehicles, assuming AFR_{stoich} for all conditions introduces little error and is sufficient for the goals of this project. For the diesel-powered TDI, AFR was determined continuously from the air and fuel mass flow rates. Equation 2.13 can be used to calculate the total exhaust mass flow rate, while the exhaust gas temperature is measured with a thermocouple mounted in the vehicle exhaust system. The test cell temperature is also measured and used as the reference state temperature for the temperature differential. Finally, Equation 2.11 is used to calculate the enthalpy change.

$$\dot{m}_{exhaust} = \dot{m}_{fuel} + AFR * \dot{m}_{fuel}$$

■ Equation 2.13

This section would be incomplete without a brief discussion of fuel economy. The numbers most often reported to consumers when discussing the performance of a particular vehicle correspond to the distance the vehicle is able to travel on a given quantity of fuel. Typically, the units used in the U.S. are miles per gallon, or mpg. This measurement has become familiar to consumers because of its widespread use. However, this metric becomes complicated when the fuel in question is no longer easily measured in gallons; such is the case with vehicles operating on gaseous fuels (CNG, Hydrogen) and electric vehicles.

The relation of fuel economy to vehicle efficiency is also nebulous, and depends on several factors. Vehicle efficiency depends chiefly on the operating points of the engine and driveline with regard to speed, applied load, and thermal state. In a hybrid-electric vehicle, the regenerative braking energy recaptured is a further important

consideration. Fuel economy, however, is more difficult to parameterize. It depends both on the efficiency with which fuel is utilized, and also on the amount of work required of the vehicle over the distance traveled. Because the fuel economy measurement alone provides no means to separate these two factors, further metrics such as vehicle efficiency are beneficial in order to properly illuminate the vehicle's operating characteristics. Fuel economy is given by Equation 2.14.

$$\text{Fuel Economy} = \frac{\text{Distance Travelled}}{\text{Fuel Used}}$$

■ Equation 2.14

2.2 Modern Passenger Vehicle Powertrain Technology & Architecture

Fuel economy of passenger vehicles has become an issue of significant importance. It is a topic that has received a great deal of research and development focus and has garnered steady public interest, especially over the past 15 years. This is due to a number of factors, including governmental Corporate Average Fuel Economy (CAFE) regulations, recent increased interest in environmentalism and green motoring, and concerns over U.S. dependence on foreign oil (In 2012, 46.5% of petroleum used in the U.S. was imported [1]).

The quest for improved fuel economy is largely a quest for efficiency improvements, and many new technologies have come to market to address these issues. A 2003 paper by authors Sovran and Blaser investigates the factors affecting vehicle fuel economy and the potential benefits of advanced technology application to passenger vehicles. A variety of techniques for improving efficiency are available, and several are discussed in their paper including shifting engine operation to more efficient speed and load points, improving the efficiency contour topology of the engine map, reducing fuel use on deceleration, and decreasing engine idling time [2]. Additional efficiency gains can be made in other areas, such as power transmission efficiency, road load reduction,

and in the case of hybrid-electric vehicles, recapture of kinetic energy through regenerative braking.

A number of technologies have surfaced to provide a means for improvement in each of these areas. One technique for improving engine efficiency is the application of over-expanded cycles. Sovran and Blaser posit that the major driver of peak engine efficiency is the thermodynamic efficiency of the engine process, which is directly influenced by the engine's geometric compression ratio [2]. In gasoline engines, further increasing compression ratio is made difficult by the octane rating of the fuel; a numerically high compression ratio contributes to elevated peak cylinder pressures and temperatures, which can cause combustion knock. One means for mitigating this effect is to apply an over-expanded cycle to reduce the effective compression ratio while preserving a large expansion ratio. Toyota details their implementation of this strategy on the 2ZR-FXE engine in a 2009 SAE paper. The authors show that the implementation of the Atkinson cycle reduced the brake-specific fuel consumption of the engine by 8.5% over the base engine utilizing a conventional cycle [3]. It should also be noted that diesel engines are able to sustain much higher compression ratios than equivalent gasoline engines, which results in generally higher brake thermal efficiency values for these engines [4,5].

Engine downsizing provides a second approach to maximizing efficiency. Gasoline engines require careful control of the air to fuel ratio (AFR) in order to ensure stable combustion and effective operation of the traditional three way aftertreatment catalyst. In order to facilitate careful AFR control, these engines are fitted with throttling valves to restrict the amount of air flowing into the engine at part load conditions. These valves often cause the intake manifold pressure to drop below atmospheric values, forcing the engine to work harder to pump air into the cylinders. In general, a smaller engine must operate with a wider throttle opening to produce an equivalent torque output. This serves to reduce throttling losses, improving engine efficiency under part load conditions. Downsized engines are typically turbocharged to maintain power density. These engines also typically benefit from reduced friction losses stemming from smaller

required bearing and piston ring contact surfaces. A 2004 SAE paper published by Ricardo UK and Ford-Werke details the development of a downsized engine that yielded a 21% improvement in efficiency over the naturally aspirated base engine it was developed to replace, chiefly due to the aforementioned advantages [6]. Similarly, a 2007 paper released by Hyundai-Kia Motors explores the development of 2.0L I4 turbocharged GDI engine to replace a 3.3L V6. In their testing, it was found that the downsized engine exhibited 17% better fuel economy than the V6 in city driving. It was also shown that the downsized engine was able to provide greater torque across the majority of the operation range [7].

It should be noted that technologies for improving engine efficiency often present challenges as well. Over-expanded engine cycles reduce engine power density, while engine downsizing reduces the overall power output of an engine. Turbochargers can be implemented to pressurize the intake manifold. This increases charge density and engine power output, but also increases intake air temperature and peak combustion temperatures [4,5]. This often necessitates lower compression ratios in turbocharged engines, reducing efficiency at part load conditions. Direct fuel injection (DI) architecture can help to cool the charge mixture as the injected fuel vaporizes in the cylinder. A 2009 paper published by Mahle Powertrain Ltd discusses the challenges involved in turbocharging modern gasoline engines. The authors state that implementation of DI architecture can serve to allow an increase in compression ratio of at least 1 point over port fuel injected (PFI) engines, improving part-load efficiency. [8]

It should also be noted that advanced engineering modeling techniques are enabling more robust optimization efforts in engine design. This helps to ensure that each of the technologies employed in the development of a new engine is developed in such a way as to minimize fuel consumption. A 2007 paper published by the University of Malaysia discusses a multi-dimensional modeling strategy to optimize a multitude of engine parameters to aid in engine design [9].

Vehicle transmission technologies are also continuously improving. One trend is the conversion from torque converters to automated clutch units for power transfer. A 2005 paper by Borg Warner Transmission Systems shows that dual clutch transmissions can improve power transmission efficiency by as much as 10% over conventional automatic transmissions [10]. Another trend in this market is the development of hydraulically optimized torque converter transmissions with increased gear ratio counts. ZF produced a paper in 2009 detailing the development of a new 8-speed automatic transmission that increased power transmission efficiency by 6% over a legacy unit [11]. A 2010 paper by Honda R&D details the development of a modern 6-speed torque converter automatic transmission. Through the addition of an extra gear ratio and hydraulic optimization of the gear change mechanisms, the new transmission yielded a 5% increase in fuel economy when installed in a test vehicle and evaluated on a chassis dynamometer [12]. It should be noted that a greater number of available ratios provides increased engine utilization flexibility, allowing the engine to operate at peak efficiency points as often as possible.

Hybridization of the vehicle powertrain can serve to improve engine utilization flexibility while also providing a means of kinetic energy recovery. Though these systems are more complex than traditional powertrains, the ability to modulate engine load and provide regenerative braking are unique and beneficial. Toyota released a technical paper in 2009 detailing the development of their latest hybrid vehicle architecture. The authors discuss several of the design innovations that allow for high fidelity control over engine utilization, which also provided the opportunity to optimize the engine efficiency islands accordingly [13,3].

Each of these engine and powertrain technologies has been steadily applied to modern passenger vehicles. This has resulted in the creation of several popular platform architectures. Those tested for this thesis work are introduced and discussed below.

2.2.1 Modern Conventional Gasoline

The majority of passenger vehicles sold in the United States are equipped with a gasoline engine and a torque converter automatic transmission. This broad formula dates back many years, but has been extensively updated with the application of new technologies. The 2012 Ford Fusion included in this study falls into this category.

Engines in this segment are universally fitted with fuel injection systems that provide fine control over the fuel/air mixture to minimize emissions and maximize economy. Some are fitted with gasoline direct injection (GDI) which provides additional control over injection timing and an additional cooling effect that can allow for increased compression ratios to improve engine efficiency and power density. Variable valve timing is common and helps to improve the efficiency of the gas exchange process, reducing the required engine pumping work. Common displacements range from 1.8 to 2.5 liters, with most engines incorporating dual overhead camshafts and four valves per cylinder to further improve breathing efficiency. There has also been a trend toward the use of lighter-viscosity lubricating oils to reduce engine friction.

Transmissions of modern conventional gasoline vehicles have also benefitted from numerous updates. Though torque converter automatic transaxles are sometimes considered an older technology, the newest transmissions benefit from hydraulic optimization and an increased ratio count, ranging from five to eight forward speeds.

2.2.2 Modern Conventional Turbodiesel

Turbodiesel engines have also benefitted from a great deal of development in recent years. Though sales numbers have been historically low in North America, vehicles equipped with these engines are beginning to gain traction in the market.

Diesel engines have a number of advantages over traditional gasoline engines. Because the fuel and air mixture is ignited via compression of the cylinder charge, it is no longer important to concentrate a fuel-rich kernel around a single ignition source. This frees the engine from the need for stoichiometric combustion and allows for non-throttled

operation over a wide variety of conditions, largely eliminating throttling losses. Because of the relatively violent nature of compression ignition, diesel components are typically designed to be stronger than those used in gasoline engines, tolerating higher compression ratios and producing comparatively large brake torque at lower engine speeds. This helps to enhance drivability. Diesel engines are often equipped with one or more turbochargers to provide greater power density and finer control over the amount of air introduced into the cylinder.

Diesel engine fuel systems have been trending towards common rail designs, where all injectors are fed from a single high pressure fuel source. The injectors themselves are increasingly fitted with piezoelectric actuators, allowing for extremely fast cycling (often multiple injection events per engine cycle). Exhaust aftertreatment technologies have been advancing and are fitted to almost all modern diesel engines in passenger car use. These have helped to drastically reduce tailpipe emissions such as particulate soot and oxides of nitrogen (NO_x).

The increased efficiency and drivability of the diesel engine are helping diesel-powered vehicles gain a greater market share that merits their investigation in this study. Here, the turbodiesel is represented by the 2009 Volkswagen Jetta TDI.

2.2.3 Downsized, Forced-Induction Gasoline Conventional

Another school of thought that has been gaining popularity involves improving the efficiency of conventional gasoline engines at part load through downsizing. In general, a smaller displacement engine will be forced to run at a greater throttle opening to produce equivalent torque, diminishing throttling losses and improving efficiency.

In order to maintain the full load capabilities of the larger engines they replace, downsized gasoline engines are typically fitted with a turbocharger to increase power density. Variable valve timing is ubiquitous, and turbocharged engines are increasingly fitted with GDI systems to permit higher compression ratios for further efficiency increases. With the advent of low-inertia (and sometimes variable geometry)

turbochargers, these engines are able to deliver large amounts of torque at lower engine speeds than was previously possible within the constraints of drivability and power density.

Vehicles in this segment are typically fitted with advanced transmissions. The most popular among these is the automated manual gearbox. These transmissions typically contain at least six forward ratios and transmit power through a set of twin clutches. This allows for extremely quick shifting for smooth power delivery. The absence of a torque converter helps to reduce parasitic slip losses.

In this study, the downsized gasoline configuration is represented by a 2010 European-spec Volkswagen Jetta TSI.

2.2.4 Gasoline-Electric Hybrid

Another increasingly popular answer to the question of increasing passenger vehicle fuel economy is the gasoline-electric hybrid vehicle. Several architectures exist that describe the powertrain layout and hybridization strategy, but in general vehicles in this class are powered by a gasoline engine coupled with an electric motor/generator and a battery pack for energy storage.

Hybrid electric vehicles (HEV's) increase their efficiency through two novel means depending on the vehicle's operating regime. The first is a kinetic energy recovery strategy in which the electric traction motor can be used during braking, reducing the load on the friction brakes and charging the battery pack in a process known as regenerative braking. This can be quite effective on drive cycles that require large decelerations, but is generally ineffective during prolonged periods of highway cruising where opportunities for regeneration are few.

The second means of increasing efficiency can be broadly defined as optimization of engine usage. This involves shifting the engine operating point to locations of highest efficiency. In low power demand situations, HEV's are often capable of forward motion

relying only on electric power without the aid of the IC engine. The battery power expended here can be reclaimed by regenerative braking, or it can be recharged using the engine. The latter process can be further optimized by strategically recharging during periods of relatively light load, increasing the total engine load to improve efficiency.

Hybrid-electric vehicles in the United States are generally equipped with gasoline engines. Because the engine usage strategy is considerably more flexible than that of a conventional vehicle, there are opportunities for engine optimization that are otherwise difficult to implement. Because engine power is supplemented by the traction motor, specific output becomes less important, allowing for over-expanded cycles that promote efficiency at the expense of power density. It is also true that it is less important to have an engine whose map has broad efficiency islands; instead, these can be sacrificed for smaller islands with higher efficiencies via aggressive cam timing and base engine design. The hybrid system can then be utilized to maximize the amount of time the engine spends operating at peak efficiency. Most hybrid vehicle engines are small displacement inline configurations with four power cylinders.

HEV powertrain configurations range from mild electric assist conversions of conventional vehicles to complete integrated powertrains designed specifically for hybrid use. As such, transmissions similar to those used in conventional vehicles can be found in the segment, as well as purpose-built ‘power split’ devices involving planetary gear systems.

In this study, hybrid-electric vehicles are represented by a 2010 Toyota Prius. Its configuration is discussed in detail in Chapter 6.

Chapter 3 MY2012 Ford Fusion 2.5

3.1 Relevant Vehicle Features

The baseline vehicle chosen for this research project is a MY2012 Ford Fusion. The vehicle is of FF configuration, denoting a front-engine, front-wheel-drive layout. The Fusion is equipped with a four-cylinder spark-ignited gasoline engine, displacing 2.5

liters. The engine output is robust among the subjects of this study, and is rated at 175 brake horsepower at 6,000 rpm and 172 lb.-ft. of torque at 4,500 rpm. This engine is of reasonably modern architecture, with 4 valves per cylinder, variable valve timing and port fuel injection (PFI), with a compression ratio of 9.7:1.

The Fusion's engine is coupled to a conventional six-speed automatic transmission that transmits engine power through a hydraulic torque converter. The sixth ratio is an overdrive gear, helping to maximize fuel economy at cruising speeds.

The Fusion is classified as a mid-size sedan. Its test weight category as assigned by the Environmental Protection Agency (EPA) is 3625 lbs.

The Ford Fusion was chosen in part to provide a datum from which the performance of the other vehicles in this study could be measured. Though the Fusion platform was refreshed in MY2010, the engine is based on an earlier design that dates back to MY2003, and lacks newer efficiency improvement technologies such as direct fuel injection and sports a relatively low compression ratio. The use of a torque converter is also indicative of the vehicle's conventional design principles; more modern vehicles are making use of larger ratio counts and automated manual transmissions to increase efficiency without sacrificing drivability or performance. Table 3.1.1 catalogues the relevant vehicle parameters for the Fusion, while fuel properties are found in Table 3.1.2. The vehicle is pictured in Figure 3.1.1.

Table 3.1.1: Ford Fusion Vehicle Metrics

Year/Make/Model		2012 Ford Fusion
Body Type		4 dr Sedan
Engine		2.5L 16V VVT I4 Gasoline
Compression Ratio		9.7:1
Rated Power		130 kW (175 hp) @ 6,000 rpm
Rated Torque		233 N-m (172 lb.-ft.) @ 4,500 rpm
Transmission		6 Spd Torque Converter Automatic
Gear Ratio	1st	4.58:1
	2nd	2.96:1
	3rd	1.91:1
	4th	1.44:1
	5th	1.0:1
	6th	0.746:1
	7th	-
	Final Drive	3.20:1
EPA Fuel Economy	Urban	23
	Highway	33
	Combined	26
Road Load Coefficients	Test weight	3625
	Cd	0.32
	a	33.9204
	b	0.364
	c	0.0166
Vehicle Performance		
WOT Acceleration	0-60	10.5 s (ANL)
	30-50	3.5 s (ANL)
	50-70	5.3 s (ANL)

Table 3.1.2: Ford Fusion Fuel Specifications

Fuel Name:	Tier II EEE HF437	Density:	0.74	[g/ml]
Carbon Weight Fraction:	0.8631	Net HV:	18490	[BTU/lbm]



Figure 3.1.1: 2012 Ford Fusion

3.2 Instrumentation Specifics

In order to facilitate the collection of study data, the Fusion was fitted with a number of sensors and measurement devices. The intent was to observe the vehicle's operating characteristics unobtrusively so as not to influence the vehicle's performance during testing.

Fuel flow to the engine was directly measured using the Re-Sol RS840-060 fuel cart discussed previously. The Fusion is equipped with a returnless fuel system, allowing for measurement of the fuel supplied by splicing the meter into the supply line to the fuel rail. With this setup, fuel is pushed through the meter by the stock fuel pump as is done in normal operation.

The Fusion's cooling system was fitted with a pair of Omega FTB series flow meters in order to measure engine coolant flow rates. An FTB 1306 was installed in the radiator loop, while an FTB 1304 was installed in the heater core loop. Both sensors were supplied with calibration curves and were installed with the help of hose barb fittings.

The vehicle was also instrumented with a number of thermocouples. A total of four were placed in the cooling system at the engine inlets and outlets to both the radiator and heater core loops. These allowed for the monitoring of coolant temperatures in real time. Additionally, thermocouples were placed in the exhaust manifold to monitor the exhaust gas temperature.

Combustion parameters were monitored with the help of an AVL IndiModul and IndiCom software. The stock engine position signal was tapped and used in conjunction with an AVL 4CA1 crank angle calculator to determine crankshaft position in real time with an interpolated resolution of 0.1 degrees. Alignment between the measured cylinder top dead center (TDC) and crank angle signal was facilitated using an AVL 428 TDC determination probe. Cylinder pressure signals were measured in cylinder #1 with an AVL piezoelectric pressure transducer housed in the cylinder's spark plug. The transducer was calibrated using a dead weight calibrator to verify the manufacturer's calibration.

Several of the parameters reported by the engine control unit (ECU) were recorded with the use of a Ford diagnostic tool and optical character recognition software. These included the real time engine equivalence ratio and mass air flow, as well as the throttle plate position.

As with the other vehicles in this test, tailpipe emissions were measured with the use of a Sensors, Inc. SEMTECH and an AVL Dynamic Vehicle Exhaust system.

Figure 3.2.1 below showcases the Fusion's engine bay as configured during testing.

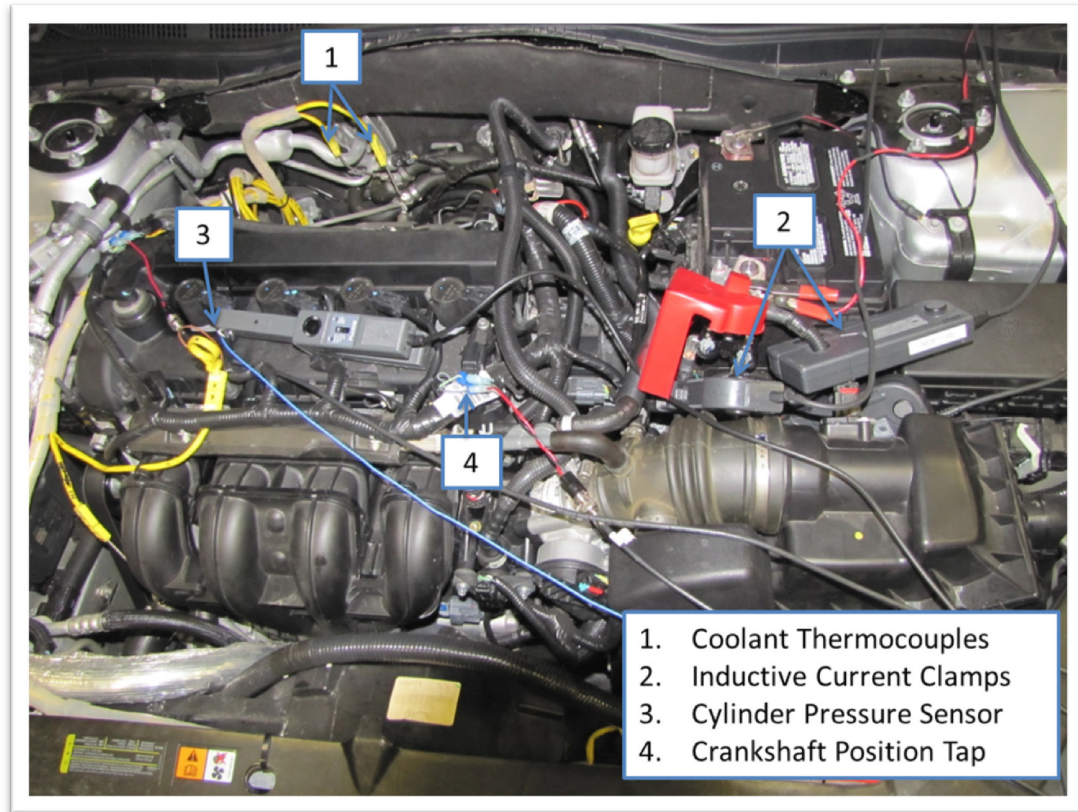


Figure 3.2.1: Ford Fusion Engine Bay

3.3 Drive Cycle Performance

The Fusion was subjected to a number of drive cycles in order to evaluate the vehicle's performance characteristics. A sample of the test plan used for this work can be found in Appendix A. The fuel economy of the vehicle was calculated along with the overall vehicle efficiency as defined in Equations 2.9 and 2.14. Table 3.3.1 catalogues these results. It should be noted that the label 'CS' designates a cold start, meaning that the test was conducted after the vehicle was allowed to soak without operation at the test temperature of 72° F for a minimum of 12 hours. Conversely, the label 'HS' designates a hot start test where the vehicle powertrain has already attained operating temperature before the test is started.

Table 3.3.1: Ford Fusion Drive Cycle Economy and Vehicle Efficiency

Test Description	Test #	Fuel Economy (mpg)	Vehicle Efficiency
UDDS CS	71210032	23.9	12.0%
UDDS HS	71210033	26.4	13.3%
UDDS #3	71210034	26.5	13.3%
HWFET	71210035	40.6	17.7%
US06 CS	71210048	23.6	18.7%
US06 CS City	71210048	14.2	16.6%
US06 CS Hwy	71210048	29.1	19.9%
US06 HS	71210038	26.1	20.8%
US06 HS City	71210038	16.9	19.9%
US06 HS Hwy	71210038	31.0	21.3%

Cycle fuel economy performance for the Fusion ranges from 14.2 mpg on the aggressive US06 city portion to 40.6 mpg on the more gentle HWFET cycle. The vehicle's economy on the UDDS cycle falls in between these two values. The order of these results is typical for the majority of vehicles due to the relative energy requirements of these three drive cycles.

It can be seen that the thermal state of the vehicle powertrain has a notable impact on the Fusion's fuel economy. The vehicle was able to achieve 26.4 mpg on the second UDDS cycle and 26.5 mpg over the third UDDS cycle. By the time the third UDDS is performed, the vehicle has reached a quasi-steady thermal state where the powertrain temperatures throughout the test are typical for repeated cycles. The warmer drivetrain lubricants and engine coolant reduce mechanical and thermal losses, providing ideal conditions for best economy. In contrast, the Fusion returned 23.9 mpg on the same cycle when performed with a cold engine and powertrain – a reduction in fuel economy of 9.8%.

It was noted that the thermal impact on fuel economy is even more pronounced when the vehicle is driven more aggressively. Fuel economy on the city portion of the

US06 cycle drops from 16.9 mpg under hot start conditions to 14.2 mpg for cold start conditions, yielding a reduction of 16.0%.

The Fusion's vehicle efficiency numbers also vary significantly across the test cycles. They range from 12.0% on the cold start UDDS to 21.3% on the hot start US06 highway portion. It is important to understand the apparent disconnect between vehicle efficiency and fuel economy. It can be seen that the Fusion achieves its best fuel economy on a cycle where the overall vehicle efficiency is significantly lower than for other cycles. Similarly, the best efficiency is achieved on a cycle that does not return the highest fuel economy. This is due to the fact that fuel economy depends both on vehicle efficiency and cycle energy requirements as discussed in section 2.1.5.

The Fusion's vehicle efficiency is greatest for the US06 cycle. The aggressive nature of this particular drive cycle translates to large throttle openings and medium engine speeds, facilitating operation in areas of greater engine efficiency. In contrast, efficiency is considerably lower on the UDDS cycle, where the engine is operated under comparatively light load where throttling losses are more significant.

One factor that helps to illustrate the relationship between the drive cycle and the vehicle's fuel economy performance is the percentage of fuel used during idle periods. This factor is illustrated for each drive cycle in Figure 3.3.1. It can be seen that the Fusion uses as much as 10.3% of the total drive cycle fuel energy while the vehicle is idling. This effect is especially pronounced on the UDDS cycle as it includes several stops where a conventional vehicle is forced to idle. The vehicle's thermal state has a clear impact here; we see a 4% increase in idle fuel use between the cold start and hot start versions of the US06 city portion. This is likely due to an aggressive catalyst warm up strategy that drastically increases the idle fuel flow rate when the vehicle is cold. Analysis of these cycles shows the idle fuel flow rate after the first US06 hill to be approximately 0.59 cc/s for the cold start test. This figure is reduced to 0.36 cc/s when run at operating temperature. It should also be noted that the HWFET cycle has extremely low idle fuel use as the vehicle has almost no idle opportunity during this test.

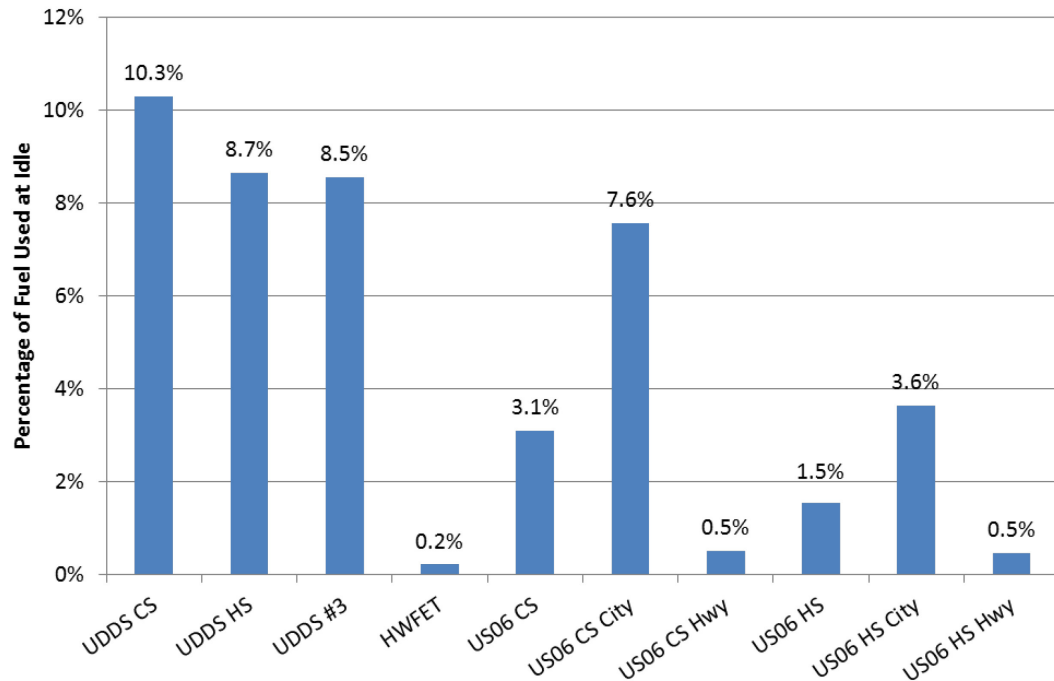


Figure 3.3.1: Ford Fusion Idle Fuel Use

Another contributing factor to fuel economy figures is the vehicle's behavior during deceleration fuel cutoff (DFCO). During braking periods, the work measured at the wheel does not move the vehicle down the road. Therefore it is considered to be negative and doesn't contribute to the cycle vehicle tractive work. Some fuel is consumed during this time to handle accessory loads, reduce engine braking during gentle decelerations where the brakes are not applied, and to provide proper drivability. This fuel use necessarily reduces both vehicle efficiency and fuel economy.

The amount of fuel supplied to the engine during deceleration can be shown to vary depending on the conditions under which the deceleration takes place. Figure 3.3.2 shows the end of the first 'hill' of the UDDS hot start cycle for the Fusion. Here it is shown that though the Fusion reduces fuel flow during deceleration, it continues to provide power to the engine while the driver is braking. This is a relatively small deceleration event, braking from approximately 32 mph to a stop over 11 seconds. Figure 3.3.3 shows the end of the first hill of the US06 hot start cycle. This is a larger

deceleration where the vehicle brakes from 70 mph to a stop over about 30 seconds. Though the average deceleration rates are comparable, the Fusion ceases fuel flow to the engine during the higher speed event. Once the vehicle speed drops below 20 mph, the engine resumes fueled operation.

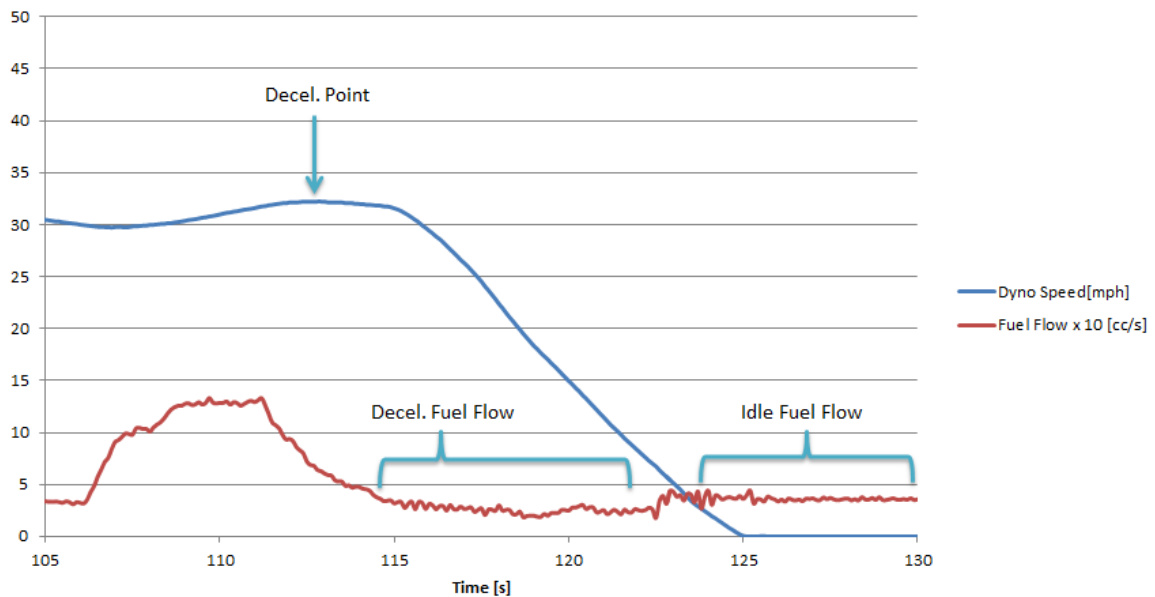


Figure 3.3.2: Ford Fusion Deceleration Fuel Cutoff (DFCO), UDSS HS

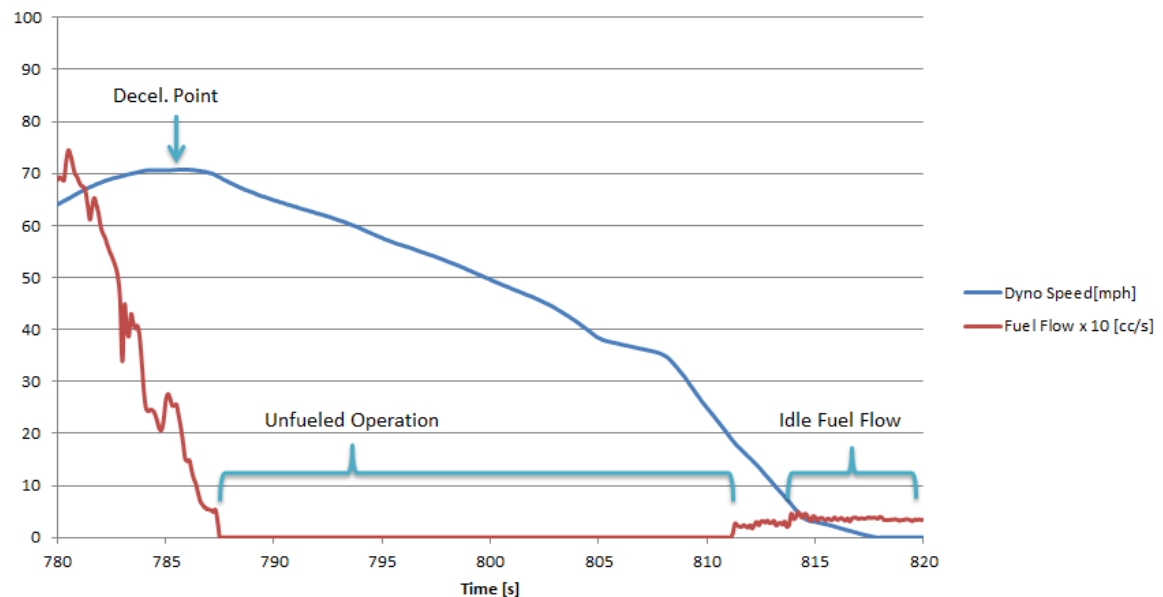


Figure 3.3.3: Ford Fusion Deceleration Fuel Cutoff (DFCO), US06 HS

The DFCO behavior of the Fusion can be better illustrated through the creation of a DFCO map for the vehicle. This is done by examining all of the transient acceleration and fueling data for the UDDS, HWFET, and US06 cycles and applying a filter to determine which points show a significant reduction in fuel as the vehicle decelerates. The criteria applied to create the DFCO map labels only points where the vehicle acceleration is negative and the fuel flow rate is less than 0.1 cc/s. The latter number was chosen because it allows for slight noise in the fuel scale while still being significantly less than the vehicle's idle fuel flow rate. Figure 3.3.4 shows the DFCO map for the Fusion.

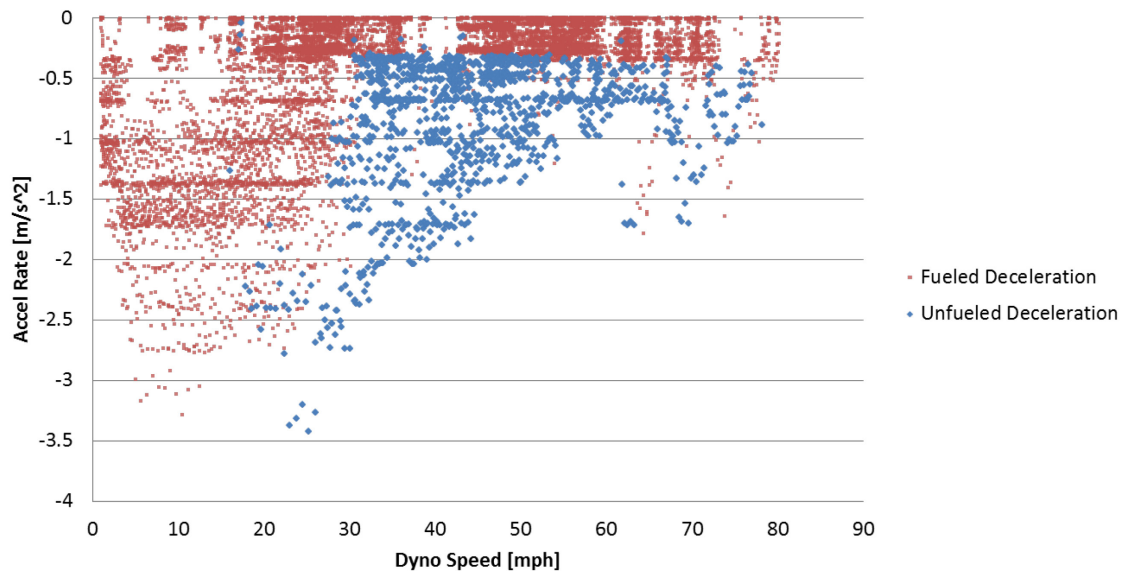


Figure 3.3.4: Ford Fusion Deceleration Fuel Cutoff (DFCO) Map

Examination of the DFCO map for the Fusion shows that the vehicle has a propensity to reduce fuel on deceleration at speeds above approximately 25 mph and decelerations greater than 0.4 m/s^2 . Decelerations at lower speeds are typically fueled regardless of magnitude, possibly due to vehicle transmission constraints or to achieve the drivability characteristics desired for this particular vehicle.

Table 3.3.2 catalogues the fuel energy, indicated work, and indicated engine efficiency for the Fusion over the drive cycles conducted. The indicated engine efficiency is calculated using Equation 2.5. This gives a measure of the amount of fuel energy that is converted to work on the engine's pistons. On a conventional vehicle, this typically relates directly to the overall vehicle efficiency because the internal combustion engine is the only source for motive power. Figure 3.3.5 shows the vehicle efficiency and indicated engine efficiency plotted for each of the test cycles. It can be seen that increased engine efficiency yields a corresponding increase in overall vehicle efficiency for each cycle. It should be noted that the variance in vehicle efficiency is greater than the variance in engine efficiency. This shows that the magnitude of the losses between the engine and drive wheels are dependent on additional factors such as the amount of power transmitted through the driveline and the thermal state of the components.

Table 3.3.2: Ford Fusion Cycle Indicated Engine Efficiency

Test Description	Test #	Fuel NRG In (kJ)	Indicated Engine Work (kJ)	Indicated Engine Efficiency
UDDS CS	71210032	37448	10679	28.5%
UDDS HS	71210033	33833	9681	28.6%
UDDS #3	71210034	33800	9682	28.6%
HWFET	71210035	30432	10169	33.4%
US06 CS	71210048	40743	13570	33.3%
US06 CS City	71210048	14966	4751	31.7%
US06 CS Hwy	71210048	25777	8819	34.2%
US06 HS	71210038	36851	12660	34.4%
US06 HS City	71210038	12623	4228	33.5%
US06 HS Hwy	71210038	24228	8431	34.8%

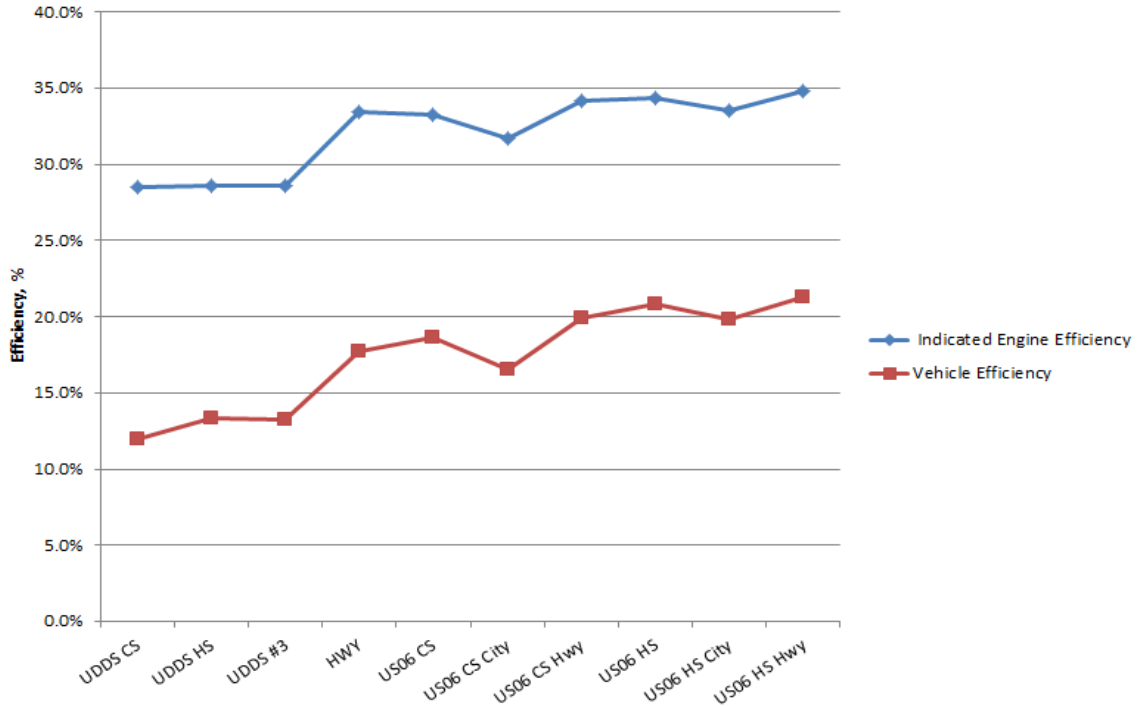


Figure 3.3.5: Ford Fusion Indicated Engine Efficiency and Vehicle Efficiency

The introduction of indicated engine efficiency allows for further illumination of the effect of the vehicle's thermal state on drive cycle vehicle efficiency. It can be seen in Table 3.3.2 that the indicated efficiency of the Fusion's engine suffered relatively little during the UDDS CS cycle. The change in efficiency between the cold and hot start UDDS cycles was a mere 0.1%. Put another way, it appears that the additional 3.6 MJ of fuel energy consumed during the UDDS CS was largely expended to overcome additional driveline losses and engine spin losses rather than to overcome any additional combustion chamber heat loss.

In the case of the more aggressive US06 cycle, the variance between the hot and cold start indicated engine efficiency was 1.1%. This effect can be further illustrated by focusing analysis on the first part of the US06 where the engine climbs to operating temperature in a cold start test; the difference when only considering the city portion of the US06 is 1.8%. In order to better understand the duration of the cold start effect, the Fusion's oil and coolant temperatures during the hot and cold start US06 are plotted in

Figure 3.3.6. It is shown that the engine coolant does not reach full operating temperature until the last third of the test, while the engine oil does not reach operating temperature for the duration of the cold start test.

While thermal effects have been shown to account for as much as a 1.8% difference in indicated engine efficiency, Table 3.3.2 shows that indicated efficiency varied from 28.5% to 34.8% across the drive cycles conducted. This makes it clear that factors besides the thermal state of the engine affect the indicated efficiency. It is commonly discussed in IC engine literature that several factors are at play in determining engine efficiency, and that efficiency generally varies with the engine speed and the load placed on the engine [4]. With this in mind, it is pertinent to study the speed and load utilization of the Fusion's engine over the drive cycles conducted for this thesis.

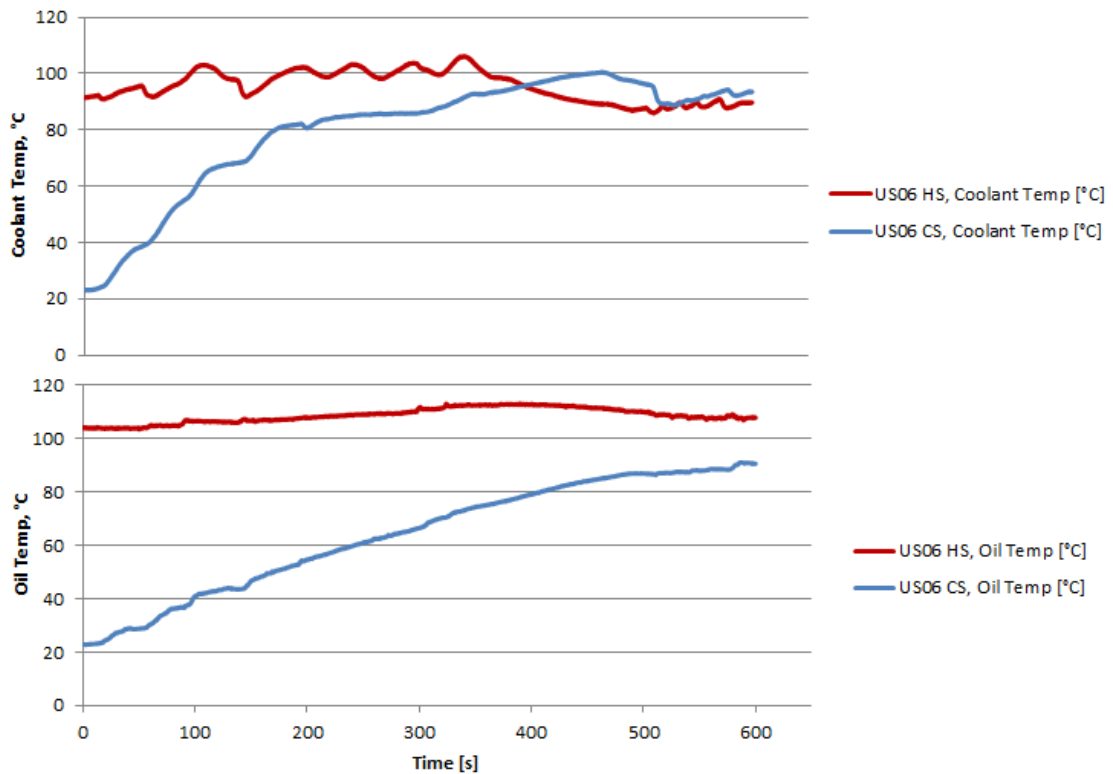


Figure 3.3.6: Ford Fusion Oil and Coolant Temperatures, US06 Cycles

Figures 3.3.7 through 3.3.9 show the Fusion's engine utilization on the hot start UDDS, HWFET, and US06 drive cycles. The amount of time spent at each speed and load is denoted by the color profile and is scaled as a percentage of total drive cycle time spent in a given speed and load bin. The bins used for these figures are sized in increments of 200 rpm and 0.5 bar IMEP.

The Fusion's engine utilization during the UDDS hot start cycle is shown in Figure 3.3.7. It can be seen that the engine spends the majority of its time at relatively low speed and load. A centroid can be seen at approximately 1700 rpm and 2.0 bar IMEP where the vehicle tends to operate most often during this cycle. Because the power demand is relatively low for the UDDS, the transmission attempts to keep the engine speed as low as possible in order to maximize load for best efficiency. There is also a significant amount of time spent at 1.8 bar IMEP and 700 rpm, which is the vehicle's idle point. In general, operation during the UDDS cycle occupies a relatively narrow speed and load range. Some DFCO operation can be seen between 900 and 1500 rpm with IMEP values less than 0.5 bar, as well as the transition from DFCO to the idle state.

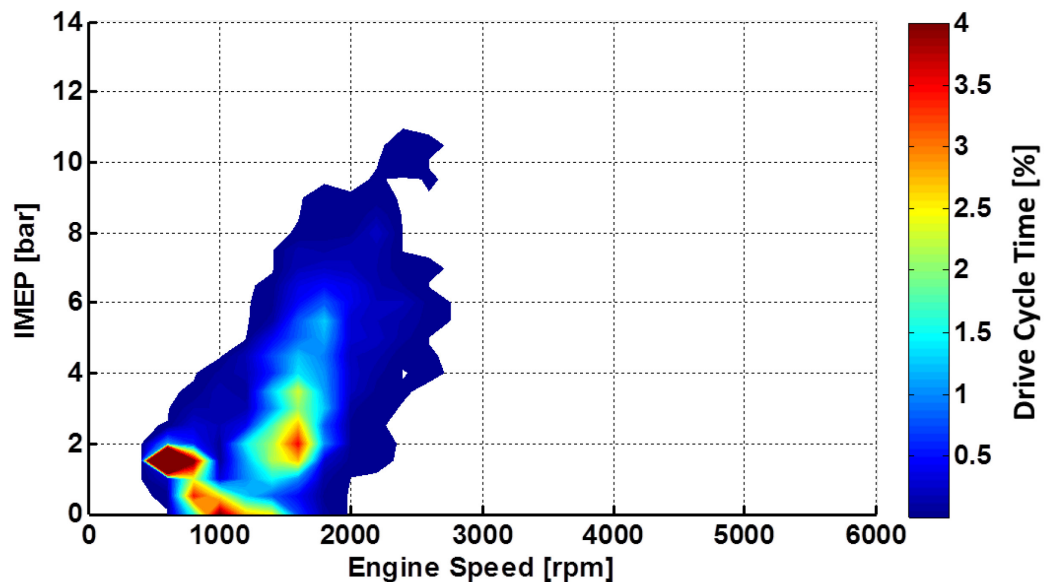


Figure 3.3.7: Ford Fusion Engine Utilization, UDDS HS Cycle

Figure 3.3.8 showcases the Fusion's engine utilization during the US06 hot start cycle. As previously discussed, the US06 is an aggressive cycle with periods of relatively high power demand. This is immediately obvious in the wide spread of speeds and loads shown in the utilization map. During this cycle the engine is operated between 700 and 5,500 rpm at loads as high as 12 bar IMEP. A teal colored band can be seen centering around 2000 rpm between 1.8 and 8.5 bar where the engine is operated most commonly under power. This largely represents the cruising portions of the US06 where the Fusion elects to remain in a high gear and increase engine load to meet the power demands. In contrast, the area above 2300 RPM largely represents more transient operation where the vehicle is accelerating through the powerband. As in the UDDS cycle, we can again see the Fusion's propensity to keep the engine operating at low speed as often as possible. It can further be seen that the engine spends a significant amount of time operating at idle, though less than that seen on the UDDS cycle. Finally, a band is visible at near zero IMEP between 1200 and 2200 RPM. This represents the vehicle's DFCO behavior for which the US06 provides significant opportunity.

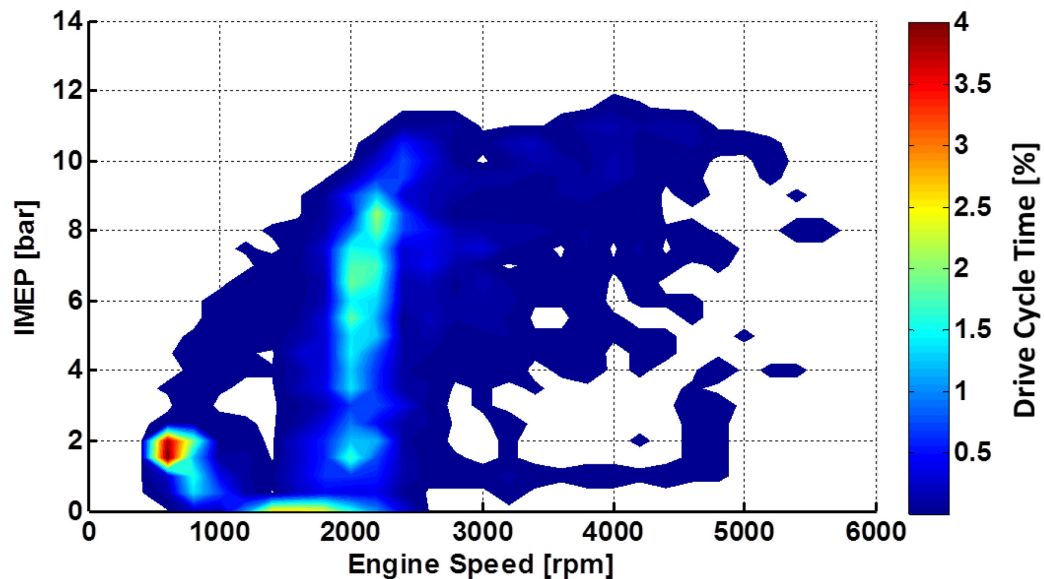


Figure 3.3.8: Ford Fusion Engine Utilization, US06 HS Cycle

The Fusion's engine utilization on the HWFET cycle can be seen in Figure 3.3.9. This test cycle contains mostly gentler accelerations and entails a great deal of time cruising without large changes in throttle position. The figure shows that the majority of engine operation on this cycle takes place centering around 4 bar IMEP and 1750 RPM. Engine load for the cycle is higher than the UDDS, peaking at 10.5 bar during the most aggressive acceleration event. The speed range is relatively narrow, never exceeding 2800 RPM. A small DFCO band can also be seen, though this is not as significant as that found in the US06 cycle. Finally, it is important to note that there is almost no opportunity for idle operation during this test.

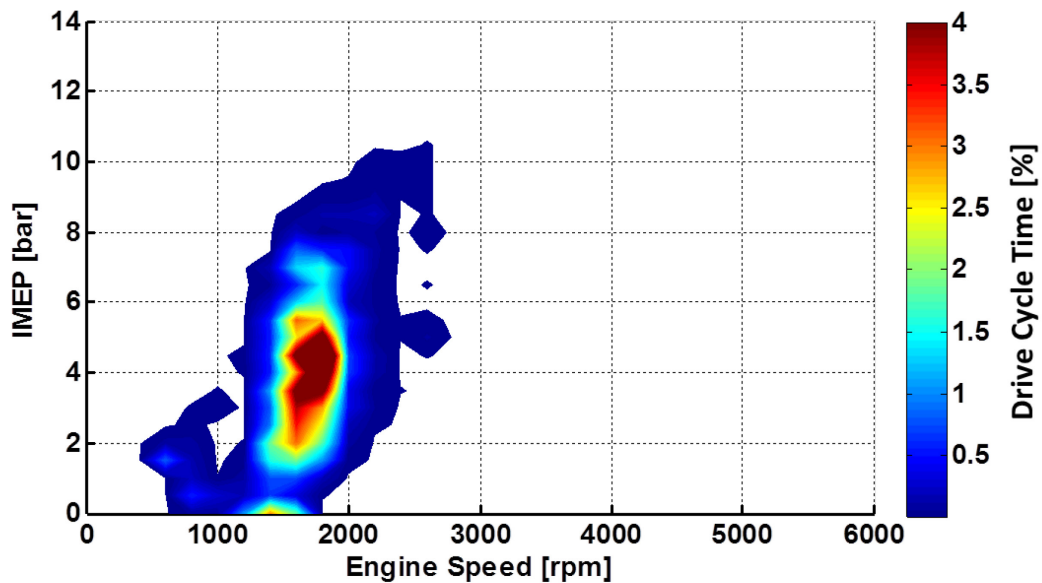


Figure 3.3.9: Ford Fusion Engine Utilization, HWFET HS Cycle

The Fusion's performance on the different drive cycles can be further understood by examining the steady state behavior of the vehicle at a range of speeds. In order to facilitate this, the vehicle was subjected to a steady state speed test as defined in section 2.1.1. The average fuel economy and vehicle efficiency were determined for each speed, and plotted along with the selected transmission gear and wheel power in Figure 3.3.10.

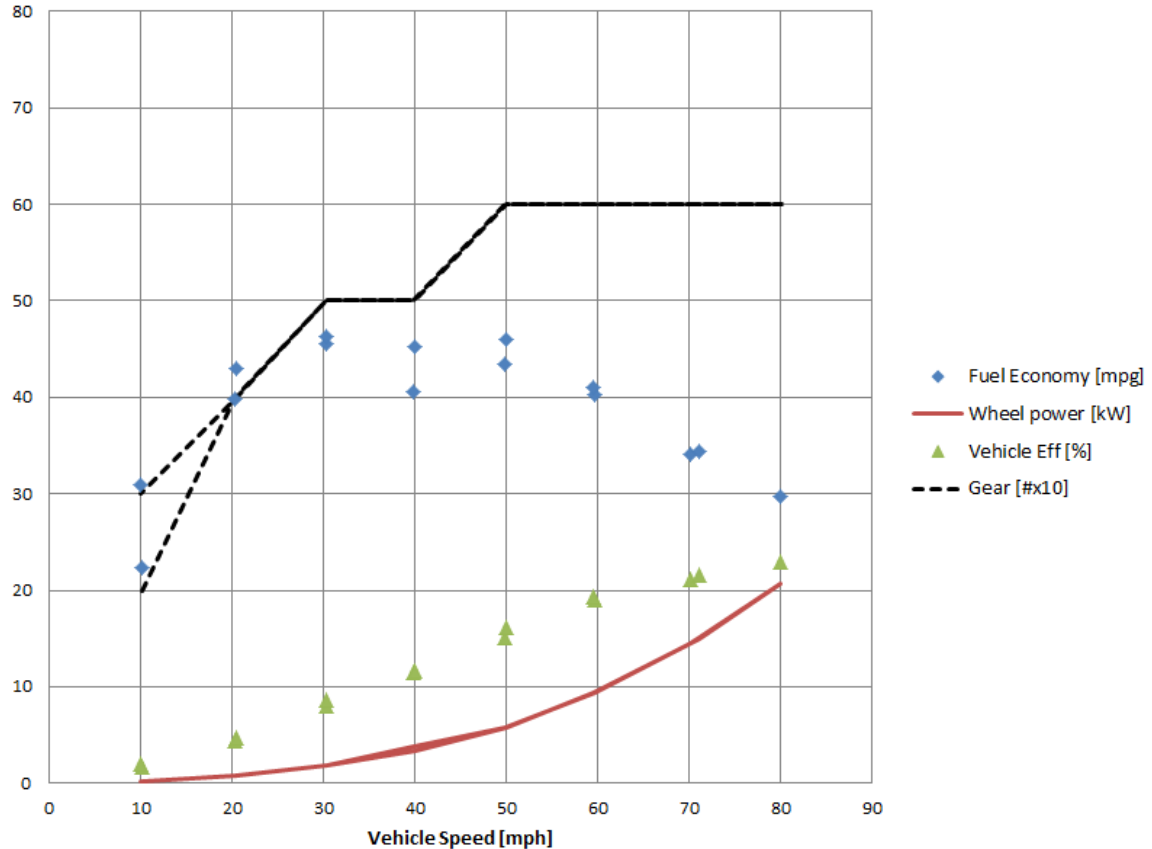


Figure 3.3.10: Ford Fusion Steady State Performance

Examining Figure 3.3.10, we see that the Fusion's fuel economy appears to have two maxima: the first peak of 46.3 mpg at 30 mph and the second peak of 46.0 mpg at 50 mph after the transmission upshifts to its final gear. As the required road load increases with speed, so does the measured power at the vehicle's wheel. Vehicle efficiency rises also as the engine load increases to supply the required road load. The transmission exhibits hysteresis at the 10 mph speed; during the first hold the transmission is in second gear, while third gear is selected during the latter hold. This figure also illustrates the fact that higher vehicle efficiency does not necessarily translate to better fuel economy; though the Fusion's economy falls after 50 mph with rising road load, vehicle efficiency continues to increase.

For the most part, the differences in fuel economy between the two instances of each speed are within reason at less than 10% with the exception of the 10 mph mark where the vehicle performed the holds in two different gears. Differences are typically attributable to some difficulty in holding the vehicle perfectly steady at speed, especially at the lower speeds.

3.4 Cycle-Based Heat Loss Proportions

As seen in section 3.3, between 12% and 21.3% of the fuel energy supplied to the Fusion is measured as positive work output at the vehicle's wheels over the drive cycles considered. In order to better understand where the remainder of the energy is lost, thermocouples and flow sensors were placed in the Fusion's cooling system in order to capture the coolant flow rates and temperature differentials across the vehicle radiator and cabin heater core. Additionally, exhaust gas temperatures were measured continuously. Using the equations defined in Section 2.1.5, these values were used to determine the energy lost by the vehicle to the surroundings.

The nature of the vehicle cooling system presents problems for instantaneous analysis of energy loss. The vehicle operates with a given volume of engine coolant which must be brought to operating temperature before the thermostat opens and energy can be shed through the radiator. Even when the engine and fluids have reached operating temperature, it is difficult or impossible to directly measure the complete temperature profile throughout the cooling system. Energy absorbed into the water jacket from the engine cylinders must be transported through the cooling system until it can reach the radiator to be effectively shed. In order to combat the issues of engine thermal inertia and transport delay, the analysis of heat loss is first restricted to warm start cycles, and then is only considered in terms of total losses for a given drive cycle. Measurement and analysis of instantaneous heat loss proportions is left to other studies.

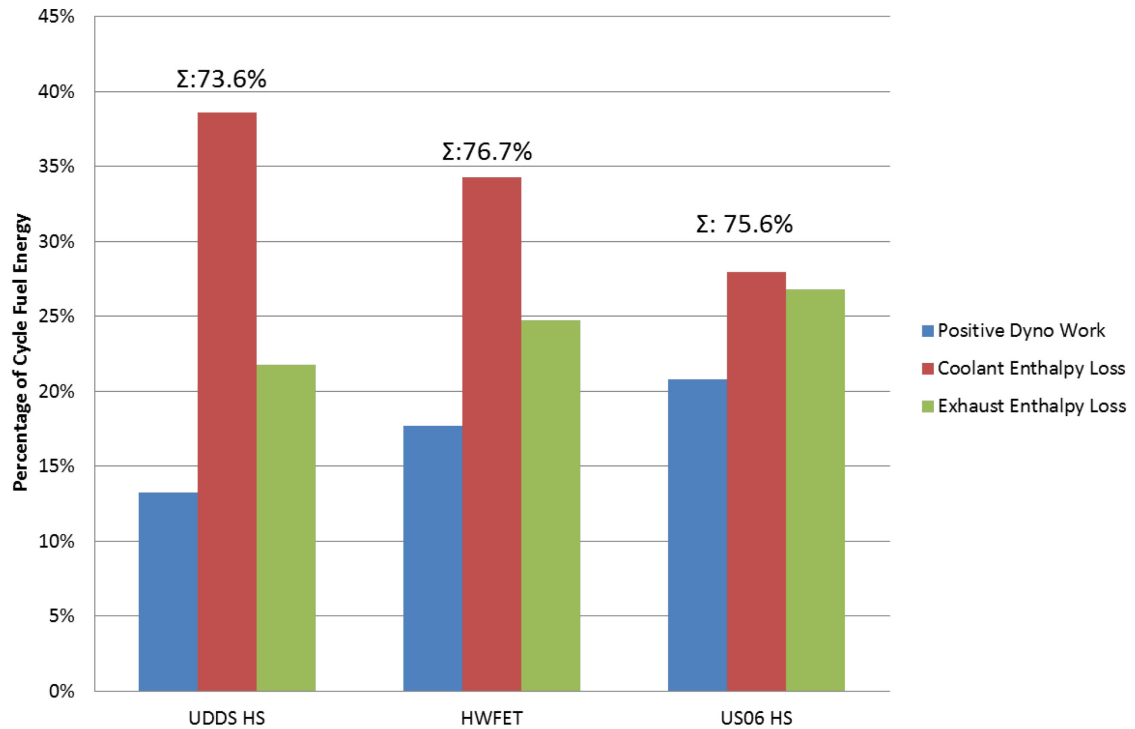


Figure 3.4.1: Ford Fusion Cycle-Based Fuel Energy Usage

Figure 3.4.1 catalogues the measured vehicle energy output for the UDDS, HWFET and US06 cycles. In all cases, the total measured proportion of fuel energy consumed is near 75%. The remaining 25% of fuel energy unaccounted for is likely the result of several factors, such as radiated heat loss from the engine surfaces, engine and drivetrain mechanical losses, incomplete combustion and any coolant losses facilitated by extraneous plumbing apart from the radiator and heater core.

In all three of the cycles shown, the greatest proportion of the measured fuel energy is lost to the engine coolant. This is especially true for the UDDS cycle where the engine is run at relatively low speed and load. It is typically accepted that as a vehicle's engine is operated more aggressively and at higher speeds, exhaust temperatures rise and combustion efficiency dips, increasing exhaust enthalpy [4]. At the same time, the amount of time available for each cylinder charge to lose heat to the cylinder wall is diminished. The engine efficiency also increases to a point, improving the total positive

dyno work fraction. The Fusion's performance on the HWFET and US06 cycles reflects this, with the positive dyno work fraction and exhaust enthalpy increasing as the cycle becomes more aggressive. The coolant proportion diminishes accordingly.

Figure 3.4.2 shows the enthalpy losses of the Fusion's radiator and heater core for the UDDS hot start, HWFET, and US06 hot start cycles. The enthalpy change across the heater core is almost negligible in comparison to the radiator, especially in the case of the HWFET and US06 cycles. As the vehicle's HVAC fan was switched off during all tests, the temperature change across the heater core was minimal. In the case of the US06 hot start test, the enthalpy change across the heater core is actually negative, indicating that the coolant passing through the core increased in temperature. This effect is likely due to the location of the Fusion's heater core return hose, which is near the exhaust manifold.

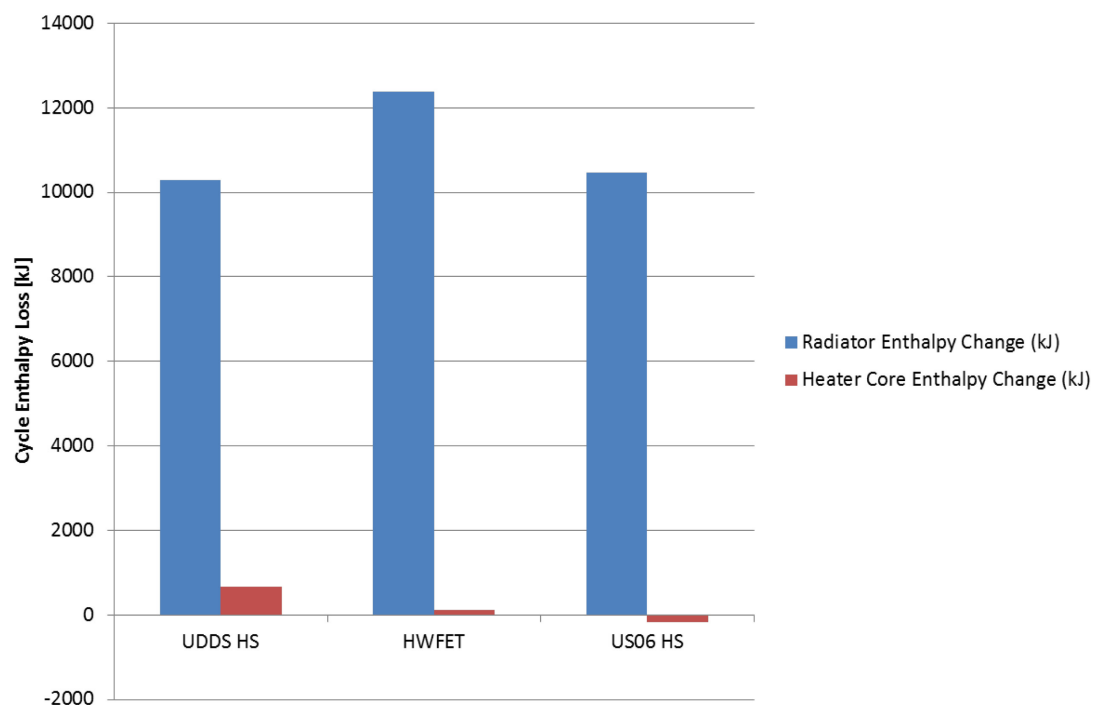


Figure 3.4.2: Ford Fusion Coolant Enthalpy Change by Source

3.5 Cycle-Based Emissions Measurements

Though vehicle emissions are not intended to be a significant focus of this thesis work, the Fusion's emissions behavior is catalogued here. The tailpipe emissions measured in this study include CO, THC, and NOx. Table 3.5.1 catalogues the total tailpipe emissions for several drive cycles.

Table 1.5.1: Ford Fusion Total Emissions by Cycle

Test Description	NOx [mg]	THC [mg]	CO [mg]
UDDS CS	135.3	294.8	4175.2
UDDS #3	8.9	69.2	3275.7
HWY	26.4	18.0	1407.2
US06 CS	260.2	493.5	9199.8
US06 HS	120.4	59.1	3953.5

Two conclusions can be drawn directly from the table. It can be seen that in general, emissions are significantly higher for the more aggressive US06 cycle. This is generally unsurprising, as more fuel is burned during the course of this cycle. We can also see that emissions are much higher for cold start tests than for hot start tests. This is primarily due to the fact that the exhaust system catalysts responsible for scrubbing tailpipe emissions are ineffective below a given operating temperature. To better illustrate this fact, Figures 3.5.1 and 3.5.2 show the integrated emissions for the US06 cold and hot start tests respectively.

The hot start emissions shown in Figure 3.5.2 climb gradually throughout the drive cycle. Quick increases in the emissions level correspond with hard accelerations during which additional fuel is added. Combustion efficiency typically drops slightly during throttle transients, resulting in more cylinder-out emissions [4]. Emissions increase rapidly when a hard acceleration is performed after a long deceleration event. This is likely due to a decrease in catalyst efficiency caused by the cooling of the substrate.

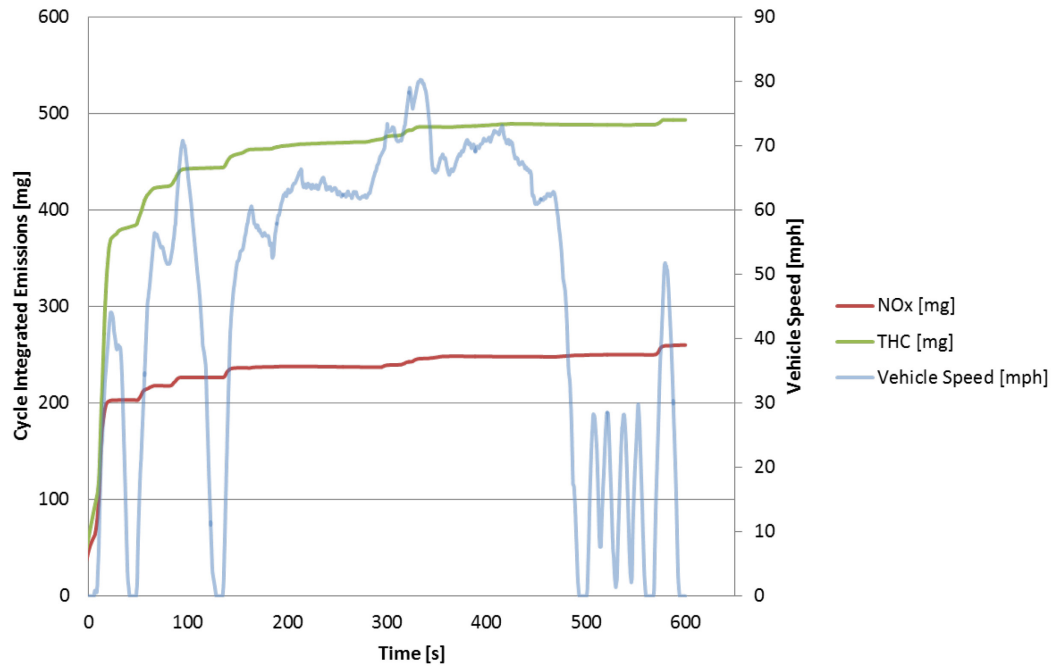


Figure 3.5.1: Ford Fusion US06 Cold Start Integrated NOx and THC

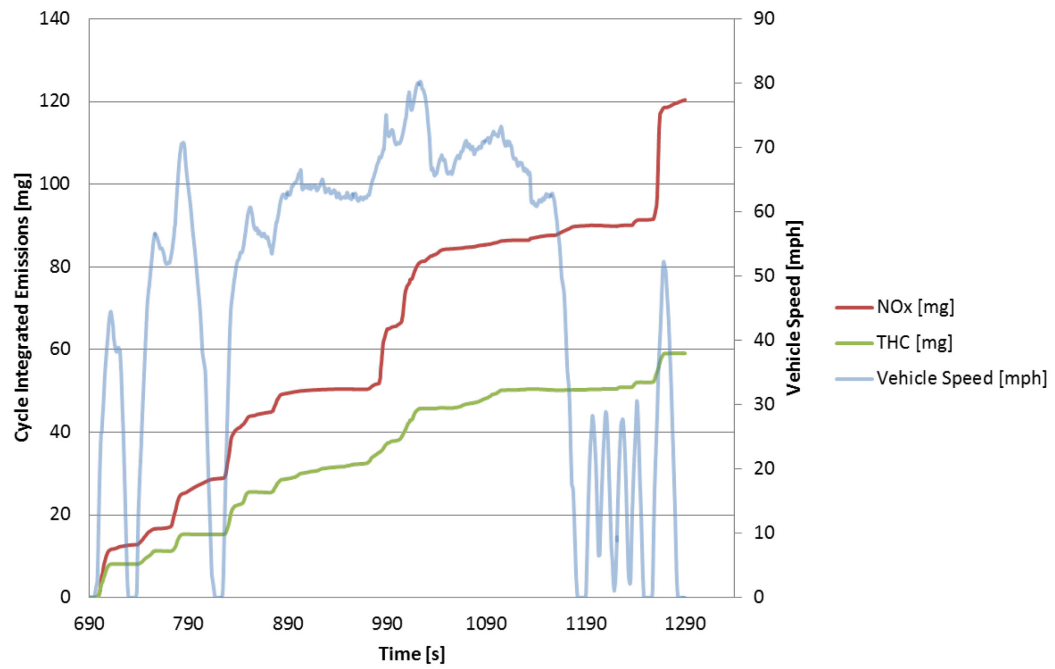


Figure 3.5.2: Ford Fusion US06 Hot Start Integrated NOx and THC

In general, emissions for the cold start US06 cycle show similar behavior with marked rises in the total emissions levels corresponding most often to hard acceleration events. It should be noted that the majority of the increased emissions over the hot start test come during the first 20 seconds of the test in the period directly following the cold engine start. During cranking extra fuel is placed in the cylinder for fast starting, and timing is often significantly retarded to help the exhaust catalysts reach operating temperature as quickly as possible to minimize further tailpipe emissions. Additionally, the supplied fuel does not always vaporize or combust completely due to low cylinder temperatures resulting in additional cylinder-out THC and CO [5]. After this initial “light-off” period, emissions behavior is similar to that of the hot start test. This is best illustrated in Figure 3.5.3.

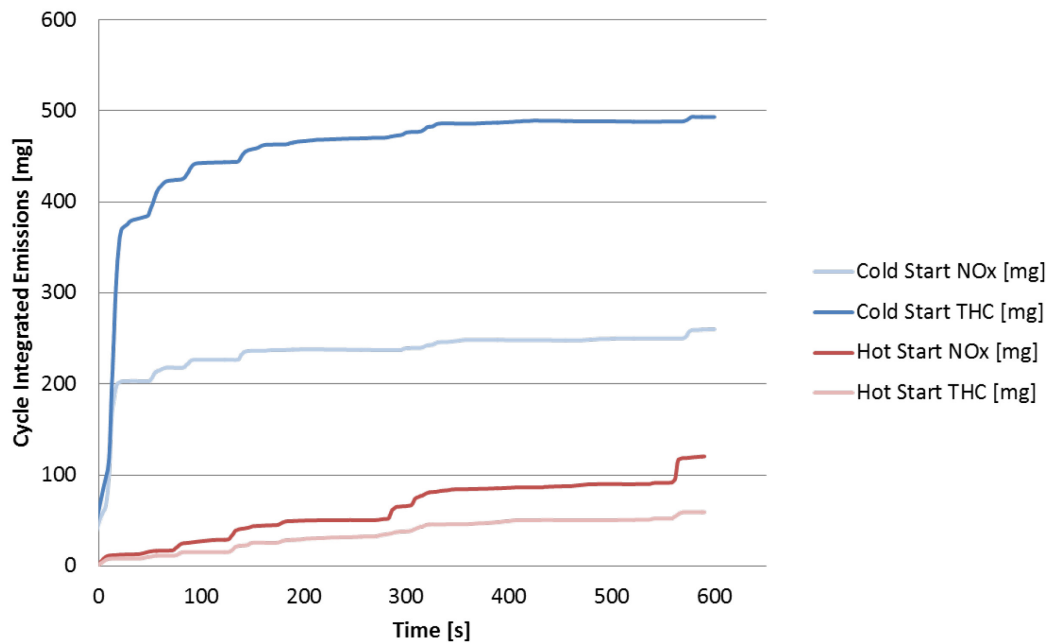


Figure 3.5.3: Ford Fusion US06 Hot and Cold Start Emissions

3.6 Engine Indicating System Measurements

During the course of testing, the IndiModul and IndiCom system were used to calculate and export engine IMEP in real-time, facilitating the indicated efficiency calculations discussed in Section 3.3. The system was also used to record crankshaft-angle-based pressure data. Data of this nature can be used to accomplish a number of tasks related to combustion analysis in engine-centric research. In this study this data was used in order to qualitatively examine engine design and operating characteristics.

Three engine operating points are chosen for examination. The first point is at engine idle with the vehicle in neutral gear and at operating temperature. The second point is at moderate speed and load as the vehicle is under power. The last point is at high speed and load near the engine's peak power point. Table 3.6.1 catalogues several parameters describing these points. Figures 3.6.1 through 3.6.3 display the pressure-volume (P-V) diagrams on a log-log scale. The engine strokes are labeled in Figure 3.6.1 for convenience. It should be noted that the operating points discussed here were chosen from single engine cycles. Due to the transient nature of drive cycle testing, it is difficult to choose a sufficient number of consecutive cycles at a single operating condition for averaging. Instead, the cycles shown here are used mainly to illuminate general P-V behavior as it is effected by engine architecture.

Table 3.6.1: Ford Fusion Engine Operating Points

		Point 1	Point 2	Point 3
Engine Speed	[rpm]	660	3354	4827
IMEP	[bar]	1.7	5.1	11.7
Peak Pressure	[bar]	6.8	26.7	58.6
Burn Duration	[ms]	5.9	2.2	1.5
Angle, 50% MFB	[CAD]	32 ATDC	7.2 ATDC	10.2 ATDC
Angle, PMAX	[CAD]	40 ATDC	13 ATDC	16 ATDC

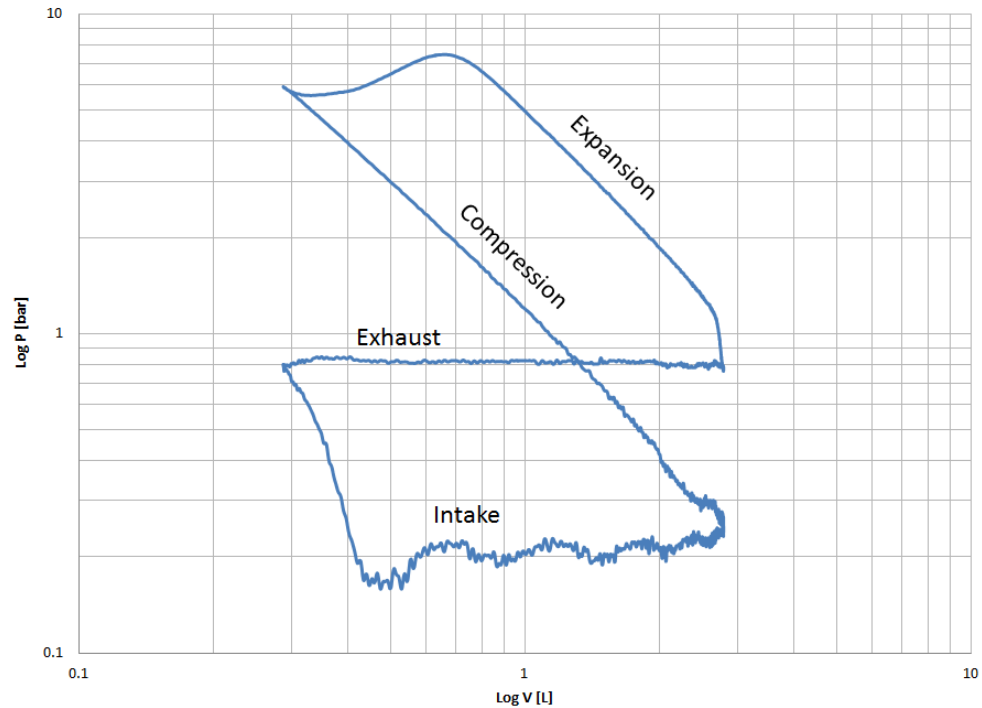


Figure 3.6.1: Ford Fusion P-V Diagram, Point 1

During the idle conditions shown in Point 1, all of the power generated by the engine is used to overcome heat, friction, and vacuum losses in order to allow the engine to continue to idle. The relatively large pumping loop shows that the engine is aggressively throttled and that vacuum losses are significant. Also notable is the retarded combustion timing. Measurements show that the point at which 50% of the combustion charge heat release (50% mass fraction burned, or 50% MFB) occurs at a relatively late 32 degrees after TDC. This can also be observed in the shape of the positive work loop; we see that the beginning of the expansion stroke occurs at pressures similar to those seen during the end of the compression stroke, indicating that combustion has yet to take place. As the piston returns we see a second pressure rise as the cylinder charge is ignited.

The reason for this late timing may be twofold; first, it helps to keep exhaust gas temperatures higher during idle periods in order to keep the exhaust catalysts in the proper operating range. Secondly, it provides a means to sharpen the throttle response at

initial tip-in. Because the engine is idled slightly less efficiently, more power is already available at the present fuel flow rate and can be accessed quickly by advancing the engine timing. The timing change can happen almost instantaneously as opposed to AFR adjustment, which is subject to air and fuel flow dynamics. The initial timing advancement helps to reduce the delay while fuel flow is increased to produce additional power.

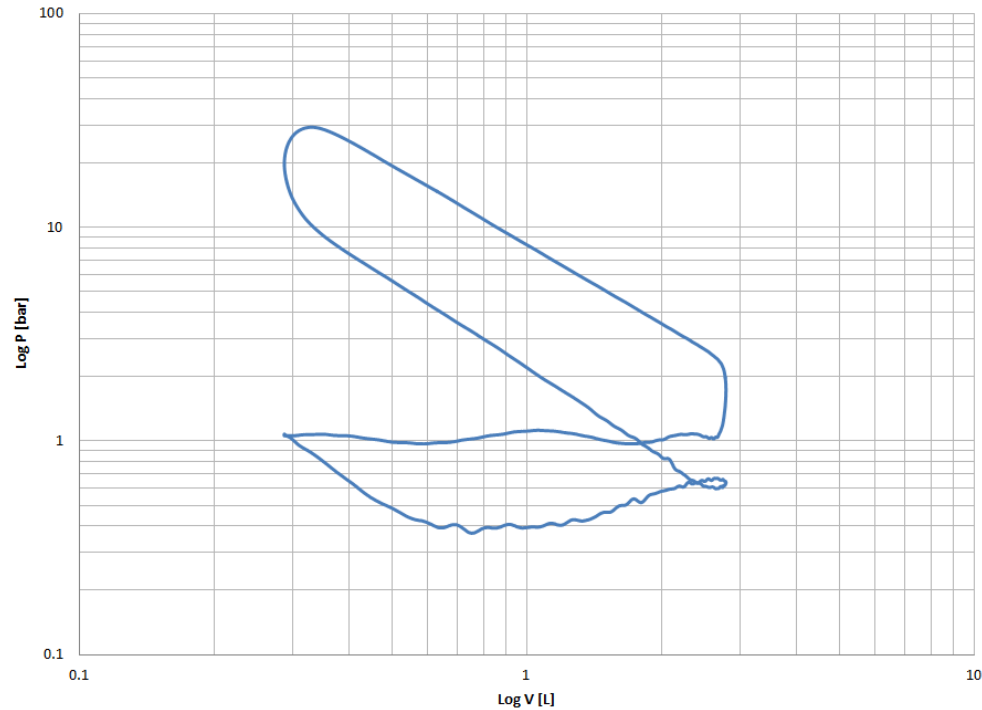


Figure 3.6.2: Ford Fusion P-V Diagram, Point 2

The second operating state, labeled Point 2, was taken during a steady-state cruise at 80 mph. The engine is operating at 3354 RPM with indicated mean effective pressure of 5.1 bar. This type of moderate loading is common for the vehicle, especially during the HWFET cycle and the higher speed portion of the US06. It should be noted that the retarded ignition timing exhibited at Point 1 is no longer present. Instead, the entirety of the expansion stroke takes place at significantly higher cylinder pressure than the compression stroke in order to maximize the engine's work output. The pumping loop is significantly smaller in size than that seen in Point 1, indicating that the engine is not so

aggressively throttled. The exhaust stroke also takes place at slightly higher pressure, indicating greater exhaust backpressure at the higher engine speed.

It is generally accepted that for best efficiency and torque output, the greatest amount of heat release should take place around 5 to 10 degrees ATDC [4]. Engine timing at Point 2 is such that the peak cylinder pressure occurs at 13 degrees after top dead center, which is consistent with the literature. The burn duration is significantly shorter than at idle speed, indicating that the combustion speed is greater due to the denser cylinder charge.

Also of note is the transition area between the exhaust and intake strokes. According to the measurements, the cylinder pressure at the end of the intake stroke is greater than that at the beginning of the compression stroke. This is most likely due to the intake runner gas dynamics combined with the valve timing strategy. It appears as though gas velocities are being maximized for optimal cylinder-filling, resulting in an inertial effect raising the pressure near the transducer at the end of the intake stroke.

The third point considered was taken at 4827 RPM and 11.3 bar IMEP. This represents the upper segment of the Fusion's speed and load capability, with the throttle nearly completely open. It can be seen that the pumping loop is smaller than in both Points 1 and 2 as a result. Pressure during the exhaust stroke is the highest of the three points chosen. This is likely due to increased exhaust backpressure as the exhaust gas velocities increase with engine speed.

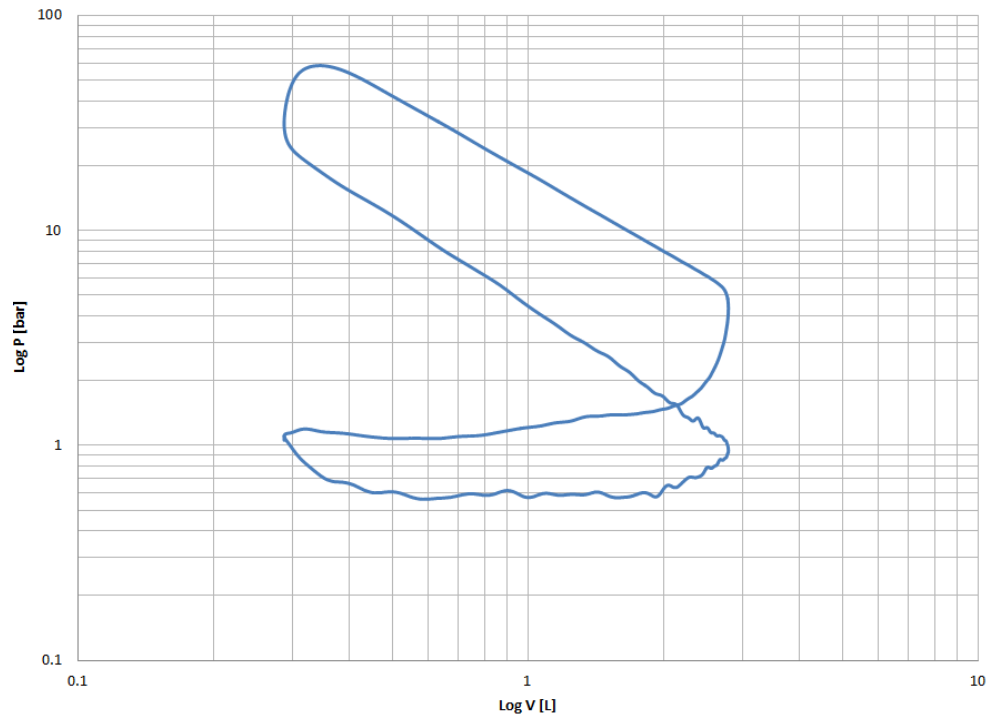


Figure 3.6.3: Ford Fusion P-V Diagram, Point 3

The peak cylinder pressure was measured at 58.6 bar and took place at 16 degrees ATDC, showing slightly later timing than Point 2. This later timing is likely due to the need for knock prevention at high loads with lower octane fuel. Again, the combustion duration decreased with increasing load, suggesting that flame speed is increasing. This increase is most likely due to the greater cylinder charge density along an additional gas turbulence affect; the faster mean piston speed helps to promote better mixing of the fuel and air constituents for faster combustion. Finally, we note that the pressure increase at the end of the intake stroke as seen at Point 2 has disappeared, likely a result of changing gas dynamics with engine speed.

Chapter 4 MY2009 Volkswagen Jetta TDI 2.0

4.1 Relevant Vehicle Features

A MY2009 Volkswagen Jetta TDI was included in this study in order to represent the modern turbodiesel vehicle architecture. The TDI is of FF configuration, with the front wheels powered by a four-cylinder turbocharged diesel engine that displaces 2.0 liters. This engine, designated CBEA, produces 140 brake horsepower at 4,000 rpm and has a broad and robust torque curve, producing 236 lb-ft. of torque between 1,750 and 2,500 rpm.

Architecturally speaking, the CBEA engine sports dual overhead camshafts and has four valves per cylinder. It is fitted with a high-pressure common-rail fuel injection system with injectors controlled by piezoelectric actuators capable of multiple injection events per combustion cycle. Fuel injection pressure capability is as high as 1800 bar. The engine is fitted with a variable-geometry turbocharger that is used to adjust engine airflow across the operating range for optimal combustion with quick transient response.

In order to meet diesel engine emissions regulations, the TDI is fitted with a complex emissions system including an oxidation catalyst, diesel particulate filter, NO_x catalyst, and hydrogen sulfide catalyst as well as high and low-pressure exhaust gas recirculation systems. Unlike the three-way catalysts used to reduce emissions of gasoline engines, the TDI's aftertreatment system requires a regeneration process wherein combustion timing and injection quantity are adjusted to raise the temperature of the components to 650-750 °C to burn away accumulated emissions. The frequency of these regeneration events depends on the manner in which the vehicle is operated. For the purposes of this study, only drive cycles in which the vehicle was not exhibiting regeneration behavior were used and regeneration behavior is not studied in detail. For reference, the emissions system layout is depicted in Figure 4.1.1.

The TDI's engine is mated to an advanced dual clutch automated transmission with six forward ratios. These gears are housed on two shafts, with two final drive ratios

available. Advantages of this transmission architecture typically include fast gear changes and a high degree of mechanical efficiency.

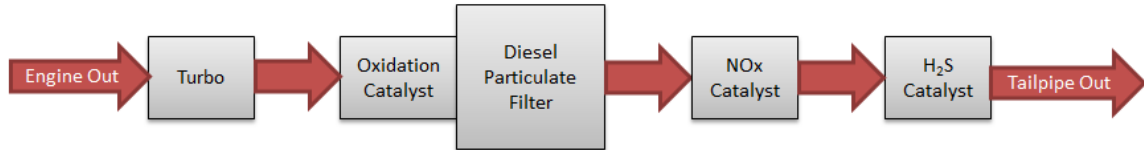


Figure 4.1.1: Volkswagen Jetta TDI Exhaust Aftertreatment System Schematic

The Volkswagen Jetta TDI is classified as a compact sedan. Its test weight class is 3,625 lbs. The test vehicle is pictured in Figure 4.1.2. Relevant vehicle features are catalogued in Table 4.1.1, while fuel properties are found in Table 4.1.2.



Figure 4.1.2. 2009 Volkswagen Jetta TDI

Table 4.1.1: Volkswagen Jetta TDI Vehicle Metrics

Year/Make/Model		2009 Volkswagen Jetta TDI
Body Type		4 dr Sedan
Engine		2.0 L 16V VVT I4 Turbodiesel
Compression Ratio		18.0:1
Rated Power		104 kW (140 hp) @ 4,000 rpm
Rated Torque		320 N-m (236 lb.-ft.) @ 1,750 - 2,500 rpm
Transmission		6 Spd Dual Clutch Transmission (VW DSG)
Gear Ratio	1st	3.46:1
	2nd	2.05:1
	3rd	1.30:1
	4th	0.90:1
	5th	0.91:1
	6th	0.76:1
	7th	-
	Final Drive	Gears 1-4: 4.12:1, Gears 5-6: 3.04:1
EPA Fuel Economy	Urban	29
	Highway	40
	Combined	33
Road Load Coefficients	Test weight	3625
	Cd	0.31
	a	35
	b	0.18
	c	0.0193
Vehicle Performance		
WOT Acceleration	0-60	10.6s (ANL)
	30-50	3.6s (ANL)
	50-70	5.7s (ANL)

Table 4.1.2: Volkswagen Jetta TDI Fuel Specifications

Fuel Name:	2007 Cert. Diesel	Density:	0.85	[g/ml]
Carbon Weight Fraction:	0.8686	Net HV:	18355	[BTU/lbm]

4.2 Instrumentation Specifics

A number of instruments were installed on the TDI in order to monitor the performance and operating characteristics of the vehicle during testing. The nature of this vehicle presented several measurement challenges. These are discussed in this section.

Modern diesel engines with high pressure common-rail injection systems have a fuel supply strategy wherein the bulk of the fuel supplied to the injectors is returned to the fuel tank in a continuous supply loop. This provides for significant fuel flow to the injectors which helps to keep the sensitive electronics at stable and reasonable temperatures. Unfortunately, the result is a large bulk fuel mass flow rate wherein the quantity of fuel consumed must be measured as a differential of the supply and return line mass flow rates. The fuel consumption rate is often so small in relation to the bulk flow rate that it makes this strategy difficult or impossible to implement with acceptable accuracy.

In order to determine the relation between bulk fuel flow rate and fuel consumption rate for the TDI, the fuel supply pump was run for a period of 30 seconds with the output redirected into a graduated cylinder. From this simple test the bulk fuel flow rate was found to be 3,650 ml/min. Previous testing of the vehicle with fuel flow rates calculated from emissions bench measurements showed the idle fuel rate to be around 13.5 ml/min at operating temperature. It was concluded that the measurement turn-down ratio and the resulting measurement sensitivity required was so great as to make physical measurement with traditional flow sensors impractical.

It should be noted that alternative physical solutions for diesel fuel flow measurement are available. The accepted method used in engine test stand applications is to implement a fuel measurement system that eliminates the stock fuel return system. The bulk fuel flow requirements are maintained by the measurement system in a fuel flow loop whose pressure is carefully monitored. As fuel is consumed by the engine, a corresponding quantity of makeup fuel is added to the loop to maintain the bulk quantity.

This quantity can be directly measured by a smaller, more sensitive meter that does not need to accommodate large bulk flow rates. These systems are expensive and require extensive engine modifications, and as such were considered impractical for this work.

In order to measure the fuel flow for the TDI, vehicle CAN bus decoding was utilized to identify and record a signal corresponding to the amount of fuel injected for each combustion event. This signal was then used in conjunction with engine speed to determine the mass flow rate of fuel. To ensure that the decoded signal provided accurate measurements, fuel mileage figures for the UDDS, HWFET and US06 cycles were calculated. The figures were then compared to those determined from exhaust carbon balancing during legacy tests with a Horiba emissions bench. The fuel economy provided by the CAN signal was found to be within 4.5% of that calculated by the emissions bench. Based on this result the CAN-based fuel flow measurement was determined to be suitable for this study.

The TDI's radiator and heater core coolant loops were instrumented with Omega FTB 1306 and FTB 1304 flow sensors in order to measure the coolant mass flow. Thermocouples were also installed at the heat exchanger inlets and outlets. These measurements were used in conjunction with the mass flow rate to determine the coolant enthalpy loss across the heat exchangers. Additional thermocouples were placed in the exhaust to measure exhaust gas temperatures.

In addition to the fuel injection quantity, several other parameters were read from the vehicle's CAN bus including the selected transmission gear and mass air flow rate for exhaust lambda calculations. Additional signals included engine speed and intake manifold pressure.

Considerable effort was expended to instrument the TDI engine with an indicating transducer for in-cylinder pressure measurement. A custom adapter was purchased from AVL in order to provide a means of mounting a GH13P transducer in the engine's glow plug bore. A further adapter was machined in-house in order to facilitate the use of an

AVL 428 TDC alignment probe in the combustion chamber in place of a fuel injector to determine the cylinder 1 TDC location. The adapter and the alignment in process are depicted in Figures 4.2.1 and 4.2.2.

After TDC determination, the engine was reassembled and the vehicle was operated with the indicating transducer in place. It was found during testing that the vehicle exhibited extremely high exhaust gas temperatures and returned significantly worse fuel economy than was observed in previous tests with the vehicle. After some investigation, it was determined that the transducer should be removed and replaced with the stock glow plug. After this change the vehicle's operation returned to normal. It was determined that the only acceptable approach to instrument the engine with an indicating transducer would involve the removal and machining of the cylinder head to accommodate a sensor mounted directly in the combustion chamber. This approach is typically expensive and time consuming. As such, the drive cycles considered in this thesis were performed without the benefit of the cylinder pressure indicating system installed on the vehicle. This situation is discussed in more detail in section 4.5.

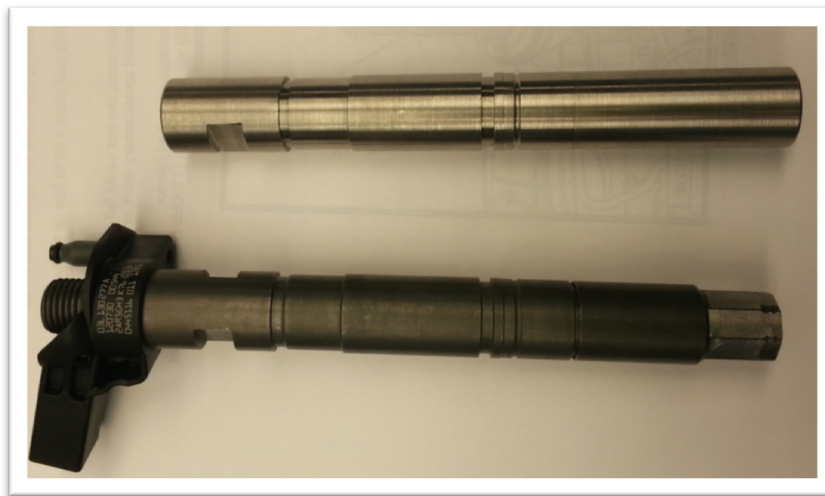


Figure 4.2.1: Volkswagen Jetta TDI TDC Adapter & Fuel Injector

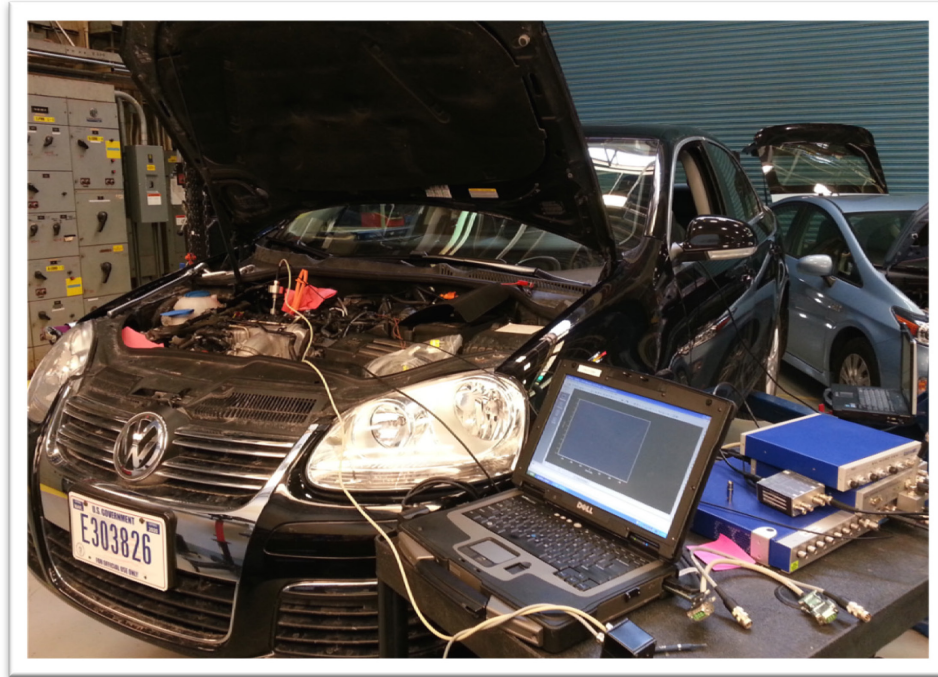


Figure 4.2.2: Volkswagen Jetta TDI TDC Determination

4.3 Drive Cycle Performance

The Jetta TDI was subjected to the same selection of drive cycles as the other vehicles in this test in order to measure its performance and investigate its operational tendencies. A copy of the test plan is found in Appendix A. The vehicle's fuel economy was calculated along with the overall vehicle efficiency as calculated in Section 2.1.5 of this thesis. As stated before, it is important to note that a test name followed by the designation 'CS' denotes a cold start test wherein the vehicle was allowed to rest at ambient test cell temperature for a minimum of 12 hours. The designation 'HS' denotes a hot start test where the vehicle is already at normal operating temperature prior to the beginning of the test. Table 4.3.1 catalogues the TDI's performance.

Table 4.3.1: Volkswagen Jetta TDI Drive Cycle Economy and Vehicle Efficiency

Test Description	Test #	Fuel Economy (mpg)	Vehicle Efficiency
UDDS CS	71307026	32.5	15.3%
UDDS HS	71307014	36.8	17.3%
UDDS #3	71307015	36.8	17.0%
HWFET	71307012	52.1	21.6%
US06 Cold	71307016	31.9	23.4%
US06 Cold City	71307016	21.8	22.9%
US06 Cold Hwy	71307016	36.7	23.7%
US06 Hot	71307010	35.5	25.9%
US06 Hot City	71307010	24.8	26.0%
US06 Hot Hwy	71307010	40.5	25.9%

The TDI's drive cycle economy ranges from 21.8 miles per gallon on the city portion of the cold start US06 cycle to 52.1 miles per gallon on the less aggressive HWFET cycle. As is typical for most vehicles, mileage on the UDDS cycle falls in between these two extremes.

Cold start operation has a significant effect on the TDI's fuel economy. It manages to return 36.8 mpg on the second and third iterations of the UDDS cycle. The fact that there is no variation between these tests supports the fact that the vehicle has reached its operating temperature by the third UDDS cycle. When the powertrain and engine temperatures are lower, the TDI only manages to achieve 32.5 mpg over this same cycle. The cold start fuel economy penalty for this test is then calculated to be 11.6%. In the case of the more aggressive US06 cycle, the TDI achieves 35.5 mpg for the hot start test, but only 31.9 mpg for the cold start iteration, yielding a cold start penalty of 10.1%.

The TDI's calculated vehicle efficiency varies significantly over the different drive cycle tests. The portion of fuel energy measured as work at the wheels varies from 15.3% for the cold start UDDS cycle to 26.0% on the hot start city portion of the US06 cycle. The vehicle appears to return the greatest efficiency when it is highly loaded during aggressive acceleration events.

One of the key advantages of the diesel engine is that it does not require a throttling valve in the intake tract for air/fuel ratio control. The resulting decrease in part-load throttling losses is a significant benefit that helps to increase vehicle efficiency on lightly loaded drive cycles. Despite the light loads required, the TDI still manages to return over 17% vehicle efficiency for both warm UDDS tests.

In order to better understand the effect of cold start tests on the TDI's vehicle efficiency, the oil and coolant temperatures are plotted for the hot and cold start iterations of the US06 cycle in Figure 4.3.1 below. It can be seen that the TDI typically operates with coolant temperatures in the range of 90°C. Oil temperatures are typically not regulated as carefully by design, but during the US06 cycle the TDI runs between 105°C and 110°C measured in the engine sump. For the cold start US06 cycle, it can be seen that the oil never reaches the full operating temperature achieved in the hot start test. Conversely, engine coolant reaches operating temperature about 60% of the way through the drive cycle. These observations indicate that the TDI's engine and vehicle efficiency are subject to temperature-related effects for a significant portion of the cold start drive cycles.

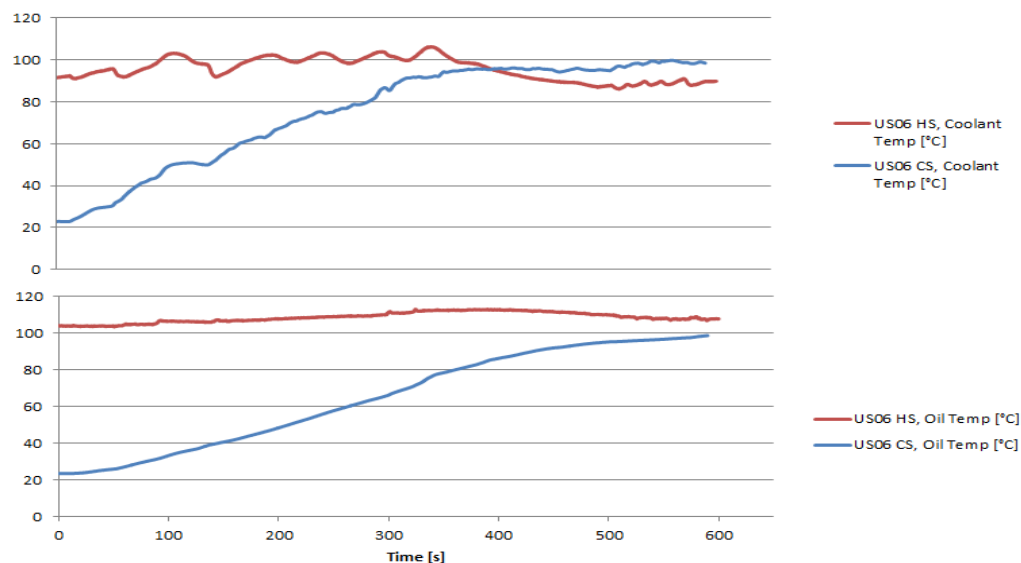


Figure 4.3.1: Volkswagen Jetta TDI Oil and Coolant Temperatures, US06 Cycles

Examining the percentage of fuel used during idle periods helps to illuminate both the idle opportunity for a given drive cycle as well as the vehicle's fuel requirements at idle, both of which are factors contributing to cycle fuel economy. The UDDS cycle provides ample opportunity for idle, and the TDI uses as much as 7.9% of the total cycle fuel energy at idle conditions during this cycle. It is interesting to note that this proportion does not change significantly with vehicle thermal state. A closer look at the UDDS cycle data shows that when operating under cold start conditions, the TDI increases all fuel injection events commensurately; put another way, the increase in idle fuel flow rate is of the same magnitude as the increase in cruising fuel flow rate. Because of this, though the magnitude of the idle fuel flow is greater during the cold start test, the proportion of fuel spent at idle conditions changes very little. The TDI's idle fuel consumption as a percentage of total drive cycle fuel requirements is depicted in Figure 4.3.2.

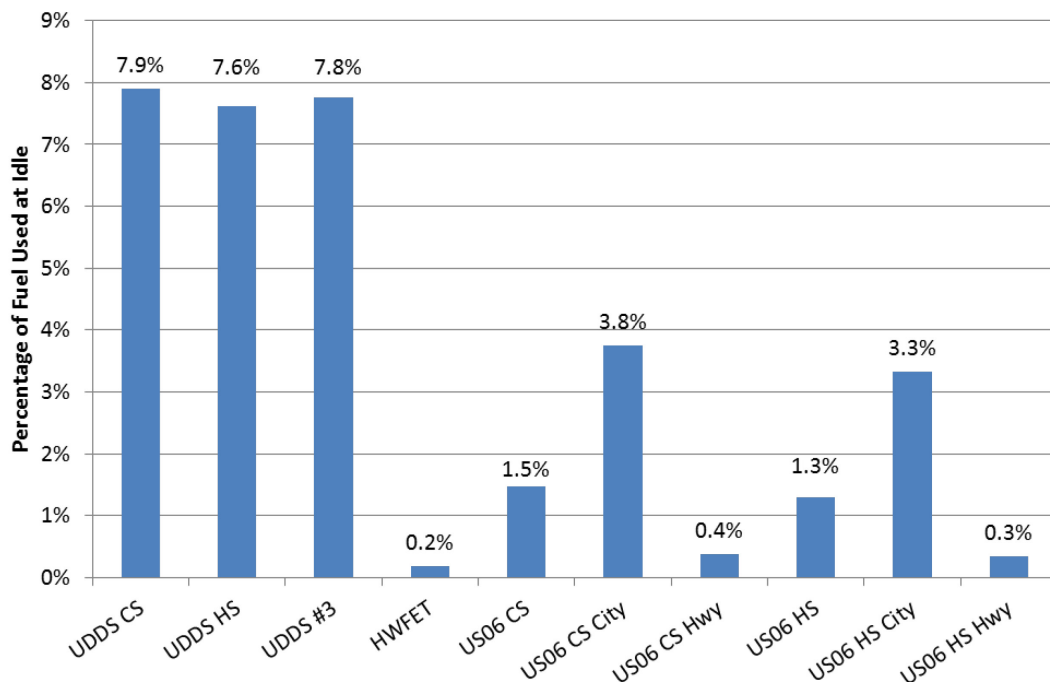


Figure 4.3.2: Volkswagen Jetta TDI Idle Fuel Use

Vehicle fueling behavior during deceleration (often termed ‘decelerative fuel cutoff’, or ‘DFCO’) is another important contributor to cycle fuel economy. While the

vehicle is braking, no positive tractive work is required at the wheels to move the vehicle down the road. However, some fuel is sometimes consumed during this time to handle accessory loads and to provide desired drivability characteristics. Careful management of this fueling behavior can have a significant effect on the vehicle's fuel economy. To illustrate the TDI's DFCO behavior, two deceleration events are shown below.

Figure 4.3.3 portrays the end of the first 'hill' of the UDDS hot start cycle. This comprises a relatively gentle deceleration event in which the vehicle slows to a stop from 32 mph over 11 seconds. It can be seen that while the TDI reduces fuel flow to idle levels, it does not completely shutoff fuel flow under these deceleration conditions. Figure 4.3.4 shows the end of the first 'hill' of the US06 hot start cycle. This deceleration starts at considerably higher speed, requiring the vehicle to come to a stop from 70 mph over a period of 30 seconds. Though the average deceleration rates are similar, the TDI completely cuts fuel flow until vehicle speed drops below 12 mph at which time the vehicle repowers the cylinders at the idle fuel flow rate.

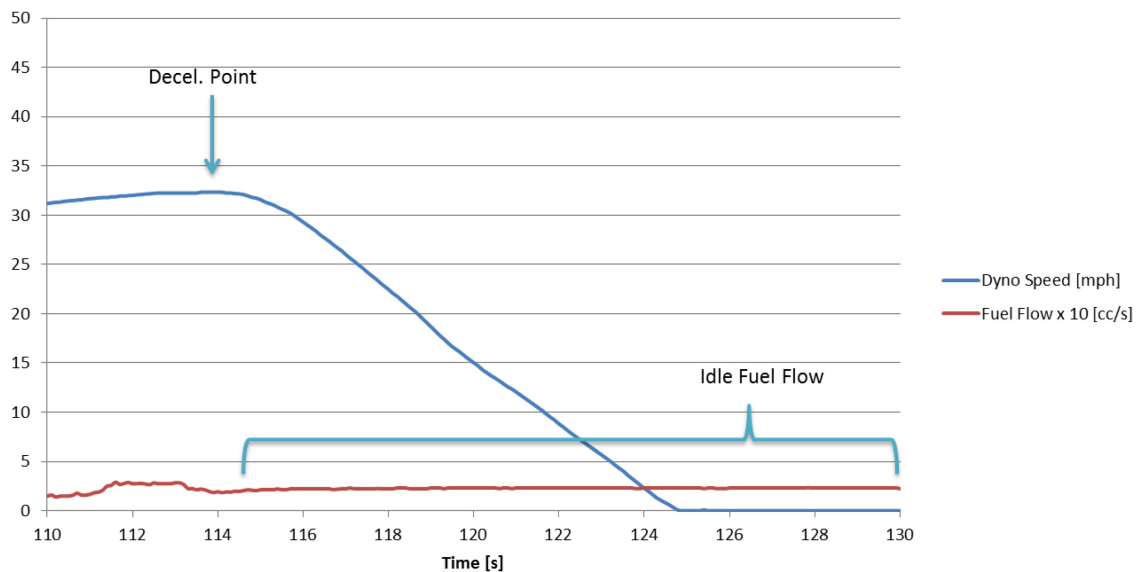


Figure 4.3.3: Volkswagen Jetta TDI Deceleration Fuel Cutoff (DFCO), UDDS HS

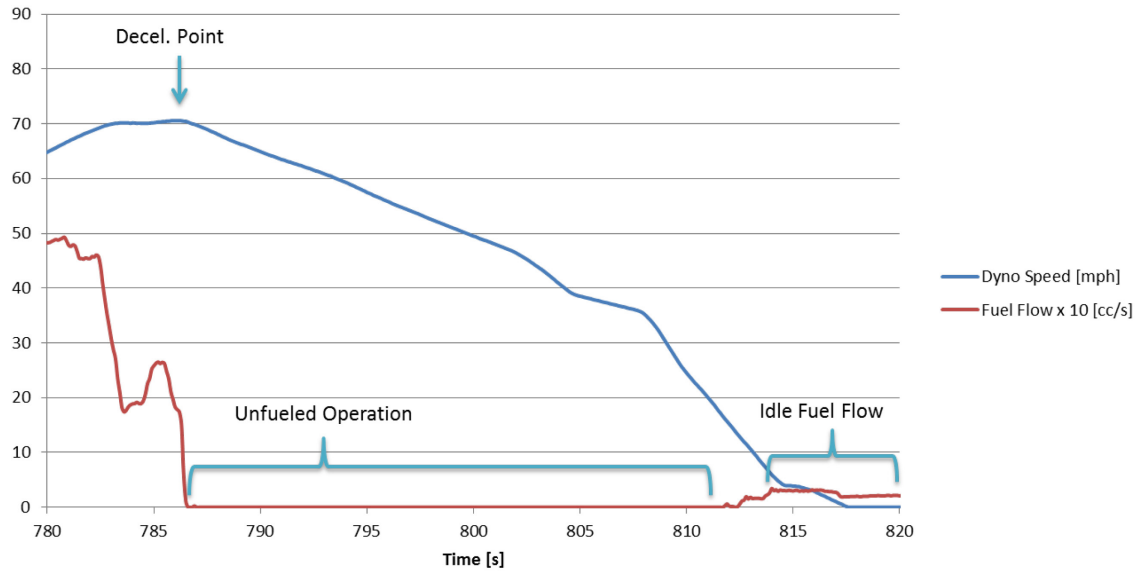


Figure 4.3.4: Volkswagen Jetta TDI Deceleration Fuel Cutoff (DFCO), US06 HS

To further illustrate the DFCO behavior of the TDI, all deceleration events over the hot start UDDS, hot start US06, and HWFET cycles were considered. After all the events are gathered, a filter is applied to recolor those points where the vehicle is decelerating and fuel flow is less than 0.3 mg per engine revolution. This latter value is chosen so as to allow for some signal noise while being significantly less than the warm idle fuel flow rate of 6.2 mg per revolution. Figure 4.3.5 portrays the deceleration fuel cutoff map for the TDI.

The DFCO map for the Jetta TDI shows that the vehicle exhibits significant decelerative fuel cutoff over the majority of the deceleration field gathered from the drive cycles used in this thesis work. The vehicle aggressively reduces fuel during decelerations greater than 0.35 m/s^2 above approximately 12 mph. Once the vehicle speed or acceleration rates drop below these levels, the vehicle resumes fueled operation.

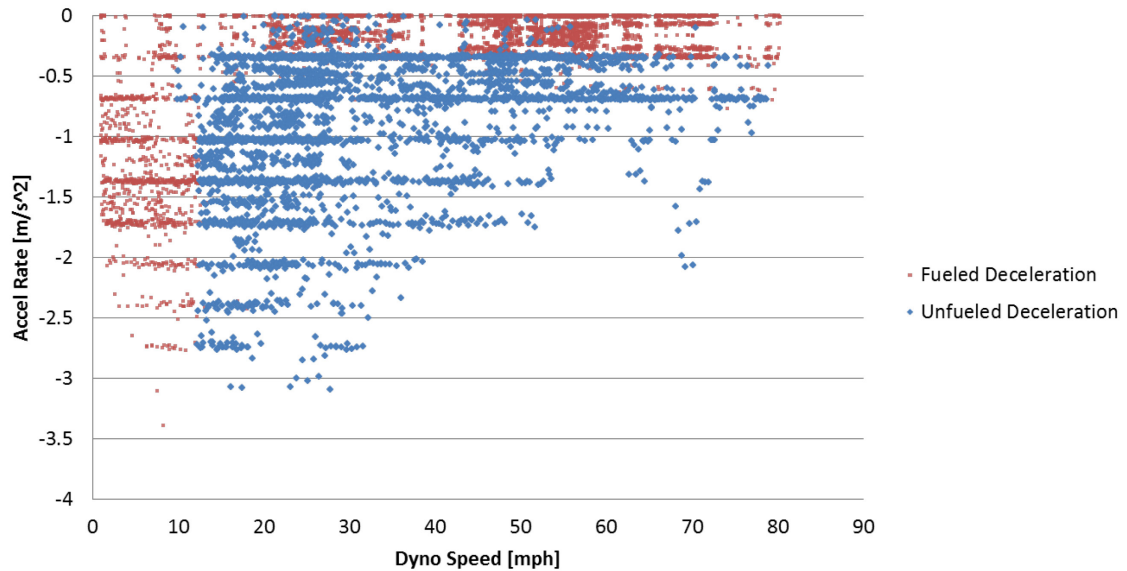


Figure 4.3.5: Volkswagen Jetta TDI Deceleration Fuel Cutoff (DFCO) Map

As discussed elsewhere in this document, it is commonly understood that the efficiency of the internal combustion engine varies with engine speed and load. As such, it is important to consider the speed and load utilization of the TDI in order to understand the vehicle's capability to utilize the highest efficiency areas on the map. Because indicating transducer measurements (and thus engine IMEP) are not available for the TDI, the quantity of fuel injected and normalized by engine speed was used to quantify engine load. Figures 4.3.6 through 4.3.8 show the TDI's engine utilization for the hot start UDDS, HWFET, and US06 cycles. The total time spent in operation at each speed and load point is denoted by the color profile, scaled as a percentage of total drive cycle time. The bins used to generate these figures were sized in increments of 150 rpm and 5 mg of fuel injected per engine revolution.

The TDI's engine usage for the hot start UDDS cycle is shown in Figure 4.3.6. During this cycle the engine is operated primarily at low speed and light load. The low power requirements of the UDDS cycle combined with the robust torque output of the CBEA engine and six available gear ratios allow engine speed to stay below 2500 rpm at all times. The majority of the time while the vehicle is underway is spent at

approximately 1300 rpm and 20 mg/rev, with forays to higher load regions when needed. A band with near zero fueling rate between this first centroid and idle speed represents the vehicle DFCO behavior. A final centroid exists at 820 rpm and 15 mg/rev which represents the significant idle opportunity of the UDDS cycle.

Figure 4.3.7 portrays the TDI's engine usage behavior for the US06 HS cycle. The power requirements for the US06 cycle are more demanding, and as such the engine is operated at higher speeds and loads to supply the desired road load. The range of operation is as high as 3100 rpm with as much as 130 mg/rev of fuel injected. A vertical band can be seen near 1900-2300 rpm where the engine is operated most commonly under power. It is clear that the TDI elects not to shift gears when possible, but increases load to meet the power demand while keeping engine speeds low. As in the UDDS cycle it can be seen that there is opportunity for idle as well as a significant DFCO band. We also note that the area near 1300 rpm and 20 mg/rev, heavily favored on the UDDS cycle, is not utilized at all for the US06 test.

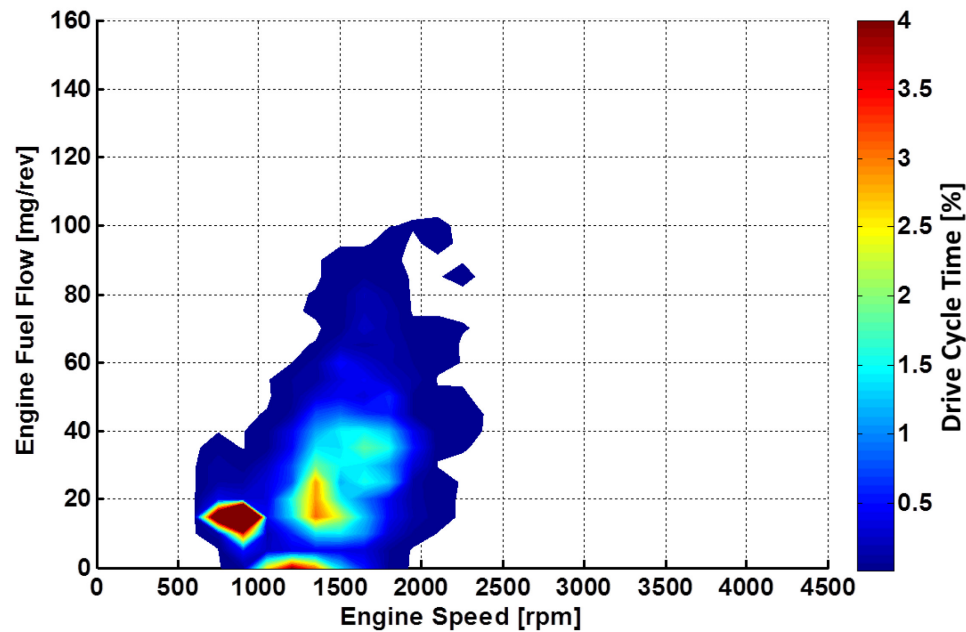


Figure 4.3.6: Volkswagen Jetta TDI Engine Utilization, UDDS HS Cycle

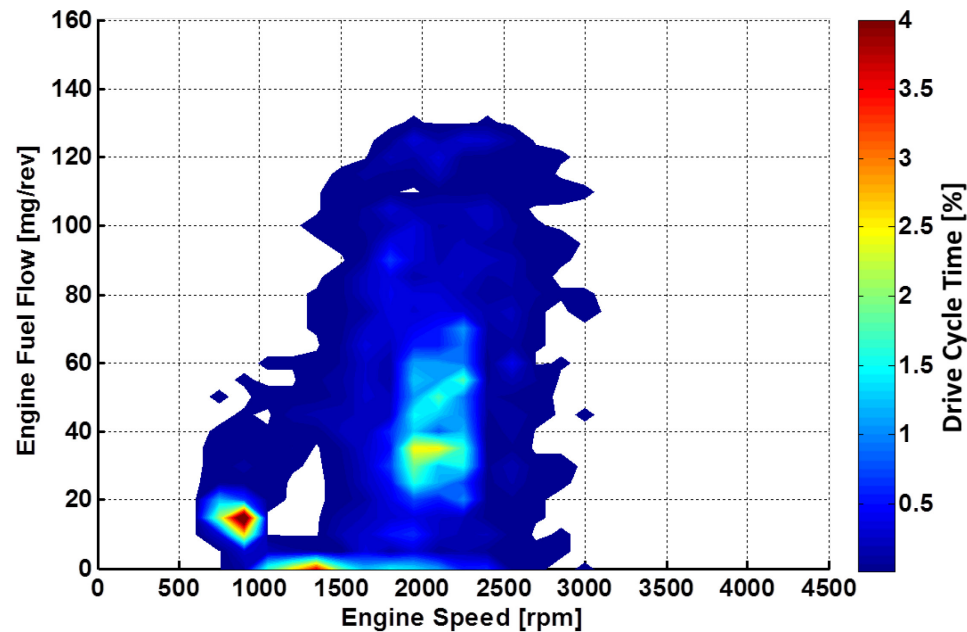


Figure 4.3.7: Volkswagen Jetta TDI Engine Utilization, US06 HS Cycle

Figure 4.3.8 catalogues the engine utilization for the TDI over the HWFET cycle. This cycle is spent primarily at relatively light load in two different cruising speeds; one band between 40 and 50 mph, and the other between 50 and 60 mph. These two bands are easily seen in the figure as two centroids at 1500 and 1750 rpm respectively. We also note that there is almost no opportunity for idle, and that the DFCO speed window is much narrower as the decelerations do not typically span the large vehicle speed ranges present in the other drive cycles. It is also interesting to note the higher load region shown in the figure. Though it is seldom used, it can be seen that when necessary the TDI elects to again increase engine load significantly without increasing engine speed, showcasing the flexibility of the diesel engine's broad torque curve.

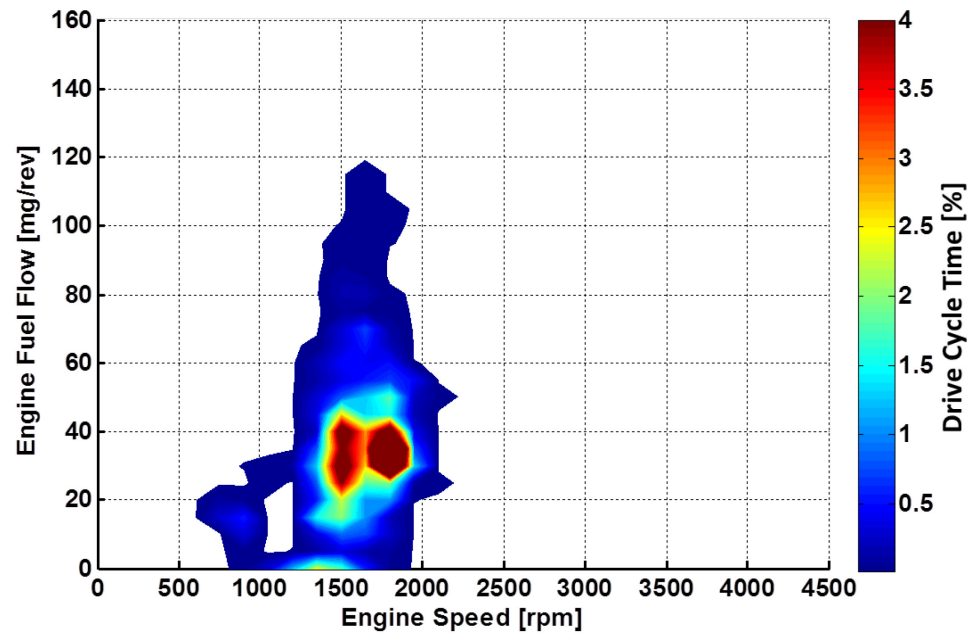


Figure 4.3.8: Volkswagen Jetta TDI Engine Utilization, HWFET Cycle

In order to further investigate the TDI's drive cycle performance, it is pertinent to investigate its behavior at a selection of steady state speeds. Toward this end, the vehicle was operated over a steady state speed drive cycle as shown in Section 2.1.1. For each speed the vehicle fuel economy, efficiency, wheel power and gear selection were calculated and are shown in Figure 4.3.9 below.

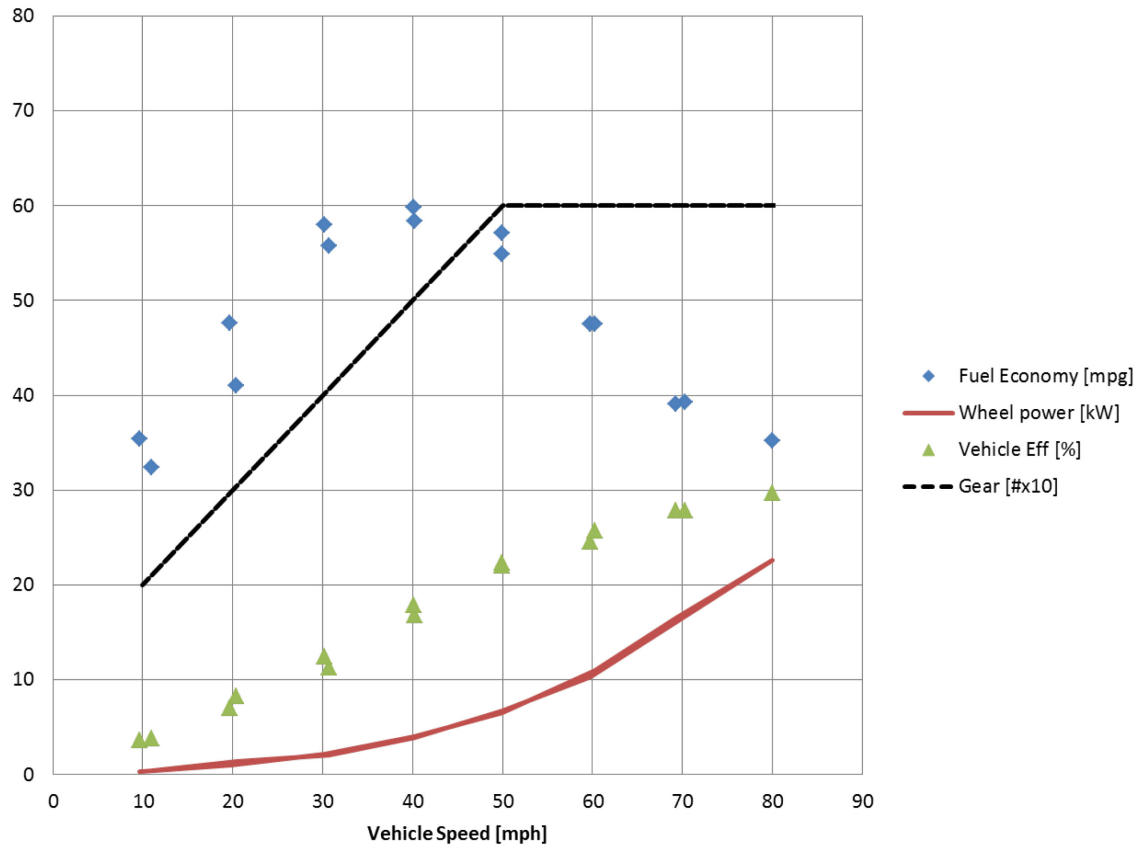


Figure 4.3.9: Volkswagen Jetta TDI Steady State Performance

Figure 4.3.9 shows that the TDI's fuel economy peaks at 40 mph at nearly 60 miles per gallon. Under the relatively low loads required to operate at steady state speed, the TDI upshifts as quickly as possible and selects the transmission's final gear by the 50 mph speed. Vehicle efficiency increases with increasing road and engine load, peaking at 30% at a speed of 80 miles per hour. The required road load is higher for this vehicle than the other's considered in this test; at 80 mph, the TDI must generate 2.3 kW of power to maintain speed. As is the case with other vehicles in the test, fuel economy falls at higher speeds as the road load power increases. The speeds ranging from 10 mph to 70 mph are repeated as part of the test plan, and as such show two data points each. The differences are for the most part very small, with the exception of the 20 mph speed. Closer inspection of the data shows some difficulty in keeping a constant load at this speed

during the first hold, resulting in the lower of the two economy figures. Actual vehicle performance at this speed is better represented by the 48 mpg data point.

4.4 Cycle-Based Heat Loss Proportions

It was shown in section 4.3 that between 15.3% and 26.0% of the total fuel energy consumed by the TDI on a given drive cycle is measured as positive tractive work at the vehicle's wheels. This naturally leaves anywhere between 74.0% and 84.7% of the fuel energy that is lost to conversion inefficiencies between the fuel tank and the work measured at the vehicle's wheels. In order to better understand where these losses take place, the enthalpy changes occurring in the TDI's coolant and exhaust systems were measured and considered for each drive cycle. The cooling system was instrumented with a pair of flow sensors and four thermocouples to measure the enthalpy drop across the radiator and heater core, while the exhaust mass flow rate was calculated from the air and fuel flow rates reported by the vehicle's onboard sensors through the CAN bus. A thermocouple was placed in the exhaust in order to measure the bulk gas temperature, and the test cell temperature was used as the dead state temperature to gauge the enthalpy added to the exhaust gases.

As discussed elsewhere in this work, the nature of the vehicle's cooling system presents some challenges to enthalpy change measurements conducted in this manner. The engine operates with a volume of coolant that must come up to operating temperature before it begins to flow through the radiator. There also exists a transport delay between the time that a given amount of energy is transferred to the coolant and the time it is shed through a given heat exchanger. Measurement of this transport delay would require a prohibitively detailed set of thermocouples installed throughout the coolant flow passages in order to understand the instantaneous temperature gradients involved in this process. In order to get around these issues, we only consider heat loss proportions for cycles conducted at operating temperature, and then only consider heat loss proportions for entire drive cycles.

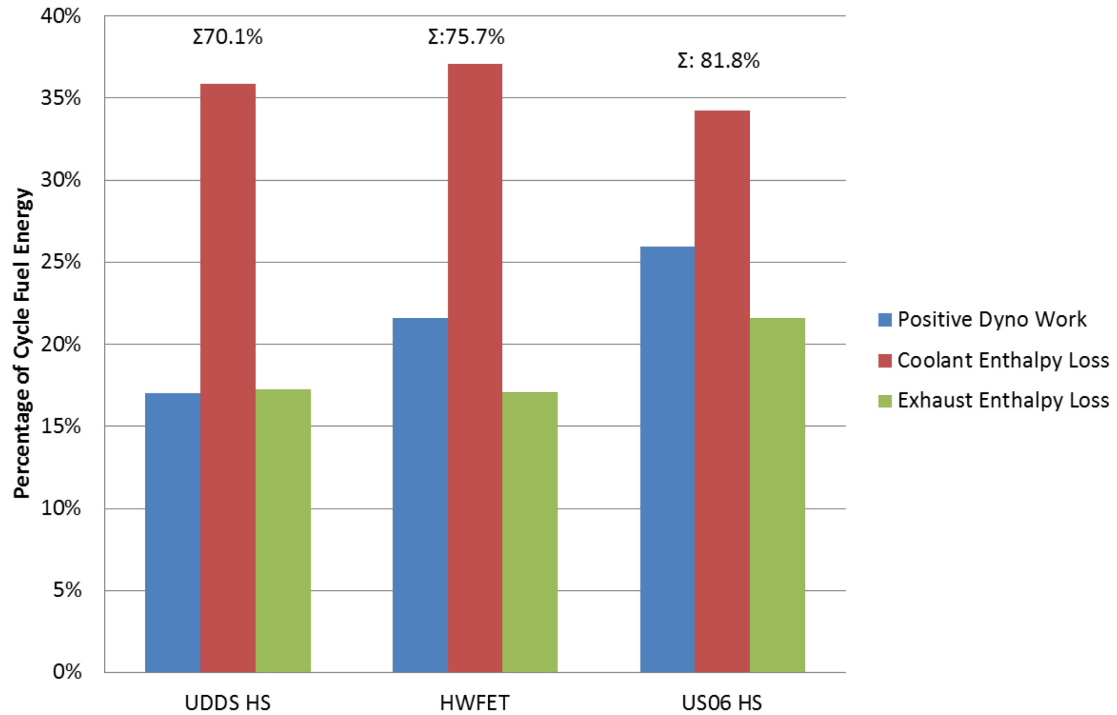


Figure 4.4.1: Volkswagen Jetta TDI Cycle-Based Fuel Energy Usage

Figure 4.4.1 shows the measured proportions of energy at the wheels, enthalpy lost through the cooling system, and enthalpy lost through the exhaust system for the Jetta TDI. The total measured proportion of energy lost varies over the three cycles and ranges from 70.1% on the UDDS hot start cycle to 81.8% on the US06 hot start cycle. The remaining energy is shed through other sources that are difficult to measure, such as radiant and convective heat from the engine surfaces and exhaust components, drivetrain mechanical losses, coolant losses not captured across the heat exchangers. Any losses from incomplete combustion also contribute to the unmeasured fraction, but these are not typically large for diesel engines because of their globally lean combustion strategy.

Coolant loss proportions are steady across the cycles ranging between 34 and 36% of fuel energy. In all three cases, the majority of the measured energy is lost through this source. Both the positive dynamometer work fraction and the exhaust enthalpy losses increase markedly as the engine is loaded more heavily on the US06 cycles. It should be

noted that the dynamometer work fraction is equivalent to vehicle efficiency; this relationship is presented in Section 2.1.5 and the TDI's vehicle efficiency figures are detailed in Section 4.3. Figure 4.4.2 shows the TDI's coolant losses separated between the two heat exchangers. Because the HVAC fan was not operated during these tests, it can be seen that the heat losses across the heater core are almost negligible in comparison to those across the vehicle radiator.

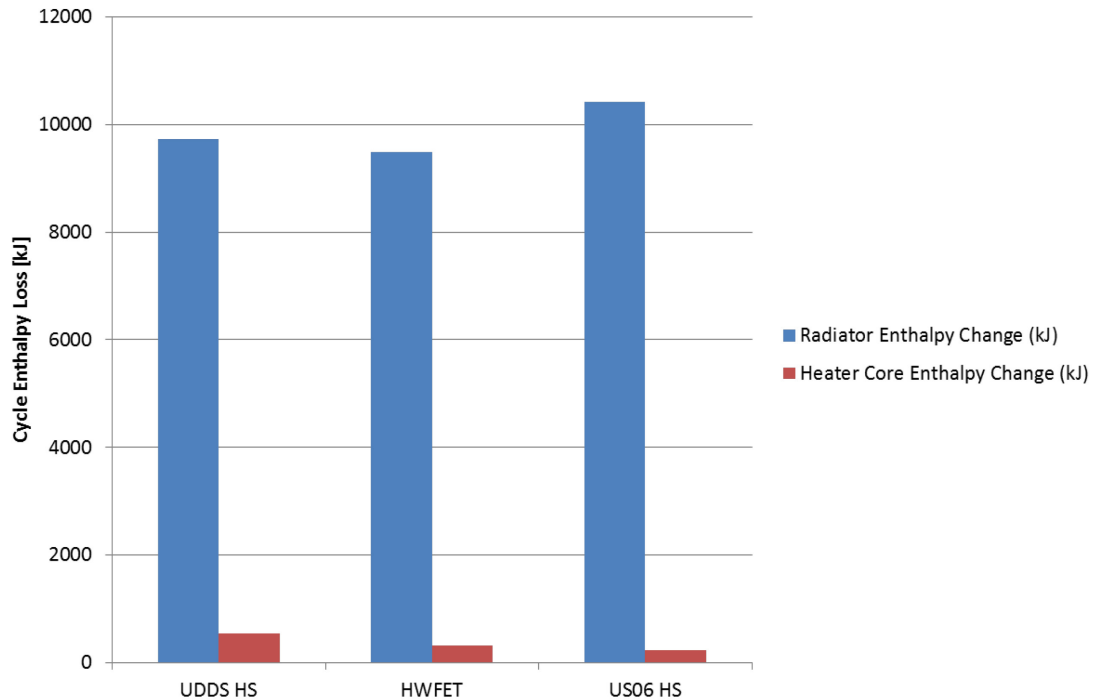


Figure 4.4.2: Volkswagen Jetta TDI Coolant Enthalpy Change by Source

It is generally accepted that as engine speed and load increase, combustion efficiency dips and exhaust gas temperatures and mass flow rates rise, thereby increasing the proportion of fuel energy that is measured as a change in exhaust gas enthalpy [4]. It is interesting to note that the TDI's exhaust gas temperatures are quite low among the vehicles studied, and are on the order of 300°C to 400°C. Because of the lean air/fuel ratios typical in diesel combustion, the total mass and therefore the heat capacity of the cylinder charge is typically much higher for a given amount of fuel, resulting in a smaller bulk temperature rise over the combustion cycle. However, the exhaust gas mass flow

rate is much higher, causing the total exhaust losses to be similar in magnitude to the gasoline-fueled vehicles in this test. Further comparative analysis is left to Chapter 7.

4.5 Cycle-Based Emissions Measurements

The cycle-based tailpipe emissions for the TDI were measured with the help of the Semtech and AVL DVE equipment detailed in Section 4.1. Table 4.5.1 catalogues the total tailpipe emissions on a per-cycle basis.

Table 4.5.1: Volkswagen Jetta TDI Total Emissions by Cycle

Test Description	NOx [mg]	THC [mg]	CO [mg]
UDDS CS	230.9	2203.5	7584.1
UDDS #3	26.7	457.9	977.2
HWY	157.9	43.6	318.7
US06 CS	2473.2	981.2	1462.5
US06 HS	2704.4	529.3	731.1

From the table we note that the aggressive US06 cycle generated the highest levels of NOx emissions. NOx emissions are typically formed at high combustion temperatures in the presence of excess oxygen, two conditions that are typical of diesel combustion because of a globally-lean, high compression ratio combustion strategy [4,5]. It is interesting to note that while the greatest level of NOx occurs on the hot start US06 cycle, the cold start test results in greater THC and CO emissions. This may be because the engine peak combustion temperatures are higher during the hot start test; the warm engine bay and turbocharger generate higher intake air temperatures that can have a significant effect on peak combustion temperatures because of the high 18.0:1 compression ratio. Extra fuel is added during the cold start to stabilize combustion, lowering combustion efficiency as the cooler temperatures slow the rate of fuel vaporization. This combined with the cold starting temperatures of the aftertreatment catalysts results in greater THC emissions.

The highest levels of THC and CO emissions were observed on the cold start version of the UDDS test. This may have to do with the extended warmup period that occurs on this cycle because of comparatively gentle vehicle operation at low engine loads, resulting in richer air/fuel ratios. With the exception of this test, CO numbers for the TDI are relatively low. CO is typically formed when there is a shortage of oxygen to bond with the carbon supplied by the fuel. Such a shortage is typically not found in diesel combustion because of predominantly lean air/fuel ratios.

Figures 4.5.1 and 4.5.2 show the integrated NO_x and THC emissions for the TDI over the hot and cold start versions of the US06 drive cycle. Quick increases in integrated NO_x emissions levels often correspond to hard accelerations at high engine loads, regardless of whether the engine has attained operating temperature. THC emissions exhibit similar behavior, especially when the engine is cold and at very high engine loads. Because of a slight delay inherent in turbocharger dynamics, increasing the engine load very quickly often results in momentarily richer mixture conditions while the turbocharger increases speed and supplies additional airflow to the engine. This can result in THC spikes such as those seen in the figures below.

A large increase in THC can be seen during the cold start US06 cycle beginning approximately 250 seconds into the test. This event does not appear to correspond to a large acceleration event. Instead it may have to do with catalyst temperature maintenance or a change in the engine EGR rate causing a transient effect on combustion efficiency or catalyst efficiency. Without further exhaust gas sampling on both sides of each aftertreatment catalyst, further exploration of this event is not possible.

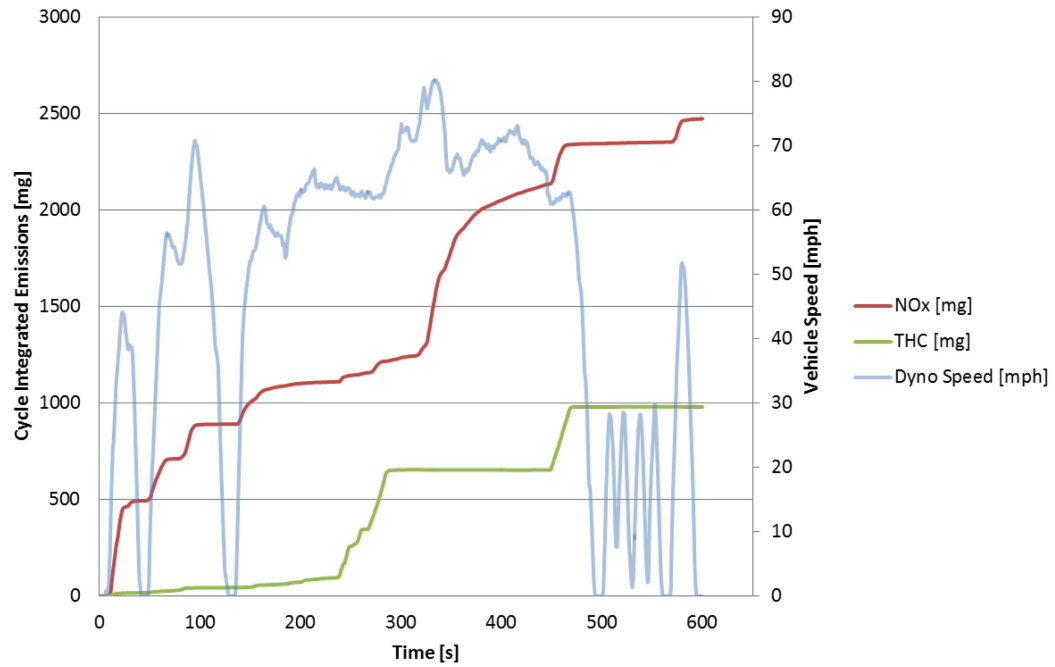


Figure 4.5.1 Volkswagen Jetta TDI US06 Cold Start Integrated NOx and THC

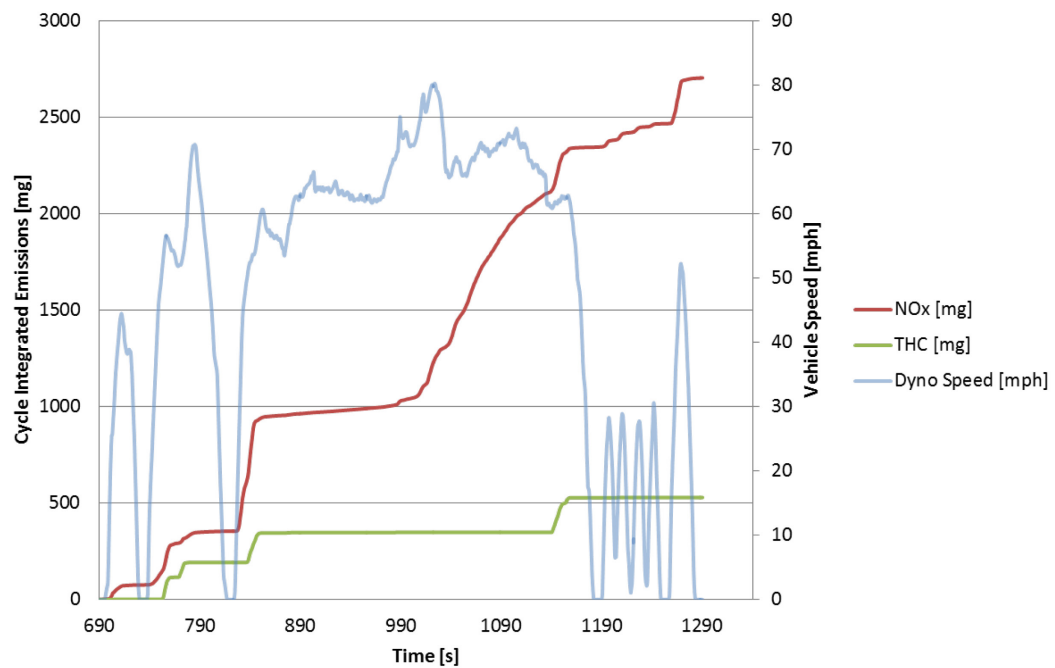


Figure 4.5.2 Volkswagen Jetta TDI US06 Hot Start Integrated NOx and THC

4.6 Engine Indicating System Measurements

As discussed previously in Section 4.2, considerable effort was expended to meet the unique challenges of implementing a non-invasive piezoelectric pressure transducer in the combustion chamber of the Volkswagen TDI. Because a diesel engine has no spark plug, the traditional method of using a pressure transducer housed in a custom spark plug body is not viable. Fortunately, the TDI is equipped with glow plugs that are used to create a very hot locus for combustion in the chamber during cold start conditions. Because the vehicle was operated at ambient temperatures of 72 degrees Fahrenheit it was thought that removing the glow plug on cylinder one would allow for the use of a custom adapter to facilitate the use of a pressure transducer without causing significant cold start difficulty.

It was soon discovered that the TDI is instrumented with a type of cylinder pressure transducer from the factory. Materials from Volkswagen AG indicate that the stock glow plugs incorporate a membrane exposed to combustion chamber pressures and instrumented with strain gauges. As combustion pressure changes and the membrane is stressed, the resulting strain is measured and provides an indication of the cylinder pressure. This information is used to monitor combustion timing for cylinder balancing and emissions reduction.

It was anticipated that if the stock transducer were replaced with a high-sensitivity piezoelectric unit, the vehicle would likely display a malfunction indicator light. It was hoped that the missing signal would not cause an operational change in combustion strategy and that the vehicle could be tested as normal. To this end the vehicle was tested with an AVL GH-13P piezoelectric pressure transducer installed in the cylinder in place of the stock transducer. The vehicle did immediately display an indicator light, but appeared to operate as normal; no loss in power or change in strategy was observed by the test driver.

However, when the vehicle was run through several drive cycles, it was found that the resulting fuel economy was as much as 20% below results obtained in prior testing of the vehicle. In addition to this, exhaust gas temperatures on higher speed cycles were as much as 300°C above those seen in prior testing. At first it was thought that the vehicle was exhibiting aggressive regeneration behavior. In order to allow the regeneration process to run its course, the vehicle was operated at 55 mph for a period of 30 minutes while exhaust gas temperatures were carefully monitored. When the temperature measurements failed to return to normal levels, it was decided that the stock glow plug transducer should be replaced and the tests repeated; this resulted in lower exhaust gas temperatures and proper fuel economy, suggesting that the loss of the stock glow plug transducer had a significant influence on the vehicle's operating strategy.

After much consideration, it was decided that in order to properly implement a piezoelectric transducer the cylinder head should be removed and the combustion chamber modified to incorporate the sensor. Because of the cost, complexity, and time requirements of this solution, the vehicle was operated without indicating system measurements for drive cycle analysis.

Alternative solutions for pressure measurement were discussed, such as carrying the pressure signal from an adjacent cylinder to the cylinder one pressure measurement wiring harness. This would likely require a microprocessor to repeat the signal and offset it by a time equivalent to the passing of 180 crank angle degrees. Because this required time would change directly with engine speed, it would require extremely precise measurement of the crankshaft speed. Additionally, the vehicle ECU's ability to accurately apply fuel timing adjustments to cylinder one would be compromised. Utilizing the signal provided by the stock pressure transducer for indicating measurements was also considered, but with no information available as to the repeatability or temperature sensitivity of the strain gauges as well as lack of a means to calibrate the sensor led to the decision to forgo engine indicating pressure measurements for this vehicle.

With all this said, measurements were collected for several engine operation points while the AVL transducer was installed. It must be noted that these measurements are likely not indicative of the typical engine operating strategy. However, they are still instructive of some of the combustion characteristics of the TDI. The operating points detailed are all the results of single engine cycles and are not representative of sustained steady-state operation. Table 4.6.1 details three operating points discussed in this section.

Table 4.6.1: Volkswagen TDI Engine Operating Points

		Point 1	Point 2	Point 3
Engine Speed	[rpm]	830	1607	3006
IMEP	[bar]	1.9	4.5	19.6
Peak Pressure	[bar]	43.8	55.9	160.2
Burn Duration	[ms]	1.33	2.45	7.45
Angle, 50% MFB	[CAD]	14.7 ATDC	18.2 ATDC	16.9 ATDC
Angle, P _{MAX}	[CAD]	0.2 ATDC	4.7 ATDC	5.7 ATDC

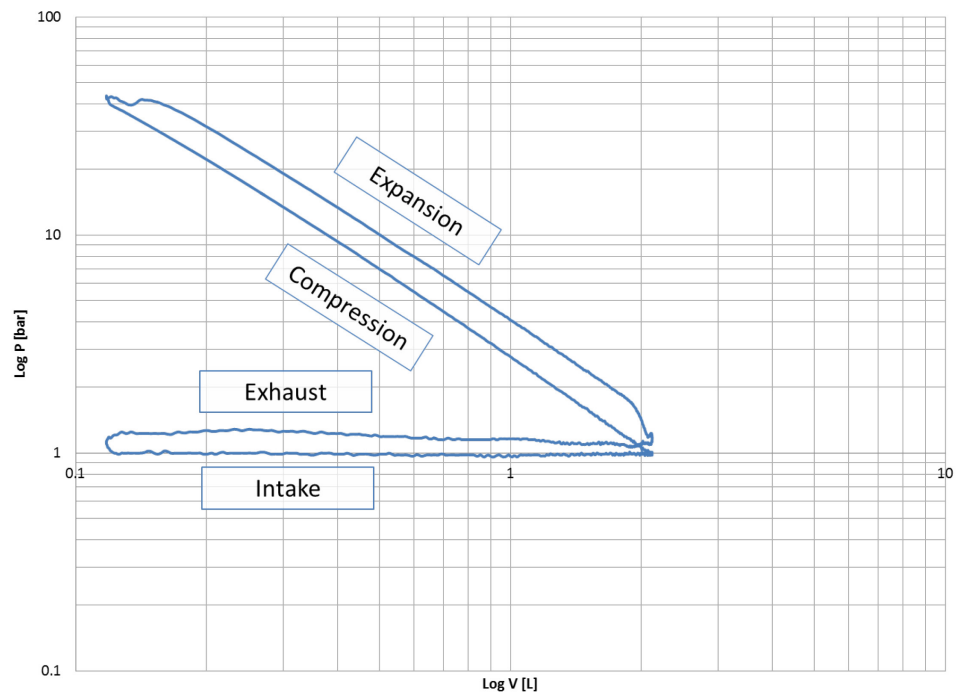


Figure 4.6.1: Volkswagen Jetta TDI P-V Diagram, Point 1

The first point detailed in Table 4.6.1 was taken during idle conditions at 830 rpm and 1.9 bar IMEP. The P-V diagram on a log-log scale is represented in Figure 4.6.1 with engine strokes labeled for convenience. Thanks to a high compression ratio of 18.0:1, the TDI exhibits a peak combustion pressure of 43.8 bar with minimal fuel energy input. The measurements show that peak combustion pressure occurs almost exactly at top dead center, but this is somewhat misleading regarding overall combustion timing. Examining the P-V diagram shows that while a small initial injection of fuel is burning and raises the pressure just after TDC, a second, larger bolus of fuel causes a significant pressure rise several degrees later. Modern piezoelectric fuel injectors allow the latest generation of diesel engines to inject fuel multiple times per combustion event in varying quantities to control combustion characteristics, and this is exhibited here. It is also interesting to note the position of the pumping loop; because the diesel engine has no throttling valve, the intake process takes place at atmospheric pressure or approximately 1 bar. While this helps to drastically reduce throttling losses, it must also be noted that large idle air flow rates in combination with the presence of a turbocharger and complicated exhaust aftertreatment increase engine backpressure significantly, pushing the exhaust stroke pressure significantly above ambient pressure. Regardless of this fact, the required pumping work is low in comparison to a gasoline engine of comparable displacement at similar operating conditions.

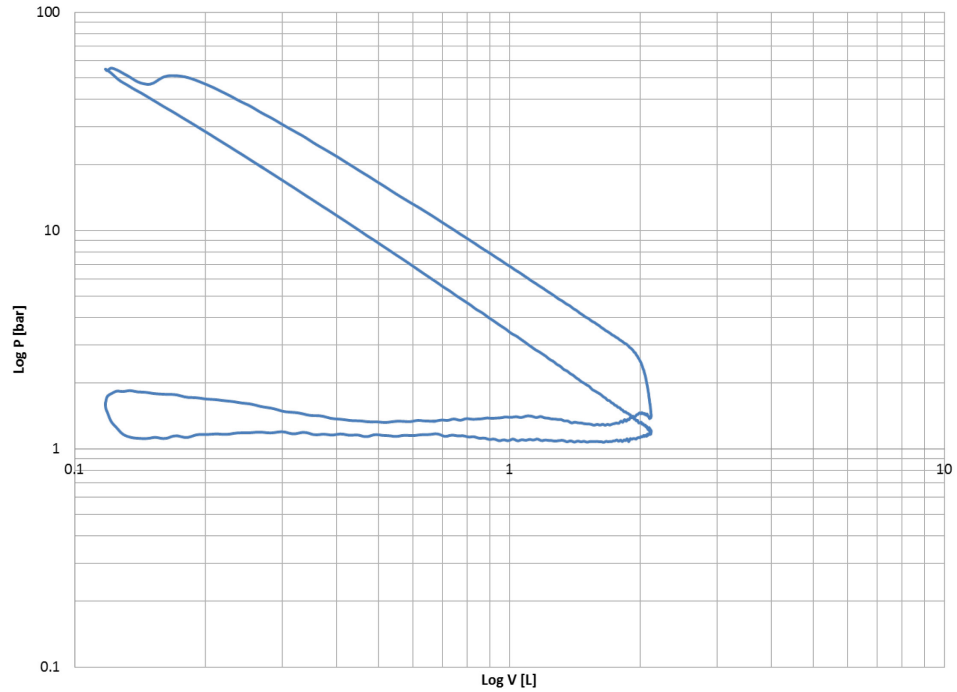


Figure 4.6.2: Volkswagen Jetta TDI P-V Diagram, Point 2

Figure 4.6.2 illustrates the pressure to volume relationship of the second operating point detailed in Table 4.6.1. This operating point is taken at 1600 rpm and 4.5 bar IMEP which is representative of highway cruising speeds for the TDI. The maximum cylinder pressure of 55.9 bar again takes place close to TDC. Injection behavior here is similar to that found at Point 1; a pilot injection occurs very near TDC while a second, larger event follows later. This behavior may be due in part to NO_x-reducing combustion strategy; moving the bulk of combustion later in the expansion process helps to lower peak cylinder temperatures, combatting formation of oxides of nitrogen [4,5]. It is also possible that combustion is moved later in the cycle because of the missing pressure transducer.

We can also see at Point 2 that combustion duration increases, likely because of the greater amount of fuel injected during the combustion process to make the additional power required at cruise. Because the engine load and speed are higher, it follows that turbocharger speeds are significantly greater than in Point 1. Because of this, we see that

the intake stroke now takes place entirely above 1 bar. Exhaust backpressure also rises with increasing airflow rate, and the work related to the pumping loop is similar in magnitude to Point 1.

Figure 4.6.3 showcases the third operating point considered for the TDI. Point 3 is taken at 3006 rpm and 19.6 bar IMEP, which is representative of an aggressive acceleration at peak loads. The 19.6 bar IMEP capability of the TDI is far greater than the gasoline-fueled vehicles in this thesis, and it is this number that is responsible for the diesel's robust torque rating. In the search for maximum power, the multiple injection event strategy that was clear in Points 1 and 2 is no longer apparent; here the TDI favors one long combustion event, resulting in a rounded and even pressure curve on the expansion stroke. Peak pressure occurs 5.7 degrees ATDC, and crests at 160.2 bar. We also see that the turbocharger is providing a dramatic increase in intake pressure; the entire intake stroke takes place above 1.9 bar. As seen in Point 2, exhaust backpressure increases with the larger airflow rate, and pumping work is comparable to the gasoline engines in this thesis when those engines are operated at WOT.

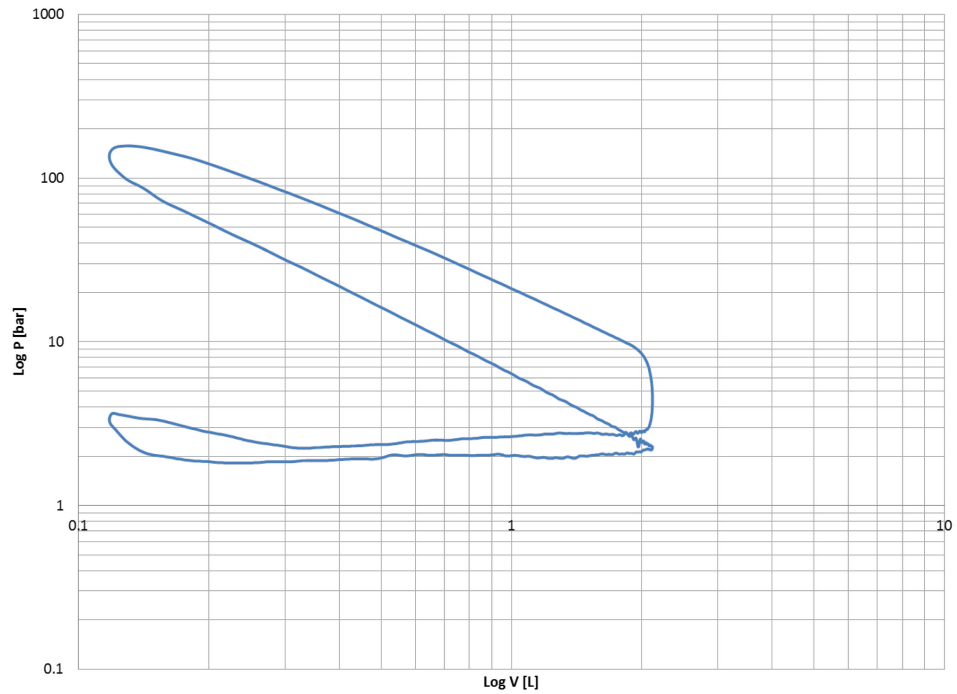


Figure 4.6.3: Volkswagen Jetta TDI P-v Diagram, Point 3

A final word regarding the combustion changes exhibited by the TDI; the noted symptoms were primarily a loss in fuel economy and a dramatic rise in exhaust gas temperature. The reason for these changes is unknown, and attempts to explain them without further access to the vehicle ECU's fuel injection quantity and timing metrics are largely conjecture. However, it is worth noting that modern turbodiesels are subjected to increasingly strict emissions standards for NO_x and THC. Volkswagen materials state that one of the primary reasons for the inclusion of pressure transducers as part of the CBEA engine package is to reduce emissions and fuel consumption. It is possible that upon recognizing the missing pressure transducer signal, the ECU assumes irregular or incomplete combustion is taking place in the missing cylinder and implements a strategy to keep the aftertreatment catalysts hot in order to burn off unburned hydrocarbons before they become particulate and THC emissions escaping the tailpipe. Such a strategy could explain the increased fuel use and high EGT's observed during testing.

Chapter 5 MY2010 Volkswagen Jetta TSI 1.4

5.1 Relevant Vehicle Features

The third vehicle chosen for inclusion in this thesis work was a MY2010 Volkswagen Jetta TSI. The vehicle is equipped with a small displacement 1.4L gasoline engine fitted with a turbocharger. So equipped, the TSI is representative of downsized, forced-induction engine architecture. Like the other vehicles in this study, the TSI is of FF configuration, driving the front wheels with its powertrain located in the front of the vehicle.

The TSI's gasoline engine incorporates direct fuel injection and air to water intercooling, and produces 120 brake horsepower at 5,000 rpm and 148 lb-ft of torque between 1,500 and 3,500 rpm. It features four valves per cylinder and dual overhead camshafts with variable intake camshaft phasing. The vehicle is equipped with two separate cooling systems. The first features a mechanical water pump that circulates coolant to the engine components and heater core. The second cooling system is dedicated to the air to water intercooler and turbocharger, and utilizes an electric water pump to drive coolant only when needed. The second system is sometimes referred to as the auxiliary system in this thesis. The cooling systems utilize separate heat exchangers, both of which are packaged in a single radiator unit at the front of the vehicle.

The Jetta TSI is equipped with an advanced dual clutch transmission. It features seven forward ratios and a dry clutch assembly. This gearbox provides high-efficiency power transmission and allows for gear changes with minimal interruption in tractive force.

Like the Jetta TDI with whom it shares dimensions, the Jetta TSI is classified as a compact sedan. The vehicle test weight is 3,500 lbs. It should be noted that because the Jetta was not available in the United States with this powertrain, the test vehicle was imported from Europe.

The TSI's vehicle parameters are catalogued in Table 5.1.1. Fuel properties are found in Table 5.1.2. The vehicle is pictured in Figure 5.1.1.

Table 5.1.1: Volkswagen Jetta TSI Vehicle Metrics

Vehicle Information		
Year/Make/Model		2010 Volkswagen Jetta TSI
Body Type		4 dr Sedan
Engine		1.4 L 16V VVT I4 DI Gasoline
Compression ratio		10.0:1
Rated Power		90 kW (120 hp) @ 5,000 rpm
Rated Torque		200 Nm (148 lb.-ft.) @ 1,500 - 3,500 rpm
Transmission		7 Spd Dual Clutch Automated Manual (DSG)
Gear Ratio	1st	n/a
	2nd	n/a
	3rd	n/a
	4th	n/a
	5th	n/a
	6th	n/a
	7th	n/a
	Final Drive	n/a
EPA Fuel Economy	Urban	Not Reported
	Highway	Not Reported
	Combined	Not Reported
Road Load Coeff.	Test weight	3500
	Cd	0.31
	a	30
	b	0.2
	c	0.0186
Vehicle Performance		
WOT Acceleration	0-60	10.4 s (ANL)
	30-50	3.7 s (ANL)
	50-70	6.0 s (ANL)

Table 5.1.2: Volkswagen Jetta TSI Fuel Properties

Fuel Name:	Tier II EEE HF437	Density:	0.74	[g/ml]
Carbon Weight Fraction:	0.8646	Net HV:	18489	[BTU/lbm]



Figure 5.1.1: 2010 Volkswagen Jetta TSI

5.2 Instrumentation Specifics

The Jetta TSI was fitted with an extensive instrumentation package in order to collect data to illuminate the vehicle's performance and behavior during testing. The intent was to instrument the vehicle in such a way as to observe its characteristics without affecting its operating strategy.

Like the other gasoline-powered vehicles in this work, fuel supplied to the TSI's engine was measured using a RE-Sol RS840-060 fuel cart. The positive-displacement

meter is plumbed into the fuel supply line and fuel is measured as it is supplied to the fuel rail. Tailpipe emissions were measured with the use of a Sensors, Inc. SEMTECH and an AVL Dynamic Vehicle Exhaust system.

The TSI's cooling system was instrumented with a collection of Omega FTB series flow meters to measure coolant flow across the two radiator heat exchangers and the vehicle's heater core. An FTB 1306 was installed in the base engine radiator loop, while the FTB 1304 was selected for the heater core and secondary radiator loops because of their lower flow rates.

Combustion characteristics were monitored using an AVL IndiMicro 602 indicating system and IndiCom software. The signal from the stock engine position hardware was utilized to read the crankshaft position in real time with resolution interpolated to 0.1 degrees. As with the other test vehicles, the signal was aligned to the cylinder 1 top dead center position using an AVL 428 TDC determination probe. A piezoelectric transducer incorporated into a replacement spark plug was used to generate pressure signals. The transducer was calibrated using a dead weight calibrator to ensure accurate measurements.

A physical tap of the vehicle bus communication wires was used to log raw CAN signals. A scan tool was used to decode a number of signals in order to record vehicle parameters such as the commanded lambda value, throttle plate position, and engaged gear. In addition to this, the intake manifold pressure sensors were removed and a calibration curve was generated using a Merriam pressure transducer calibrator. The stock signals were then tapped and translated to yield useable manifold pressure signals.

The vehicle was also fitted with a number of thermocouples to measure the temperature of critical fluids, such as engine and transmission oil and engine coolant. Engine coolant temperatures were measured in a number of places to facilitate enthalpy change calculations across the heat exchangers. A thermocouple was also placed in the exhaust system to measure exhaust gas temperature.

Finally, the 12V battery power was monitored using a Hioki power analyzer with voltage taps and an inductive current measurement clamp.

Figure 5.2.1 shows an example of a flow sensor and thermocouple installation in the return line from the radiator associated with turbocharger cooling.

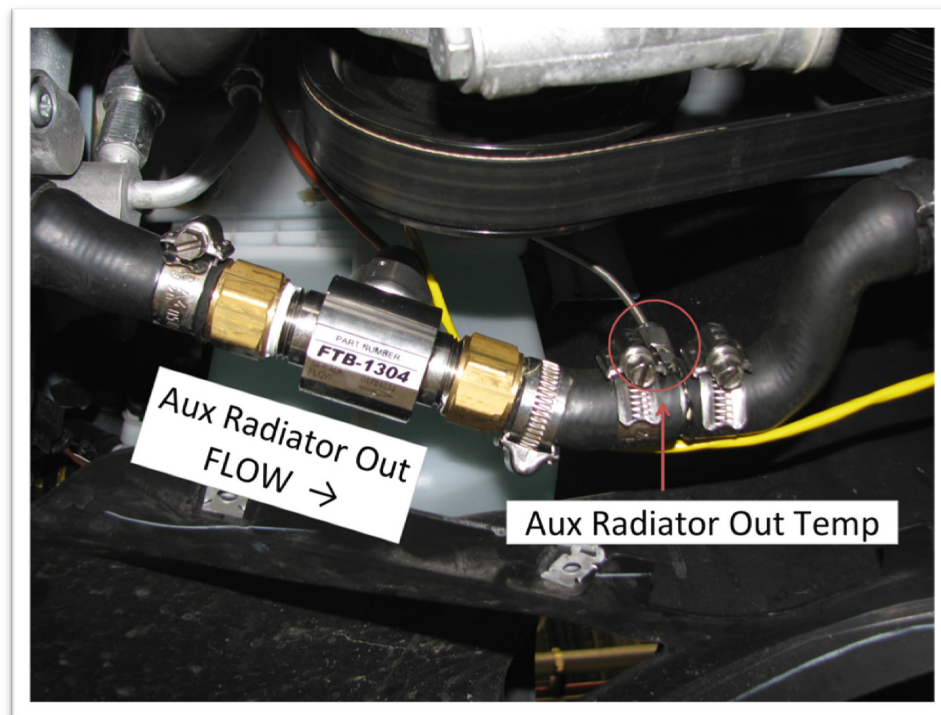


Figure 5.2.1: Volkswagen Jetta TSI Flow Sensor & Thermocouple Installation in Coolant Hose

5.3 Drive Cycle Performance

The Jetta TSI was subjected to a series of chassis dynamometer drive cycles in order to evaluate its performance and operating behavior. The test plan can be found in Appendix A. The TSI's fuel economy was calculated along with the powertrain efficiency as discussed in Section 2.1.5. It is important to note that test cycles with designation 'CS' denote a test performed under cold start conditions where the vehicle rested without operating in the test cell for at least twelve hours prior to the test. Tests

designated ‘HS’ were run with the vehicle beginning at operating temperature. Table 5.3.1 shows the TSI’s fuel economy and efficiency results over the drive cycles.

Table 5.3.1: Volkswagen Jetta TSI Drive Cycle Economy and Vehicle Efficiency

Test Description	Test #	Fuel Economy (mpg)	Vehicle Efficiency
UDDS CS	71309014	35.4	17.4%
UDDS HS	71309015	39.0	19.1%
UDDS #3	71309016	39.0	19.2%
HWFET	71309017	50.3	22.1%
US06 CS	71309027	28.2	22.1%
US06 CS City	71309027	17.3	19.8%
US06 CS Hwy	71309027	34.3	23.3%
US06 HS	71309018	31.6	24.6%
US06 HS City	71309018	20.9	23.9%
US06 HS Hwy	71309018	36.9	24.9%

The Jetta TSI returned fuel economy results ranging from 17.3 mpg on the city portion of the cold start US06 cycle to 50.3 mpg on the gentler HWFET cycle. In keeping with other conventional vehicles tested in this study, mileage for the UDDS cycle fell between these values; the TSI returned 39.0 mpg on the hot start UDDS tests.

The TSI exhibits a measurable decrease in fuel economy during cold start operation. The vehicle achieved 35.4 mpg on the cold start UDDS test, falling 9.2% below the economy achieved under hot start conditions. The cold start economy penalty for aggressive US06 operation is slightly higher, coming in at 10.8%.

To better understand the duration of cold start effects on the TSI’s operation, oil and coolant temperatures are plotted for the US06 cycle in Figure 5.3.1. The TSI typically operates with oil temperatures slightly above 100°C on the US06 cycle, with coolant temperatures are closer to 90°C. When the vehicle is operated under cold start conditions, coolant temperatures converge about 250 seconds into the test. Oil temperatures, however, do not fully converge over the course of a single US06 cycle.

This suggests that the vehicle is subjected to increased friction losses throughout the cold start cycle.

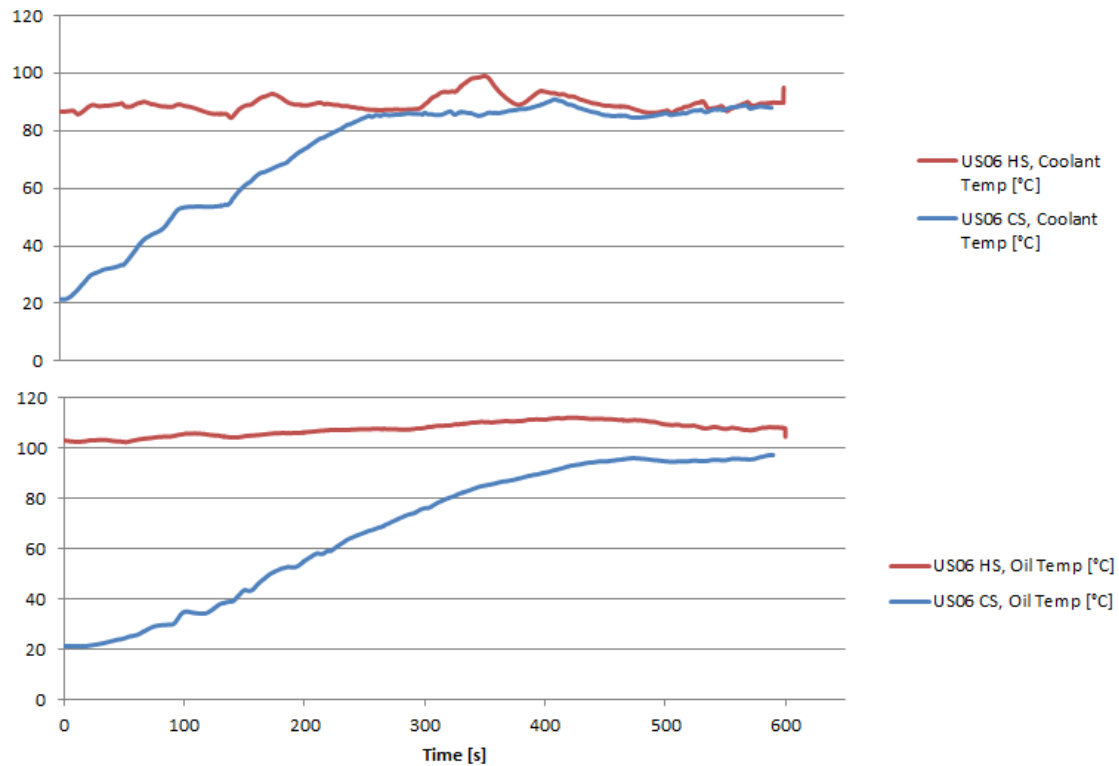


Figure 5.3.1: Volkswagen Jetta TSI Oil and Coolant Temperatures, US06 Cycles

The TSI returns its best vehicle efficiency values when it is operated at moderate loads with little idle opportunity. The vehicle achieved 24.9% vehicle efficiency on the highway portion of the US06 HS cycle where the vehicle cruises at high speeds with moderate engine loads. Vehicle efficiency was considerably lower during the UDDS cycle, ranging from 17.4% to 19.2% depending on whether the cycle was run under cold start or hot start conditions.

The TSI's efficiency behavior is typical of the conventional vehicles in this study, but the variance between the minimum and maximum efficiency values is smaller than is usual. This is partially due to the vehicle's downsized and boosted architecture. Because the engine is required to operate with wider throttle openings to generate the same torque

as a larger-displacement equivalent, throttling losses are reduced. This boosts efficiency at lighter loads. However, when the engine is asked to generate higher loads, it must do so by significantly boosting manifold pressure with the turbocharger. In order to mitigate combustion knock in these situations, the fuel mixture is often richened and ignition timing retarded to reduce peak cylinder temperatures. These phenomena are further explained in Section 5.6. The additional fuel injected during these conditions does not contribute appreciably to engine power, and therefore reduces vehicle efficiency. This operating strategy is employed during aggressive accelerations and can be seen during the US06 cycle as illustrated in Figure 5.3.2.

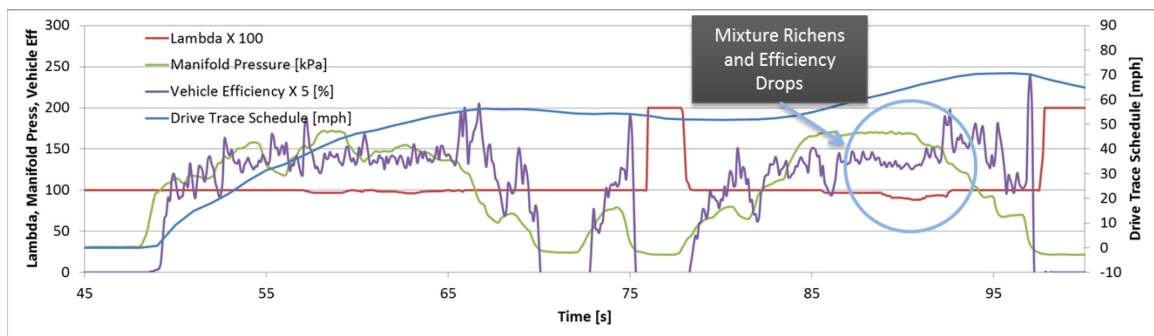


Figure 5.3.2: Volkswagen Jetta TSI Fuel Mixture Enrichment During Aggressive Operation, US06 Cycle

Idle fuel use is another contributing factor to the TSI's relative performance on each drive cycle. The UDDS cycle provides ample opportunity for idle consumption, as the vehicle spends 20.4% of the total cycle time at rest. Here the TSI spends approximately 6% of the fuel energy at idle under hot start conditions. Under cold start conditions, this figure increases to 8% because of the additional fuel used during cold start and catalyst warmup. Idle fuel usage on the other cycles is considerably lower, with the US06 city portion showing the next highest usage rates. Again the cold start test shows considerably higher idle fuel usage. The TSI's idle fuel usage by cycle is shown in Figure 5.3.3.

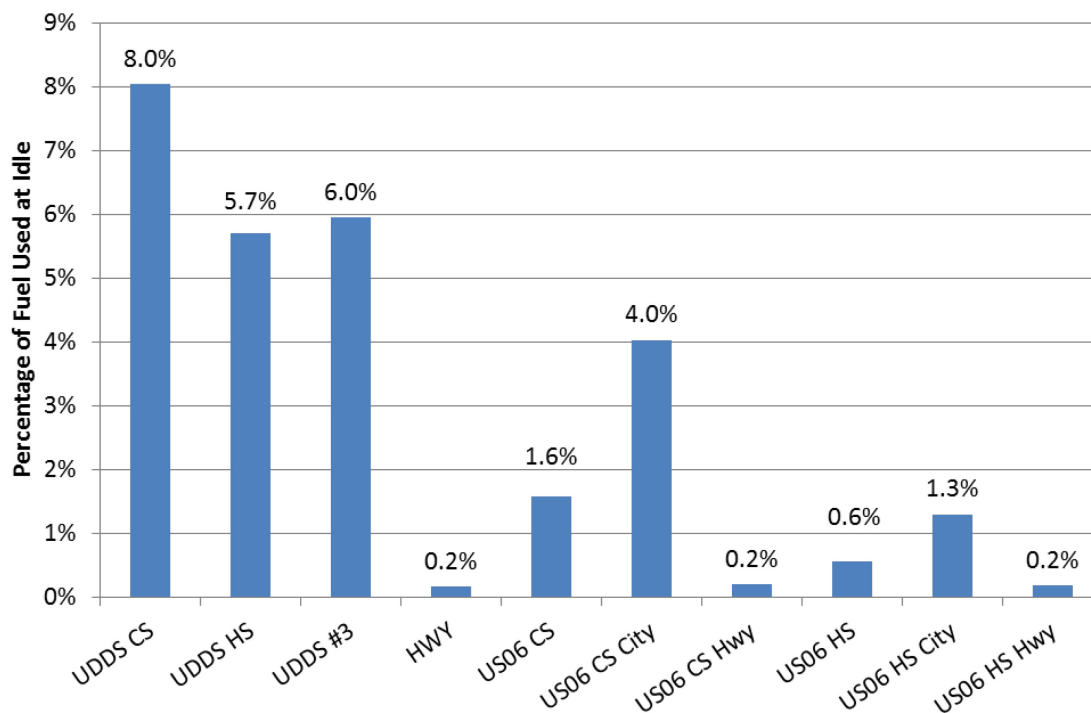


Figure 5.3.3: Volkswagen Jetta TSI Idle Fuel Use

Another important factor contributing to cycle fuel consumption is fueling behavior during deceleration events, or decelerative fuel cutoff (DFCO). During braking events, no tractive effort is required of the vehicle and fuel rates can be drastically reduced so long as drivability is not adversely affected. To show the TSI's DFCO behavior, an example deceleration event is discussed.

Figure 5.3.4 illustrates a sample deceleration event at the end of the first 'hill' of the UDDS hot start cycle. The vehicle slows from 32 mph to a stop over 11 seconds, comprising a fairly gentle deceleration. Though the rate of deceleration is gentle, the vehicle exhibits aggressive fuel cutoff behavior. At the 115 second mark, the driver releases the throttle and the fueling rate drops to near zero cc/s. Fueled operation does not resume until the vehicle comes to a complete stop and the transmission declutches from the engine.

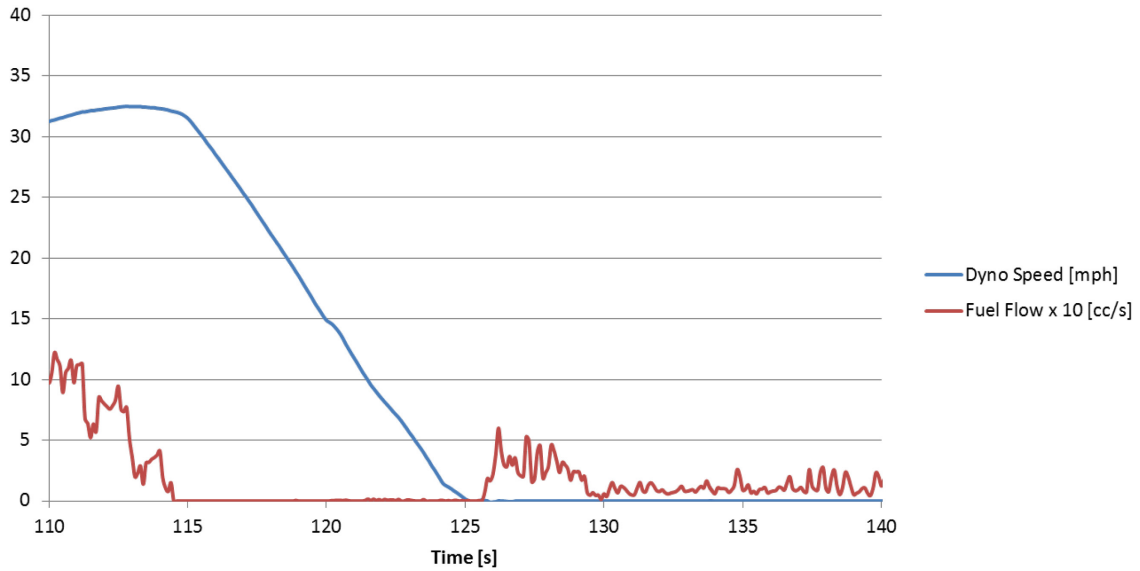


Figure 5.3.4: Volkswagen Jetta TSI Deceleration Fuel Cutoff (DFCO), UDDS HS

The TSI's DFCO behavior is similar for more aggressive decelerations. To illustrate this, a DFCO map is shown in Figure 5.3.5. All deceleration points for the UDDS, US06, and HWFET cycles are considered and plotted in blue. A filter is then applied that considers only the points during which the vehicle exhibits fuel flow rates less than 0.05 cc/s. This value was chosen to illuminate points significantly below the idle fuel flow rate while being resilient to noise in the fuel measurement signal. The DFCO points are plotted in red.

The TSI's DFCO behavior can best be described as aggressive. Unlike the other conventional vehicles included in this work, the vehicle does not exhibit a clear speed below which the vehicle begins refueling the engine. Refueling is instead blended directly with declutching the transmission. While it appears that the vehicle does not always cut fuel at small deceleration rates at higher speeds, these points are indicative of fueled decelerations where the reduction in vehicle speed is facilitated by the vehicle road load with slight throttle applied. There is a significant reduction of this behavior below 40 mph where the vehicle cuts fuel regardless of deceleration rate so long as the throttle is released. Such aggressive fuel reduction is likely the result of a combination of factors

including the vehicle's transmission choice and GDI architecture. The DSG transmission is not equipped with a torque converter, and as such is able to quickly transfer power in transient conditions. The DI fuel injection strategy provides quick, accurate control over engine air fuel ratios, and likely reduces the need to inject fuel early in anticipation of acceleration demands.

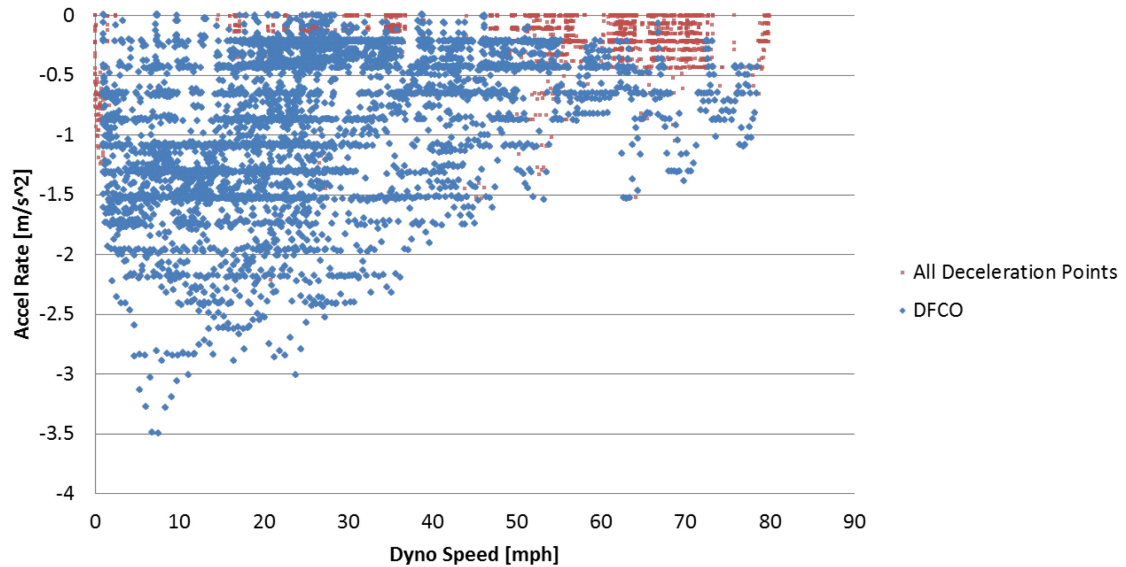


Figure 5.3.5: Volkswagen Jetta TSI Deceleration Fuel Cutoff (DFCO) Map

It is also pertinent to investigate the TSI's engine utilization strategy. Figures 5.3.6 to 5.3.8 display the vehicle's engine usage of the speed and load space, with a color map representing the percentage of cycle time spent at a given operating condition. The bins used to generate these figures are sized in increments of 200 rpm and 0.5 bar IMEP.

The TSI's engine utilization map for the hot start UDDS cycle is shown in Figure 5.3.6. As is common for conventional vehicles on the UDDS cycle, the TSI shows a significant portion of time spent idling, which occurs at approximately 700 rpm and 1 bar IMEP. A significant band can be seen along the bottom of the map between 800 and 1500 rpm and approximately 0 IMEP, which represents the vehicle's DFCO behavior. A series of vertical clouds at 1300 rpm and 1-6 bar IMEP represent operation during cruise.

An interesting characteristic unique to the TSI is the general shape of the utilization cloud. The vehicle shows a relatively narrow speed band with a wide variance in engine load, yielding a tall usage map. This is indicative of the TSI's tendency to increase engine load rather than downshift to provide power, reducing throttling losses while minimizing friction for optimal efficiency.

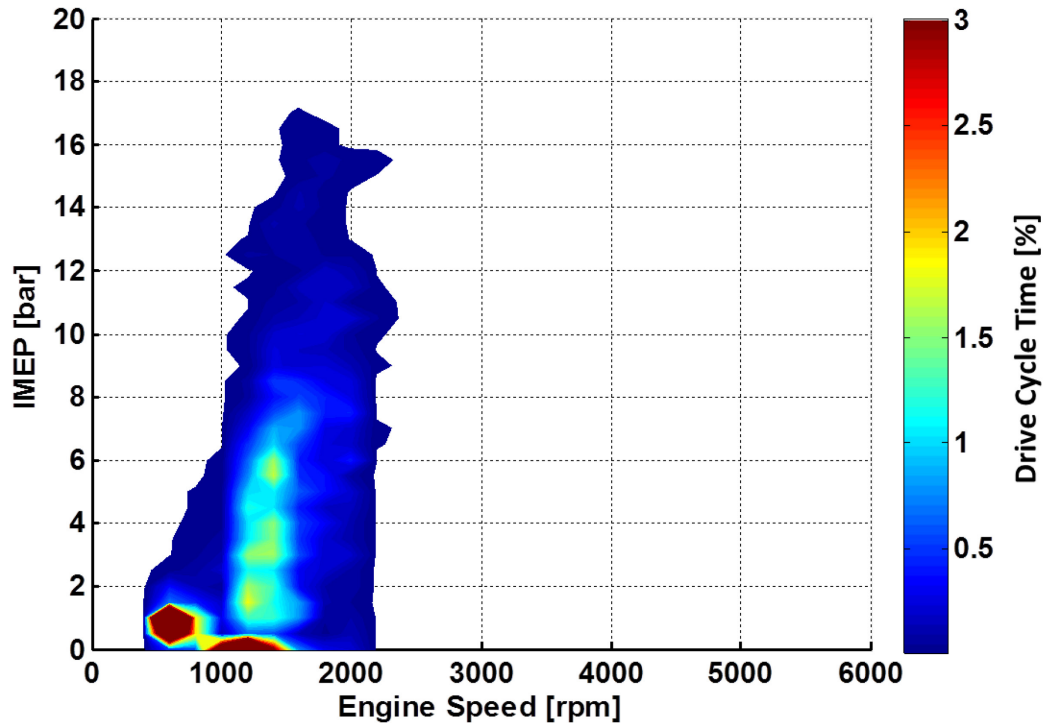


Figure 5.3.6: Volkswagen Jetta TSI Engine Utilization, UDDS HS Cycle

The TSI's operation over the more aggressive US06 cycle is shown in Figure 5.3.7. The size of the utilization map grows considerably for this aggressive cycle, reaching peak loads of 21 bar IMEP. IMEP values this high are usually prohibited by combustion knock in turbocharged gasoline engines, but the cooling effect of direct fuel injection helps to mitigate this issue. Efficient intercooling of the charge air may also play a role. Though a couple of excursions to higher speed ranges are shown, the engine spends the vast majority of time below 3000 RPM. This behavior is again indicative of the vehicle's strategy to use low speed, high load operation wherever possible. As in the

UDDS cycle, a centroid representing idle operation is visible as well as a band representing the vehicle's DFCO behavior. Another high utilization area falls around 2200 rpm between 6 and 10 bar, which represents operation during the majority of the highway portion of the US06 cycle.

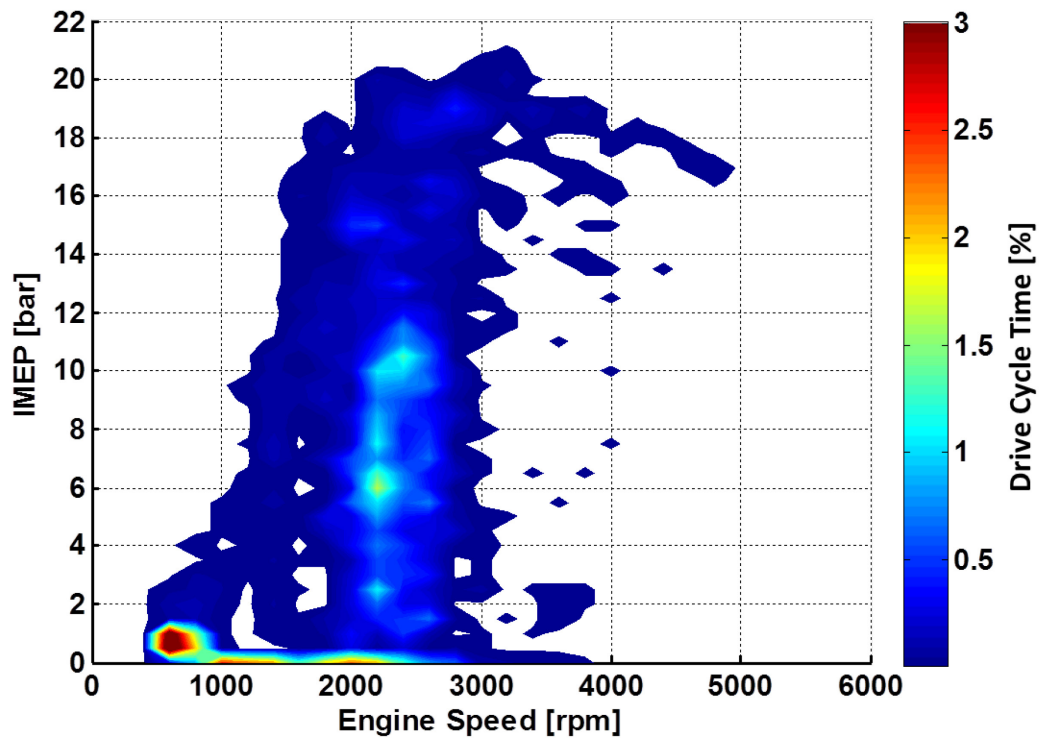


Figure 5.3.7: Volkswagen Jetta TSI Engine Utilization, US06 HS Cycle

Figure 5.3.8 shows the TSI's engine utilization over the HWFET cycle. Because of the nature of the cycle, there is very little opportunity for the vehicle to idle. A small band can be seen representing the TSI's aggressive DFCO behavior. Despite brief periods of operation at high load, the TSI spends the vast majority of cycle time operating around 2000 rpm and 5-7 bar IMEP, which is representative of cruising conditions over this cycle. Engine speed never exceeds 2400 rpm. It is worth noting that among the conventional vehicles in this study, the TSI exhibits the highest indicated engine load

during highway operation. This again reduces throttling losses and improves efficiency, and is a direct result of the engine's comparatively small displacement.

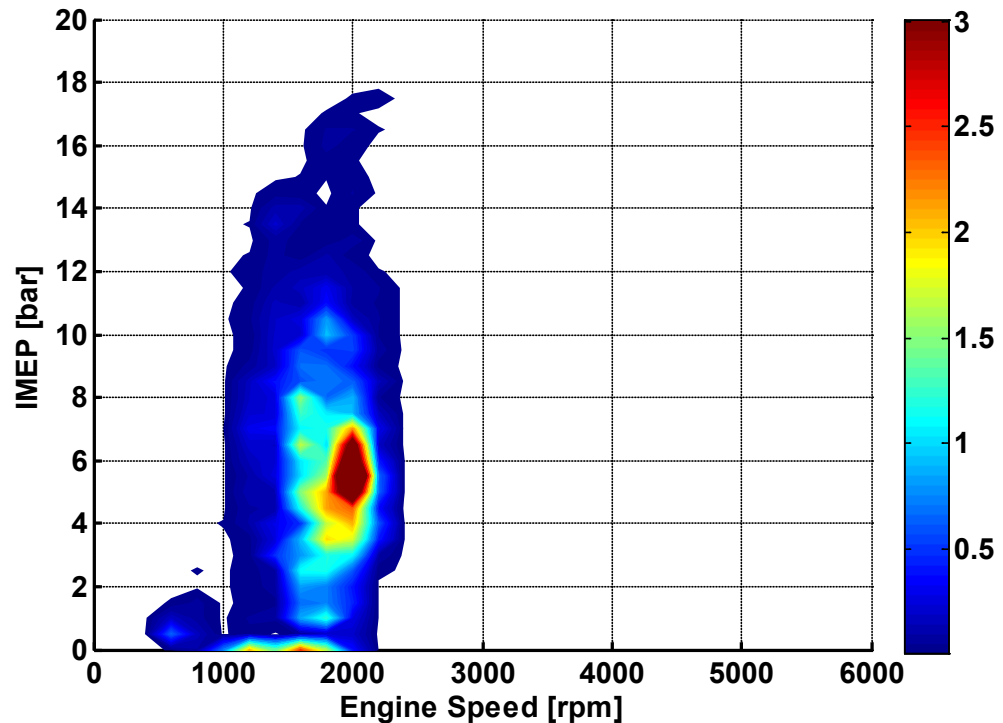


Figure 5.3.8: Volkswagen Jetta TSI Engine Utilization, HWFET Cycle

The TSI's fuel economy and efficiency can be further understood by examining the vehicle's performance at a range of steady state speeds. To accomplish this, the vehicle was tested on a steady state drive cycle involving 30 second steady state holds at a range of speeds as defined in Section 2.1.1. The TSI's average fuel economy and vehicle efficiency along with gear selection and required road load power are plotted in Figure 5.3.9.

The Jetta TSI's fuel economy peaks at 30 mph, achieving as much as 73 mpg in steady state operation. The fuel economy peak is fairly broad; the vehicle manages to return better than 50 mpg from 20 to 50 mph. The transmission upshifts as early as possible to minimize engine speed and maximize load; 4th gear is selected by 20 mph,

and 7th is engaged by the time the vehicle reaches 40 mph. Vehicle efficiency increases with increasing road load, peaking at 26% at 80 mph. As discussed in previous sections, vehicle efficiency and fuel economy do not necessarily correlate directly; fuel economy is a metric dependent on both vehicle efficiency and vehicle work requirements as determined by the operator's driving habits and the vehicle road load coefficients.

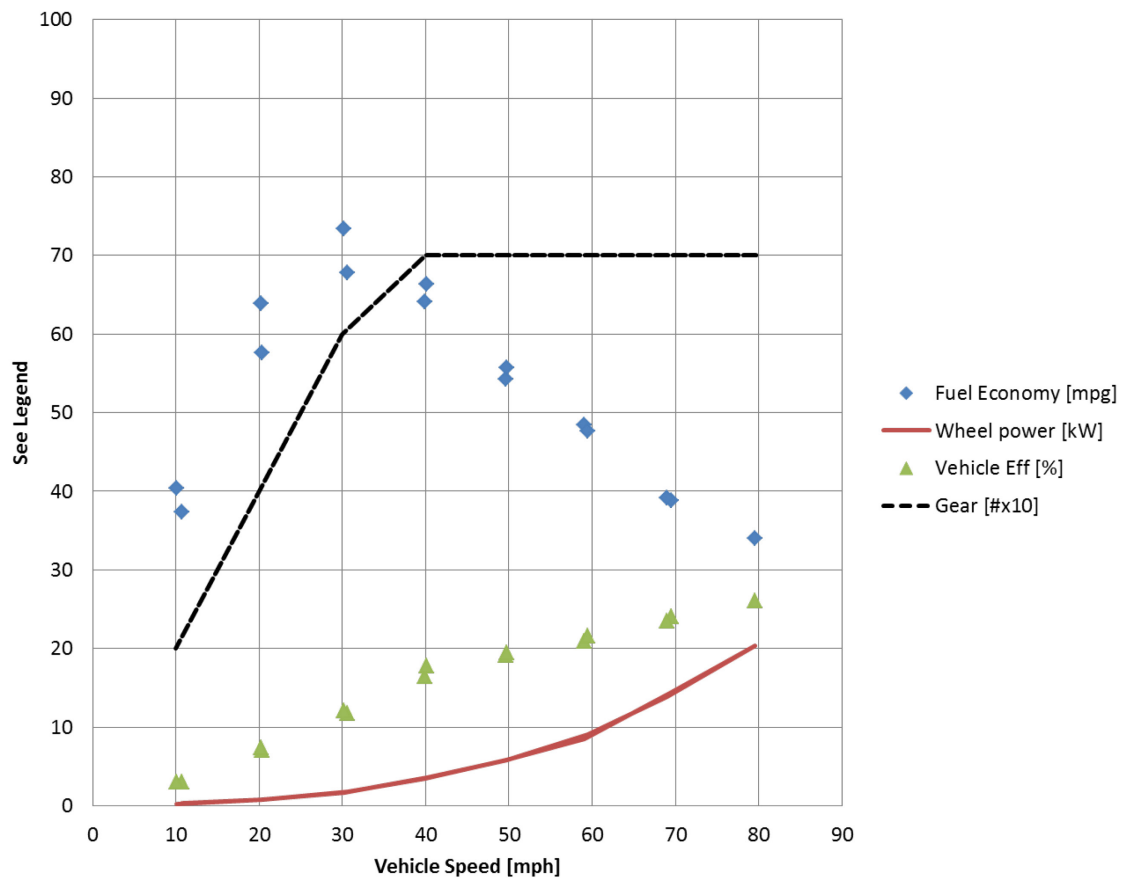


Figure 5.3.9: Volkswagen Jetta TSI Steady State Performance

5.4 Cycle-Based Heat Loss Proportions

In Section 5.3, it was shown that the Jetta TSI's cycle-based vehicle efficiency varied from 17.4% to 24.9% depending on the nature of the drive cycle and whether the test was performed under cold start or hot start conditions. In order to better understand where the remainder of the vehicle's fuel energy is lost, the TSI was instrumented with

flow sensors and thermocouples to measure coolant enthalpy and exhaust enthalpy changes during each drive cycle. Coolant flow rates were measured with turbine-based Omega FTB flow sensors, while exhaust mass flow was calculated using the measured fuel flow rate and vehicle-reported exhaust equivalence ratio. Coolant enthalpy calculations were performed using the coolant temperature change across the vehicle's heat exchangers, while exhaust enthalpy was calculated using exhaust temperature measured via thermocouple and the test cell ambient temperature as the reference or dead state.

Care must be taken when measuring coolant-based heat losses to account for the thermal capacity of the system. During cold starts, a considerable amount of time passes during which the coolant within the engine block is warmed to operating temperature by heat losses from combustion and engine friction. During this time the vehicle's thermostat remains closed and coolant flow remains static through the heat exchangers. Once the vehicle's fluids have reached operating temperature, the thermostat opens and flow is driven by the water pump. Only in this latter case can coolant losses be measured effectively. There also exists a transport delay between the time that a given amount of heat is transferred to the coolant and the time when it is shed through the heat exchangers. For these reasons, analysis in this section is restricted to hot start conditions and full drive cycles.

Figure 5.4.1 shows the measured proportions of fuel energy expended by the TSI during the UDDS, HWFET, and US06 cycles. The total measured proportion varies between 63.4% on the UDDS cycle to 74.5% on the US06 test. The remaining fraction of fuel energy is lost through other sources, such as heat loss from engine and ancillary component surfaces, coolant losses not captured across the heat exchangers, mechanical friction, and incomplete combustion (though emissions requirements and efficiency targets drive these to be quite small).

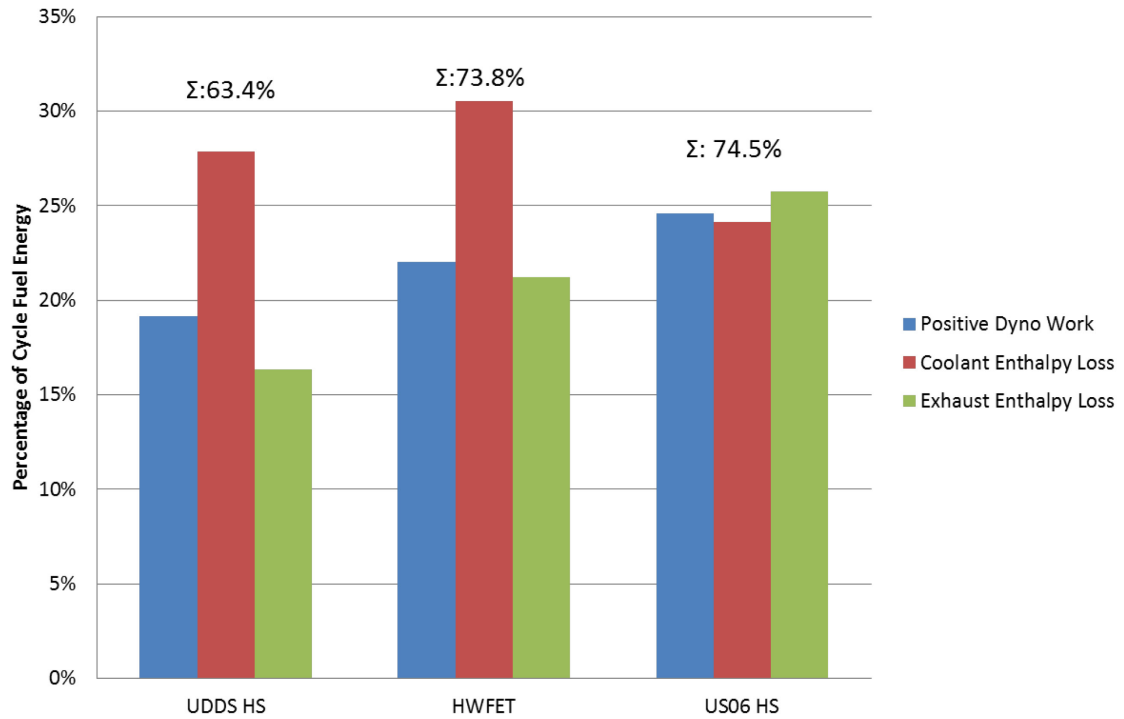


Figure 5.4.1: Volkswagen Jetta TSI Cycle-Based Fuel Energy Usage

In all three cases, coolant losses are a significant source of waste heat over the course of an engine cycle. In the UDDS and HWFET cycles, coolant losses represent the greatest proportion of measured energy lost, followed by the positive dynamometer work fraction (which is equivalent to vehicle efficiency as defined in Section 2.1.5). As the average engine load over the drive cycle increases, both measured vehicle efficiency and exhaust losses increase markedly, with the latter peaking at 25.8% on the US06 cycle.

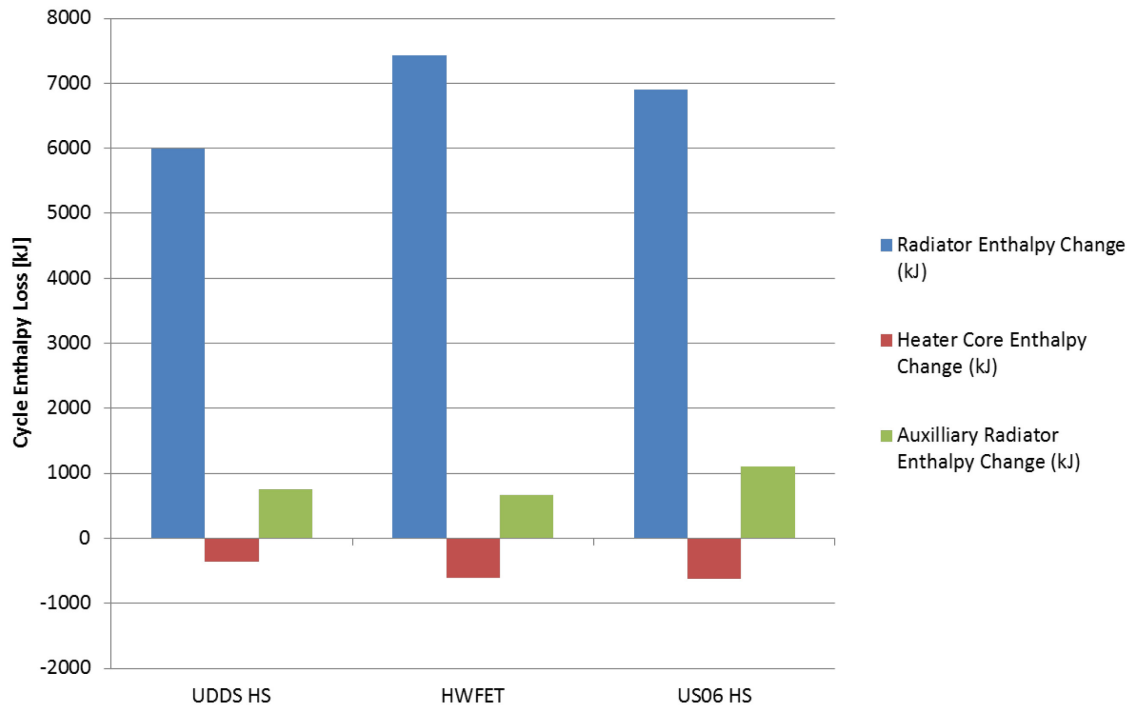


Figure 5.4.2: Volkswagen Jetta TSI Coolant Enthalpy Change by Source

Figure 5.4.2 shows the enthalpy change across each of the TSI's three heat exchangers for the UDDS, HWFET and US06 cycles. The thermal energy shed through the radiator is significantly larger than that shed through the auxiliary radiator. The auxiliary radiator is responsible only for cooling the turbocharger and intercooler and is driven by an electric water pump which operates generally only during periods of high intake manifold pressure (significant boosting) during aggressive acceleration. Even during the US06 cycle, coolant flow through this exchanger is minimal in comparison to the primary radiator. The heater core also showed minimal enthalpy loss. In this case the flow rate of coolant is directly related to engine speed, but the change in temperature across the heat exchanger is minimal because the HVAC fan was not operated. In all three cases the enthalpy change across the heater core was actually negative, indicating that the enthalpy of the coolant rose as it passed through the heater core loop. In the case of the HWFET cycle, the thermocouples on either side of this heat exchanger exhibit a consistent offset of roughly 1.3 degrees Celsius. This may have to do with the

temperature profile distribution in the engine bay affecting coolant temperature in the hoses.

5.5 Cycle-Based Emissions

The TSI's tailpipe constituents were measured in order to observe the vehicle's emissions behavior over the drive cycles. NO_x, THC and CO were measured, and the total level of each substance for each drive cycle is listed in Table 5.5.1.

Table 5.5.1: Volkswagen Jetta TSI Total Emissions by Cycle

Test Description	NO _x [mg]	THC [mg]	CO [mg]
UDDS CS	170.0	355.7	2523.5
UDDS #3	366.2	18.8	367.9
HWY	121.2	88.5	437.5
US06 CS	768.1	1224.2	34114.6
US06 HS	334.1	526.0	18790.4

The cold start US06 cycle shows the greatest level of tailpipe emissions for the TSI by a fair margin for all three measured emissions. Trends concerning the relative levels of tailpipe emissions for the hot start iteration are similar, but the total emissions are only 43-53% of those seen for the cold start test. This largely has to do with the cold start behavior of the vehicle. Emissions of NO_x and THC are plotted for the US06 hot and cold start cycles in Figure 5.5.1 and 5.5.2.

The TSI exhibits a very aggressive catalyst warmup strategy during cold start. Combustion timing is retarded to the point where the engine was found to misfire occasionally, suggesting a very aggressive cold start calibration. The vehicle exhibits this behavior regardless of whether the pressure-indicating spark plug or stock spark plug is installed. Such aggressive retardation results in high exhaust gas temperatures that speed catalyst warmup, but also results in high engine-out emissions levels of THC. This, combined with low catalyst temperatures, results in a large emissions spike during warmup. This can be seen in Figure 5.5.1 as a large increase in integrated emissions

levels directly following engine start at the beginning of the test. This same behavior is much less evident for the hot start test.

Catalyst temperature rises quickly, both due to the aggressive nature of this cycle as well as the dedicated catalyst lightoff strategy. Rates of emissions generation are higher for the cold start test during the first third of the cycle. After this, the emissions system is operating as designed and further emissions are very similar between the two tests.

Marked rises in the rate of emissions generation typically correspond to hard acceleration events. As seen in Section 5.3, the TSI chooses to operate under high loads with significant boost in order to generate sufficient power for hard accelerations. This results in high peak temperatures that favor NO_x production. The vehicle also exhibits a tendency to richen the fuel mixture during very aggressive operation, resulting in higher THC emissions. Outside of these conditions, emissions levels are quite low.

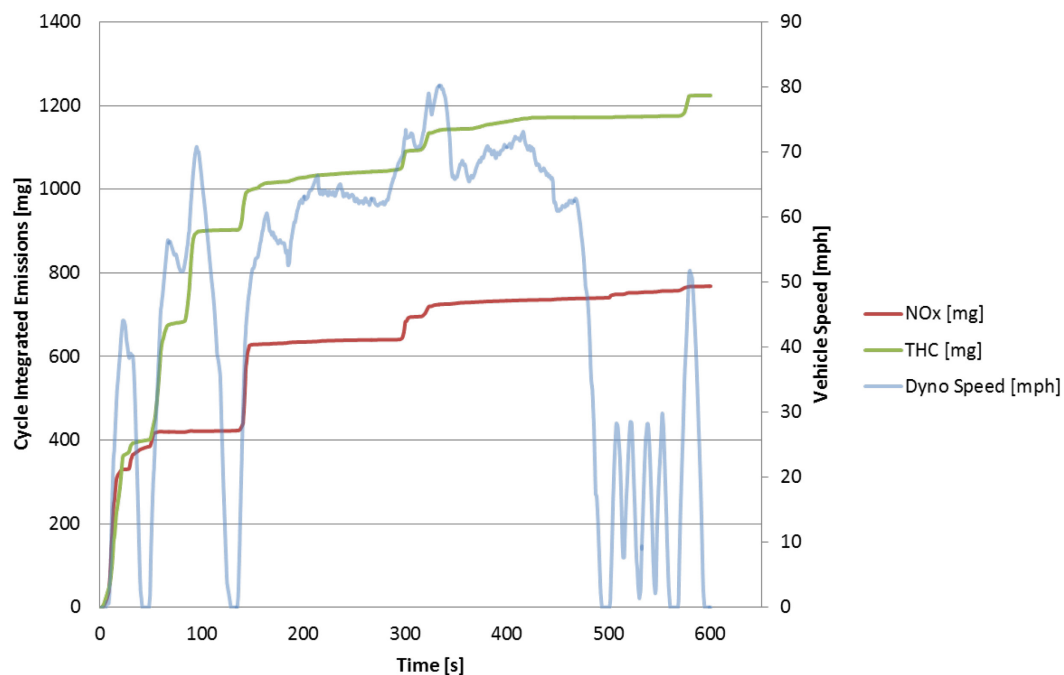


Figure 5.5.1: Volkswagen Jetta TSI US06 Cold Start Integrated NO_x and THC

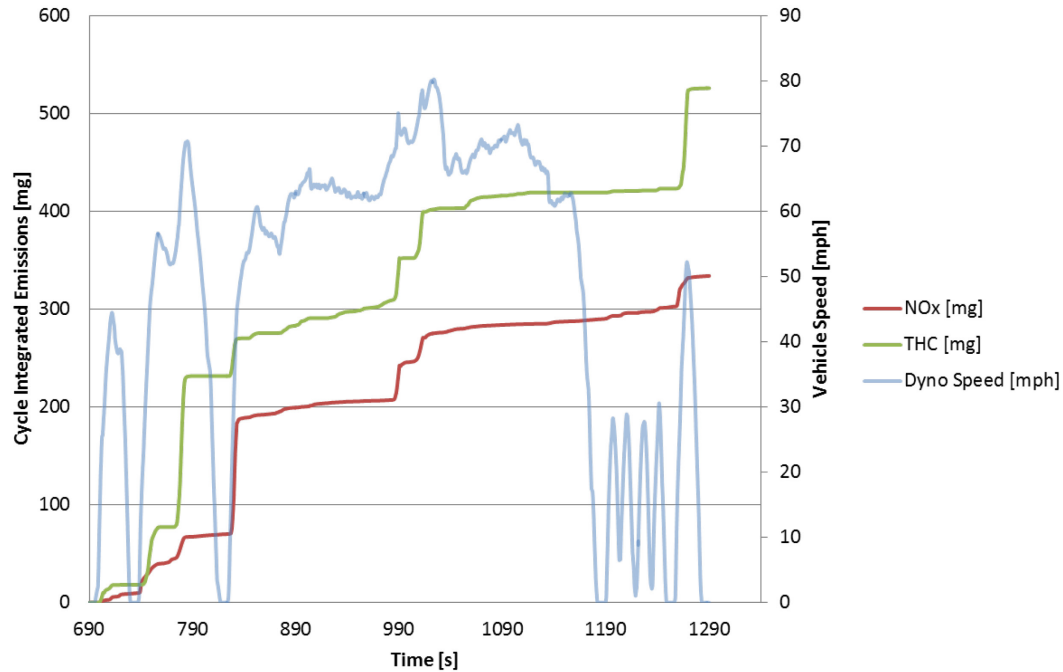


Figure 5.5.2: Volkswagen Jetta TSI US06 Hot Start Integrated NOx and THC

5.6 Engine Indicating System Measurements

During the course of drive cycle testing, cylinder pressure data was recorded for the TSI over all cycles on a crank angle basis. This data can be used to understand the characteristics of the engine's combustion system by observing parameters including IMEP, combustion timing, and heat release rates. It should be noted that the operating points are representative of single engine cycles. Due to the transient nature of drive cycle testing, it is difficult to extract sufficient data to provide averaged engine pressure traces. Instead, the cycles shown here are used mainly to illuminate general P-V behavior. For the purposes of this study, the data was used to draw qualitative conclusions about the engine's operating strategy.

Three engine operating points are examined in this section. Point 1 is representative of idle conditions at 659 RPM and 0.7 bar IMEP with the vehicle stopped and the transmission clutch open. Point 2 is taken at 2165 RPM and 5.7 bar IMEP and is

representative of cruising conditions like those found during the HWFET cycle. Point 3 involves aggressive engine loading at medium speed, which is the vehicle's preferred method of delivering power for acceleration and passing maneuvers. All points were taken with the vehicle at full operating temperature. Table 5.6.1 catalogues several parameters that illustrate engine behavior at these points. Figures 5.6.1 through 5.6.3 display pressure-volume (P-V) diagrams illustrating the engine cycle during each operating point using a log-log scale. Engine strokes are labeled in Figure 5.6.1 for convenience.

Table 5.6.1: Volkswagen Jetta TSI Engine Operating Points

		Point 1	Point 2	Point 3
Engine Speed	[rpm]	659	2165	3164
IMEP	[bar]	0.7	5.7	19.6
Peak Pressure	[bar]	5.37	35.98	73.3
Burn Duration	[ms]	10	2.2	1.6
Angle, 50% MFB	[CAD]	48.9 ATDC	5.9 ATDC	22.7 ATDC
Angle, PMAX	[CAD]	0 ATDC	11.9 ATDC	27.9 ATDC

Figure 5.6.1 illustrates the idling behavior of the TSI. At this point, all of the power generated is used to overcome losses related to friction and pumping work to allow the engine to maintain a steady speed. The intake manifold pressure is quite low because the engine is aggressively throttled, leading to a large pumping loop indicating significant pumping losses. Though pumping losses are greatest at idle, the small size of the engine helps to limit friction losses and reduce the work required for idle; the engine idle load is a low 0.7 bar IMEP.

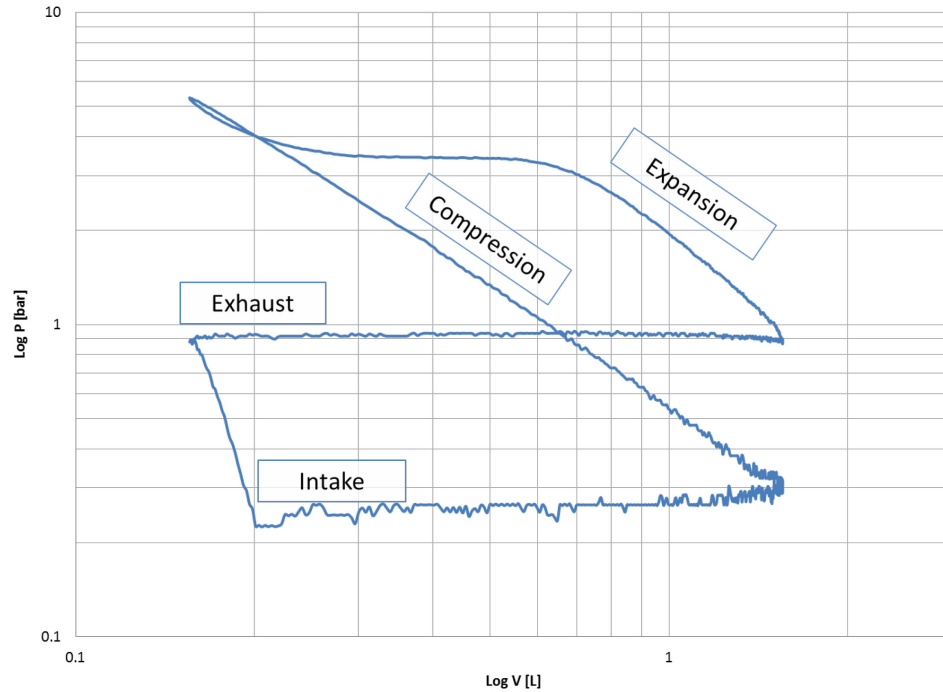


Figure 5.6.1: Volkswagen Jetta TSI P-V Diagram, Point 1

It can also be seen that the vehicle idles with very late ignition timing at idle. Following the compression and expansion strokes on the PV diagram shows that cylinder pressure drops slightly after TDC. Because no combustion is occurring yet, heat lost from the compressed cylinder charge results in a slight but noticeable pressure drop until combustion begins later in the cycle. This late timing is used for two reasons: First, late combustion timing raises exhaust gas temperatures and helps to keep the aftertreatment catalyst at operating temperature. Second, idling with late ignition timing provides a quickly accessible torque reserve that can be used to provide fast off-idle response by quickly advancing spark and to stabilize idle speed in response to transient accessory loads such as the alternator and A/C compressor. The cost of this behavior is reduced idle efficiency. At this condition, maximum cylinder pressure actually occurs at TDC, with the 50% mass-fraction-burned (MFB) point falling much later at 48.9 degrees after TDC.

Figure 5.6.2 illustrates the TSI's engine behavior while the vehicle is at medium speed cruising conditions. Here the engine is rotating at 2165 RPM. The engine's small

displacement requires a higher load to produce the required motive power, resulting in an IMEP measurement of 5.7 bar. This characteristic also results in lower throttling losses which can be observed in the smaller area covered by the pumping loop at this condition. These factors help to improve the efficiency of the engine at part load conditions.

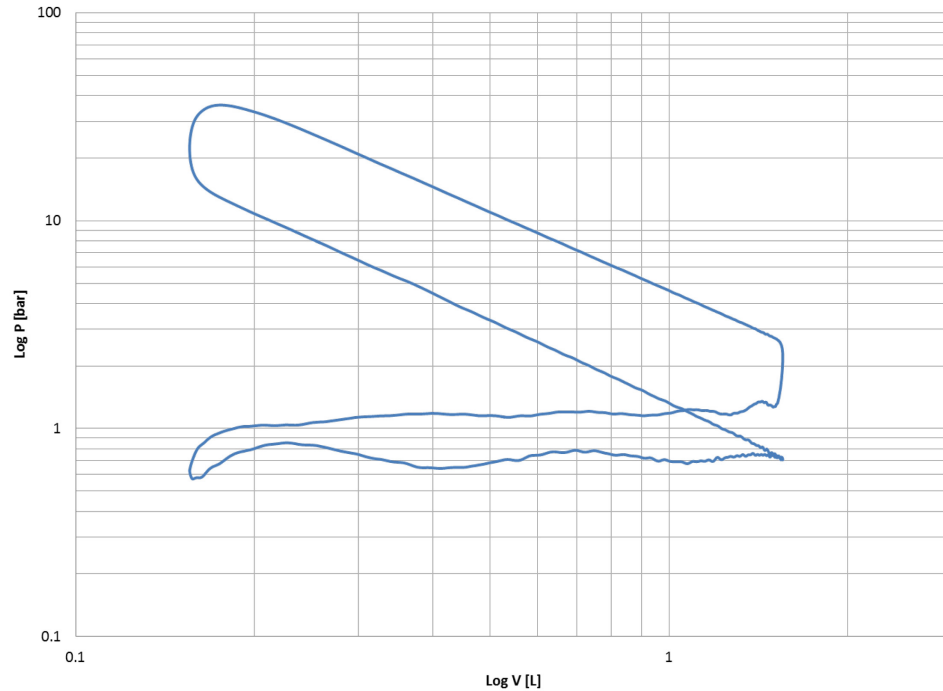


Figure 5.6.2: Volkswagen Jetta TSI P-V Diagram, Point 2

Engine timing is also advanced considerably at this operating condition. The maximum cylinder pressure of 35.98 bar occurs 11.9 degrees after TDC. This facilitates more efficient engine operation by increasing peak expansion stroke pressures. The engine mass flow rate is also higher at this condition, resulting in higher exhaust backpressure which increases pumping work somewhat. Combustion duration is also significantly shorter than at idle. This is affected by several factors, including in-cylinder turbulence, charge density and ignition timing.

Figure 5.6.3 illustrates a point of extremely high load for the TSI's engine. IMEP at this point is 19.6 bar, with a peak cylinder pressure of 73.3 bar occurring 27.9 degrees after TDC. At this point, the engine is operating with the throttle nearly wide open, and the turbocharger is making appreciable boost. This can be observed in the pumping loop, where both intake and exhaust manifold pressures are well above atmospheric pressure. The turbocharger both helps to minimize pumping losses and to increase the mass flow rate of air, thereby enabling larger mass flow rates of fuel that provide high load capability and favorable power density.

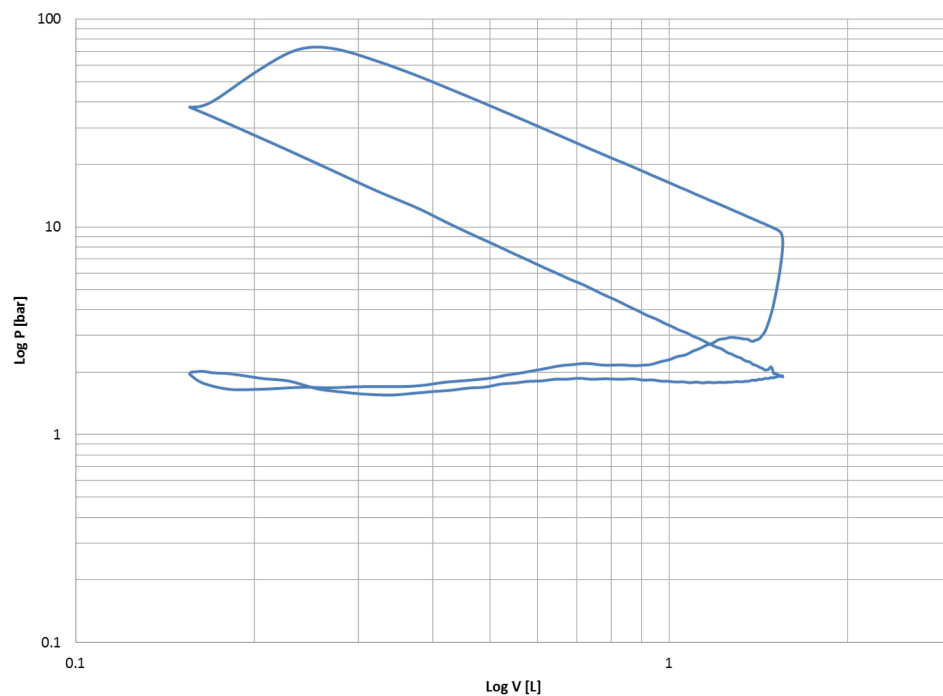


Figure 5.6.3: Volkswagen Jetta TSI P-V Diagram, Point 3

It is interesting to note that ignition timing at Point 3 is considerably later than at Point 2, with the 50% MFB point occurring almost 17 crank angle degrees later in the cycle. This phenomenon is also visible in Figure 5.6.3 as the piston begins the expansion stroke before appreciable pressure rise takes place. The retarded timing is most likely implemented to mitigate knock; the engine is operating at very high loads and medium speed, providing for high charge pressures and temperatures that can result in high end

gas temperatures. These end gas temperatures carry forward to the next cycle, elevating peak temperatures and increasing the likelihood of an engine-damaging knock event. Retarding the combustion timing reduces peak temperatures and helps to prevent knock. Similarly, it was explained in Section 5.3 that the vehicle richens the fuel mixture under high loads; additional fuel hurts efficiency, but the resulting higher specific heat of the mixture also contributes to reduced cylinder temperatures. These factors allow the engine to be able to endure high loads at the expense of efficiency.

A final interesting phenomenon visible at Point 3 is that the intake manifold pressure is higher than the exhaust pressure at the beginning of the intake stroke. This is a direct result of the engine being equipped with a turbocharger supplying significant boost. When the intake valve opens, the pressurized air in the intake manifold does positive net work on the piston. As the piston travels toward BDC, pressure is reduced as the charge is inducted.

Chapter 6 MY2010 Toyota Prius 1.8

6.1 Relevant Vehicle Features

The final vehicle considered for this thesis work is a 2010 Toyota Prius. The Prius is a gasoline-electric hybrid vehicle and was designed with the goals of maximizing fuel economy while simultaneously reducing tailpipe emissions. This vehicle was designed from the ground up to implement an advanced hybrid architecture, and it features a number of innovations that help to push efficiency and fuel economy to high levels.

The Prius' 2ZR-FXE engine is a purpose-built inline four-cylinder gasoline unit displacing 1.8 liters. It features an over-expanded Atkinson combustion cycle, wherein the expansion stroke is longer than the compression stroke. The geometric compression and expansion ratios are identical at 13.0:1, but the effective compression ratio is reduced by late closure of the intake valve. This serves to prevent combustion knock while preserving the large expansion ratio for optimum thermal efficiency. The 2ZR-FXE also incorporates a cooled exhaust gas recirculation (EGR) system and variable valve timing on the intake cam. It is also fitted with an electric water pump that reduces parasitic losses on the crankshaft and allows for coolant flow to be adjusted independently of engine speed. In order to speed engine warmup during cold start conditions, the vehicle incorporates a heat exchanger in the exhaust system that serves to reclaim exhaust waste heat to increase engine coolant temperature. The engine output is rated at 98 brake horsepower @ 5,200 rpm and 105 lb.-ft. of torque at 4,000 rpm.

The 2ZR-FXE engine is incorporated into the Prius' Toyota Hybrid System. This system consists of the gasoline engine, a 1.4 kWh energy storage battery and power inverter, a pair of motor/generators that are used to provide motive force and reclaim kinetic energy, and a power split device that consists of a system of planetary gears that allows the motors to interact with the engine and the drive axles. This system provides a high degree of engine operating flexibility, allowing the 2ZR-FXE to operate in the most efficient manner possible at any given time. Excess energy converted by the engine or

recovered during regenerative braking is stored in the battery for later use. The Toyota Hybrid System is pictured in Figure 6.1.1.

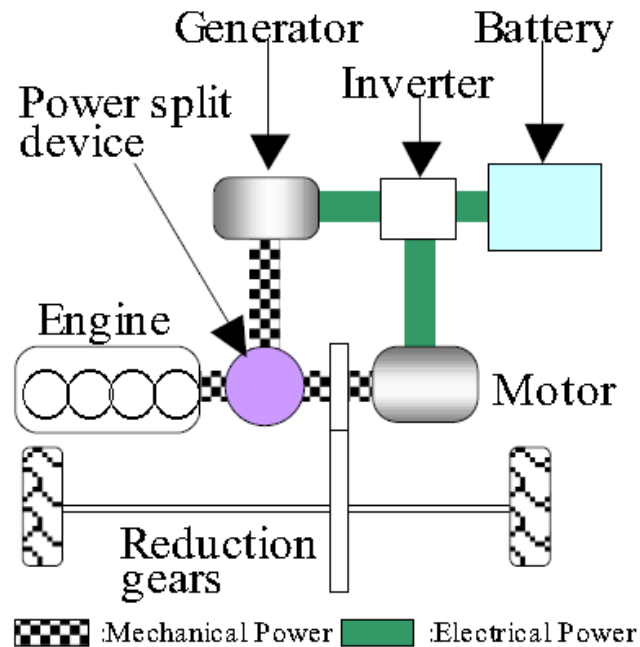


Figure 6.1.1: Toyota Hybrid System Architecture. Reprinted with permission from SAE Paper 2009-01-1061 © 2009 SAE International. Further use or distribution is not permitted without permission from SAE.

The Prius' power split device houses a planetary gear set that serves to facilitate interaction between the engine, motor/generators and differential. It allows the Prius to operate with the engine providing motive force, charging the battery, or both. This transmission can provide an infinite number of effective gear ratios depending on the input speeds of the three components, and as such is termed a continuously variable transmission (CVT).

Like the other vehicles studied in this work, the Prius is of FF configuration denoting a front-engine, front-wheel-drive layout. It is classified as a midsize car, and its test weight category as defined by the EPA is 3,375 lbs. Relevant vehicle parameters for the Prius are listed in Table 6.1.1. Fuel properties are available in Table 4.2.2, and the vehicle is pictured on the chassis dynamometer in Figure 6.1.2.

Table 6.1.1: Toyota Prius Vehicle Metrics

Year/Make/Model		2010 Toyota Prius
Body Type		4 dr Hatchback
Engine		1.8L 16V VVT "Atkinson" I4 Gasoline
Compression Ratio		13.0:1
Rated Power		73 kW (98 hp) @ 5,200 rpm
Rated Torque		105 lb.-ft. @ 4,000 rpm
Hybrid System		Electric Motor & 1.4 kW-hr NiMH Battery Pack
Total System Output		97 kW (130 hp)
Transmission		Planetary Gearset CVT
EPA Fuel Economy	Urban	51
	Highway	48
	Combined	50
Road Load Coefficients	Test weight	3375
	Cd	0.25
	a	18.5
	b	0.0223
	c	0.0181
Vehicle Performance		
WOT Acceleration	0-60	11.0 s (ANL)
	30-50	3.8 s (ANL)
	50-70	5.9 s (ANL)

Table 6.1.2: Toyota Prius Fuel Properties

Fuel Name:	Tier II EEE HF437	Density:	0.74	[g/ml]
Carbon Weight Fraction:	0.8647	Net HV:	18493	[BTU/lbm]

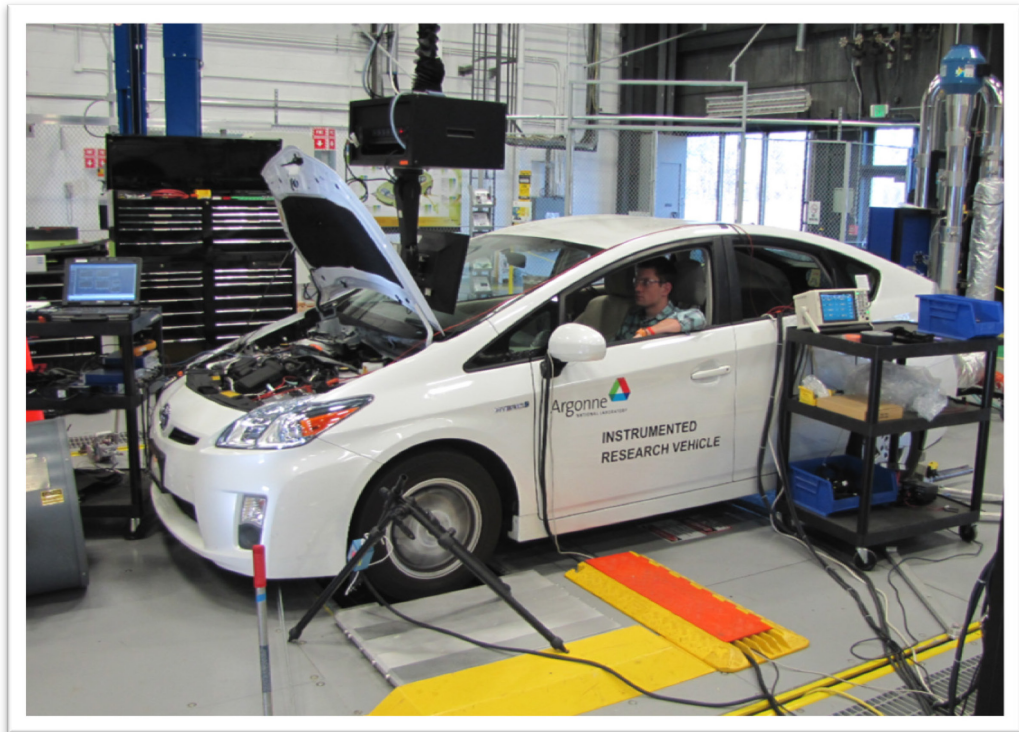


Figure 6.1.2: Toyota Prius on Chassis Dynamometer

6.2 Instrumentation Specifics

In order to gather data to facilitate the research goals of this project the Prius was instrumented with a collection of sensors that measure vital operating signals. The Prius has been the subject of previous research at Argonne National Laboratory and significant investments in time, expertise and materials have been made in order to make the vehicle's operation as transparent as possible on the dynamometer. Signals used in this thesis work are detailed in this section.

In order to reduce the necessary investment required for physical instrumentation, a number of signals reported by the vehicle over the CAN bus were decoded and recorded. These include high voltage battery pack current and voltage, motor/generator speed, mechanical friction brake torque, accelerator pedal position, and exhaust equivalence ratio among others.

The Prius was also instrumented with a number of thermocouples to provide comprehensive temperature measurements. Engine and transmission oil temperatures are available, as well as battery pack temperatures and battery cooling air temperature. Exhaust temperature was also measured in order to calculate exhaust gas enthalpy changes. Several thermocouples were installed in the cooling system to provide the temperature change across the radiator, heater core, and exhaust waste heat recovery exchanger. Like the other vehicles in this test, the Prius was also equipped with Omega FTB series flow sensors to aid in the calculation of coolant enthalpy changes.

In order to paint a detailed picture of mechanical powertrain efficiency, the Prius was fitted with a custom engine torque sensor. This required the removal and disassembly of the vehicle powertrain to facilitate the installation of a modified transmission input shaft incorporating a series of strain gauges and a wireless inductive antenna. The strain gauges were chosen with similar expansion rates to the material to negate measurement drift caused by material expansion. They were carefully calibrated to a range of known torques applied to the input shaft. The resulting calibration curve is used to determine the engine output torque at any given time. This combined with engine speed allows for the calculation of brake engine power. The custom input shaft and antenna are shown mounted in the Prius' transaxle in Figure 6.2.1.

In order to accommodate for the extra axial length of the modified input shaft cause by the addition of the strain gauges, a custom spacer was designed to engage the engine output shaft and transmission input shaft. A spacer plate of similar width was between the transaxle bell housing and engine block. The modified powertrain was then reinstalled in the vehicle. In order to preserve driveline geometry, the transmission's location in the engine bay remained unchanged while the engine was shifted approximately 1.2" towards the passenger frame rail by means of a modified engine mount. The transmission and spacer plate are shown in Figure 6.2.2.

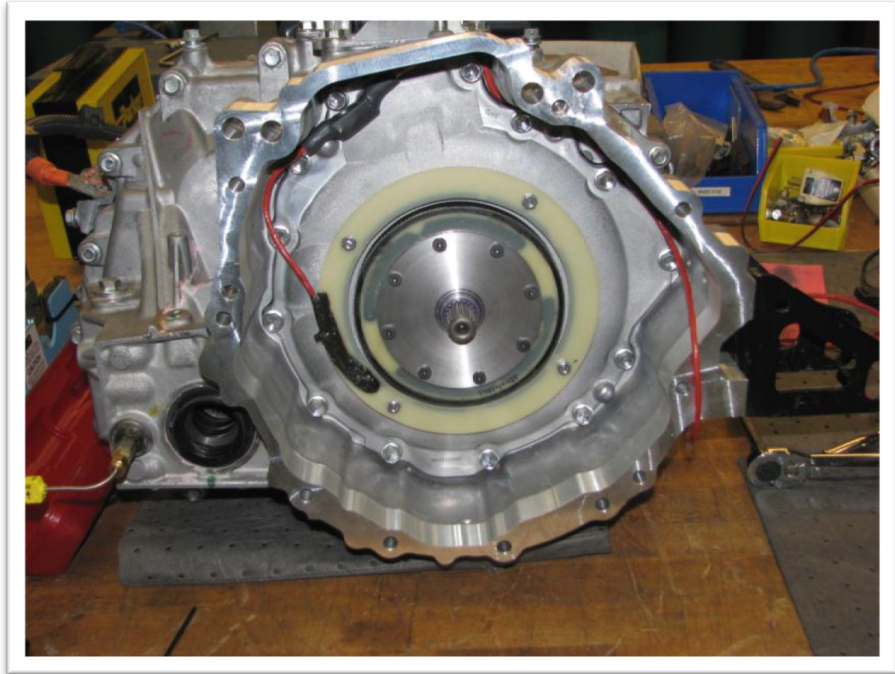


Figure 6.2.1: Toyota Prius Engine Output Torque Sensor

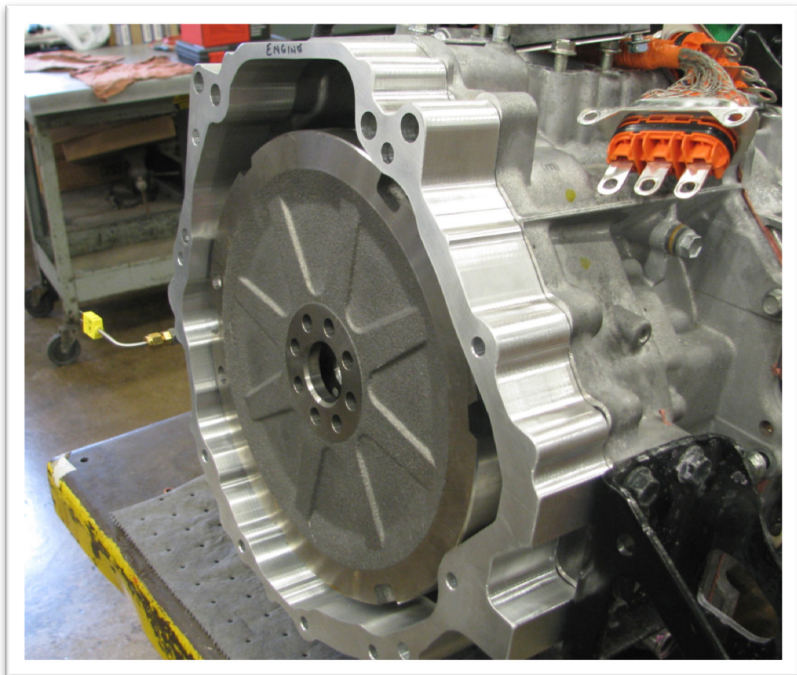


Figure 6.2.2: Toyota Prius Transaxle with Spacer Plate

In order to measure the combustion parameters of the 2ZR-FXE engine, a modified spark plug was purchased from AVL that incorporates a piezoelectric pressure transducer. The spark plug was installed in engine cylinder 1 in place of the stock spark plug and served to preserve proper engine functionality while providing high resolution cylinder pressure measurements. The engine's top dead center offset was determined using an AVL 428 TDC alignment probe while the stock engine position system was used in conjunction with an AVL Vehicle Interface module to provide high resolution crank angle data at 0.5 degrees per mark for use in calculating IMEP.

As with the other vehicles studied in this work, the Prius' emissions were measured with the combination of a Sensors, Inc. Semtech emissions measurement system in conjunction with an AVL Direct Volume Exhaust device.

Finally, a Hioki power analyzer was used to provide a physical measurement of electrical power expenditures via voltage taps and inductive current clamps. The high voltage battery pack, DC-DC converter used to provide accessory power and the 12 volt battery system were each instrumented in this manner.

6.3 Drive Cycle Performance

As with the other vehicles included in this work, the Toyota Prius was subjected to a series of chassis dynamometer drive cycles in order to gauge its performance under different operating conditions. The tests were conducted according to the test plan document found in Appendix A. It should be noted that in this context the label 'CS' designates a test performed under cold start conditions wherein the vehicle is allowed to soak at the test cell temperature for a period of at least twelve hours. Conversely, the label 'HS' designates a hot start test where the vehicle has already attained operating temperature prior to the beginning of the drive cycle. The Prius' extensive instrumentation plan allowed for the calculation of a number of illuminating vehicle metrics as discussed in Section 2.1.5. Table 6.3.1 catalogues the Prius' fuel economy and overall vehicle efficiency.

Table 6.3.1: Toyota Prius Drive Cycle Economy and Vehicle Efficiency

Test Description	Test #	Fuel Economy (mpg)	Vehicle Efficiency
UDDS CS	71306040	59.2	26.0%
UDDS HS	71306041	70.2	30.9%
UDDS #3	71306042	72.0	31.6%
HWFET	71306044	69.4	25.2%
US06 CS	71306051	38.8	27.2%
US06 CS City	71306051	24.9	26.8%
US06 CS Hwy	71306051	46.2	27.5%
US06 HS	71306050	43.7	30.7%
US06 HS City	71306050	29.3	31.4%
US06 HS Hwy	71306050	50.8	30.4%

It should be noted that when testing hybrid-electric vehicles for fuel economy, care must be taken to ensure that the results are not significantly affected by a change in total onboard electric energy. During a given drive cycle, the vehicle battery's state of charge (SOC) may change significantly. If this change in battery energy is not accounted for, the effect of this energy on fuel consumption is unknown and the fuel economy measurements are not representative of the overall propulsion energy. Fortunately, most non-plug-in hybrid-electric vehicles utilize a 'charge sustaining' strategy. When subjected to multiple iterations of the same drive cycle, the vehicle battery's state of charge will normalize to a given level depending on the demands of the drive cycle. So long as this particular charge level is reached at the beginning and end of the drive cycle, the net energy change of the battery is small enough that the SOC-related effect on fuel economy is negligible. The criteria given for this in SAE J1711, "Recommended Practice for Measuring the Exhaust Emissions and Fuel Economy of Hybrid-Electric Vehicles, Including Plug-in Hybrid Vehicles" is that the total net energy change (NEC) of the battery over a drive cycle must be less than 1% of the total fuel energy consumed during that same cycle. All tests conducted for the Prius for this thesis were properly charge-sustaining, with battery NEC of less than 1% of consumed fuel energy. Figure 6.3.1 illustrates the Prius' NEC behavior for a hot start UDDS cycle. The total battery NEC in this case is 0.17 kWh, or about 0.5% of the consumed fuel energy.

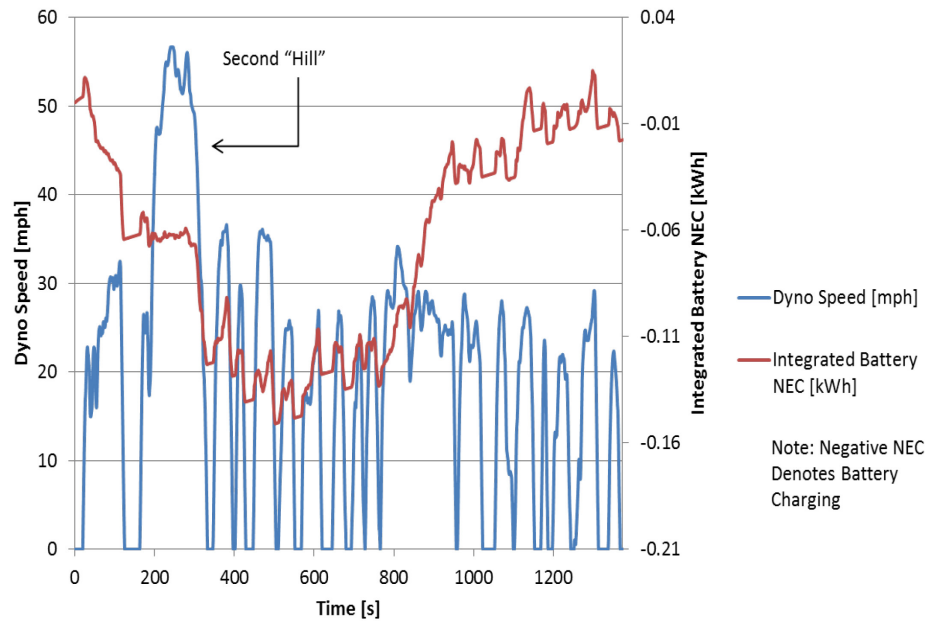


Figure 6.3.1: Toyota Prius Battery Net Energy Change, UDDS Hot Start Cycle

The Prius’ drive cycle fuel economy ranges from 24.9 mpg on the city portion of the cold start US06 cycle to 72.0 mpg on the hot start UDDS test. It is interesting to note that the Prius’ fuel economy peaks on the relatively low speed, low load UDDS cycle; the vehicle’s ability to recapture kinetic energy under braking plays a significant role in this result. Fuel economy on the HWFET cycle was measured at 69.4 mpg.

Though detailed comparison between vehicles is left to Chapter 7, it can be said that the Prius exhibits significant efficiency gains over the other vehicles considered in this thesis. The Prius’ vehicle efficiency peaks on the UDDS cycle at 31.6%, and this figure never drops below 25% over a given drive cycle. These dramatic increases in efficiency are due largely to the benefits of hybridization; namely regenerative braking, EV operation, idle fuel reduction, and increased authority over engine usage.

When the Prius is decelerating, the motor/generators can be used to slow the vehicle while generating electric power that is used to replenish the battery. Unless the vehicle’s battery SOC is so high that it will not permit further energy recovery,

regenerative braking is used often and is a significant benefit inherent in hybrid-electric architecture. Careful inspection of Figure 6.3.1 shows that the battery NEC often realizes significant negative changes (denoting battery charging) during long decelerations, such as the end of the second hill of the UDDS cycle as denoted in the figure. These changes primarily represent the energy recaptured during regenerative braking, and are significant on the UDDS and US06 drive cycles.

During low speed operation, the Prius is able to operate in EV mode, stopping the combustion engine and operating solely on battery power. Figure 6.3.2 illustrates the Prius' engine operating behavior over the hot start UDDS cycle. It can be seen that for large portions of the cycle, the Prius chooses to operate in EV mode with an engine speed of 0 rpm. The Prius operates its engine only 33.2% of the time during the UDDS hot start drive cycle. The engine is most often operated under acceleration conditions that require significant power output, but is stopped during deceleration events. This saves a significant amount of fuel by eliminating inefficient, low-load engine operation.

In order to better understand the EV mode capability of the Prius, the vehicle's behavior over the UDDS, HWFET, and US06 cycles was considered. All positive acceleration events were plotted against the speed at which they take place. A filter was then applied to determine which points were achieved with the engine unfueled, signifying EV operation. Figure 6.3.3 illustrates these results.

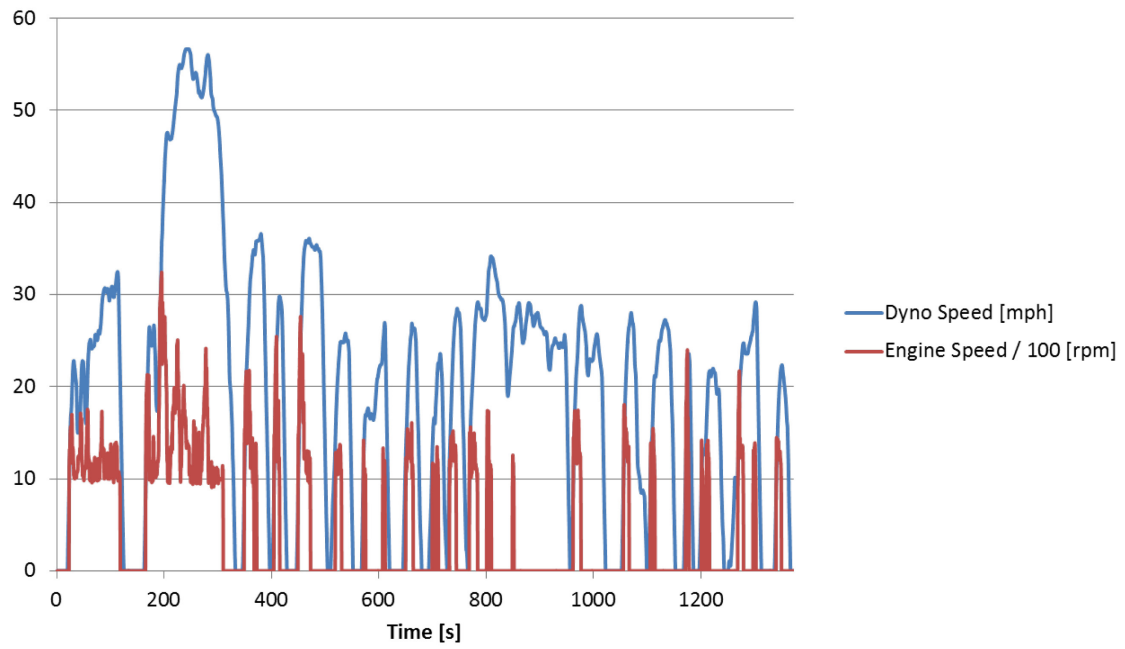


Figure 6.3.2: Toyota Prius EV Operation, UDDS Hot Start Cycle

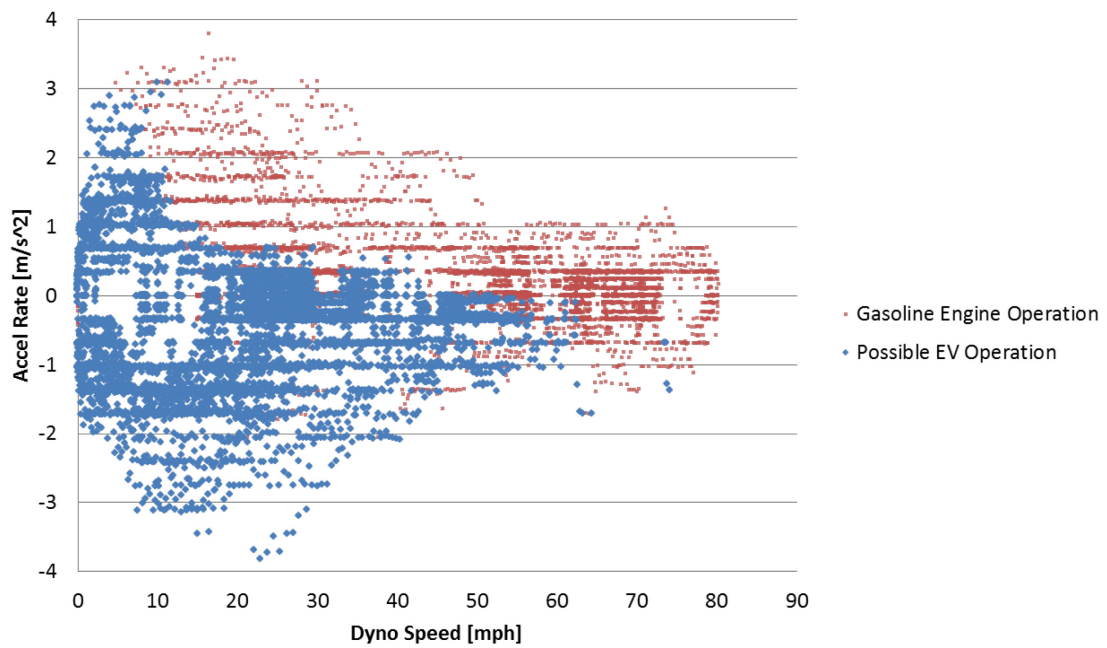


Figure 6.3.3: Toyota Prius EV Operation, UDDS, HWFET and US06 Cycles

Examining Figure 6.3.3 shows that the Prius' opportunity for EV operation is most significant at low speeds. As vehicle speed increases, greater accelerations require that the gasoline engine be run to provide the required motive force. It is important to understand that the blue points denote that there is an opportunity for EV operation, but not necessarily that EV operation always occurs; under varying SOC levels the Prius may choose to operate its gasoline engine at times when it otherwise would operate in EV mode. Finally, it can be seen that the Prius does not operate in EV mode above approximately 60 miles per hour. This may be largely due to drivability constraints; when braking gently from high speed as represented in these drive cycles, there is a significant chance the operator will transition to accelerating again and will require additional tractive effort. Rather than attempt to fill this high torque demand with the electric motor, the Prius instead chooses to operate its gasoline engine. As vehicle speed decreases, the Prius will often continue to spin the gasoline engine at around 1,000 rpm using the motor/generators. This continues to protect drivability by providing for fast restarts. The presence of speed differential constraints imposed by the planetary gear set in the power split device may also contribute to this behavior. If this is the case, in order to keep the motor/generators spinning below their respective speed limits the engine must also be rotating. At the speeds required, it is no longer prudent to drive the engine with the motor/generators and the engine is fueled instead.

Also shown in Figure 6.3.3 is the EV mode deceleration behavior of the Prius. This can also be thought of as the Prius' decelerative fuel cutoff map. Below approximately 60 mph, the Prius has significant opportunity to stop its engine entirely while the vehicle is braking. A combination of regenerative braking and friction braking is then used to slow the vehicle. Because the Prius has the ability to instantly provide motive force with its motor/generators, the DFCO map does not feature a cutoff speed or acceleration rate below which the engine is always fueled. This further contributes to the vehicle's fuel efficiency gains.

Another benefit that stems from the Prius' ability to instantly provide drive torque with the motor/generators is the ability to stop the gasoline engine when the vehicle is at

rest. While most conventional vehicles idle the engine to provide fast transient response and to handle accessory loads such as air conditioning, the Prius meets these demands with its motor/generators and the electrification of auxiliary loads. As such, the Prius is almost always seen to stop its engine at idle unless engaged in catalyst warmup. The percentage of fuel used at idle on a given cycle is often zero as a result. These values are detailed in Figure 6.3.4.

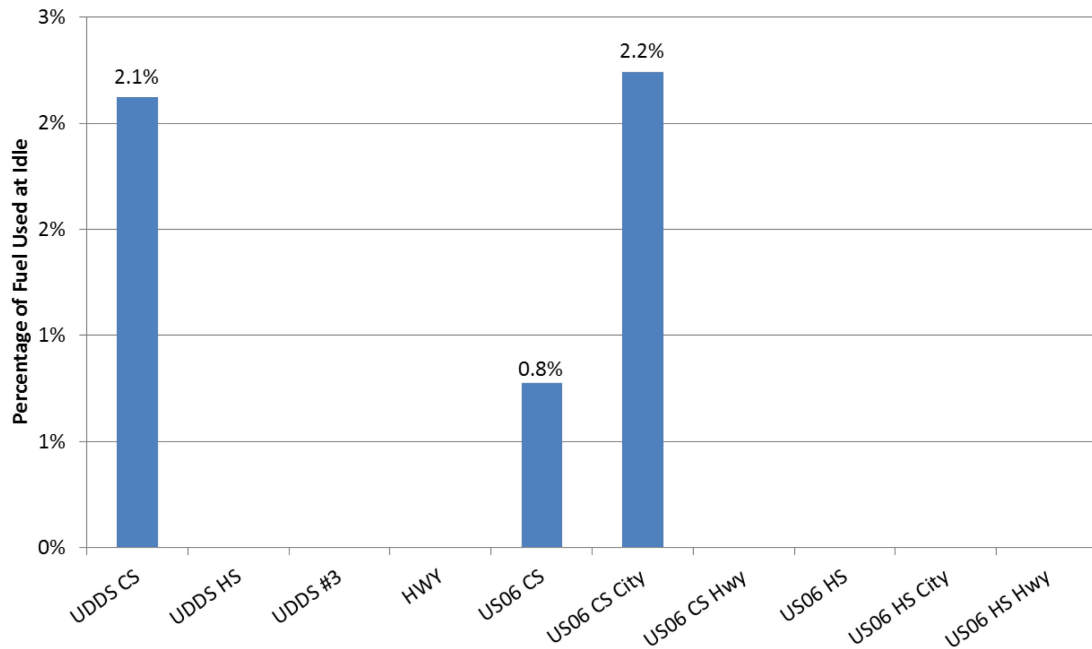


Figure 6.3.4: Toyota Prius Idle Fuel Use

As discussed previously, the Toyota Hybrid System architecture allows for a large degree of authority regarding the operating strategy of the combustion engine. Depending on the battery SOC, the engine load can be adjusted independently of the required road load by using the engine to drive the motor/generators to generate electric energy. This allows the Prius to continuously operate the engine in regions of peak efficiency. Figures 6.3.5 through 6.3.7 show the Prius' engine operation over the UDDS, HWFET, and US06 hot start cycles in the form of density plots.

Figure 6.3.5 shows the Prius' engine operation over the UDDS cycle. It can be seen that the engine is often stopped. When it is fueled, it can be seen to almost always run at high load above 6 bar IMEP. This helps to reduce throttling losses and improve efficiency.

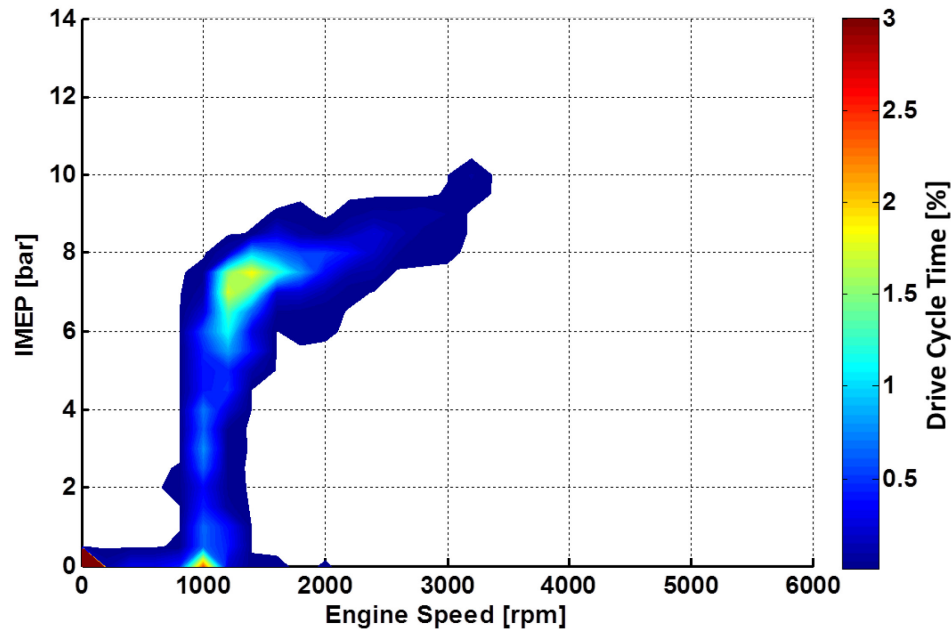


Figure 6.3.5: Toyota Prius Engine Utilization, UDDS HS Cycle

Figure 6.3.6 illustrates the Prius' engine utilization over the US06 cycle. Because of the aggressive nature of this drive cycle, the engine is operated much more frequently and over a wider range of speeds and loads. A visible map feature still exists at 0 rpm, denoting that engine stop behavior is still significant. A second centroid is found at 1,000 rpm and approximately 1 bar IMEP, showing that the Prius does spend some amount of time operating the engine at light load during this test. This operation occurs during decelerations from speeds above 60 mph and likely done to protect for the possibility of fast torque demands as discussed previously. A final dense area of operation exists between 1500 and 2500 rpm and 7 to 9 bar IMEP. This relatively high load operation occurs during periods of heavy acceleration requiring large tractive power generation.

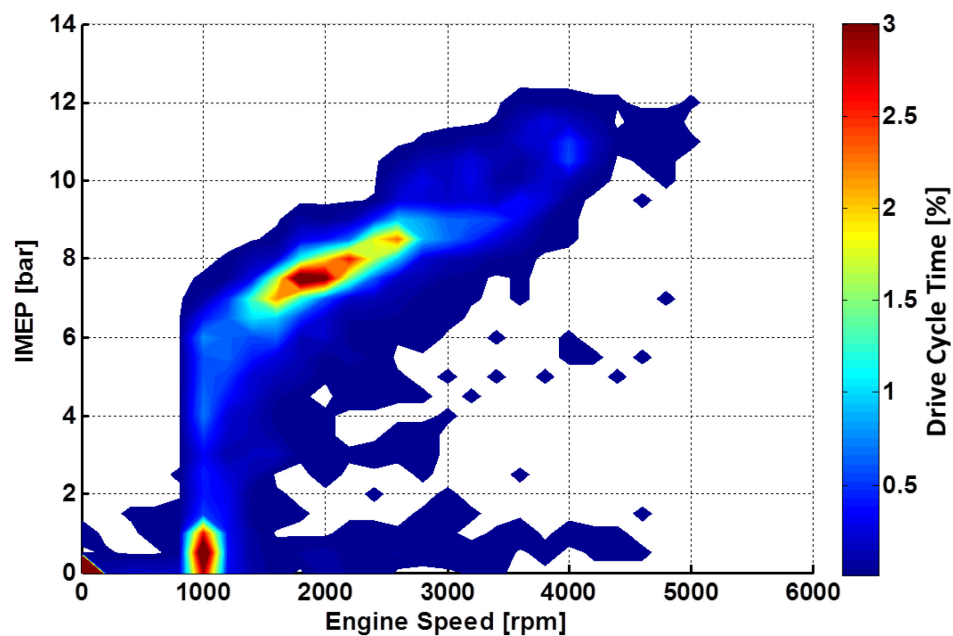


Figure 6.3.6: Toyota Prius Engine Utilization, US06 HS Cycle

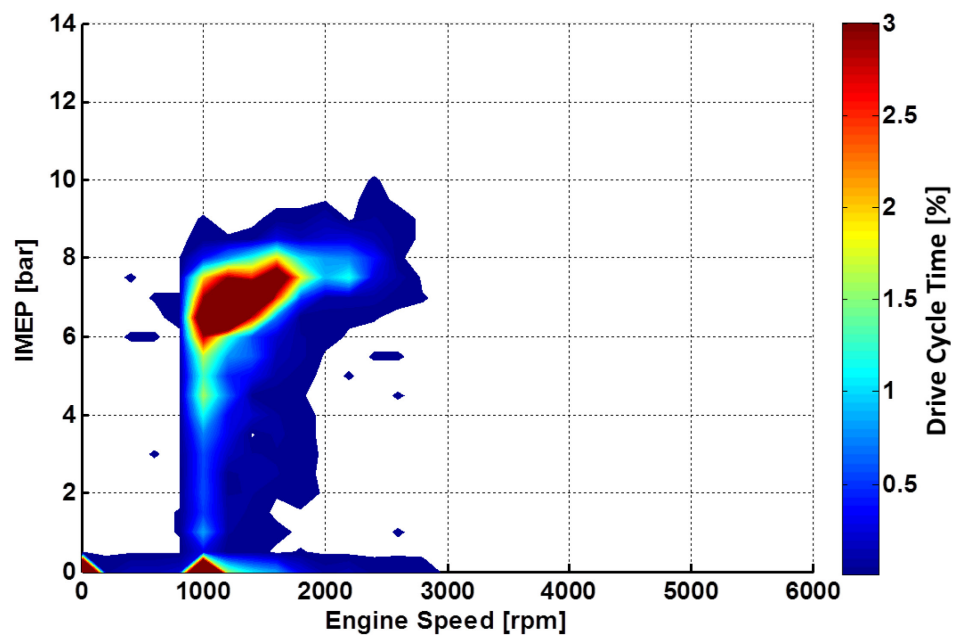


Figure 6.3.7: Toyota Prius Engine Utilization, HWFET Cycle

Figure 6.3.7 shows the operation of the Prius' engine over the HWFET cycle. Again a centroid exists at zero speed denoting the presence of some EV operation, which covers about 9% of the cycle time. A second dense area exists at 1000 rpm and zero IMEP. This occurs during deceleration events and is again due to drivability concerns. In this case, the deceleration events occur at lower vehicle speeds, and the Prius elects to expend some electric power to spin the engine rather than injecting fuel. Because the likely torque demand is typically less at lower speeds, the Prius can fill a greater portion of the demand with its electric machines to provide adequate transient response while fuel is resupplied to the engine. Finally, a large centroid shows the majority of the engine operation between 1000 and 1800 rpm and 6 to 8 bar IMEP, which takes place during high speed cruising.

A very interesting facet of the Prius' engine operation is illustrated by the engine utilization during the US06 cycle. Because the hybrid system provides such a high degree of flexibility over the engine operation, the Prius is able to adopt an operating strategy that involves keeping the engine as close to the most efficient operating point as possible. Figure 6.3.8 shows the US06 engine utilization map modified with a line plotted through the areas where the engine spends the majority of its time operating. This line can be thought of as the Prius' engine operating line, and can be seen in other literature describing the behavior of this particular vehicle. It represents an optimal path through the efficiency islands of the 2ZR-FXE engine map [3]. It is worth noting that the operating line is near vertical at 1,000 rpm, signifying that the engine is almost never operated at light loads where throttling losses are high. By operating the engine in the most efficient spaces possible, the Prius is able to make the most of any quantity of fuel that is consumed.

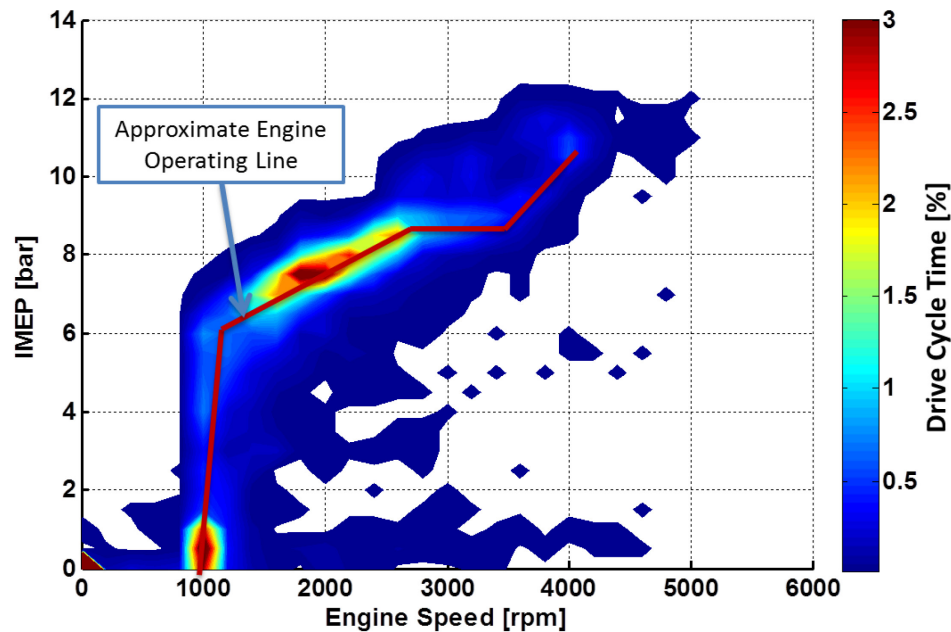
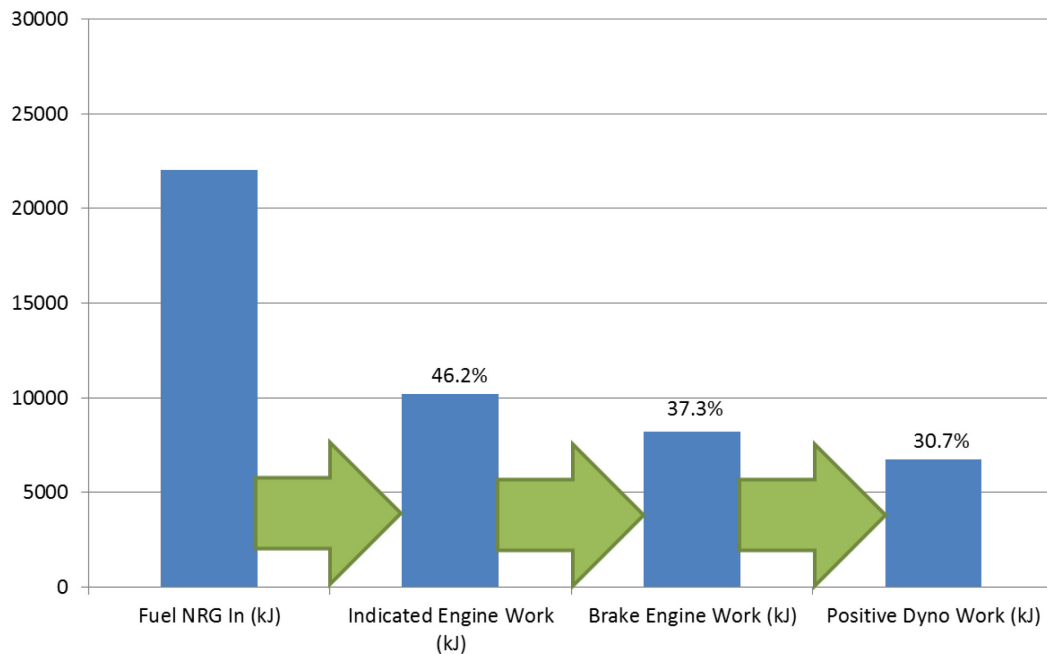


Figure 6.3.8: Toyota Prius Engine Operating Line

The extensive instrumentation plan implemented on the Prius allows for the calculation of a number of efficiency metrics that help to illustrate the Prius' energy transfer behavior. Table 6.3.2 catalogues the fuel energy, indicated engine efficiency, brake engine efficiency, and vehicle efficiency for the vehicle on a per-cycle basis. While higher figures for indicated and brake engine efficiency do increase vehicle efficiency, it is shown that vehicle efficiency reaches its peaks of 31.6% on the UDDS hot start cycle, while the Prius returns its best engine efficiency results on the highway portion of the US06 cycle. Though the engine is less efficient in the case of the UDDS cycle, the vehicle is able to take advantage of significant opportunity for regenerative braking, paying large dividends in terms of vehicle efficiency. Figure 6.3.9 shows the total amount of energy measured for each efficiency metric over the US06 hot start cycle.

Table 6.3.2: Toyota Prius Cycle-Based Efficiencies

Test Description	Fuel NRG In (kJ)	Indicated Engine Efficiency	Brake Engine Efficiency	Vehicle Efficiency
UDDS CS	15127	40.1%	32.2%	26.0%
UDDS HS	12744	43.1%	35.9%	30.9%
UDDS #3	12434	43.3%	35.0%	31.6%
HWFET	17797	45.9%	37.8%	25.2%
US06 CS	24809	42.8%	34.0%	27.2%
US06 CS City	8565	39.5%	30.8%	26.8%
US06 CS Hwy	16244	44.5%	35.6%	27.5%
US06 HS	22048	46.2%	37.3%	30.7%
US06 HS City	7273	43.0%	35.7%	31.4%
US06 HS Hwy	14775	47.8%	38.0%	30.4%

**Figure 6.3.9: Toyota Prius Measured Energy Proportions, US06 Hot Start Cycle**

It is also important to consider the effect of operating temperature. The thermal state of the Prius' powertrain has a significant effect on the vehicle's fuel economy and efficiency. Returning to table 6.3.1, it can be seen that the Prius' fuel economy on the UDDS cycle falls from 72.0 mpg in the hot start case to 59.2 for cold start conditions,

decreasing by 17.8%. This effect is less pronounced on the more aggressive US06 cycle, where fuel economy falls by 11.2% from 43.7 mpg to 38.8 mpg.

The majority of the additional fuel used on a cold start is due to an aggressive catalyst light-off strategy. According to a 2010 paper published by Toyota, during cold start conditions the Prius will operate its gasoline engine for approximately 50 seconds in order to increase catalyst temperatures to 400°C [15]. During this time, the vehicle provides tractive force with the battery and motor/generators. The fuel used during this period does help to generate electric power, but the engine is purposely operated with late valve timing to increase EGT's, hampering efficiency. To illustrate this behavior, the Prius' behavior during the three UDDS cycles is shown in Figure 6.3.10, with the cold start cycle shown in blue.

During the first 60 seconds of the cold start test, the Prius' engine is operated with very steady fueling rates while the aftertreatment catalyst comes up to temperature. Accelerative tractive effort demands during this time are met by the electric traction motor, visible as negative spikes in battery power. The vehicle also increases regenerative braking to recover as much of this energy as possible. During the deceleration event at the end of the first 'hill' of the cycle, the engine cycles off for each cycle. The fuel consumed during the first acceleration event of the second hill is greater than that required for the latter two cycles. This is due to both increased friction losses due to cold start conditions as well as a need to recharge the battery pack to compensate for the energy expended during the catalyst lightoff period. Though the specialized cold start behavior is finished approximately 60 seconds into the test, the Prius' fuel demands for the cold start test are greater for most of the cycle.

More information on this topic can be found in an upcoming SAE paper titled "*A Comparison of Cold-Start Behavior and its Impact on Fuel Economy for Advanced Technology Vehicles*" by Anderson et al., to be published in 2014 [16].

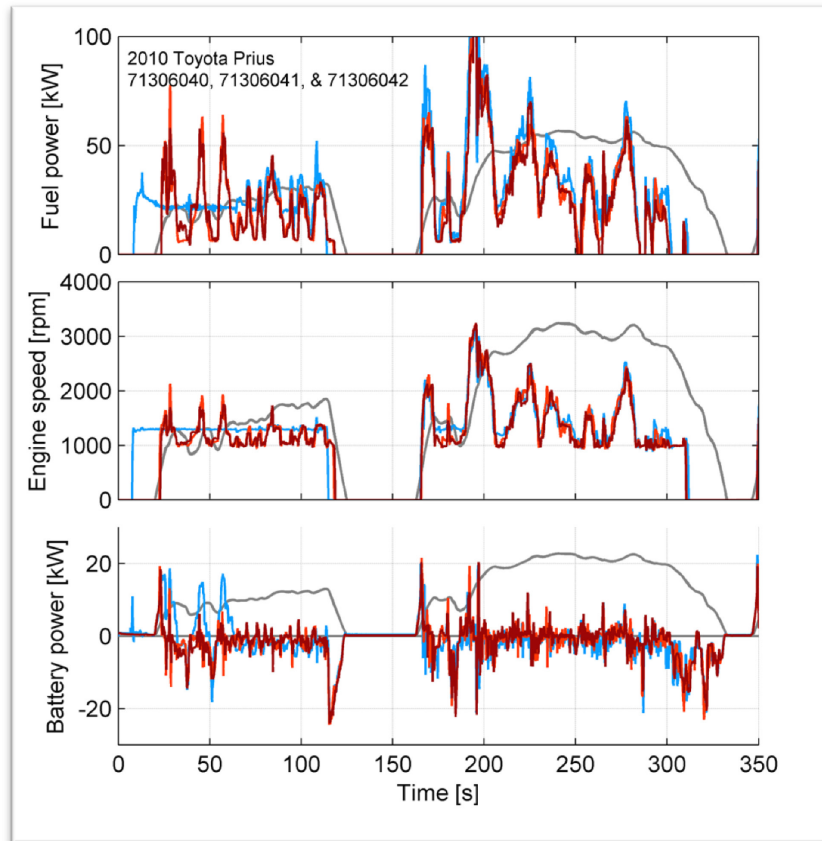


Figure 6.3.10: Toyota Prius Cold Start Behavior, UDDS Cycles

Additional losses are imposed by cold coolant and driveline fluids. In order to better understand the duration of these effects, the Prius' coolant and oil temperatures for the hot start and cold start US06 cycles are plotted in Figure 6.3.11. It can be seen that while the coolant temperatures converge around 250 seconds into the test, the lubricating oil never reaches full operating temperature during the cold start test.

To help further illuminate the drive cycle performance of the Prius, the vehicle was operated at a selection of steady state speeds until the battery state of charge stabilized. Once SOC was stable, the vehicle was operated for an additional 30 seconds to determine fuel economy, efficiency, and wheel power. In the case of the 30 mph speed, the vehicle was operated for one full cycle of EV and engine-on operation, over which the results are averaged. These results are shown in Figure 6.3.12.

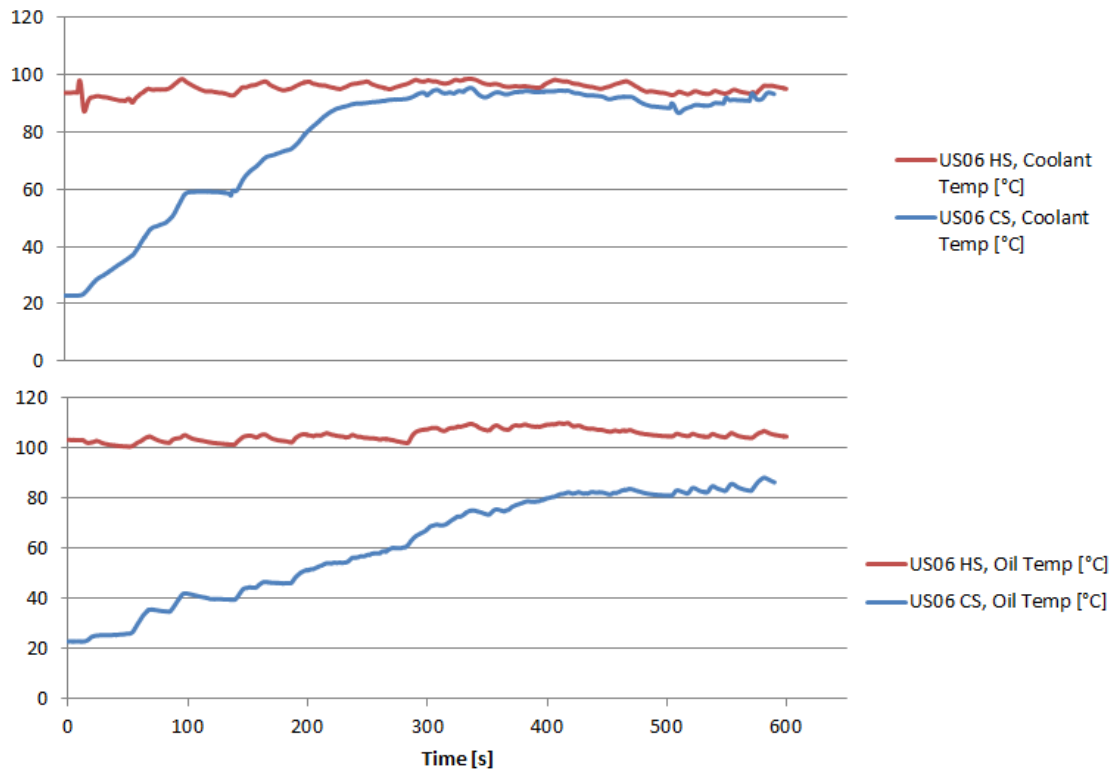


Figure 6.3.11: Toyota Prius Oil and Coolant Temperatures, US06 Cycles

It can be seen in Figure 6.3.12 that the Prius delivers its greatest fuel economy of 108 mpg at a steady speed of 30 mph. At this speed, the vehicle transitions between EV operation where the battery charge is depleting and engine-on operation where the battery is actively charged. Using the motor/generators to increase the engine load in order to maximize engine efficiency in this manner is one of the prime advantages of hybrid-electric architecture. As the vehicle speed increases, fuel economy drops, eventually reaching a minimum value of 43 mpg at 80 mph. Vehicle efficiency is seen to increase with additional road load. This is due to the fact that operating the vehicle at steady state conditions eliminates any opportunity for regenerative braking, and vehicle efficiency becomes primarily dependent on engine efficiency. As seen in Table 6.3.2, the Prius' engine is most efficient when loaded more heavily, such as in the case of the highway portion of the US06 cycle. The results shown in Figure 6.3.12 are consistent with these observations.

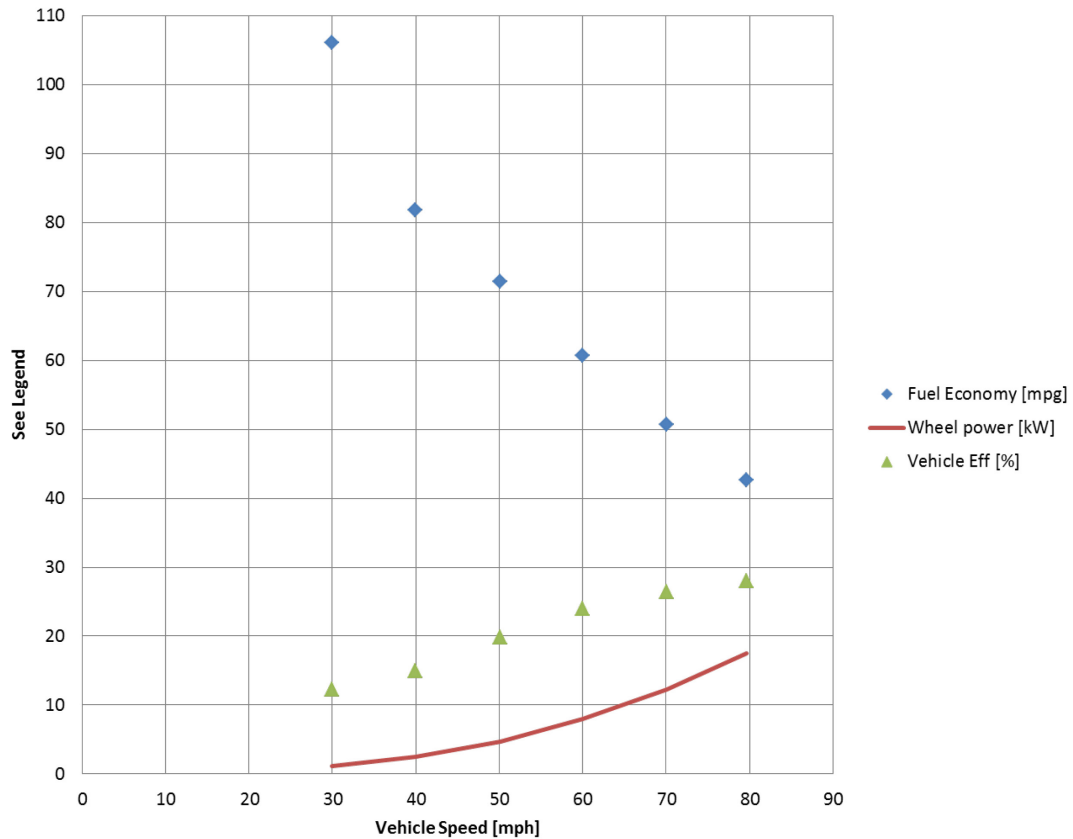


Figure 6.3.12: Toyota Prius Steady State Performance

6.4 Cycle-Based Heat Loss Proportions

It was shown in section 6.3 that between 25.2% and 31.6% of the fuel energy consumed by the Prius during a given drive cycle can be measured as positive work output at the vehicle's wheels. In order to better understand where the remaining energy is lost, the Prius was instrumented with a suite of thermocouples and flow sensors in order to measure the losses associated with the engine cooling system and exhaust gases.

As discussed elsewhere in this work, the nature of the vehicle cooling system makes the measurement of instantaneous enthalpy loss proportions difficult or impossible. Because the coolant volume has a significant heat capacity and takes time to come up to operating temperature, coolant losses were only considered for cycles in which the vehicle had already attained operating temperature prior to the start of the test.

As is the case with the other subjects of this study, analysis was further restricted to integration over complete drive cycles.

Figure 6.4.1 shows the measured energy proportions attributed to positive dynamometer work, cooling system losses, and exhaust gas losses over the hot start UDDS, HWFET, and US06 cycles. As much as 82.9% of the total energy consumed by the Prius can be measured. The remainder is lost to sources not measured in this work, such as heat lost from the engine by radiation, or lost from the other powertrain components apart from the coolant heat exchangers. Power conversion losses also play a part in the Prius' total losses as energy is converted from mechanical to electrical form and back again.

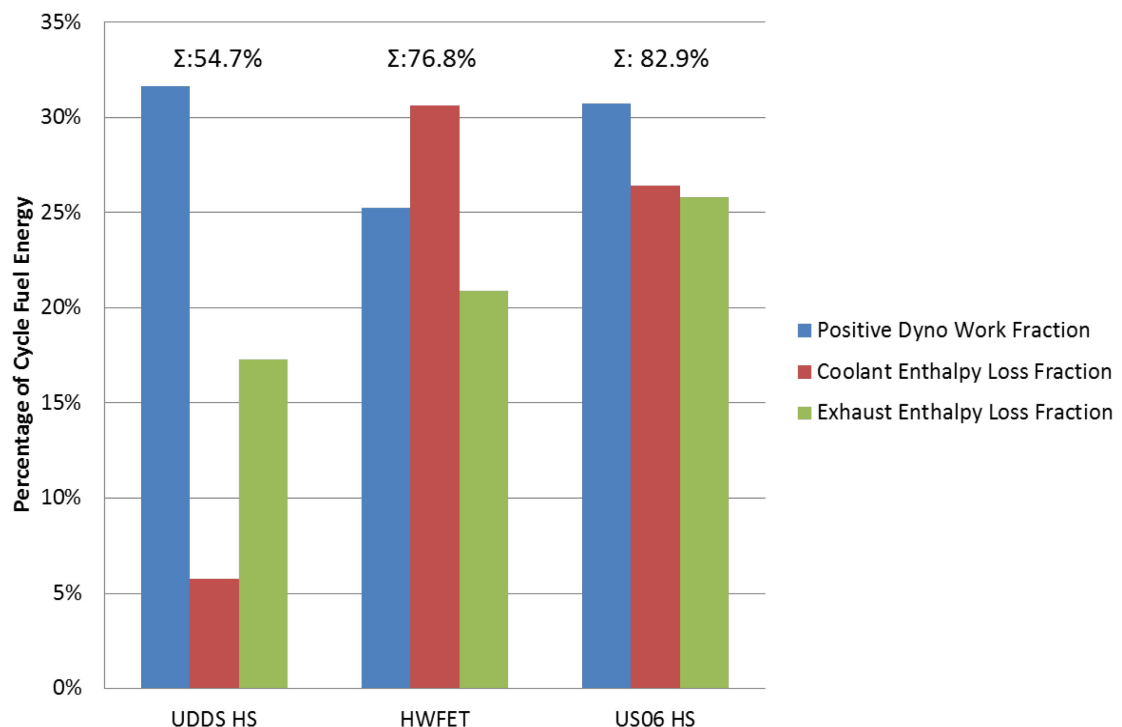


Figure 6.4.1: Toyota Prius Cycle-Based Fuel Energy Use

It is interesting to note that in the case of the UDDS cycle only 54.7% of the total fuel energy is successfully measured. This is largely because the Prius only operates its engine 33% of the time during this test. The extended engine-off operation causes the

engine coolant to remain below operating temperature. The thermostat remains closed, limiting coolant flow and drastically reducing measurable enthalpy losses.

In the case of the UDDS and US06 cycles, the greatest proportion of fuel energy can be found at the vehicle's wheels. As discussed in the preceding section, regenerative braking plays a significant role in these cycles, helping to reduce the total fuel energy required to perform the required accelerations. In the case of the HWFET cycle, regenerative braking opportunity is almost nonexistent and the engine is operated for the entire cycle. Here the Prius acts most like a conventional vehicle, and coolant enthalpy losses become the dominant loss mode.

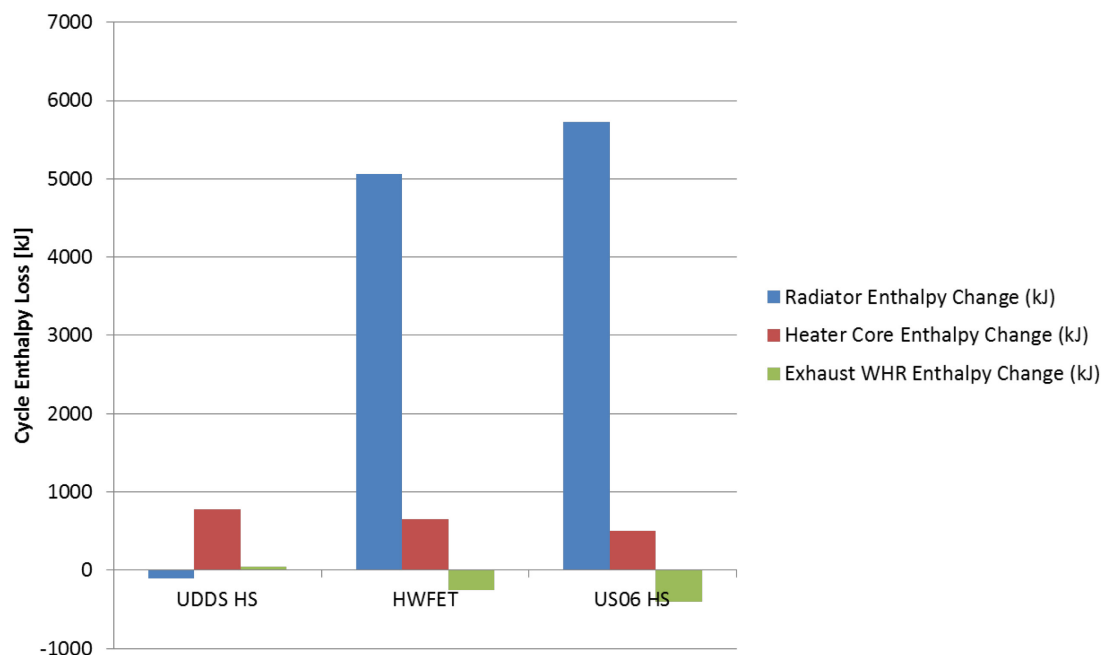


Figure 6.4.2: Toyota Prius Coolant Enthalpy Change by Source

Figure 6.4.2 shows the proportions of the coolant enthalpy changes by source for the three cycles. The reason for the extremely low coolant losses in the UDDS cycle is seen clearly here; the actual enthalpy change measured across the radiator is near zero as the vehicle's thermostat is closed for the duration of the cycle. In the case of the US06 and HWFET cycles, the Prius does reclaim some exhaust energy from the waste heat

recovery system in the exhaust manifold, but the numbers are small in comparison to the energy shed through the radiator. The HVAC fan was not operated during testing, but the Prius does show a small but consistent heat loss across the heater core in all cases. It may be that this effect is exacerbated by the proximity of the heater core lines to the EGR cooler and exhaust manifold, which may push the heater core inlet temperature above normal levels.

6.5 Cycle-Based Emissions Measurements

Tailpipe emissions were also measured as a part of the work performed for this thesis. NO_x, THC and CO were among the constituents measured, and are catalogued on a per-cycle basis in Table 6.5.1.

Table 6.5.1: Toyota Prius Total Emissions by Cycle

Test Description	NO _x [mg]	THC [mg]	CO [mg]
UDDS CS	11.3	76.6	309.2
UDDS #3	46.1	25.9	184.6
HWY	14.2	0.0	283.6
US06 CS	545.5	237.9	1965.6
US06 HS	3.6	7.1	925.9

In general, the Prius exhibits extremely low levels of tailpipe emissions. The cold start US06 cycle stands out as the test with the highest levels of emissions by a wide margin for all three measured constituents. In order to minimize overall emissions levels, the vehicle's hybrid architecture helps to minimize fast engine load transients by providing instantaneous torque with the electric motor/generators. Only when the engine is operating aggressively under cold start conditions does this strategy become less effective.

It is beneficial to better understand the conditions that result in tailpipe emissions for this vehicle. To this end, Figures 6.5.1 and 6.5.2 show the integrated NO_x and THC emissions for the Prius over the hot and cold start versions of the US06 test.

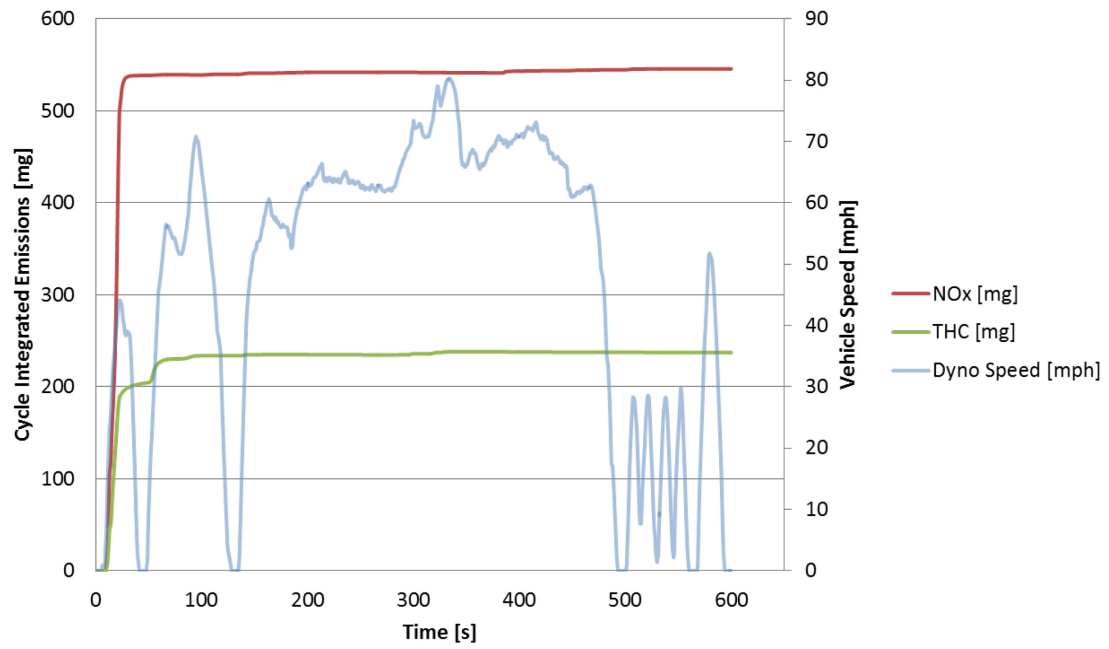


Figure 6.5.1: Toyota Prius US06 Cold Start Integrated NOx and THC

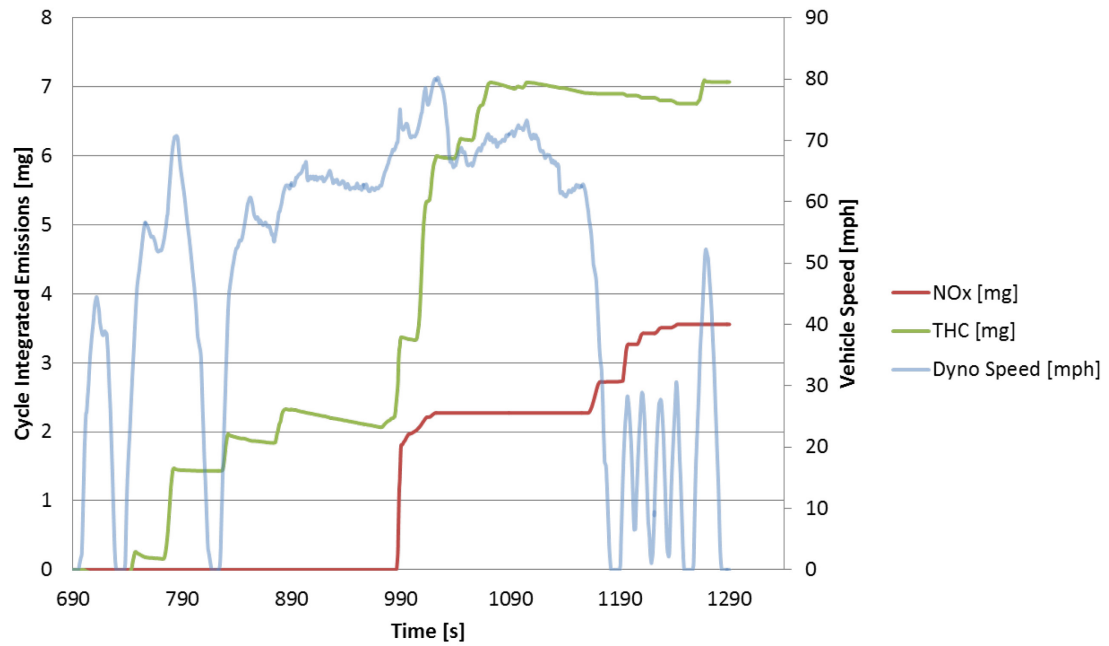


Figure 6.5.2: Toyota Prius US06 Hot Start Integrated NOx and THC

It can be seen that in general, increases in emissions take place during demanding accelerations. Under these conditions the Prius cannot meet the driver's acceleration demands with the electric drivetrain alone, and must operate the engine somewhat aggressively to make up the difference. It can also be seen that the majority of the increased emissions for the cold start US06 occur in the first 30 seconds of the test. In this brief window the exhaust catalysts have not yet come up to temperature and are significantly less effective at treating the cylinder-out emissions caused by the aggressive acceleration of the first hill.

Some interesting behavior is also noted in Figure 6.5.2 with regards to the integrated THC figures. During each dwell period after a spike in total hydrocarbon emissions, the total measured THC appears to decrease. During testing, the Semtech unit is calibrated several times per day using specific gas cylinders with predetermined concentrations of compounds found in tailpipe emissions. Before a test is begun, the unit takes a background reading of ambient air in order to establish baseline emissions levels against which to judge those produced by the vehicle. Occasionally, environmental conditions can temporarily increase background levels of these constituents in the air. An example of this might be a diesel-powered delivery truck idling near the test cell. When background levels return to normal, the Semtech may then actually read negative concentrations of exhaust gas constituents. Typically these errors are very small, but in the case of the Prius, tailpipe emissions are low enough that this was noticeable during the hot start US06 cycle.

6.6 Engine Indicating System Measurements

As discussed previously, the Prius's gasoline engine was instrumented with an indicating transducer in order to measure cylinder pressures in real time during testing. Engine IMEP was calculated in real time and used to calculate the indicated efficiency metrics discussed in Section 6.3. In order to better understand the operating characteristics of the 2ZR-FXE, several representative operating points were chosen and are discussed in this section. Table 6.6.1 details these operating points.

It must be noted that the operating points shown are the result of single engine cycles. Because the data for this study was collected mainly over transient drive cycles, it is difficult to provide averaged engine cycles as is customary for engine-centric research projects. The cycles provided here are used to draw largely qualitative conclusions about the Prius' combustion behavior and how that behavior relates to the design of the engine.

Point 1 detailed in Table 6.6.1 showcases the operation of the Prius' 2ZR-FXE engine at idle conditions. It is rare that the Prius chooses to operate at this point; these conditions are usually seen at the beginning of a cold start test where the vehicle runs the gasoline engine with the intent of bringing the exhaust catalyst up to temperature. This operating strategy involves operating the engine with retarded combustion timing in order to increase exhaust gas temperatures. This is evidenced by the 50% mass fraction burned measurement, which takes place at 31.5 degrees ATDC at this point.

Table 6.6.1: Toyota Prius Engine Operating Points

		Point 1	Point 2	Point 3
Engine Speed	[rpm]	1086	1545	4971
IMEP	[bar]	0.9	7.1	11.8
Peak Pressure	[bar]	5.1	39.8	50.3
Burn Duration	[ms]	7.1	2.3	0.9
Angle, 50% MFB	[CAD]	31.5 ATDC	11.6 ATDC	17.8 ATDC
Angle, PMAX	[CAD]	10.5 ATDC	17 ATDC	19.9 ATDC

Figure 6.6.1 shows the P-V diagram on a log-log scale for this operating point. The four engine strokes are labeled for convenience. The 2ZR-FXE has a relatively high compression ratio for a port-injected gasoline-fueled unit at 13.0:1. A paper released by Toyota indicates that in order to mitigate combustion knock, the engine utilizes a late intake valve closing strategy wherein the intake valve is held open through part of the compression stroke to reduce peak combustion temperatures [3]. This can be seen clearly in Figure 6.6.1, as the measured cylinder pressure does not begin to rise sharply until the compression stroke is well underway. This strategy also results in a comparatively long expansion stroke, evidence of which is seen at the beginning of the exhaust stroke in the diagram; cylinder pressure falls below ambient pressure until the exhaust valve is opened at the end of the expansion stroke. Finally, it is interesting to note the sharp curve at the beginning of the intake stroke. It appears that the intake valve does not open until the intake stroke is underway, perhaps to facilitate a degree of internal exhaust gas recirculation (EGR).

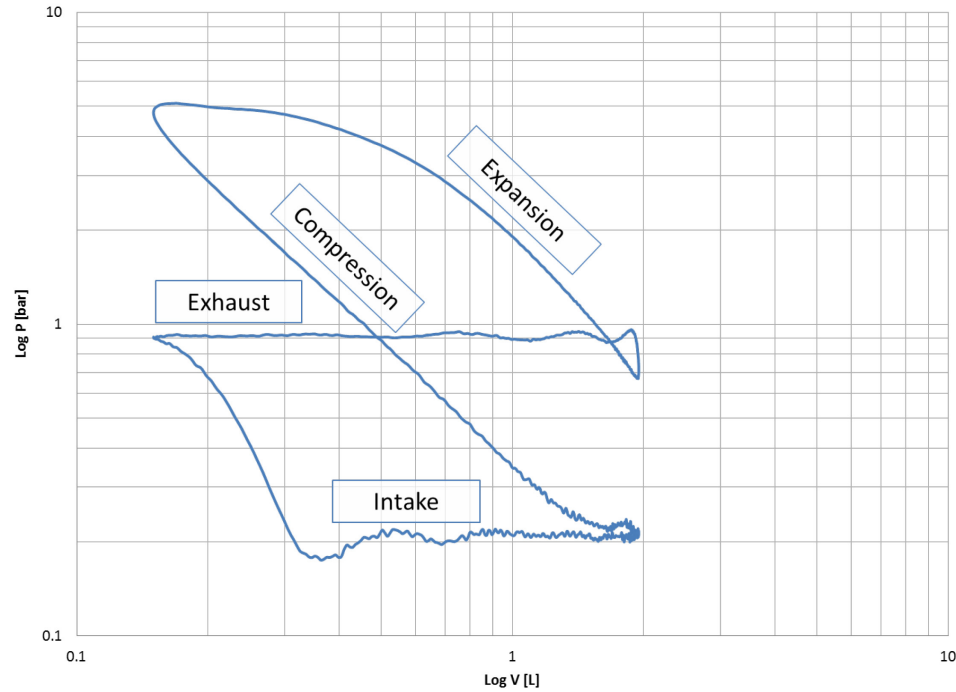


Figure 6.6.1: Toyota Prius P-V Diagram, Point 1

The second operating point shown in Table 6.6.1 is commonly utilized by the Prius, especially during low speed urban driving. In order to increase the efficiency of the engine, the Prius uses the electric drivetrain to apply additional load. The electrical energy generated here is stored in the battery pack for later use. At this operating point, combustion timing has been advanced considerably from Point 1, with the 50% MFB point located 11.6 degrees after top dead center (ATDC). Peak pressure increases markedly to 39.8 bar, and combustion duration falls significantly, primarily due to increased charge density.

Figure 6.6.2 shows the P-V diagram for Point 2. Some of the operating characteristics of Point 1 are evidenced here as well, such as the late intake valve closure represented by the lack of an immediate rise in pressure at the start of the compression stroke. It can also be seen that the pumping work loop is considerably smaller in magnitude with minimum intake pressures above 0.5 bar, indicating that the engine is much less aggressively throttled in this case. The more advanced combustion timing can

also be seen here, as the bulk of the combustion pressure increase takes place between the end of the compression stroke and the beginning of the expansion stroke, rather than later in the expansion stroke as seen in Point 1.

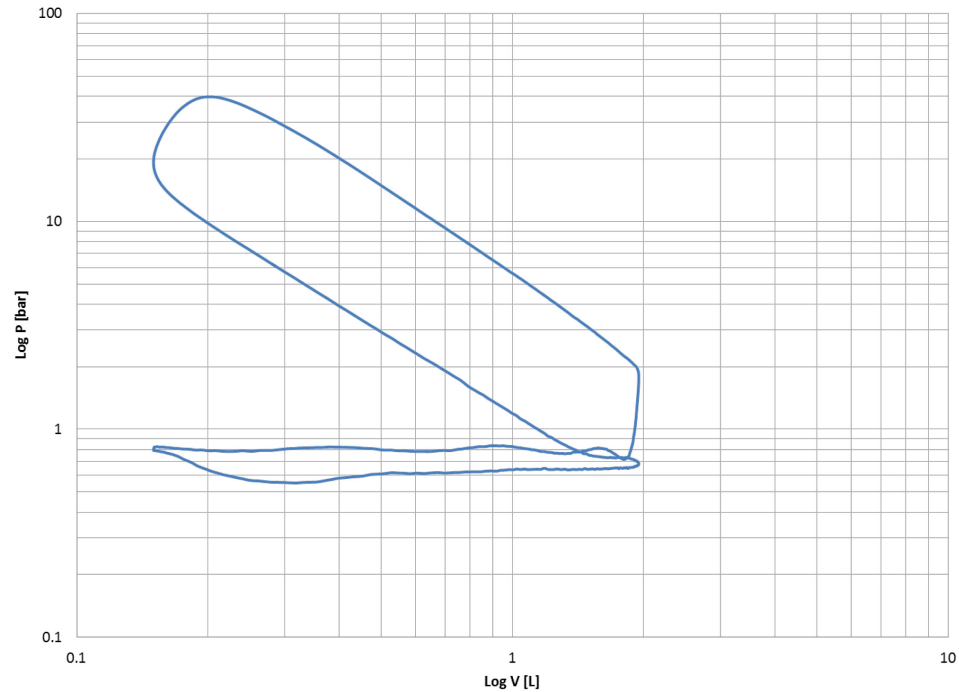


Figure 6.6.2: Toyota Prius P-V Diagram, Point 2

Operating Point 3 is shown in Figure 6.6.3. This represents the Prius' engine operation during a wide open throttle (WOT) acceleration event where the vehicle is generating as much power as possible. The engine achieves 11.8 bar IMEP with a peak pressure of 50.3 bar. Combustion timing is retarded somewhat in comparison to Point 2, with the 50% MFB point located at 17.8 degrees ATDC, likely for knock mitigation. Combustion duration is a very short 0.9 ms, likely due to efficient charge mixing caused by a large degree of turbulence in the gas exchange process.

Examining the P-V diagram shows that the Prius' engine begins to look like its more conventional counterparts when operated at high speed and load. The lag in pressure rise at the end of the intake stroke is no longer as apparent as was the case in

Points 1 and 2. Likewise, the lag in pressure reduction at the beginning of the intake stroke is no longer observable. It is difficult to say for certain whether the valve timing strategy has been adjusted, or if these changes are due to localized pressure changes near the transducer caused by inertial effects of the gas exchange process occurring at high speeds. The latter theory is in part supported by the shape of the exhaust blowdown event occurring at the end of the expansion stroke; in this case, the pressure drop occurs over approximately 1/3 of the exhaust stroke, whereas this happens over a much smaller volume differential in Point 2.

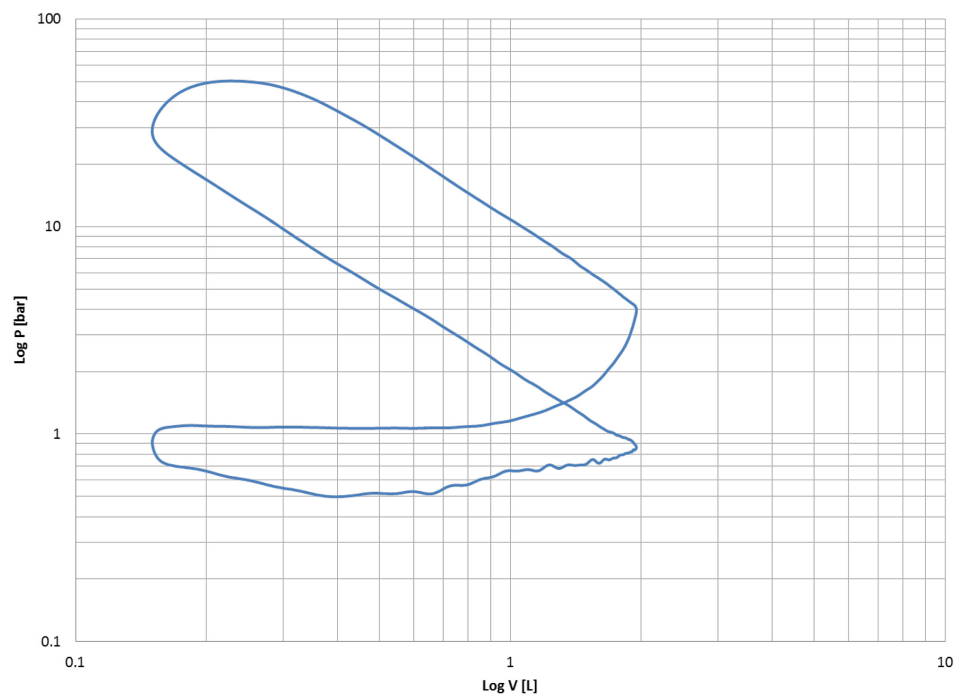


Figure 6.6.3: Toyota Prius P-V Diagram, Point 3

Chapter 7 Data Synthesis and Comparative Analysis

The purpose of this section is to consider the behavior and performance of the test vehicles with respect to one another. To this end, several sections are presented for the purpose of comparing results with different areas of focus. The intent is not to repeat the results given in previous chapters, but instead to bring these results together for relative comparison.

7.1 Vehicle Parameters and Performance Envelopes

The main objective of this thesis work was to consider several different passenger vehicle architectures in order to compare their performance in terms of efficiency and operational behavior. Ideally, each vehicle would be identical in terms of vehicle mass, road load coefficients, and powertrain output. However, choosing a single vehicle model with powertrains available to represent each of the architectures considered here proves difficult and expensive.

Instead, research subjects were chosen from a pool of vehicle available at Argonne National Laboratory. Because the chosen vehicles exhibit differences in parameters affecting their performance, it becomes important to consider these factors as well as the capability envelope of each vehicle. This provides context for the fuel economy performance returned by each vehicle and provided later in this chapter.

Table 7.1.1 provides a selected set of parameters for the four research vehicles. One of the factors directly affecting vehicle performance and economy is the vehicle mass. This figure determines vehicle inertia, which is a significant factor contributing to the amount of work that must be done when the vehicle accelerates. The Fusion and Jetta TDI are the heaviest vehicles in this thesis, both with test weights of 3625 lbs. The Jetta TSI falls in the 3500 lb class, while the Toyota Prius is the lightest vehicle tested at 3375 lbs.

Table 7.1.1: Selected Vehicle Parameters

		Fusion	Jetta TDI	Prius	Jetta TSI
Test Weight		3625	3625	3375	3500
Road Load Coefficients	Cd	0.32	0.31	0.25	0.31
	A	33.9204	35	18.5	30
	B	0.364	0.18	0.0223	0.2
	C	0.0166	0.0193	0.0181	0.0186

The vehicle's drag coefficient is a factor that directly affects the vehicle road load and the determination of the road load coefficients. Though this factor is represented in the final road load coefficients, it is worthy of consideration because it provides an indication of the aerodynamic drag losses contributing to the total road load. The Jetta TDI and TSI share the same vehicle body and drag coefficient of 0.31. The Fusion is only slightly less aerodynamic with a value of 0.32. The Prius stands out from the crowd in this metric with a drag coefficient of 0.25. This indicates that the vehicle's shape was heavily optimized to reduce aerodynamic drag.

As discussed in Chapter 2, road load coefficients are used to simulate the total forces opposing forward motion as the vehicle proceeds at speed. The equation used to model the load curve is a second order polynomial making use of three coefficients. Visualization of the effects of road load coefficients is difficult without plotting the calculated load for consideration. Figure 7.1.1 provides the calculated road load for each vehicle as a function of vehicle speed.

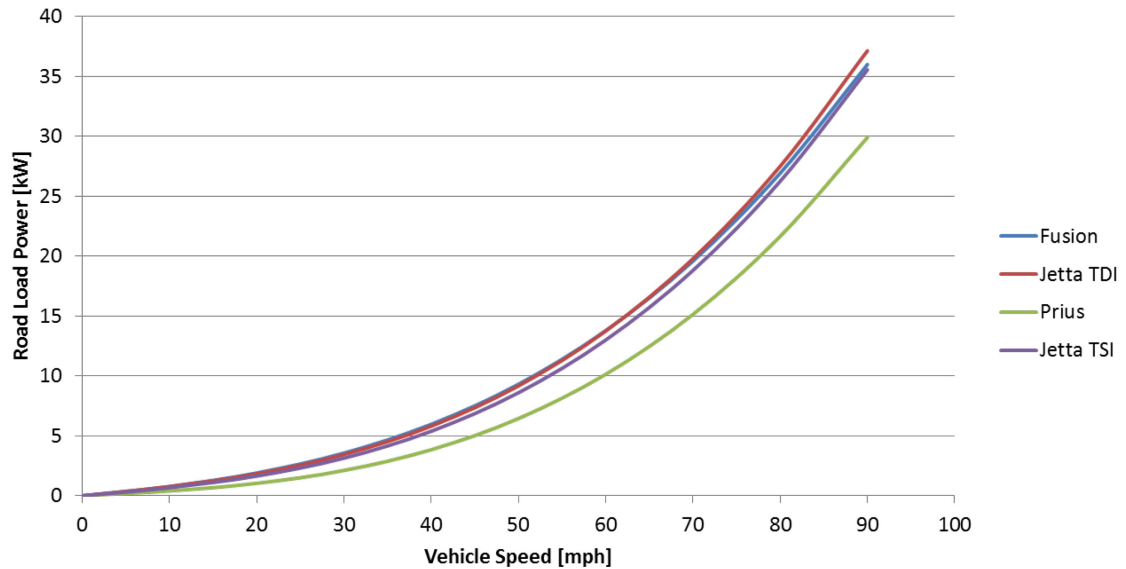


Figure 7.1.1: Road Load Power vs. Speed

The total road load power for the three conventional vehicles is similar. At speeds below 60 mph, the Fusion requires the greatest amount of power to propel the vehicle down the road at steady speed. Over 60 mph, the Jetta TDI surpasses the Fusion's road load. The Jetta TSI is comparable, but comes in slightly below the Fusion and TDI. The Toyota Prius manages a considerable reduction in road load, requiring the least amount of power to achieve steady state cruising regardless of speed. As discussed previously, these numbers take into account all losses acting on the vehicle including aerodynamic losses, tire losses, and mechanical losses due to bearings and windage in the drivetrains. In order to further illustrate the difference in required road loads, Table 7.1.2 provides the road load relative to the Fusion at 80 mph for each vehicle. Here the Prius shows a reduction in required road load of nearly 19.6%.

Table 7.3.3: Vehicle Road Load Relative to Fusion, 80 mph

	Fusion	Jetta TDI	Prius	Jetta TSI
Relative Road Load	0.00%	+2.15%	-19.59%	-2.50%

It should also be noted that the vehicles chosen for this thesis have differing performance envelopes. The most robust powertrain included produces 175 horsepower at rated engine speed and load, while the least powerful is rated at 98 horsepower. Table 7.1.3 provides acceleration values that help to illustrate the total tractive effort capability of each vehicle.

Table 7.1.3: Vehicle Acceleration Performance

		Fusion	Jetta TDI	Prius	Jetta TSI
Acceleration	0-60 [mph]	10.5 s	10.0 s	11.0 s	10.4 s
Performance	10-70 [mph]	11.2 s	11.1 s	13.1 s	12.1 s

Acceleration figures from 0-60 mph and 10-70 mph are provided. It should be noted that the acceleration times achieved on the chassis dynamometer are often slower than those available from on-road testing, especially in the case of the more powerful Fusion. This vehicle's acceleration at lower speeds was significantly limited by excessive tire slip on the dynamometer's steel rolls. For this reason, the 10-70 mph figures are provided to equalize the vehicle's launch capability. In all cases, the vehicles were operated to provide best acceleration with the transmissions left in automatic mode.

The Fusion and TDI accelerate at very similar rates with the vehicles moving from 10 to 70 mph in 11.2 and 11.1 seconds respectively. The Jetta TSI lags the more powerful TDI by one second, and the Prius trails the TSI by the same amount. It should also be noted that as successive acceleration trials are made with the Prius, performance degrades. This is because the battery is tasked with supplying significant electric power to the traction motor for maximum performance. The battery temperature climbs rapidly, and the vehicle reduces electric assist on subsequent runs to manage battery temperature.

Vehicle tractive effort provides an additional means of understanding vehicle capability. Figure 7.1.2 shows the tractive effort for each vehicle during a maximum performance acceleration trial.

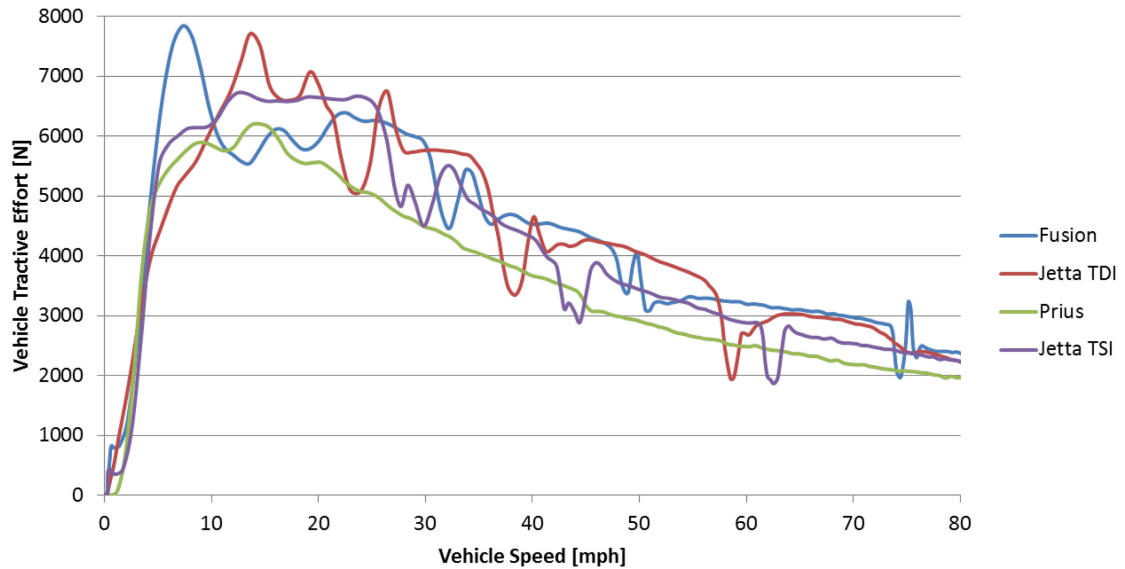


Figure 7.1.2: Vehicle Tractive Effort Capability

Several interesting phenomena are visible in Figure 7.1.2. The Fusion and TDI are able to provide the largest amounts of tractive effort, with both vehicles peaking at greater than 7500 N. The Fusion is able to provide maximum capability early in the acceleration run, peaking below 10 mph. This is likely a function of both the gear ratio choice as well as the torque-multiplying abilities of the transmission's torque converter. The TDI and TSI both provide maximum tractive effort at higher vehicle speeds as their engines develop peak torque in first gear. Each of the conventional vehicles also exhibits clear drops in tractive effort that correspond to gear changes. During these events engine torque is managed to protect the transmission and provide proper drivability. The Prius is unique among the test subjects in that it is able to utilize a continuously variable gear ratio due to its planetary gearset equipped e-CVT. The vehicle exhibits no clear shifting behavior and provides the smoothest tractive effort curve of the test subjects.

Though the vehicles do provide widely varying performance envelopes, test weights, and body volumes, it is important to remember that each vehicle is capable of carrying 4-5 passengers and some degree of cargo. While the design philosophy inherent

in each vehicle is different, each is able to carry out the tasks required in the light duty passenger vehicle market.

7.2 Drive Cycle Performance

As discussed in previous chapters, the research vehicles were each subjected to a series of drive cycle tests to facilitate equitable performance and behavior comparisons. The test plan is found in Appendix A.

The vehicle comparison metric foremost in the consumer's mind is often fuel economy as expressed in miles per gallon (mpg). As discussed in Section 2.1.5, this figure is not without shortcomings as a comparison metric. Fuel economy in miles per gallon is dependent both on the efficiency of a given vehicle as well as the amount of work required by the road load and inertia forces. This duality can cause the data to be counter-intuitive. For example, a more efficient vehicle required to do a large amount of work per mile may return worse fuel economy than an inefficient vehicle tasked with doing very little work per mile. These pitfalls make direct powertrain comparison based on fuel mileage difficult. For this reason, while fuel mileage for all vehicles is catalogued in Table 7.2.1, comparative discussion is reserved for other metrics.

Table 7.2.1: Cycle Fuel Economy (mpg) by Test Vehicle

Test Description	Fusion	Jetta TDI	Prius	Jetta TSI
UDDS CS	23.9	32.5	59.2	35.4
UDDS HS	26.4	36.8	70.2	39.0
UDDS #3	26.5	36.8	72.0	39.0
HWFET	40.6	52.1	69.4	50.3
US06 CS	23.6	31.9	38.8	28.2
US06 CS City	14.2	21.8	24.9	17.3
US06 CS Hwy	29.1	36.7	46.2	34.3
US06 HS	26.1	35.5	43.7	31.6
US06 HS City	16.9	24.8	29.3	20.9
US06 HS Hwy	31.0	40.5	50.8	36.9

A more robust metric for comparing the performance of different architectures is vehicle efficiency. As defined in Section 2.1.5, vehicle efficiency takes into account the total fuel energy consumed as well as the work done during the course of the drive cycle. It provides an effective means of normalizing vehicle performance based on the amount of work required. This metric is not typically discussed in consumer literature because accurate measurements of work performed require the use of a chassis dynamometer. Table 7.2.2 provides vehicle efficiency results for each cycle by vehicle. Figure 7.2.1 provides a more visual representation of the data.

Table 7.2.2: Cycle Vehicle Efficiency by Test Vehicle

Test Description	Fusion	Jetta TDI	Prius	Jetta TSI
UDDS CS	12.0%	15.3%	26.0%	17.4%
UDDS HS	13.3%	17.3%	30.9%	19.1%
UDDS #3	13.3%	17.0%	31.6%	19.2%
HWFET	17.7%	21.6%	25.2%	22.1%
US06 CS	18.7%	23.4%	27.2%	22.1%
US06 CS City	16.6%	22.9%	26.8%	19.8%
US06 CS Hwy	19.9%	23.7%	27.5%	23.3%
US06 HS	20.8%	25.9%	30.7%	24.6%
US06 HS City	19.9%	26.0%	31.4%	23.9%
US06 HS Hwy	21.3%	25.9%	30.4%	24.9%

The Prius returns the highest cycle efficiency values by a fairly wide margin, with vehicle efficiency peaking at 31.6% on the hot start UDDS cycle. The closest competitor on this particular cycle is the Jetta TSI, whose vehicle efficiency measured 19.2%, trailing the Prius significantly. The Jetta TDI and Fusion bring up the rear with values of 17.0% and 13.3% respectively. The Prius' exceptional performance here is largely a result of the vehicle's hybrid architecture. The hybrid-electric powertrain allows for regenerative braking and electric propulsion at low load, both of which can be utilized often during the UDDS cycle. These behaviors are discussed in more detail in Chapter 6. The range of vehicle efficiencies is narrower on the more aggressive cycles, ranging from 20.8% to 30.7% on the US06 HS cycle.

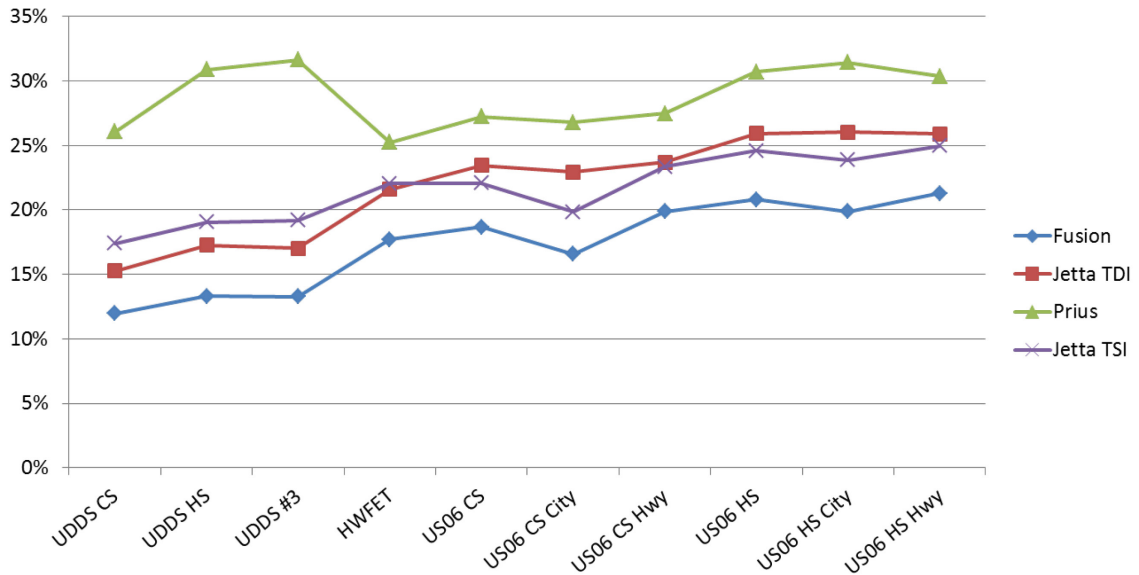


Figure 7.2.1: Vehicle Efficiency by Cycle

Several trends are visible in Figure 7.2.1. In general, efficiency increases with the average powertrain load over the cycle. This translates to better overall efficiency on the HWFET and US06 cycles where engine loads are high. This trend holds true for the conventional vehicles considered in this study. The Prius proves to be the exception to the rule, achieving its best vehicle efficiency on the hot start UDDS cycle.

Among the conventional vehicles, the Fusion and Jetta TDI exhibit similar efficiency trends across the cycles. Efficiency is at its lowest on the UDDS cycle, and peaks with the US06 cycle. The difference in efficiency between the UDDS HS and US06 HS tests is on the order of 7.5-8.9%. The TSI shows similar trends but exhibits a smaller change in efficiency between the UDDS and US06 cycles of 5.4%. This is likely a function of the downsized, boosted powertrain architecture adopted by the TSI. The engine's small displacement provides a significant reduction in throttling and friction losses at low loads, returning better than average efficiency on the UDDS cycle. When more power is demanded, the efficiency gain exhibited by the larger displacement engines is not as apparent. In extreme cases, efficiency falls as the vehicle richens the fuel mixture to avoid knock. This behavior is examined in more detail in Chapter 5.

The narrowest range of efficiencies returned by the research vehicles occurs on the HWFET cycle. Here, efficiency numbers ranged from 17.7% for the Fusion to 25.2% for the Prius. The nature of this cycle provides favorable vehicle efficiency numbers for the conventional vehicles, but is actually the worst-case operating condition for the Prius.

As mentioned in previous chapters, the HWFET cycle involves long periods of cruising at moderate engine loads with little opportunity for idle. Conventional vehicles do well here because throttling losses and energy-intensive transient acceleration events are minimized. Conversely, hybrid vehicles such as the Prius are unable to take advantage of some of the behaviors that make them effective at urban driving. The HWFET cycle provides little opportunity for regenerative braking, and almost no opportunity for idle stop. Similarly, the loads required at highway cruising speeds are not conducive to electric operation; the engine is efficient enough at these loads that the vehicle instead chooses to provide motive force with the engine. These factors are each partly responsible for the Prius returning its lowest economy values on the HWFET cycle.

Despite these factors, the Prius still returns the highest HWFET cycle efficiency of the vehicles included in this thesis work. It should be noted that this vehicle is heavily optimized for all driving conditions. A 2009 SAE paper released by Toyota detailing the development of the 2010 Prius powertrain explains in detail how the engine was optimized for efficiency at highway speeds [3,13].

It is also clear that all vehicles exhibit significant reductions in efficiency when operated under cold start conditions. This behavior is discussed in detail in Section 7.3.

7.3 Cold Start Mileage Penalties & Emissions Behavior

Powertrain operating temperature has a significant effect on vehicle efficiency and fuel economy. Vehicles operating under cold start conditions typically exhibit lower efficiency and consume more fuel than under hot start conditions. This phenomenon is

largely due to two factors; increased powertrain losses due to cold lubricants and tires, and modified vehicle behavior to speed warmup and minimize tailpipe emissions.

In order to explore the effects of cold start conditions on powertrain efficiency and economy, the test vehicles were subjected to cold start versions of the UDDS and US06 drive cycles. The reduction in fuel mileage resulting from cold start operation as compared to hot start operation is shown in Figure 7.3.1. UDDS cycle results are shown with blue backlighting, while US06 results are shown with a red backlight. It should be noted that the penalty for the UDDS cycle is calculated with respect to the third iteration of the test.

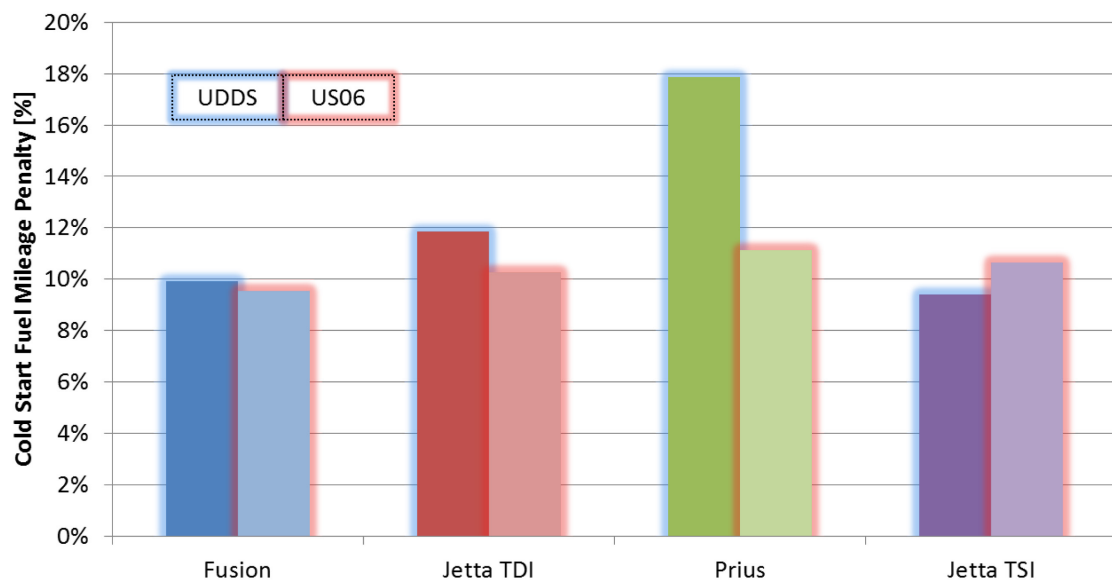


Figure 7.3.1: Cold Start Fuel Mileage Penalty by Vehicle

The vehicles in this study exhibited an average of 10.4% greater fuel consumption on the US06 cycle when driven under cold start conditions. Consumption penalties ranged from a low of 9.5% for the Fusion to 11.1% for the Prius. The aggressive nature of the US06 cycle causes the vehicles to expend a large amount of fuel energy which helps to quickly warm the powertrain lubricants and emissions catalysts. In all cases

except for the TSI, the US06 cycle shows a smaller consumption penalty than the UDDS cycle.

The cold start mileage penalties varied more widely on the UDDS cycle. Here the average fuel economy penalty was 12.3%. The conventional vehicles showed mileage penalties between 9.4 and 11.8%, which are similar in magnitude to those seen on the US06 cycle.

The Prius, however, exhibited a much larger 17.9% reduction in fuel economy on the cold start UDDS test. This is due to the aggressive catalyst lightoff strategy discussed in detail in Section 6.3. This operation causes the Prius to idle the engine with late combustion timing and lower efficiency during periods where the engine would otherwise be stopped, creating a large impact on fuel economy. During the US06 cycle, the Prius is forced to provide motive power with its gasoline engine which increases efficiency at the expense of the catalyst lightoff strategy..

Cold start behavior also has a noticeable impact on vehicle emissions. Reducing vehicle tailpipe emissions is a high priority goal that is in part responsible for cold start strategy. The normalized NO_x emissions of the four vehicles are plotted for the cold start UDDS cycle in Figure 7.3.2. Figure 7.3.3 shows the THC emissions for the same cycle. It is important to note that all values are normalized based on the maximum modal generation rate for each vehicle.

It can be seen that the most significant levels of modal NO_x and THC emissions occur during the first 100 seconds of the cold start cycle for gasoline-powered vehicles. The Prius begins generating significant emissions several seconds later than the Fusion and TSI because it exhibits initial engine start slightly later during the cycle. After the initial 100 second period, the aftertreatment catalysts of these vehicles have reached operating temperature and further tailpipe emissions are largely reduced. The Prius and TSI do show spikes in emissions during periods of heavy acceleration, but the actual magnitudes of these emissions are small, and this behavior is also apparent during hot

start conditions. With the exception of these events, emissions for the gasoline-powered vehicles are very low after the catalyst lightoff period.

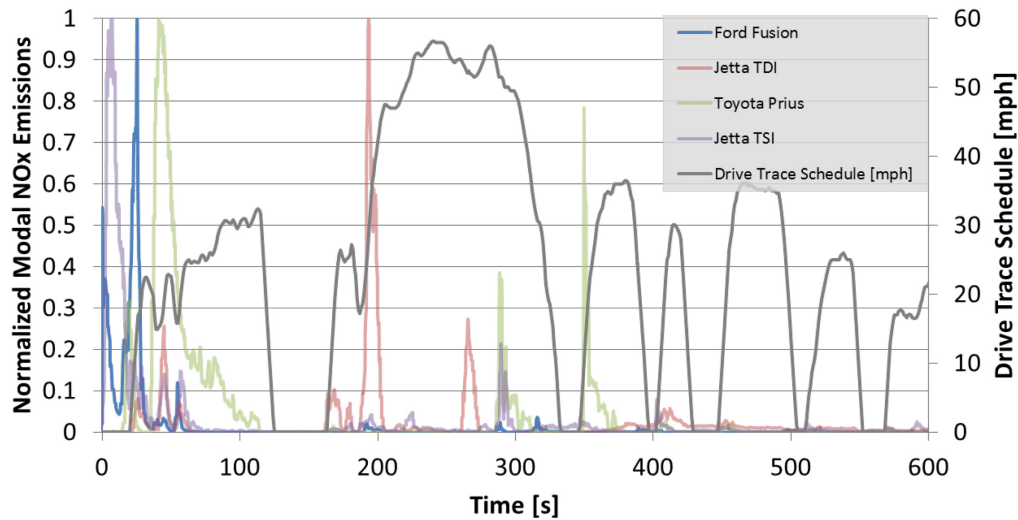


Figure 7.3.2: Normalized Modal NOx Emissions by Vehicle, UDDS CS Cycle

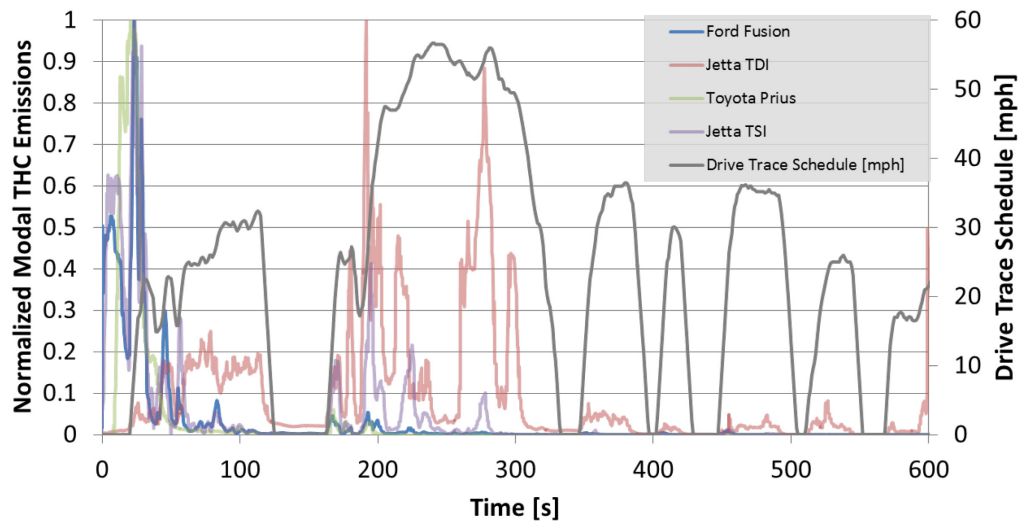


Figure 7.3.3: Normalized Modal THC Emissions by Vehicle, UDDS CS Cycle

The diesel-powered Jetta TDI was found to have significantly different emissions behavior than the gasoline-powered vehicles considered in this thesis. The TDI generates

its highest levels of NO_x and THC during the second hill of the cold start UDDS cycle. This may be due to the nature of the TDI's aftertreatment system; as discussed in Section 4.1, the TDI's aftertreatment strategy uses several different catalysts that may take longer to reach operating temperature than the close-coupled catalysts common to the gasoline vehicles. Though the TDI's peak emissions occur on the second hill, it is worth noting that the vehicle exhibits noticeable levels of emissions throughout much of the cycle, often corresponding to gear shifts and quick changes in engine load.

For each of the vehicles considered, the large modal emissions found during the early part of the cold start UDDS cycle are largely absent when the same test is performed under hot start conditions. Emissions behavior on the hot start and cold start US06 cycles shows similar trends, with greater overall emissions generated due to the aggressive nature of the cycle.

7.4 Powertrain Utilization

Regardless of the specifics of vehicle architecture, each of the research subjects here derives its primary motive force from an internal combustion engine. The strategy with which this engine is operated is a primary driver in the efficiency and fuel economy performance of the vehicle.

Differences in vehicle architecture are largely implemented either to allow a change in base engine design or to affect the way the engine is operated. In earlier chapters, engine utilization maps were provided for individual cycles to illustrate differences in utilization resulting from driving style. Figure 7.4.1 provides a consolidated utilization map for each vehicle that encompasses the hot start UDDS, HWFET, and US06 cycles. Axes are held constant to provide a visual basis for the engine operating space with the exception of the color map, which is adjusted to provide definition. In the case of the TDI, fuel injection quantity is used as the indicator of engine load because of the difficulties encountered in implementing the indicating system as discussed in Chapter 4. The peak load is approximately equivalent to 22 bar IMEP.

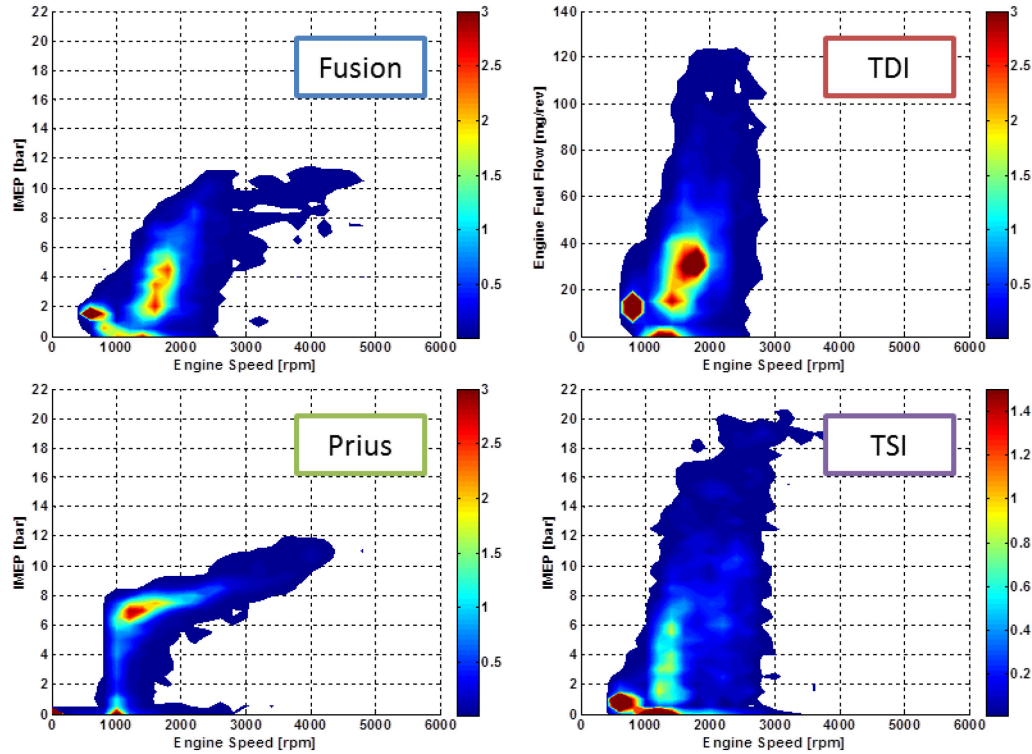


Figure 7.4.1: Engine Utilization Maps by Vehicle, UDDS, HWFET & US06 Cycles

The shape of a typical engine map is such that an area can be identified within which the combination of factors contributing to engine efficiency (friction losses, heat transfer, charge density, etc.) behaves such that efficiency is maximized. In general this area occurs at low to medium speed and at high load [4,5]. Ideally, the engine would operate in this region at all times to make the most of the consumed fuel energy. However, constraints imposed by transient power demands dictate that the engine operate over a range of speeds and loads. Careful design of engine parameters and driveline architecture can influence the required speed and load range for a given engine, directly impacting vehicle efficiency and fuel economy.

The vehicles chosen for this thesis exhibit significant variation in the shape of their engine utilization maps. The Fusion and Prius both make use of naturally aspirated, port-fuel-injected engines that have relatively low power density. The maximum load capability for these engines is around 12 bar IMEP. The TSI and TDI both make use of

aggressively turbocharged engines that are each capable of a wider load range peaking over 20 bar IMEP. This increased load capability allows these vehicles to meet increased power demands by increasing engine load instead of operating the engine at higher speeds. This limits friction losses and in the case of the TSI, it reduces throttling losses as well. The Prius and Fusion are forced to operate at higher engine speeds more often, which is generally less efficient.

Transmission design also has a noticeable effect on the shape of the engine utilization maps. Figure 7.4.2 plots engine speed against vehicle speed in order to illustrate the gear ratio utilization of each vehicle. Points in red denote fueled operation, while gray points show when the engine is unfueled such as during decelerative fuel cutoff. The figure also includes engine speed as a histogram on the left axis.

The Fusion is fitted with a traditional automatic transmission that transfers power using a torque converter. In order to provide smooth takeoff and drivability, the torque converter is often unlocked at low vehicle speed. This causes the effective total gear ratio between the engine and wheels to blend between the physical transmission gear ratios. This can cause the engine to operate over a wider range of speeds in lower gears, and results in less clearly defined lines in Figure 7.4.1. The physical ratios are more clearly defined as straight lines at higher engine speeds where the torque converter is often locked to improve power transmission efficiency.

The TSI and TDI are both equipped with Volkswagen Direct Shift Gearbox (DSG) transmissions that incorporate dual clutches. These types of transmissions are known for efficient power transfer as well as direct control over engine speed. Both transmissions are also capable of shifting quickly, and because they use direct clutch engagement instead of a torque converter, are not subject to as much blending of gear ratios. This contributes to the narrow nature of the vehicle's engine usage maps as the engine speed is more directly constrained except during gear changes. More significant unfueled engine operation is also visible for these vehicles.

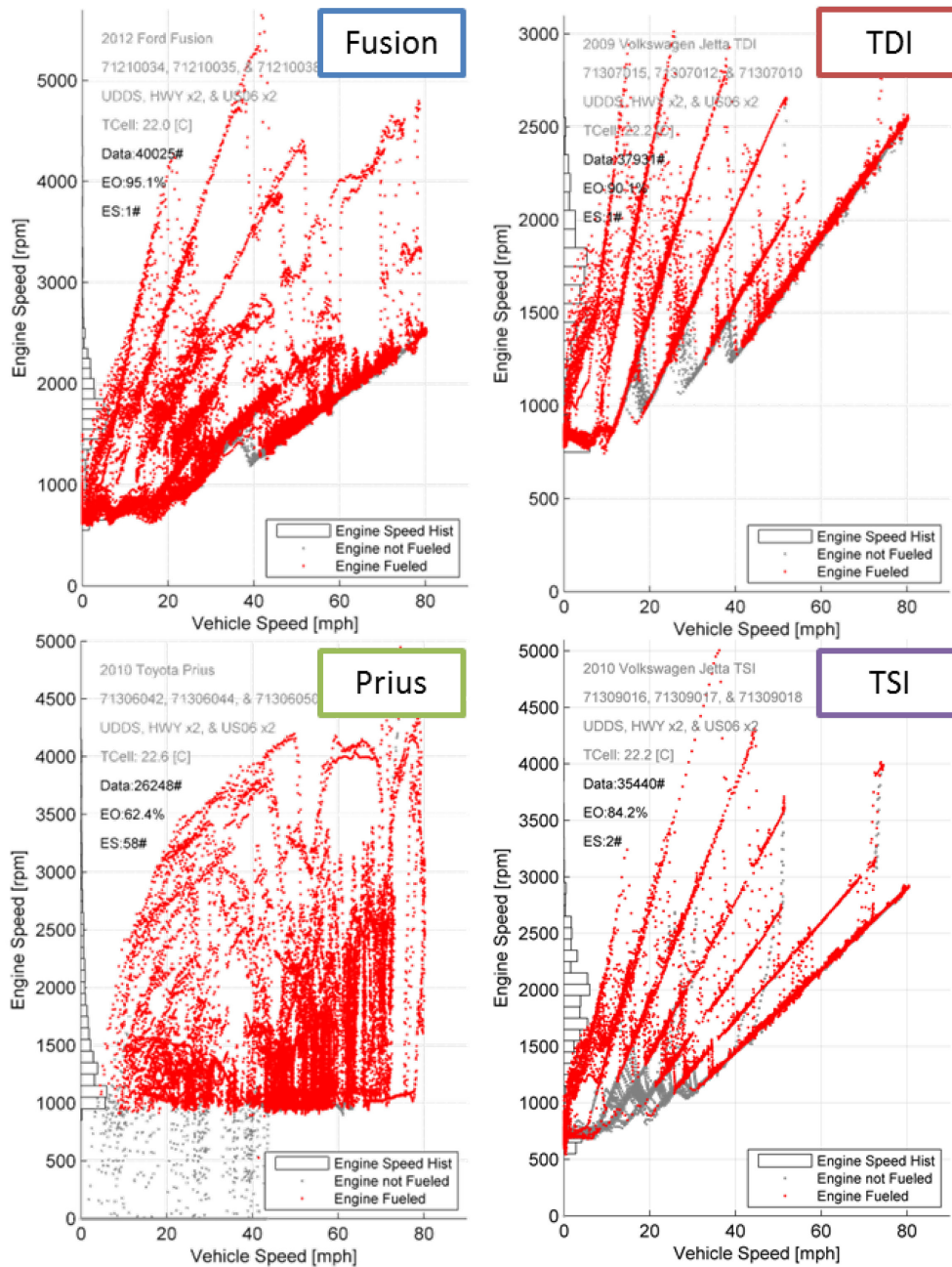


Figure 7.4.2: Engine Speed vs. Vehicle Speed, UDDS, HWFET & US06 Cycles

The Prius' power-split device and electric traction motor are largely responsible for enabling the unique shape of the vehicle's engine utilization map. The shape was

chosen by Toyota to encompass the areas of best efficiency in the engine operating space. This is discussed further in Chapter 6. The power-split transmission essentially functions as a CVT, allowing the Prius to use whichever ratio best suits the needs of the vehicle and engine at any given time. Because of this, the vehicle does not exhibit clearly defined gear ratios in Figure 7.4.2. The vehicle is also capable of full electric operation at low speeds, which is visible on the utilization map as a locus at 0 rpm and 0 bar IMEP. Engine stop events can be seen on the gear ratio map as unfueled points below idle.

The deceleration fuel cutoff behavior of the vehicles is another factor directly affecting fuel consumption on a given cycle. DFCO maps for the four vehicles are shown in Figure 7.4.3. All operation points are shown in red, while DFCO points are shown in blue.

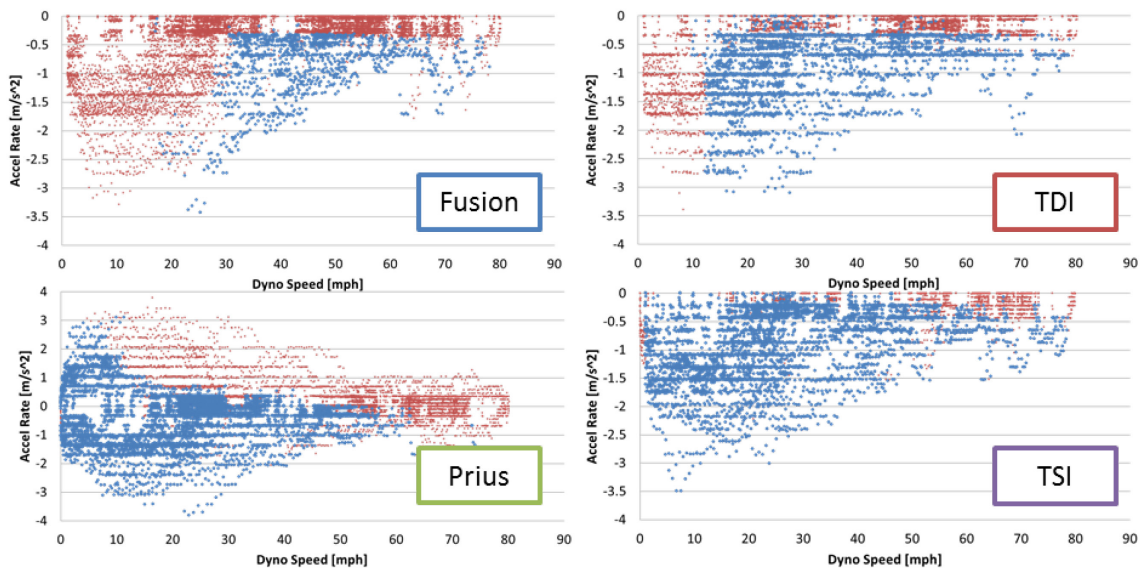


Figure 7.4.3: Deceleration Fuel Cutoff (DFCO) Maps by Vehicle

DFCO behavior is typically driven both by architecture choice and the manufacturer's particular approach toward vehicle drivability. The Fusion shows the smallest tendency to reduce fuel during deceleration, with DFCO operation largely restricted to speeds over 25 mph and decelerations greater than -0.4 m/s^2 . It is the opinion of the author that this behavior may in part be due to torque converter constraints. At

lower speeds where the torque converter is usually unlocked, the engine is fueled to provide fast transient response. Desired off-throttle deceleration behavior is another contributing factor. When the accelerator pedal is released, aggressive DFCO will result in significant engine braking while continuing to supply fuel will cause the vehicle to decelerate much more gently. The manufacturer's perception of customer preferences may have a significant effect on calibration strategy.

The TDI shows more aggressive DFCO behavior than the Fusion. The DSG transmission uses a pair of clutches in lieu of a torque converter, which allows the transmission to transfer power immediately. The nature of the direct-injected diesel engine also allows the vehicle to provide torque quickly when requested. The TDI will cut fuel on deceleration down to 12 mph so long as decelerations are greater than -0.35 m/s^2 .

Among the conventional vehicles, the TSI exhibits the most aggressive fuel cutoff during deceleration. Unlike the Fusion and TDI which have clear speeds below which the engine is commonly fueled, the TSI exhibits aggressive DFCO at all speeds. The engine is only refueled when the transmission clutch disengages to allow the engine to idle. This aggressive behavior is partially enabled by the DSG transmission's lack of a torque converter, but is also a result of aggressive fuel economy optimization. It appears likely that the calibration engineers made the decision to sacrifice some part of transient response to maximize fuel savings during deceleration.

The Prius' DFCO behavior is also very aggressive, enabled in part by the vehicle's ability to operate as an EV at low speeds. Because the traction motor is available to provide torque nearly instantaneously, the Prius provides good transient response while conserving fuel. Tractive EV operation is represented as blue points with positive acceleration rates. It is important to realize that this behavior is dependent on the thermal state of the vehicle as well as the battery's state of charge. Either of these factors may cause the vehicle to operate its gasoline engine where it would otherwise operate as an EV. The Prius does not employ DFCO above 60 mph. At high speed, the Prius spins

its gasoline engine at all times, likely to provide fast transient response when the vehicle is asked to accelerate. Though the vehicle has some ability to spin the engine with the electric motor, it elects instead to fuel the engine at high speeds. It may be that the power required to spin the engine at these speeds is more efficiently provided by fueling the engine than by draining the high voltage battery.

7.5 Cycle Based Heat Losses

Examining the proportion of fuel energy lost to the coolant and exhaust streams can help to illustrate vehicle efficiency behavior. Figure 7.5.1 shows the measured losses over the US06 hot start cycle as a percentage of total fuel energy for each vehicle. As explored previously, other losses include sources not measured such as radiative heat losses from hot surfaces, driveline spin losses and combustion inefficiencies among others.

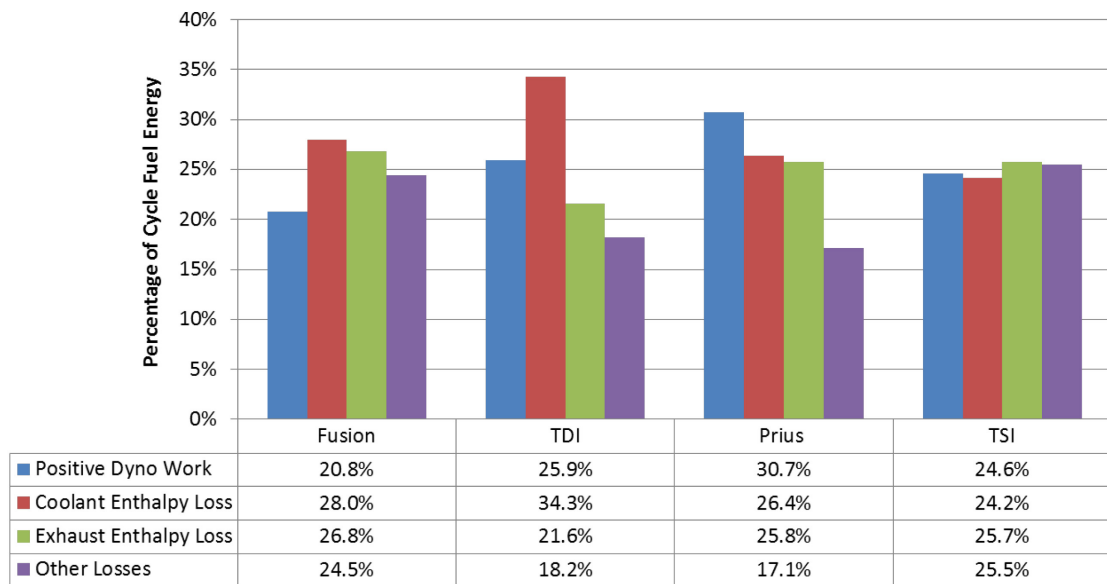


Figure 7.5.1: Fuel Energy Utilization by Vehicle, US06 HS Cycle

The aggressive US06 cycle tends to maximize both positive dynamometer work (equitable to vehicle efficiency) as well as exhaust losses because the engines tend to operate at higher than usual loads. The spark-ignited engines each shed approximately

26% of their fuel energy through increasing exhaust gas enthalpy. The Fusion loses the greatest portion through this pathway at 26.8%, while the Prius and TSI lose 25.8% and 25.7% respectively. Though the difference is minor, it is worth noting that the Prius uses an over-expanded cycle to extract the maximum amount of work from the cylinder charge. The TSI uses a turbocharger to achieve a similar effect, using exhaust gas enthalpy to power a compressor. The TDI exhibited the smallest proportion of fuel lost through the exhaust pathway at 21.6%. Though the diesel engine exhibits higher exhaust mass flow rates, significantly cooler exhaust gas temperatures lower the total enthalpy loss.

In terms of energy lost through the cooling loops, the spark-ignited vehicles exhibited greater variance. Values ranged from 24.2% in the case of the TSI to 28% in the case of the Fusion with the Prius falling in between. The TDI showed considerably higher coolant losses at 34.3% of total fuel energy. It is likely that the high compression ratio of the diesel engine yields high peak combustion temperatures that contribute to higher in-cylinder heat losses.

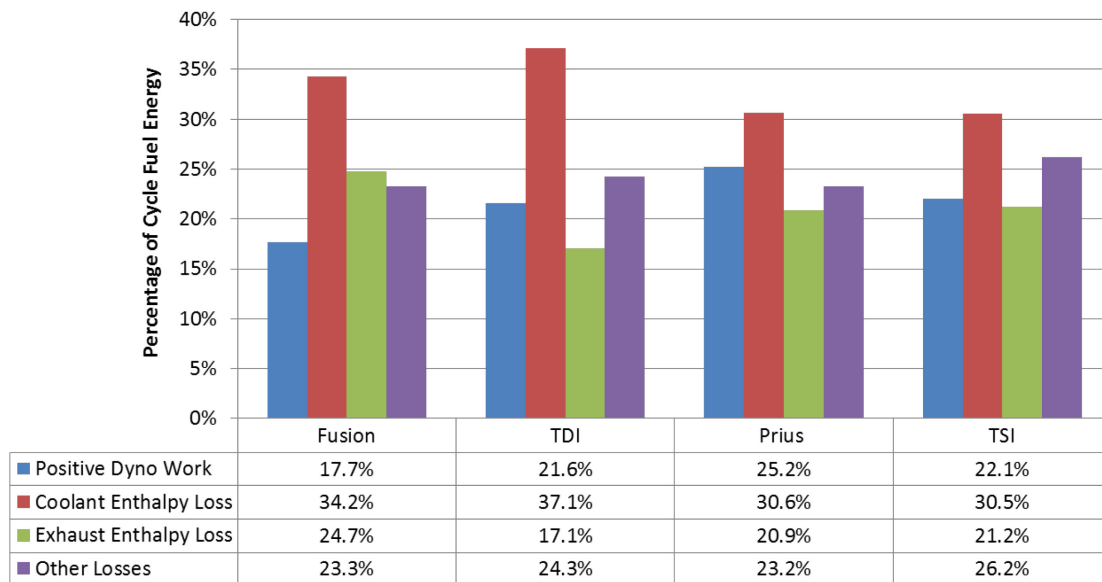


Figure 7.5.2 Fuel Energy Utilization by Vehicle, HWFET Cycle

Figure 7.5.2 shows the measured losses for each vehicle over the gentler HWFET cycle. The proportion of energy lost to the exhaust stream is considerably lower during this test because the vehicles' engines are not loaded as aggressively, causing exhaust temperatures to fall. The trends between vehicles hold true; the Fusion experiences the greatest exhaust losses, followed by the Prius and TSI with the TDI showing the least exhaust enthalpy.

The proportion of fuel energy lost to the vehicle cooling loops increases markedly in the case of the HWFET cycle. The vehicles experience sustained cruising at moderate engine loads, which contributes to constantly elevated temperatures of engine components that otherwise have opportunity to cool during deceleration. Higher engine temperatures increase the amount of heat transfer to the cooling system. Additionally, lower mean engine speeds provide more time for heat transfer from the charge gasses to the cylinder walls, and eventually to the water jacket. These phenomena increase the total proportion of fuel energy lost to the coolant.

The total measured losses for the hot start UDDS cycle are shown in Figure 7.5.3. The losses for the UDDS cycle continue the exhaust enthalpy trend apparent in the HWFET cycle; exhaust losses for all vehicles decreased with gentler operation. Total coolant losses were very similar between the two cycles except in the case of the Prius, which runs its gasoline engine during only 33% of the UDDS cycle and does not reach the coolant temperatures evident during the more aggressive drive cycles. The vehicle operates the engine so little that heat lost to the water jacket goes toward heating the coolant contained on the engine side of the system. The vehicle does not reach an operating temperature hot enough to require consistent coolant exchange between the radiator and engine as seen in the HWFET and US06 cycles. The lack of measurable coolant flow causes the Prius' coolant losses to appear artificially low.

The fact that coolant losses remain the same for the other vehicles suggests that their decreases in vehicle efficiency are not due to increased coolant losses. Instead, relatively fixed losses such as driveline friction become a larger proportion of the total

fuel energy. The Prius is the only vehicle for which efficiency on the UDDS cycle increases over that seen during the HWFET cycle. As discussed in Chapter 6, this is chiefly due to the vehicle's hybrid architecture enabling regenerative braking.

It should be noted that the total measured losses on the HWFET and US06 cycles totaled at least 73.8% of total fuel energy for each of the vehicles included in this thesis. The remaining energy not captured may be found in additional losses such as powertrain friction, convection and radiation from hot surfaces, and any losses due to incomplete combustion of the fuel. The total measured losses for the UDDS cycle are lower in most cases, ranging from 54.7% for the Prius to 73.6% for the Fusion. As mentioned previously, it is likely that the unmeasured and relatively fixed losses become more significant as the vehicles are operated in a less aggressive manner.

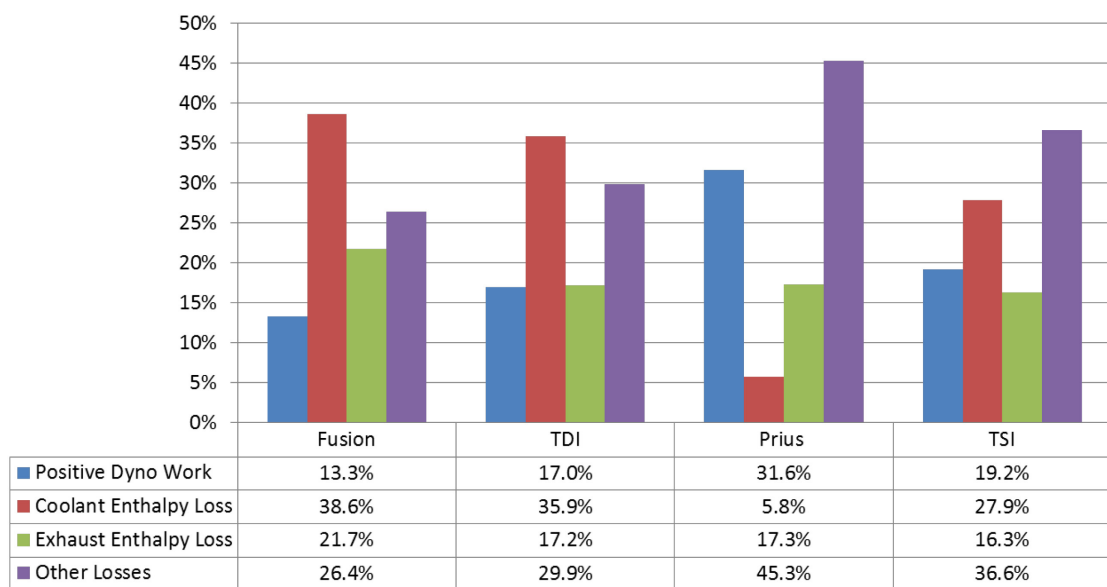


Figure 7.5.3: Fuel Energy Utilization by Vehicle, UDDS Cycle

7.6 WOT Combustion Behavior

The vehicles studied for this thesis work vary significantly in the design of their internal combustion engines. Each engine brings strengths and compromises to the powertrain. To better understand the combustion behavior in each case, pressure traces taken at wide open throttle (WOT) conditions are plotted in Figure 7.6.1. Though each engine operates at different speed and load, these traces represent the peak power generation strategy of each engine. Relevant metrics for each operating point are given in Table 7.6.1.

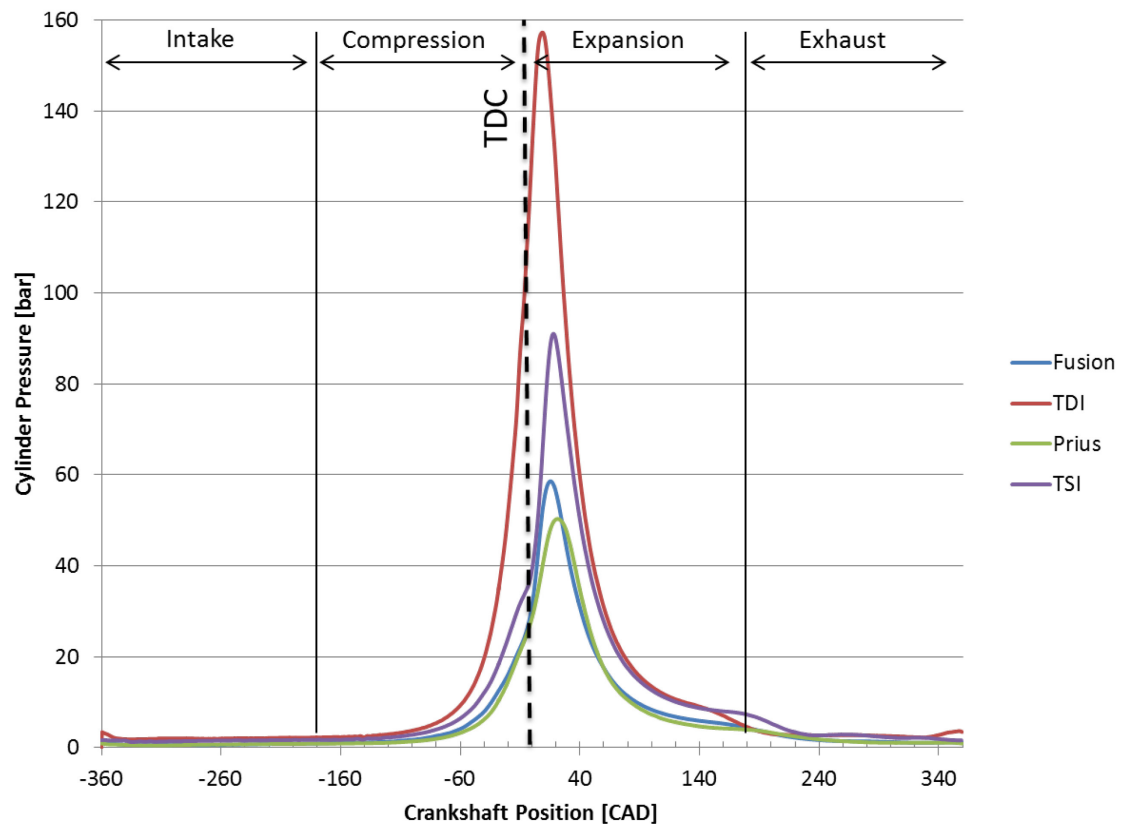


Figure 7.6.1: Pressure Traces at WOT Conditions

Table 7.6.1: WOT Combustion Characteristics

		Fusion	TDI	Prius	TSI
Engine Speed	[rpm]	4830	3006	4970	4505
IMEP	[bar]	11.5	19.6	11.8	18.0
Pmax	[bar]	58.6	160.2	50.3	91.1

It should be remembered that the Jetta TDI proved difficult to instrument with cylinder pressure indicating hardware, and that the resulting pressure traces are not necessarily indicative of normal vehicle operation, but instead should be used to draw general conclusions about the engine architecture. This compromise is discussed in detail in Chapter 5.

At high load conditions, the diesel engine in the Jetta TDI produces the greatest cylinder pressures, with the measured pressure trace peaking at 160.2 bar. These pressures are far above those generated by the gasoline engines, and are enabled by the high compression ratio of the diesel architecture as well as the presence of a turbocharger. Diesel engine components are typically designed for higher pressure to accommodate this, which contributes to the lower speed capability of the engine. Looking at the pressure trace, it would appear that the TDI would exhibit significantly higher IMEP values than the other engines, including the Jetta TSI. However, the TDI's pressure trace suggests that a significant amount of work is being done on the piston before TDC, which counts against the IMEP calculation. While the gasoline engines show less total area under the pressure trace curve, the majority of the work done by these engines is found after TDC during the expansion stroke, contributing positively to IMEP. For example, though the TSI peak cylinder pressure is nearly 70 bar below that of the TDI, the engines exhibit very similar IMEP values.

Though the TSI's cylinder pressure curve falls below that of the Jetta TDI, the gasoline-fueled Volkswagen exhibits significantly higher cylinder pressures than do the Fusion and Prius. This behavior is enabled by the TSI's turbocharger, which allows for a considerably denser cylinder charge that facilitates the burning of additional fuel. As

discussed in Chapter 5, the TSI is knock-limited at peak power, and retards combustion timing while richening the fuel mixture to avoid knock. This can be seen in Figure 7.6.1 where the TSI exhibits later peak cylinder pressure timing, as well as a leveling off of the pressure trace at the end of the compression stroke before significant combustion occurs. The latter effect is visible with the Prius and Fusion, but to a lesser extent.

The Prius exhibits the lowest peak cylinder pressure of the test subjects at 50.3 bar. As discussed in Chapter 6, the Prius employs late intake valve closing to artificially restrict the length of the compression stroke in comparison to the expansion stroke. This increases efficiency at the expense of power density and is responsible for lowering the engine's peak pressures. This effect can also be seen in the Prius' compression curve, which rises several degrees after the other vehicles.

Examining the intake and expansion strokes illuminates the gas exchange strategy of the engines. The TSI and TDI both show higher cylinder pressures during the intake stroke, facilitated by their turbochargers ability to increase intake manifold pressure while the Fusion and Prius are forced to draw air without assistance. The turbochargers also present higher exhaust backpressures, due in part to the physical exhaust restriction imposed by the turbine as well as the higher air flow rates through the engines. These engines also show higher cylinder pressures at the end of the exhaust stroke, and more significant exhaust blowdown events as the exhaust valve opens near the end of the expansion stroke. Especially notable is the TSI's later blowdown event, which may be an effort to maximize work throughout the expansion stroke.

Several of the behaviors discussed in this section can be seen in more detail in the P-V diagrams given in the individual vehicle chapters.

Chapter 8 Conclusions and Future Work

8.1 Conclusions

This thesis work was conducted with the goal of establishing the means with which advanced technology vehicles improve upon the efficiency and fuel economy of legacy technology conventional vehicles. The analysis presented in the previous chapters investigated in detail the tests conducted to illuminate the nuances of vehicle behavior, and several means of improvement were found.

The first of these is advantageous engine design. The Jetta TDI, Jetta TSI, and Prius each exhibited engine architecture strategies different from the Fusion. The TDI and TSI exhibit high engine load capability, producing robust torque that allows the engine to be more useful at lower speeds where friction losses are lower. The smaller displacement of the TSI's engine requires significant operation at high loads, which helps to minimize throttling losses to increase engine efficiency. Because the TDI's diesel architecture does not require a traditional throttling valve, it also benefits from reduced throttling losses. The Prius takes a different approach to engine design, using an over-expanded cycle to maximize efficiency and employing electrified accessories to reduce crankshaft drag. It is clear that the impact of these technologies on efficiency was considerable; going forward, modern vehicles must be fitted with advanced engine concepts to remain competitive.

Advanced engine control was discovered to be another important means of maximizing efficiency. Equipping a vehicle with the means to better utilize the most efficient areas of the engine map contributes to increased engine and vehicle efficiency as well as fuel economy. The TDI and TSI accomplish this with advanced transmissions that forgo the use of torque converters and better restrict the engine to predefined gear ratios, allowing for more precise control of engine speed. When coupled with the versatile load capability of turbocharged engines, this provides a high degree of flexibility in terms of engine utilization. The Prius facilitates usage flexibility with its advanced hybrid system. It was found that this vehicle operates its engine in a very narrow space enabled by the

hybrid system's ability to modulate total engine speed and load in response to various driving conditions. Implementation of advanced transmissions as a means of engine control is a complimentary technology to engine design and must be utilized in order to realize best efficiency numbers for modern vehicles.

One of the issues facing the three conventional vehicles in this test is the inability to recover energy. Significant quantities of kinetic energy must be bled off every time the vehicles decelerate. The Prius used its hybrid architecture to facilitate regenerative braking, recovering energy that was later used to propel the vehicle. This helped to boost the Prius' efficiency above the other vehicles studied, especially where significant opportunity for regenerative braking was available. Though the hardware required to recoup kinetic energy is expensive, the benefits are such that this technology should be strongly considered for implementation, especially in areas with large amounts of stop and go driving.

It was also found that each of the vehicles suffers from significant losses and inefficiencies. Regardless of the vehicle or drive cycle tested, greater than 65% of the total fuel energy consumed made no contribution to developing motive power. Some small quantity of this is used to power creature comforts such as the HVAC system and to maintain the powertrain with coolant and oil pressure. However, the vast majority is lost to the atmosphere by the coolant and exhaust systems. Efforts to reduce these fractions were evident in the test vehicles, but research in the area of waste heat recovery may enable greater efficiency improvements in the future. Thermoelectric materials and efforts based on the Rankine cycle are in development and show promise.

Another challenge facing each of the vehicles in this test is cold start operation. Each of the vehicles exhibited strategies to quickly warm the aftertreatment and base engine systems, but all suffered from reduced vehicle efficiency during cold start conditions. Efforts to quickly raise fluid temperatures and reduce the warming period should be utilized to minimize the impact of cold start conditions on efficiency and fuel economy.

Tailpipe emissions have been a significant driver in vehicular innovation. It was found in this work that these emissions are largely minimal for each of the gasoline vehicles, including the Fusion. These vehicles exhibit larger levels of emissions during cold start, but this behavior is largely mitigated after the aftertreatment catalysts reach operating temperature. The diesel-powered TDI did exhibit larger levels of emissions; this behavior continues to be a challenge for diesel engines as emissions standards become tighter and more difficult to meet. Advancements in aftertreatment technology will likely be required if diesel engines are to continue to be viable in the future.

It should be noted that the efficiency and fuel economy improvements yielded by the advanced technology vehicles does not come entirely without penalty. Each of the alternative architectures studied are considerably more complex than the legacy vehicle, involving complicated forced induction systems, high part count transmissions and in the case of the Prius, a complicated and expensive hybrid system. The performance of the vehicles was studied in detail to attempt to understand these tradeoffs, and it was found that the TSI and Prius exhibited less acceleration performance than the baseline Fusion. The specialty fuels required by the TDI and TSI (diesel fuel and premium gasoline) typically come with price premiums as well. Though the complex issues of life cycle impact and cost of ownership were not included in this work, these issues must also be considered to understand the economic requirements of these alternative architectures.

Regardless of the apparent costs, it is clear within this work that the means exist to significantly reduce the petroleum requirements of passenger vehicles in the modern market while maintaining acceptable performance and the creature comforts consumers have come to expect and demand.

8.2 Recommendations for Future Work

The questions addressed in this thesis work are broad in scope and complex in nature. As fuel economy requirements increase and emissions regulations tighten, additional research and development work must be conducted in order to realize further improvement. This work will involve focus at both the systems level and the individual

component level. Future architectural work will involve new engine architecture and combustion concepts as well as additional transmission concepts. Additionally, hybrid-electric systems can take several forms, each with advantages and disadvantages. Work at the component level will focus on improving existing architectures with low loss components such as electrified water pumps, variable displacement oil pumps, and advanced transmission clutches.

In addition to the continuous development of vehicle architecture and components, more focused areas of opportunity for further research were discovered during the course of this work. The first of these is the significant amount of fuel energy that does not contribute to mechanical power, but is instead lost through waste heat. Research and development work to recapture portions of this waste heat is still largely in its early stages. Efforts are currently focused on thermoelectric materials which generate electrical power when given a temperature differential and on rankine cycle waste heat recovery which uses that same temperature differential, a working fluid, and usually some form of turbomachinery to generate mechanical work. Both areas of research are currently facing difficulties in terms of cost, complexity, and efficiency. Targeted research both to improve existing components and develop optimal architectures for their implementation will help ensure that these technologies are more viable in the future.

Additionally, it was found during this research project that a considerable portion of total fuel energy cannot be measured by the means detailed in this thesis document. A significant portion is lost to other sources like convective and radiative cooling from hot engine surfaces, driveline spin losses and incomplete combustion, among others. While means are available to determine some of these losses (such as detailed emissions bench analysis for combustion efficiency), other sources, such as total heat losses, are more difficult to grasp. Research work dedicated to isolating and understanding these loss components would be valuable in determining further areas to investigate to realize further efficiency improvements.

It was also discovered that each of the vehicles suffered during cold start operation. Increased driveline friction, larger heat losses, emissions considerations and operating strategy changes each contribute to the cold start fuel economy penalties. Further work in low-viscosity lubricants may help to minimize friction losses, while development of powertrains with less thermal capacity would serve to shorten the warming period and thereby the overall economy penalty that accompanies cold start conditions.

As further research is conducted in the field and components and architectures improve, additional value will be realized by conducting further comparative research projects to understand how the advantages and compromises detailed in this work continue to develop.

Bibliography

1. "U.S. Energy Information Administration - EIA - Independent Statistics and Analysis." *United States*. N.p., n.d. Web. 25 Nov. 2012.
2. Sovran, G. and Blaser, D., "A Contribution to Understanding Automotive Fuel Economy and Its Limits," SAE Technical Paper 2003-01-2070, 2003, doi:10.4271/2003-01-2070.
3. Kawamoto, N., Naiki, K., Kawai, T., Shikida, T. et al., "Development of New 1.8-Liter Engine for Hybrid Vehicles," SAE Technical Paper 2009-01-1061, 2009, doi:10.4271/2009-01-1061.
4. Heywood, John B. *Internal Combustion Engine Fundamentals*. New York: McGraw-Hill, 1988. Print.
5. *Automotive Handbook*. Plochingen: Robert Bosch, 2011. Print.
6. Lake, T., Stokes, J., Murphy, R., Osborne, R. et al., "Turbocharging Concepts for Downsized DI Gasoline Engines," SAE Technical Paper 2004-01-0036, 2004, doi:10.4271/2004-01-0036.
7. Han, D., Han, S., Han, B., and Kim, W., "Development of 2.0L Turbocharged DISI Engine for Downsizing Application," SAE Technical Paper 2007-01-0259, 2007, doi:10.4271/2007-01-0259.
8. Fraser, N., Blaxill, H., Lumsden, G., and Bassett, M., "Challenges for Increased Efficiency through Gasoline Engine Downsizing," *SAE Int. J. Engines* 2(1):991-1008, 2009, doi:10.4271/2009-01-1053.
9. Kurniawan, W., Abdullah, S., Nopiah, Z., and Sopian, K., "Multi-objective Optimization of Combustion Process in a Compressed Natural Gas Direct Injection

- Engine using Coupled Code of CFD and Genetic Algorithm," SAE Technical Paper 2007-01-1902, 2007, doi:10.4271/2007-01-1902.
10. Matthes, B., "Dual Clutch Transmissions - Lessons Learned and Future Potential," SAE Technical Paper 2005-01-1021, 2005, doi:10.4271/2005-01-1021.
 11. Scherer, H., Bek, M., and Kilian, S., "ZF New 8-speed Automatic Transmission 8HP70 - Basic Design and Hybridization-," *SAE Int. J. Engines* 2(1):314-326, 2009, doi:10.4271/2009-01-0510.
 12. Shinbori, I., Muto, A., Takeo, H., Takahashi, T. et al., "High Efficiency 6-speed Automatic Transmission," SAE Technical Paper 2010-01-0858, 2010, doi:10.4271/2010-01-0858
 13. Matsubara, T., Yaguchi, H., Takaoka, T., and Jinno, K., "Development of New Hybrid System for Compact Class Vehicles," SAE Technical Paper 2009-01-1332, 2009, doi:10.4271/2009-01-1332.
 14. Çengel, Yunus A., and Michael A. Boles. *Thermodynamics: An Engineering Approach*. Boston: McGraw-Hill Higher Education, 2008. Print.
 15. Takagi, N., Watanabe, T., Fushiki, S., Yamazaki, M. et al., "Development of Exhaust and Evaporative Emissions Systems for Toyota THS II Plug-in Hybrid Electric Vehicle," *SAE Int. J. Fuels Lubr.* 3(1):406-413, 2010, doi:10.4271/2010-01-0831.
 16. Anderson, J., Rask, E., Lohse-Busch, H., Miers, S., "A Comparison of Cold-Start Behavior and its Impact on Fuel Economy for Advanced Technology Vehicles," Upcoming SAE Technical Paper. Submitted for Publication 11-2013.

Appendix A

A.1 Additional Figures


Vehicle 2010 Toyota Prius		Test purpose Vehicle Architecture Eval		Principal Investigator Andersson 2-3088		Folder location		Location Original Print date		2WD - 362 JJA 1.7-13 6/7/2013																																																																																																																																																																																																																																																																																																																																																																																																																																																																																																																																																																																					
Test Cycle and phases												Test Cycle and phases		Test Cycle and phases		Test Cycle and phases		Test Cycle and phases		Test Cycle and phases		Test Cycle and phases		Test Cycle and phases		Test Cycle and phases		Test Cycle and phases		Test Cycle and phases		Test Cycle and phases		Test Cycle and phases		Test Cycle and phases		Test Cycle and phases		Test Cycle and phases		Test Cycle and phases		Test Cycle and phases		Test Cycle and phases		Test Cycle and phases		Test Cycle and phases		Test Cycle and phases		Test Cycle and phases		Test Cycle and phases		Test Cycle and phases		Test Cycle and phases		Test Cycle and phases		Test Cycle and phases		Test Cycle and phases		Test Cycle and phases		Test Cycle and phases		Test Cycle and phases		Test Cycle and phases		Test Cycle and phases		Test Cycle and phases		Test Cycle and phases		Test Cycle and phases		Test Cycle and phases		Test Cycle and phases		Test Cycle and phases		Test Cycle and phases		Test Cycle and phases		Test Cycle and phases		Test Cycle and phases		Test Cycle and phases		Test Cycle and phases		Test Cycle and phases		Test Cycle and phases		Test Cycle and phases		Test Cycle and phases		Test Cycle and phases		Test Cycle and phases		Test Cycle and phases		Test Cycle and phases		Test Cycle and phases		Test Cycle and phases		Test Cycle and phases		Test Cycle and phases		Test Cycle and phases		Test Cycle and phases		Test Cycle and phases		Test Cycle and phases		Test Cycle and phases		Test Cycle and phases		Test Cycle and phases		Test Cycle and phases		Test Cycle and phases		Test Cycle and phases		Test Cycle and phases		Test Cycle and phases		Test Cycle and phases		Test Cycle and phases		Test Cycle and phases		Test Cycle and phases		Test Cycle and phases		Test Cycle and phases		Test Cycle and phases		Test Cycle and phases		Test Cycle and phases		Test Cycle and phases		Test Cycle and phases		Test Cycle and phases		Test Cycle and phases		Test Cycle and phases		Test Cycle and phases		Test Cycle and phases		Test Cycle and phases		Test Cycle and phases		Test Cycle and phases		Test Cycle and phases		Test Cycle and phases		Test Cycle and phases		Test Cycle and phases		Test Cycle and phases		Test Cycle and phases		Test Cycle and phases		Test Cycle and phases		Test Cycle and phases		Test Cycle and phases		Test Cycle and phases		Test Cycle and phases		Test Cycle and phases		Test Cycle and phases		Test Cycle and phases		Test Cycle and phases		Test Cycle and phases		Test Cycle and phases		Test Cycle and phases		Test Cycle and phases		Test Cycle and phases		Test Cycle and phases		Test Cycle and phases		Test Cycle and phases		Test Cycle and phases		Test Cycle and phases		Test Cycle and phases		Test Cycle and phases		Test Cycle and phases		Test Cycle and phases		Test Cycle and phases		Test Cycle and phases		Test Cycle and phases		Test Cycle and phases		Test Cycle and phases		Test Cycle and phases		Test Cycle and phases		Test Cycle and phases		Test Cycle and phases		Test Cycle and phases		Test Cycle and phases		Test Cycle and phases		Test Cycle and phases		Test Cycle and phases		Test Cycle and phases		Test Cycle and phases		Test Cycle and phases		Test Cycle and phases		Test Cycle and phases		Test Cycle and phases		Test Cycle and phases		Test Cycle and phases		Test Cycle and phases		Test Cycle and phases		Test Cycle and phases		Test Cycle and phases		Test Cycle and phases		Test Cycle and phases		Test Cycle and phases		Test Cycle and phases		Test Cycle and phases		Test Cycle and phases		Test Cycle and phases		Test Cycle and phases		Test Cycle and phases		Test Cycle and phases		Test Cycle and phases		Test Cycle and phases		Test Cycle and phases		Test Cycle and phases		Test Cycle and phases		Test Cycle and phases		Test Cycle and phases		Test Cycle and phases		Test Cycle and phases		Test Cycle and phases		Test Cycle and phases		Test Cycle and phases		Test Cycle and phases		Test Cycle and phases		Test Cycle and phases		Test Cycle and phases		Test Cycle and phases		Test Cycle and phases		Test Cycle and phases		Test Cycle and phases		Test Cycle and phases		Test Cycle and phases		Test Cycle and phases		Test Cycle and phases		Test Cycle and phases		Test Cycle and phases		Test Cycle and phases		Test Cycle and phases		Test Cycle and phases		Test Cycle and phases		Test Cycle and phases		Test Cycle and phases		Test Cycle and phases		Test Cycle and phases		Test Cycle and phases		Test Cycle and phases		Test Cycle and phases		Test Cycle and phases		Test Cycle and phases		Test Cycle and phases		Test Cycle and phases		Test Cycle and phases		Test Cycle and phases		Test Cycle and phases		Test Cycle and phases		Test Cycle and phases		Test Cycle and phases		Test Cycle and phases		Test Cycle and phases		Test Cycle and phases		Test Cycle and phases		Test Cycle and phases		Test Cycle and phases		Test Cycle and phases		Test Cycle and phases		Test Cycle and phases		Test Cycle and phases		Test Cycle and phases		Test Cycle and phases		Test Cycle and phases		Test Cycle and phases		Test Cycle and phases		Test Cycle and phases		Test Cycle and phases		Test Cycle and phases		Test Cycle and phases		Test Cycle and phases		Test Cycle and phases		Test Cycle and phases		Test Cycle and phases		Test Cycle and phases		Test Cycle and phases		Test Cycle and phases		Test Cycle and phases		Test Cycle and phases		Test Cycle and phases		Test Cycle and phases		Test Cycle and phases		Test Cycle and phases		Test Cycle and phases		Test Cycle and phases		Test Cycle and phases		Test Cycle and phases		Test Cycle and phases		Test Cycle and phases		Test Cycle and phases		Test Cycle and phases		Test Cycle and phases		Test Cycle and phases		Test Cycle and phases		Test Cycle and phases		Test Cycle and phases		Test Cycle and phases		Test Cycle and phases		Test Cycle and phases		Test Cycle and phases		Test Cycle and phases		Test Cycle and phases		Test Cycle and phases		Test Cycle and phases		Test Cycle and phases		Test Cycle and phases		Test Cycle and phases		Test Cycle and phases		Test Cycle and phases		Test Cycle and phases		Test Cycle and phases		Test Cycle and phases		Test Cycle and phases		Test Cycle and phases		Test Cycle and phases		Test Cycle and phases		Test Cycle and phases		Test Cycle and phases		Test Cycle and phases		Test Cycle and phases		Test Cycle and phases		Test Cycle and phases		Test Cycle and phases		Test Cycle and phases		Test Cycle and phases		Test Cycle and phases		Test Cycle and phases		Test Cycle and phases		Test Cycle and phases		Test Cycle and phases		Test Cycle and phases		Test Cycle and phases	

Figure A.1.1 – Vehicle Dynamometer Test Plan Document

A.2 Matlab Analysis Code

The following is an example of the code written to determine cycle-based economy, efficiency, and energy loss statistics.

```
close all

clear all

clc

%Manually chosen bag number

BagNo = 3;

BagNo2 = 4;

BagNo3 = 4;

BagNo4 = 4;

% Load data

% Load excel file (change the file name as needed)

data = xlsread('71309018_US06Hot.xlsx','Data');

vars = xlsread('71309018_US06Hot.xlsx','Variables');

% -----

% Exhaust Bag Definition
```

```

ct = 1;

for i = 1:length(data(:,1))

    if data(i,vars(41)) == BagNo | data(i,vars(41)) == BagNo2 |
data(i,vars(41)) == BagNo3 | data(i,vars(41)) == BagNo4

        % Store variables

        Batt12V_Curr_HiokiI1_A =
data(i,vars(1));

        Batt12V_Volt_V(ct) =
data(i,vars(2));

        ACCompSwitch_CAN(ct) =
data(i,vars(3));

        AuxRadiatorIn_C(ct) =
data(i,vars(4));

        AuxRadiatorOut_C(ct) =
data(i,vars(5));

        AxleTorque_Left_Nm(ct) =
data(i,vars(6));

        AxleTorque_Right_Nm(ct) =
data(i,vars(7));

        CabinTemp_C(ct) =
data(i,vars(8));

        CabinVentFloorTemp_C(ct) =
data(i,vars(9));

        CabinVentTemp_C(ct) =
data(i,vars(10));

```

CellPress_inHg(ct)	=
data(i,vars(11));	
CellRH_per(ct)	=
data(i,vars(12));	
CellTemp_C(ct)	=
data(i,vars(13));	
Lambda_OCR(ct)	=
data(i,vars(14));	
Cyl1_AI50_CAD(ct)	=
data(i,vars(15));	
Cyl1IMEP_bar(ct)	=
data(i,vars(16));	
Cyl1Pmax_bar(ct)	=
data(i,vars(17));	
Deltat_s(ct)	=
data(i,vars(18));	
Distance_mi(ct)	=
data(i,vars(19));	
DriveScheduleTime_s(ct)	=
data(i,vars(20));	
DriveTraceSchedule_mph(ct)	=
data(i,vars(21));	
DynoLoadCell_N(ct)	=
data(i,vars(22));	
DynoPowerCalc_kW(ct)	=
data(i,vars(23));	
DynoSpeed_mph(ct)	=
data(i,vars(24));	

DynoTargetPowerCalc_kW(ct)	=
data(i,vars(25));	
DynoTractiveForce_N(ct)	=
data(i,vars(26));	
EngClntTemp_CAN_C(ct)	=
data(i,vars(27));	
EngClntBypassTemp_C(ct)	=
data(i,vars(28));	
EngFuelFlowDirect_ccs(ct)	=
data(i,vars(29));	
EngFuelTemp_C(ct)	=
data(i,vars(30));	
EngIntakeAirTemp_CAN_C(ct)	=
data(i,vars(31));	
EngOilDipstick_C(ct)	=
data(i,vars(32));	
EngOilPan_C(ct)	=
data(i,vars(33));	
EngOil_CAN_C(ct)	=
data(i,vars(34));	
EngSpeed_rpm(ct)	=
data(i,vars(35));	
EngSpeedCAN_rpm(ct)	=
data(i,vars(36));	
ThrottlePos_CAN_per(ct)	=
data(i,vars(37));	
EngTorqueDirect_Nm(ct)	=
data(i,vars(38));	

EngTorque_CAN_Nm(ct)	=
data(i,vars(39));	
Cat_Post_Temp_C(ct)	=
data(i,vars(40));	
ExhaustBag(ct)	=
data(i,vars(41));	
ExternalLineTemp_C(ct)	=
data(i,vars(42));	
FuelFlowInt_CAN(ct)	=
data(i,vars(43));	
FuelPower_Calc_kw(ct)	=
data(i,vars(44));	
HeaterCoreFlow_gpm(ct)	=
data(i,vars(45));	
HeaterCoreIn_C(ct)	=
data(i,vars(46));	
HeaterCoreOut_C(ct)	=
data(i,vars(47));	
HiokiTime_H0_s(ct)	=
data(i,vars(48));	
I1_a(ct)	=
data(i,vars(49));	
IH1_ahr(ct)	=
data(i,vars(50));	
IntercoolerIn_C(ct)	=
data(i,vars(51));	
IntercoolerOut_C(ct)	=
data(i,vars(52));	

LocalMasterTime_s(ct)	=
data(i,vars(53));	
LocalMasterTimeOCR_s(ct)	=
data(i,vars(54));	
LocalMasterTimeExh_s(ct)	=
data(i,vars(55));	
LocalMasterTimeSemtech_s(ct)	=
data(i,vars(56));	
LocalMasterTimeVehicleDAQ_s(ct)	=
data(i,vars(57));	
LocalMasterTimeH0_s(ct)	=
data(i,vars(58));	
LocalPCTime_s(ct)	=
data(i,vars(59));	
LocalPCTimeOCR_s(ct)	=
data(i,vars(60));	
LocalPCTimeCAN_s(ct)	=
data(i,vars(61));	
LocalPCTimeExh_s(ct)	=
data(i,vars(62));	
LocalPCTimeSemtech_s(ct)	=
data(i,vars(63));	
LocalPCTimeVehicleDAQ_s(ct)	=
data(i,vars(64));	
LocalPCTimeH0_s(ct)	=
data(i,vars(65));	
MWP1_(ct)	=
data(i,vars(66));	

P1_W(ct)	=
data(i,vars(67));	
PedalAccelPosCAN_per(ct)	=
data(i,vars(68));	
PedalBrakePosCAN_per(ct)	=
data(i,vars(69));	
IntAirPress_PostThrottle_kPa(ct)	=
data(i,vars(70));	
IntAirPress_PreThrottle_kPa(ct)	=
data(i,vars(71));	
PWP1_(ct)	=
data(i,vars(72));	
AuxRadiatorFlow_gpm(ct)	=
data(i,vars(73));	
RadiatorFlow_gpm(ct)	=
data(i,vars(74));	
RadiatorIn_C(ct)	=
data(i,vars(75));	
RadiatorOut_C(ct)	=
data(i,vars(76));	
SemRawCO_mgs(ct)	=
data(i,vars(77));	
SemRawCO_ppm(ct)	=
data(i,vars(78));	
SemRawCO2_mgs(ct)	=
data(i,vars(79));	
SemRawCO2_ppm(ct)	=
data(i,vars(80));	

SemRawFuel_gs(ct)	=
data(i,vars(81));	
SemRawNO_ppm(ct)	=
data(i,vars(82));	
SemRawNOx_mgs(ct)	=
data(i,vars(83));	
SemRawNOx_ppm(ct)	=
data(i,vars(84));	
SemRawTHC_mgs(ct)	=
data(i,vars(85));	
SemRawTHC_ppm(ct)	=
data(i,vars(86));	
KickdownSwitch_CAN(ct)	=
data(i,vars(87));	
TailpipePres_inH20(ct)	=
data(i,vars(88));	
ExhVolFlow_ft3min(ct)	=
data(i,vars(89));	
ExhVolFlow_m3min(ct)	=
data(i,vars(90));	
Time_s(ct)	=
data(i,vars(91));	
TireTemp_C(ct)	=
data(i,vars(92));	
TransGear(ct)	=
data(i,vars(93));	
TransOilTemp_C(ct)	=
data(i,vars(94));	

```

        U1_(ct)                                =
data(i,vars(95));

        Clutch_CAN(ct)                        =
data(i,vars(96));

        Clutch1_CAN(ct)                      =
data(i,vars(97));

        VehicleSpeed_CAN_kph(ct)            =
data(i,vars(98));

        WP1(ct)                              =
data(i,vars(99));

        %Increase counter

        ct = ct + 1;

    end

end

% -----

```

IMEP Correction

```

for i = 1:length(Cyl1IMEP_bar)

    if Cyl1IMEP_bar(i) < 0.1;

        Cyl1IMEP_bar(i) = 0;
    end
end

```

```

        end

    end

    for i = 1:length(CyllIMEP_bar) - 1

        if (CyllIMEP_bar(i+1) - CyllIMEP_bar(i)) == 0;

            CyllIMEP_bar(i) = 0;

        end

    end
end

```

Calculations

Correct DynoTractiveForce_N for 0.4s lag of 2WD Dynamometer

```

    for i = 1:(length(DynoTractiveForce_N) - 4)

        DynoTractiveForce_N(i) = DynoTractiveForce_N(i+4);

    end

    % Dyno work = dyno speed * dyno tractive force

    DynoWork_W = DynoSpeed_mph .* 0.447 .* DynoTractiveForce_N;

    % FuelNRGIn_W = EngFuelFlowDirect_ccs * 0.74 (g/ml) * 18492
    (BTU/lbm) *

    % 2.326 (J/g per BTU/lbm)

```

```

        FuelNRGIn_W = EngFuelFlowDirect_ccs .* 0.74 .* 18492 .*
2.326;

        % Indicated Engine Power [W] = (IMEP(kPa) * Vd (L) * N (rev/s)) /
(Nr)

        IndEngineWork_W = Cyl1IMEP_bar * 100 * 1.8 .* (EngSpeed_rpm /
60) / 2;

        % Brake Engine Power [W] = Torque * Speed (rad/s)

        BrakeEngineWork_W = EngTorque_CAN_Nm .* (EngSpeed_rpm * 2 *
3.14159 / 60);

        %      % Integrated Battery Amp Hours

        %

        %      IntBattPower_Ah(1) = 0;

        %      for i = 2:length(Time_s)

        %          IntBattPower_Ah(i) = IntBattPower_Ah(i-1) +
I1_HighVoltBatt(i) * 1 / 36000;

        %      end

        %

        %      % Battery NEC

```

```

%      trip = length(IntBattPower_Ah);

%

%

%      BatteryZCV_V = mean(U1);

%      BatteryNEC_kWh =IntBattPower_Ah(trip) * BatteryZCV_V /
1000;

%      BatteryNEC_kJ = BatteryNEC_kWh * 3600;

%

%      for i = 1:length(IntBattPower_Ah)

%          IntBatteryNEC_kWh(i) = IntBattPower_Ah(i) *
BatteryZCV_V / 1000;

%      end


% Create DynoWorkPos_W vector

for i = 1:length(DynoWork_W)

    if DynoWork_W(i) > 0

        DynoWorkPos_W(i) = DynoWork_W(i);

    else

        DynoWorkPos_W(i) = 0;

    end

end

DynoWorkPos_W=DynoWorkPos_W';

```

```

% Create TEPos_N vector

for i = 1:length(DynoTractiveForce_N)

    if DynoTractiveForce_N(i) > 0

        TEPos_N(i) = DynoTractiveForce_N(i);

    else

        TEPos_N(i) = 0;

    end

end

TEPos_N=TEPos_N';

% Vehicle Eff Contour Plot Vector (CORRECTED FOR DYNO OFFSET)

VehicleEffInst_percent = (DynoWork_W./FuelNRGIn_W).*100;


for i = 1:length(VehicleEffInst_percent)

    if VehicleEffInst_percent(i) < 0

        VehicleEffInst_percent(i) = 0;

    end

end

```

```

VehicleEffPlot=diag(VehicleEffInst_percent,0);

% Create Moving Fuel NRG Vector

for i = 1:length(FuelNRGIN_W)

    if DynoSpeed_mph(i) > 1.0

        FuelNRGINMoving_W(i) = FuelNRGIN_W(i);

    else

        FuelNRGINMoving_W(i) = 0;

    end

end

% Create Idle Fuel NRG Vector

for i = 1:length(FuelNRGIN_W)

    if DynoSpeed_mph(i) < 1.0 && EngSpeed_rpm(i) > 100

        FuelNRGINIdle_W(i) = FuelNRGIN_W(i);

    else

        FuelNRGINIdle_W(i) = 0;

    end

end

```

```

% Create Acceleration State Vector

for i= 2:length(DynoSpeed_mph)

    if DynoSpeed_mph(i) > DynoSpeed_mph(i-1)

        AccelState(i) = 1;

    else

        AccelState(i) = 0;

    end

end

AccelState(1) = 0;

% Create Actual Acceleration Vector

for i = 2:length(DynoSpeed_mph)

    AccelRate_mss(i) = ((DynoSpeed_mph(i) * 0.447) -
(DynoSpeed_mph(i-1) * 0.447)) * 10;

end

AccelRate_mss(1) = 0;

% Create Tractive Fuel NRG, Fuel Flow and Work Vectors

for i = 1:length(FuelNRGIn_W)

    if AccelState(i) > 0.5

        FuelNRGInTractive_W(i) = FuelNRGIn_W(i);

    end

end

```



```

        EngFuelFlowDirectTractive_ccs(i) =
EngFuelFlowDirect_ccs(i);

        DynoWorkTractive_W(i) = DynoWork_W(i);

    else

        FuelNRGINTractive_W(i) = 0;

        EngFuelFlowDirectTractive_ccs(i) = 0;

        DynoWorkTractive_W(i) = 0;

    end

end

% Create Decel Fuel NRG Vector

for i = 1:length(FuelNRGIN_W)

    if AccelState(i) < 0.5

        FuelNRGINDecel_W(i) = FuelNRGIN_W(i);

    else

        FuelNRGINDecel_W(i) = 0;

    end

end

% Engine On State

for i = 1:length(Time_s)

```

```

        if EngSpeed_rpm(i) > 100

            EngineOn(i) = 1;

        else

            EngineOn(i) = 0;

        end

    end

    PercentEngineOn = sum(EngineOn)/numel(EngineOn) * 100;

% Idle State

    for i = 1:length(Time_s)

        if EngSpeed_rpm(i) > 100 && DynoSpeed_mph(i) < 1

            EngineIdle(i) = 1;

        else

            EngineIdle(i) = 0;

        end

    end

    PercentEngineIdle = sum(EngineIdle)/numel(EngineIdle) * 100;

% Calculate Estimated Engine Torque

```

```

        for i = 1:length(DynoWorkPos_W)

            EstEngTorque_Nm(i) = DynoWorkPos_W(i) / ( 0.85 *
EngSpeed_rpm(i) * 2 * pi / 60);

        end

% Constant Speed Constant Pedal Test Calculations (Comment for drive
cycles and other tests)

%

%      %Convert pedal voltage to %

%      PedalPos_per = (PedalPos_V - 0.746197) ./ (3.751797 - 0.746197)
.* 100;

%

%      %Define Time Steps [Start, End] in order of pedal application

%      MappingTimes = [58.2 , 69.5;           %10 pedal

%                      92.5 , 115.9;         %20 pedal

%                      298.4 , 314.2;         %30 pedal

%                      126.3 , 137.4;         %40 pedal

%                      320.1 , 335.8;         %50 pedal

%                      145.5 , 160.2;         %60 pedal

%                      345.8 , 361;           %70 pedal

```

```

%                                169.8 , 187.5;           %80 pedal

%                                376 , 389;           %90 pedal

%                                200 , 211];           %100 pedal

%

%      % Create array to store vectors between the time limits.
(Row, Column, Depth)

%      % Rows hold values, Columns 1 - 6 are vars below, and Depth
is a

%      % particular holding point

%

%      ct1 = 1;

%      for ct1 = 1:10;

%      ct2 = 1;

%      for i =1:length(Time_s);

%      if MappingTimes(ct1,1) <= Time_s(i) && Time_s(i)
< MappingTimes(ct1,2)

%      SSMap(ct2,1,ct1) = Time_s(i);

%      SSMap(ct2,2,ct1) = FuelNRGIn_W(i);

%      SSMap(ct2,3,ct1) = DynoWorkPos_W(i);

%      SSMap(ct2,4,ct1) =
(SSMap(ct2,3,ct1)/SSMap(ct2,2,ct1)) * 100;

%      SSMap(ct2,5,ct1) = EstEngTorque_Nm(i);

%      SSMap(ct2,6,ct1) = EngSpeed_rpm(i);

```

```

%                                SSMap(ct2,7,ct1) = IndEngineWork_W(i);

%                                ct2 = ct2 + 1;

%                                end

%                                end

%                                ct1 = ct1 + 1;

%                                end

%

%

%                                % Now we create arrays to develop the statistics for
plotting.

%                                %The end result is SSMapPoints. Rows 1-10 correspond to
points

%                                %1-10, and columns 1-6 correspond to the statistics
generated in

%                                %the for loop above. The points are the averages of the
stats.

%                                for MapArray_Depth = 1:10

%                                for MapArray_Col = 1:7

%                                MapArrayCount = 0;

%                                for MapArray_Row = 1:length(SSMap)

%                                if
SSMap(MapArray_Row,MapArray_Col,MapArray_Depth) > 0

%                                MapArrayCount = MapArrayCount + 1;

%                                end

```

```

%                               MapArray_Sum(MapArray_Col) =
sum(SSMap(:,MapArray_Col,MapArray_Depth));

%                               MapArray_Ct(MapArray_Col) = MapArrayCount;

%                               end

%                               end

%                               MapArray_Avg = MapArray_Sum ./ MapArray_Ct;

%                               SSMapPoints(MapArray_Depth,1) = MapArray_Avg(1,1);

%                               SSMapPoints(MapArray_Depth,2) = MapArray_Avg(1,2);

%                               SSMapPoints(MapArray_Depth,3) = MapArray_Avg(1,3);

%                               SSMapPoints(MapArray_Depth,4) = MapArray_Avg(1,4);

%                               SSMapPoints(MapArray_Depth,5) = MapArray_Avg(1,5);

%                               SSMapPoints(MapArray_Depth,6) = MapArray_Avg(1,6);

%                               SSMapPoints(MapArray_Depth,7) = MapArray_Avg(1,7);

%

%                               % Add pedal position as ninth column. Note: This is dumb.
Must be

%                               % adjusted if pedal pos changes from 10:10:100.

%                               PedalCounter = 1;

%                               for Pedal = 10:10:100

%                               SSMapPoints(PedalCounter,9) = Pedal;

%                               PedalCounter = PedalCounter + 1;

%                               end

```

```

%

%           end

%

%

%           % Make Column 8 Indicated Efficiency (%)

%           for i = 1:length(SSMapPoints)

%               SSMapPoints(i,8) = (SSMapPoints(i,7) /
SSMapPoints(i,2)) * 100;

%           end

%

```

DFCO Diagram - Used to plot points where vehicle is in Decel Fuel Cutoff (DFCO)

```

CutoffFuelFlowRate_ccs = 0.05;

count = 1;

for i = 1:length(Time_s)

    if DynoSpeed_mph(i) > 1 && EngFuelFlowDirect_ccs(i) <
CutoffFuelFlowRate_ccs && AccelRate_mss(i) < 0

        DFCO(count,1) = AccelRate_mss(i);

        DFCO(count,2) = DynoSpeed_mph(i);

        DFCO(count,3) = EngSpeed_rpm(i);

        DFCO(count,4) = EngFuelFlowDirect_ccs(i);
    end
end

```

```

        DFCO(count,5) = round(AccelRate_mss(i) * 10) / 10;

        DFCO(count,6) = DynoTractiveForce_N(i);

        count = count + 1;

    end

end

count = 1;

for i = 1:length(Time_s)

    if DynoSpeed_mph(i) > 1 && EngFuelFlowDirect_ccs(i) <
CutoffFuelFlowRate_ccs && AccelRate_mss(i) < 0 && EngSpeed_rpm(i) > 200

        DFCO1(count,1) = AccelRate_mss(i);

        DFCO1(count,2) = DynoSpeed_mph(i);

        DFCO1(count,3) = EngSpeed_rpm(i);

        DFCO1(count,4) = EngFuelFlowDirect_ccs(i);

        DFCO1(count,5) = round(AccelRate_mss(i) * 10) / 10;

        DFCO1(count,6) = DynoTractiveForce_N(i);

        count = count + 1;

    end

end

```

EV Operation


```

count = 1;

for i = 1:length(Time_s)

    if DynoSpeed_mph(i) > 1 && EngFuelFlowDirect_ccs(i) <
CutoffFuelFlowRate_ccs

        EVops(count,1) = AccelRate_mss(i);

        EVops(count,2) = DynoSpeed_mph(i);

        EVops(count,3) = DynoTractiveForce_N(i);

        count = count + 1;

    end

end

```

Emissions Matrix - Used to output integrated emissions levels against time

```

IntCO_mg(1) = 0;

IntNOx_mg(1) = 0;

IntTHC_mg(1) = 0;

for i = 2:length(Time_s)

    IntCO_mg(i) = IntCO_mg(i-1) + SemRawCO_mgs(i) / 10;

    IntNOx_mg(i) = IntNOx_mg(i-1) + SemRawNOx_mgs(i) / 10;

    IntTHC_mg(i) = IntTHC_mg(i-1) + SemRawTHC_mgs(i) / 10;

end

```

```

for i = 1:length(Time_s)

    EmissionsMat(i,1) = Time_s(i);

    EmissionsMat(i,2) = IntCO_mg(i);

    EmissionsMat(i,3) = IntNOx_mg(i);

    EmissionsMat(i,4) = IntTHC_mg(i);

end

```

Radiator Energy Loss

Properties for 50/50 Glycol/H2O at 200F SG = 1.038, p = 3.929 kg/gal cp = linear curve fit below

```

%cp Based on linear curve fit

TavgRad_K = ((RadiatorIn_C + 273) + (RadiatorOut_C + 273)) /
2;

cpRad_JkgK = 3.2675 .* TavgRad_K + 2429.1;

RadFlowNRG_W = (RadiatorFlow_gpm/60) .* 3.929 .* cpRad_JkgK .*
(RadiatorIn_C - RadiatorOut_C);

for i = 1:length(Time_s)

    if EngSpeed_rpm(i) > 50

        RadFlowNRGEngOn_W(i) = RadFlowNRG_W(i);

    else

```

```

        RadFlowNRGEngOn_W(i) = 0;

    end

end

%Integrated Radiator Loss

    IntRadNRG_kJ(1) = 0;

    for i = 2:length(Time_s)

        IntRadNRG_kJ(i) = IntRadNRG_kJ(i-1) +
RadFlowNRG_W(i)/10000;

    end

```

Auxiliary Radiator Energy Loss

Properties for 50/50 Glycol/H2O at 200F SG = 1.038, p = 3.929 kg/gal cp = linear curve fit below

```

    %cp Based on linear curve fit

    TavRad_K = ((AuxRadiatorIn_C + 273) + (AuxRadiatorOut_C +
273)) / 2;

    cpRad_JkgK = 3.2675 .* TavRad_K + 2429.1;

    AuxRadFlowNRG_W = (AuxRadiatorFlow_gpm/60) .* 3.929 .* cpRad_JkgK
.* (AuxRadiatorIn_C - AuxRadiatorOut_C);

    for i = 1:length(Time_s)

```

```

        if EngSpeed_rpm(i) > 50

            AuxRadFlowNRGEOn_W(i) = AuxRadFlowNRG_W(i);

        else

            AuxRadFlowNRGEOn_W(i) = 0;

        end

    end

    %Integrated Radiator Loss

    IntAuxRadNRG_kJ(1) = 0;

    for i = 2:length(Time_s)

        IntAuxRadNRG_kJ(i) = IntAuxRadNRG_kJ(i-1) +
        AuxRadFlowNRG_W(i)/10000;

    end

```

Heater Core Energy Loss

Properties for 50/50 Glycol/H2O at 200F SG = 1.038, p = 3.929 kg/gal cp = linear curve fit below

```

    %cp Based on linear curve fit

    TavgHeaterCore_K = ((HeaterCoreIn_C + 273) + (HeaterCoreOut_C
+ 273)) / 2;

    cpHeaterCore_JkgK = 3.2675 .* TavgHeaterCore_K + 2429.1;

```

```

        HeaterCoreFlowNRG_W = (HeaterCoreFlow_gpm/60) .* 3.929 .*
        cpHeaterCore_JkgK .* (HeaterCoreIn_C - HeaterCoreOut_C);

        for i = 1:length(Time_s)

            if EngSpeed_rpm(i) > 50

                HeaterCoreFlowNRGEngOn_W(i) = HeaterCoreFlowNRG_W(i);

            else

                HeaterCoreFlowNRGEngOn_W(i) = 0;

            end

        end

        %Integrated Heater Core Loss

        IntHCNRG_kJ(1) = 0;

        for i = 2:length(Time_s)

            IntHCNRG_kJ(i) = IntHCNRG_kJ(i-1) +
            HeaterCoreFlowNRG_W(i)/10000;

        end

        % %% Exhaust Heat Recovery Energy Loss

        %      % Properties for 50/50 Glycol/H2O at 200F

        %      % SG = 1.038, p = 3.929 kg/gal cp = linear curve fit below

        %      %cp Based on linear curve fit

```

```

%          TavgExhRecovery_K = ((ExhHeatRecovClntOutTemp_C + 273) +
(HeaterCoreOut_C + 273)) / 2;

%          cpHeaterCore_JkgK = 3.2675 .* TavgExhRecovery_K + 2429.1;

%

%          ExhRecoveryFlowNRG_W = ((HeaterCoreFlow_gpm -
EGRCoolerFlow_gpm)/60) .* 3.929 .* cpHeaterCore_JkgK .* (HeaterCoreOut_C
- ExhHeatRecovClntOutTemp_C);

%

%          for i = 1:length(Time_s)

%          if EngSpeed_rpm(i) > 50

%              ExhRecoveryFlowNRGEngOn_W(i) = ExhRecoveryFlowNRG_W(i);

%          else

%              ExhRecoveryFlowNRGEngOn_W(i) = 0;

%          end

%          end

%

%          %Integrated Exhaust WHR Loss

%          IntExhNRG_kJ(1) = 0;

%          for i = 2:length(Time_s)

%              IntExhNRG_kJ(i) = IntExhNRG_kJ(i-1) +
ExhRecoveryFlowNRG_W(i)/10000;

%          end

%

```

Fuel Stoichiometry & Exhaust Specific Heat

$C_1H_{1.84} = x(O_2 + 3.76 N_2) \rightarrow CO_2 + y(H_2O) + 3.76 * Z(N_2)$ Carbon Balance: $1C_1H_{1.84} = 1CO_2$ Hydrogen Balance: $1.84 = 2y$ Oxygen Balance: $2x = 2 + y$ Solve for x and y

```
HCx_Ratio = 1.84;

A_Stoich=[0 2;2 -1];

B_Stoich=[HCx_Ratio;2];

C_Stoich=A_Stoich\B_Stoich;

% Mass Fractions (MW CO2 = 44.01g/mol, MW H2O = 18.015 g/mol, MW
N2 =

% 28 g/mol

Mfrac_CO2 = 44.01 / (44.01 + C_Stoich(2) * 18.015 +
C_Stoich(1) * 28 * 3.76);

Mfrac_H2O = C_Stoich(2) * 18.015 / (44.01 + C_Stoich(2) *
18.015 + C_Stoich(1) * 28 * 3.76);

Mfrac_N2 = C_Stoich(1) * 28 * 3.76 / (44.01 + C_Stoich(2) *
18.015 + C_Stoich(1) * 28 * 3.76);

%Stoichiometric AFR

AFRStoich=(C_Stoich(1) * (32 + 3.76 * 28)) / (12 + HCx_Ratio
* 1.007);

%Calculate Exhaust Specific Heat

%cp CO2 @ 750K = 1148 J/kg * K

%cp H2O @ 750K = 2113 J/kg * K
```

```

%cp N2 @ 750K = 1110 J/kg * K

cpExh_JkgK = MFrac_CO2 * 1148 + MFrac_H2O * 2113 + MFrac_N2 *
1110;

```

Exhaust Gas Flow Energy Loss

Fuel Density = 0.74 g/ml

```

MdotFuel_kgs=EngFuelFlowDirect_ccs .* 0.74 / 1000;

MdotAir_kgs = AFRStoich .* Lambda_OCR .* MdotFuel_kgs; %NOTE:
EQRatio11OCR1 seems to be Lambda - i.e., goes less than 1 at high loads.

MdotExh_kgs = MdotAir_kgs + MdotFuel_kgs;

% Exhaust Enthalpy

ExhFlowNRG_W = (MdotExh_kgs) .* cpExh_JkgK .*
(Cat_Post_Temp_C - CellTemp_C);

%% Willans Fuel Economy Estimate

% Load Willans Vector (Requires File in Active Directory)

WillansMat = load('FusionWillans1.mat','WillansMat');

WillansMat_revsorted = sortrows(WillansMat,2);

% Add Fuel Power Est

for i = 1:length(FuelNRGIn_W)

    if AccelState(i) > 0.5;

```



```

%           TractiveTotalFuelUsed_Gal =
sum(EngFuelFlowDirectTractive_ccs)/10 * 0.0002642;

%

%           WillansTotalFuelError = (TractiveTotalFuelUsed_Gal -
WillansTotalFuelUsed_Gal) / TractiveTotalFuelUsed_Gal * 100;

%

%

%           %Integrated Willans Fuel Power vs Measured

%           WillansTractiveFuelInt_cc(1) = 0.0001;

%           EngFuelFlowDirectTractiveInt_cc(1) = 0.0001;

%

%           for i = 2:length(WillansTractiveFuelNRG_W)

%               WillansTractiveFuelInt_cc(i) =
WillansTractiveFuelInt_cc(i-1) + WillansTractiveFuelFlow_ccs(i)/10;

%               EngFuelFlowDirectTractiveInt_cc(i) =
EngFuelFlowDirectTractiveInt_cc(i-1) +
EngFuelFlowDirectTractive_ccs(i)/10;

%           end

```

Numeric Outputs

```

clc

format shortg

```

Fuel Energy Counts

```

TotalFuelNRG_kJ = sum(FuelNRGIn_W)/10000;

fprintf('\nTotal Fuel NRG In: %2.2f kJ \n', TotalFuelNRG_kJ)

%fprintf('\nTotal Battery NEC: %2.2f kJ \n', BatteryNEC_kJ)

%BatteryNEC_Check = BatteryNEC_kJ / TotalFuelNRG_kJ * 100;

%fprintf('\nBattery NEC as percentage of Fuel: %0.4f percent \n',
BatteryNEC_Check)

MovingTotalFuelNRG_kJ = sum(FuelNRGInMoving_W)/10000;

fprintf('\nTotal Moving Fuel NRG In: %2.2f kJ \n',
MovingTotalFuelNRG_kJ)

TotalFuelNRGInTractive_kJ = sum(FuelNRGInTractive_W)/10000;

fprintf('\nTotal Tractive Fuel NRG In: %2.2f kJ \n',
TotalFuelNRGInTractive_kJ)

DecelTotalFuelNRG_kJ = sum(FuelNRGInDecel_W)/10000;

fprintf('\nTotal Fuel NRG In on Decel: %2.2f kJ \n',
DecelTotalFuelNRG_kJ)

IdleTotalFuelNRG_kJ = sum(FuelNRGInIdle_W)/10000;

```

```

    fprintf('\nTotal Fuel NRG In at Idle: %2.2f kJ \n',
IdleTotalFuelNRG_kJ)

    IdleTotalFuelNRG_per = (IdleTotalFuelNRG_kJ / TotalFuelNRG_kJ) * 100;

    fprintf('\nPercent Total Fuel NRG In at Idle: %2.2f percent \n',
IdleTotalFuelNRG_per)

```

Total Fuel NRG In: 30534.28 kJ

Total Moving Fuel NRG In: 30363.85 kJ

Total Tractive Fuel NRG In: 25340.29 kJ

Total Fuel NRG In on Decel: 5193.99 kJ

Total Fuel NRG In at Idle: 170.43 kJ

Percent Total Fuel NRG In at Idle: 0.56 percent

Indicated Engine Work

```

TotalIndEngineWork_kJ = sum(IndEngineWork_W)/10000;

    fprintf('\nTotal Indicated Engine Work: %2.2f kJ \n',
TotalIndEngineWork_kJ)

```

Total Indicated Engine Work: 13172.81 kJ

Brake Engine Work

```
TotalBrakeEngineWork_kJ = sum(BrakeEngineWork_W)/10000;  
  
fprintf('\nTotal Brake Engine Work: %2.2f kJ \n',  
TotalBrakeEngineWork_kJ)
```

Total Brake Engine Work: 8777.11 kJ

Dynamometer Work

```
TotalDynoWork_kJ = sum(DynoWorkPos_W)/10000;  
  
fprintf('\nTotal Positive Dyno Work: %2.2f kJ \n', TotalDynoWork_kJ)  
  
TotalDynoWorkTractive_kJ = sum(DynoWorkTractive_W)/10000;  
  
fprintf('\nTotal Tractive Dyno Work: %2.2f kJ \n',  
TotalDynoWorkTractive_kJ)
```

Total Positive Dyno Work: 7507.45 kJ

Total Tractive Dyno Work: 6574.67 kJ

Cycle Efficiencies

```
CycleIndEngineEff = (TotalIndEngineWork_kJ/TotalFuelNRG_kJ) * 100;  
  
fprintf('\nIndicated Engine Cycle Efficiency: %2.2f percent \n',  
CycleIndEngineEff)
```

```

CycleVehicleEff = (TotalDynoWork_kJ/TotalFuelNRG_kJ) * 100;

fprintf('\nVehicle Cycle Efficiency: %2.2f percent \n',
CycleVehicleEff)


MovingCycleVehicleEff = (TotalDynoWork_kJ/MovingTotalFuelNRG_kJ) *
100;

fprintf('\nMoving Vehicle Cycle Efficiency: %2.2f percent \n',
MovingCycleVehicleEff)


TotalDynoWorkTractive_kJ = sum(DynoWorkTractive_W)/10000;

TotalFuelNRGInTractive_kJ = sum(FuelNRGInTractive_W)/10000;


TractiveCycleVehicleEff =
(TotalDynoWorkTractive_kJ/TotalFuelNRGInTractive_kJ) * 100;

fprintf('\nTractive Vehicle Cycle Efficiency: %2.2f percent \n',
TractiveCycleVehicleEff)


%%Thermal Efficiencies


RadFlowNRG_kJ = sum(RadFlowNRG_W)/10000;

fprintf('\nRadiator Flow Enthalpy Change: %2.2f kJ \n',
RadFlowNRG_kJ)

```

```

AuxRadFlowNRG_kJ = sum(AuxRadFlowNRG_W)/10000;

fprintf('\nAuxilliary Radiator Flow Enthalpy Change: %2.2f kJ \n',
AuxRadFlowNRG_kJ)


HeaterCoreFlowNRG_kJ = sum(HeaterCoreFlowNRG_W)/10000;

fprintf('\nHeater Core Flow Enthalpy Change: %2.2f kJ \n',
HeaterCoreFlowNRG_kJ)


%ExhRecoveryFlowNRG_kJ = sum(ExhRecoveryFlowNRG_W)/10000;

%fprintf('\nExhaust WHR Flow Enthalpy Change: %2.2f kJ \n',
ExhRecoveryFlowNRG_kJ)


RadFlowNRGEngOn_kJ = sum(RadFlowNRGEngOn_W)/10000;

fprintf('\nRadiator Flow Enthalpy Change, Engine On: %2.2f kJ \n',
RadFlowNRGEngOn_kJ)


AuxRadFlowNRGEngOn_kJ = sum(AuxRadFlowNRGEngOn_W)/10000;

fprintf('\nAuxilliary Radiator Flow Enthalpy Change, Engine On: %2.2f
kJ \n', AuxRadFlowNRGEngOn_kJ)


HeaterCoreFlowNRGEngOn_kJ = sum(HeaterCoreFlowNRGEngOn_W)/10000;

fprintf('\nHeater Core Flow Enthalpy Change, Engine On: %2.2f kJ \n',
HeaterCoreFlowNRGEngOn_kJ)

```

```

%ExhRecoveryFlowNRGEgnOn_kJ = sum(ExhRecoveryFlowNRGEgnOn_W)/10000;

fprintf('\nExhaust WHR Flow Enthalpy Change, Engine On: %2.2f kJ
\n', ExhRecoveryFlowNRGEgnOn_kJ)

ExhFlowNRG_kJ = sum(ExhFlowNRG_W)/10000;

fprintf('\nExhaust Flow Enthalpy Change: %2.2f kJ \n', ExhFlowNRG_kJ)


ThermalLossFraction = ((HeaterCoreFlowNRG_kJ + RadFlowNRG_kJ +
AuxRadFlowNRG_kJ) / TotalFuelNRG_kJ) * 100;

fprintf('\nCycle Thermal Loss Fraction: %2.2f percent \n',
ThermalLossFraction)


ThermalLossFractionEngOn = ((HeaterCoreFlowNRGEgnOn_kJ +
RadFlowNRGEgnOn_kJ + AuxRadFlowNRGEgnOn_kJ) / TotalFuelNRG_kJ) * 100;

fprintf('\nCycle Thermal Loss Fraction, Engine On: %2.2f percent \n',
ThermalLossFractionEngOn)


ExhFlowFraction = (ExhFlowNRG_kJ / TotalFuelNRG_kJ) * 100;

fprintf('\nCycle Exhaust Flow Loss Fraction: %2.2f percent \n',
ExhFlowFraction)

```

Indicated Engine Cycle Efficiency: 43.14 percent

Vehicle Cycle Efficiency: 24.59 percent

Moving Vehicle Cycle Efficiency: 24.72 percent

Tractive Vehicle Cycle Efficiency: 25.95 percent

Radiator Flow Enthalpy Change: 6897.25 kJ

Auxilliary Radiator Flow Enthalpy Change: 1098.10 kJ

Heater Core Flow Enthalpy Change: -620.91 kJ

Radiator Flow Enthalpy Change, Engine On: 6897.25 kJ

Auxilliary Radiator Flow Enthalpy Change, Engine On: 1098.10 kJ

Heater Core Flow Enthalpy Change, Engine On: -620.91 kJ

Exhaust Flow Enthalpy Change: 7858.67 kJ

Cycle Thermal Loss Fraction: 24.15 percent

Cycle Thermal Loss Fraction, Engine On: 24.15 percent

Cycle Exhaust Flow Loss Fraction: 25.74 percent

Miscellaneous Stats

```
TotalFuelUsed_Gal = sum(EngFuelFlowDirect_ccs) / 10 * 0.0002642;

TotalDist_mi = 0;

for i = 1:length(DynoSpeed_mph)

    TotalDist_mi = TotalDist_mi + DynoSpeed_mph(i) / 36000;

end

MPG = TotalDist_mi / TotalFuelUsed_Gal;

fprintf('\nCycle Economy: %2.2f mpg \n', MPG)

fprintf('\nPercent Engine On Time: %2.2f percent \n',
PercentEngineOn)

% %Willans Error

% fprintf('\nWillans Fuel Estimate Error: %2.2f percent \n',
WillansTotalFuelError)
```

Cycle Economy: 31.55 mpg

Percent Engine On Time: 100.00 percent

Table Output (Needs Work)

```
CycleStats =  
{TotalFuelNRG_kJ;TotalDynoWork_kJ;RadFlowNRG_kJ;HeaterCoreFlowNRG_kJ;ExhF  
lowNRG_kJ;CycleVehicleEff;MovingCycleVehicleEff;TractiveCycleVehicleEff;T  
hermalLossFraction;ExhFlowFraction};  
  
CycleStatslabel = {'Fuel NRG In';'Total Dyno Work';'Radiator Flow  
NRG';...  
  
    'Heater Core Flow NRG';'Exhaust Flow NRG';'Cycle Vehicle Eff';...  
  
    'Moving Vehicle Eff';'Tractive Vehicle Eff';'Thermal Loss  
Fraction';'Exhaust Flow Fracion'};
```

Plots

```
clf  
  
figure(1)  
  
columnname = {'Cycle Statistics'};  
  
t=uitable;  
  
set(t,'Data',CycleStats, 'Columnname', 'Cycle Statistics', 'Rowname',  
CycleStatslabel);  
  
set(t,'ColumnWidth',{150})
```

```

figure (2)

plot(Time_s,DynoSpeed_mph)

xlabel('Time, s')

ylabel('Speed, mph')

title('Figure 2: Drive Cycle')

% axis([0 600 0 80])


figure (3)

plot(Time_s,DynoWorkPos_W)

xlabel('Time, s')

ylabel('Work, W')

title('Figure 3: Dyno Work vs Time')

% axis([0 200 0 100000])


figure (4)

plot(Time_s,RadFlowNRG_W)

%plot(Time_s,DynoWorkPos_W)

xlabel('Time, s')

ylabel('Radiator Energy Loss, W')

title('Figure 4: Radiator Loss vs Time')

% axis([0 200 0 100000])

```

```

figure(5)

hold on

plot(Time_s,DynoWorkPos_W, 'r')

plot(Time_s,FuelNRGIn_W)

xlabel('Time, s')

ylabel('Energy, W')

title('Figure 5: Dyno Work & Fuel Energy')

% axis([0 200 0 100000])

legend('DynoWorkPos (W)', 'FuelNRGIn (W)')

hold off


figure(6)

hold on

[AX,H1,H2]=plotyy(Time_s,Cyl1IMEP_bar,Time_s,DynoSpeed_mph);

set(get(AX(1),'Ylabel'),'String','IMEP, bar')

set(get(AX(2),'Ylabel'),'String','Dyno Speed, mph')

xlabel('Time, s')

title('Cylinder 1 IMEP')

hold off

title('Figure 6')

```

```

figure (7)

plot(EngSpeed_rpm,IndEngineWork_W/1000, '*', 'MarkerSize', 5)

xlabel('Engine Speed, RPM')

ylabel('Indicated Engine Power, kW')

title('Figure 7 Vehicle Power Map')


% figure(8)

% surf(EngSpeed_rpm,TEPos_N,VehicleEffPlot)


figure(8)

hold on

plot(Time_s,ExhFlowNRG_W)

hold off

xlabel('Time, s')

ylabel('Exhaust Flow Energy, W')

title('Exhaust Flow Energy vs Time')


% figure (9)

% hold on

% plot(Time_s,SemRawTHC_ppm)

```

```

% xlabel('Time, s')

% ylabel('Total Hydrocarbons, PPM')

% title('Total Hydrocarbon Emissions')

%

% figure (10)

% hold on

% plot(Time_s,SemRawNOx_ppm)

% xlabel('Time, s')

% ylabel('Total NOx, PPM')

% title('Total NOx')

%

% figure (11)

% plot(Time_s,EQRatio11OCR1)

% xlabel('Time, s')

% ylabel('Equivalence Ratio')

% title('Equivalence Ratio vs Time')

% axis([0 700 -2 2])

figure (12)

plot(DFCO(:,2),DFCO(:,1),'*')

xlabel('Dyno Speed, mph')

```

```

ylabel('Accel Rate, m/s^2')

title('DFCO Envelope')

figure (13)

plot(DFCO(:,2),DFCO(:,5),'*')

xlabel('Dyno Speed, mph')

ylabel('Accel Rate, m/s^2')

title('DFCO Envelope, Rounded')

figure (14)

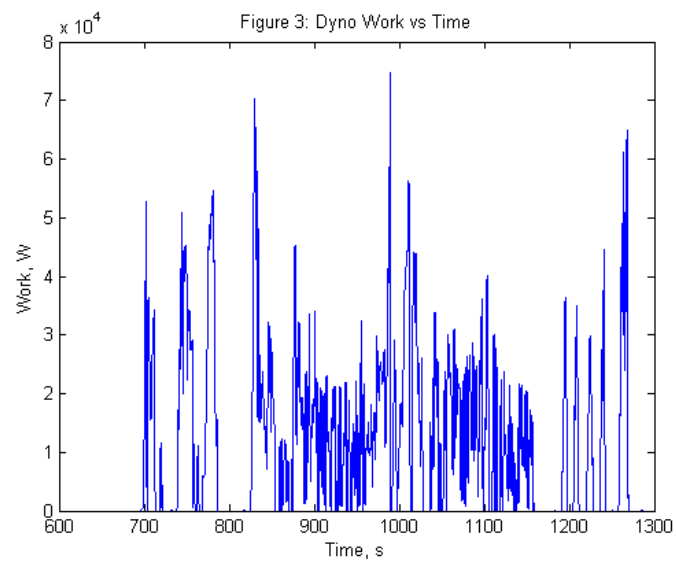
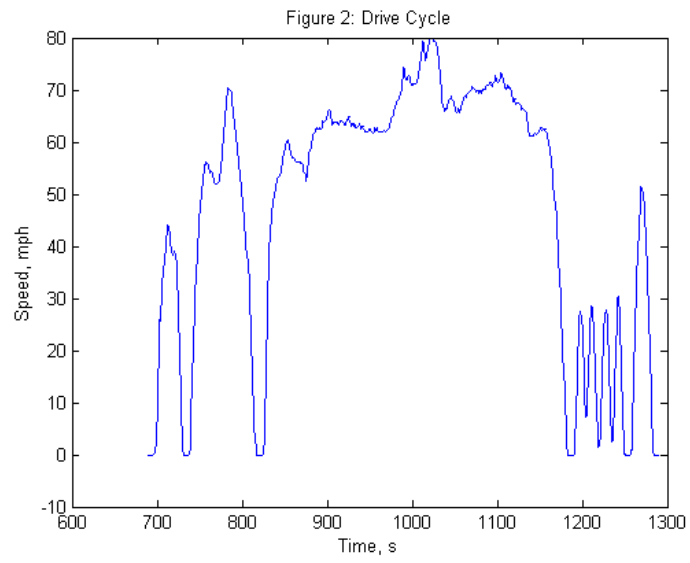
plot(DFCO(:,2),DFCO(:,6),'*')

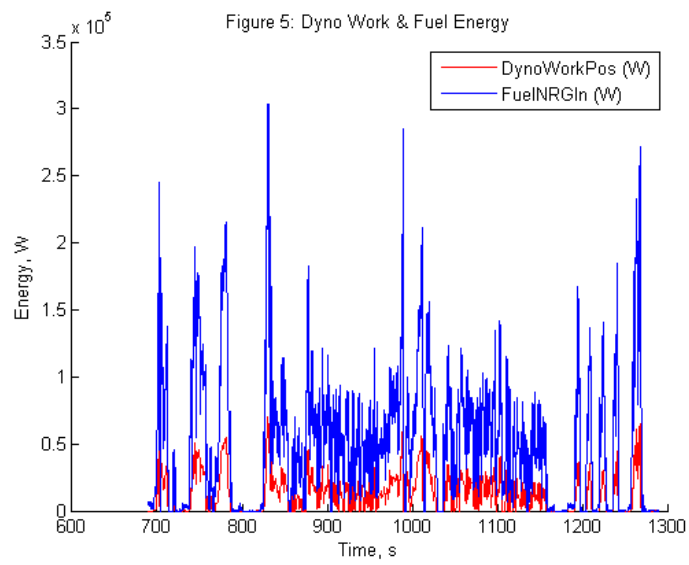
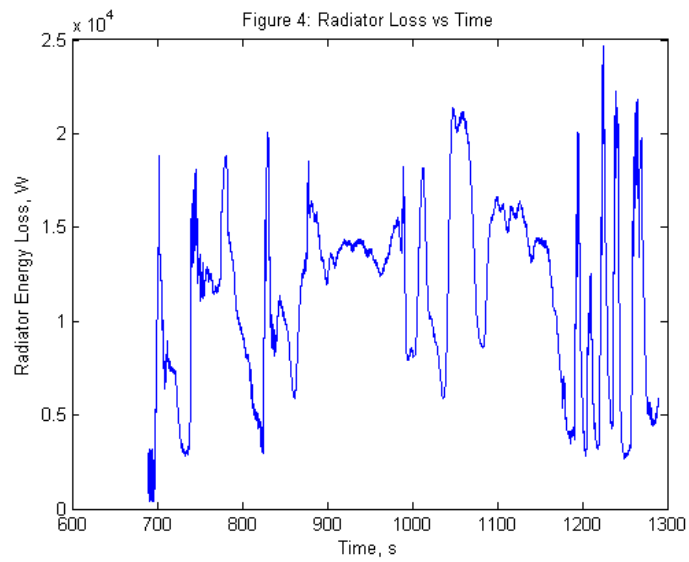
xlabel('Dyno Speed, mph')

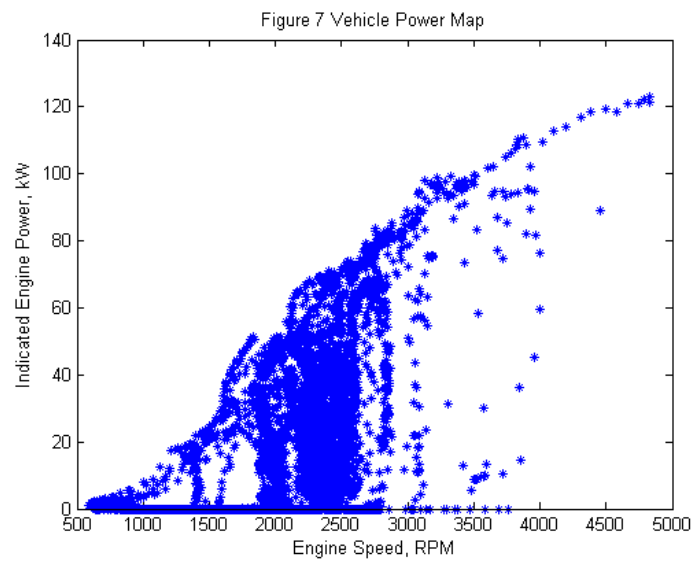
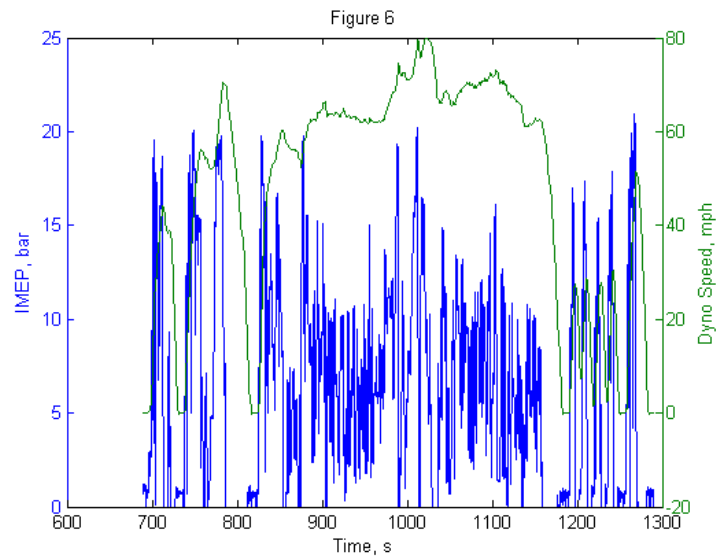
ylabel('Tractive Effort, N')

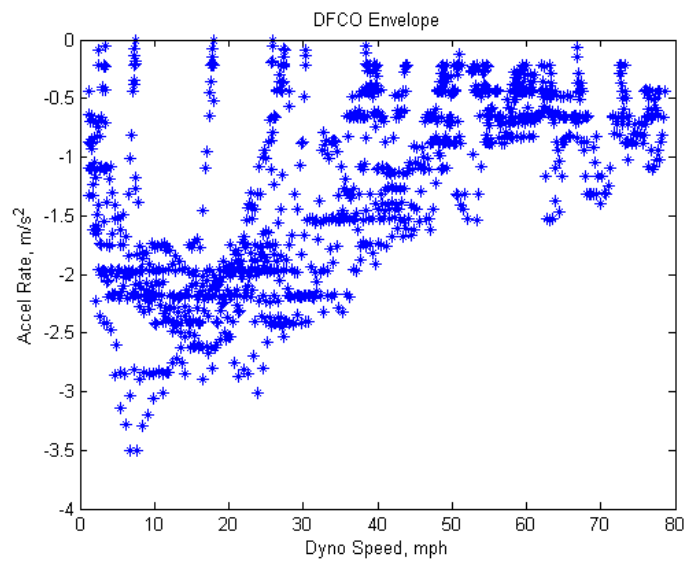
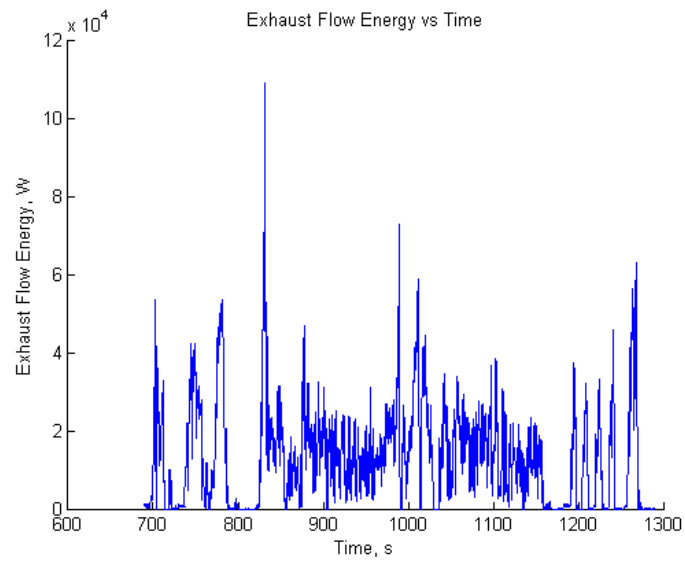
title('DFCO Envelope')

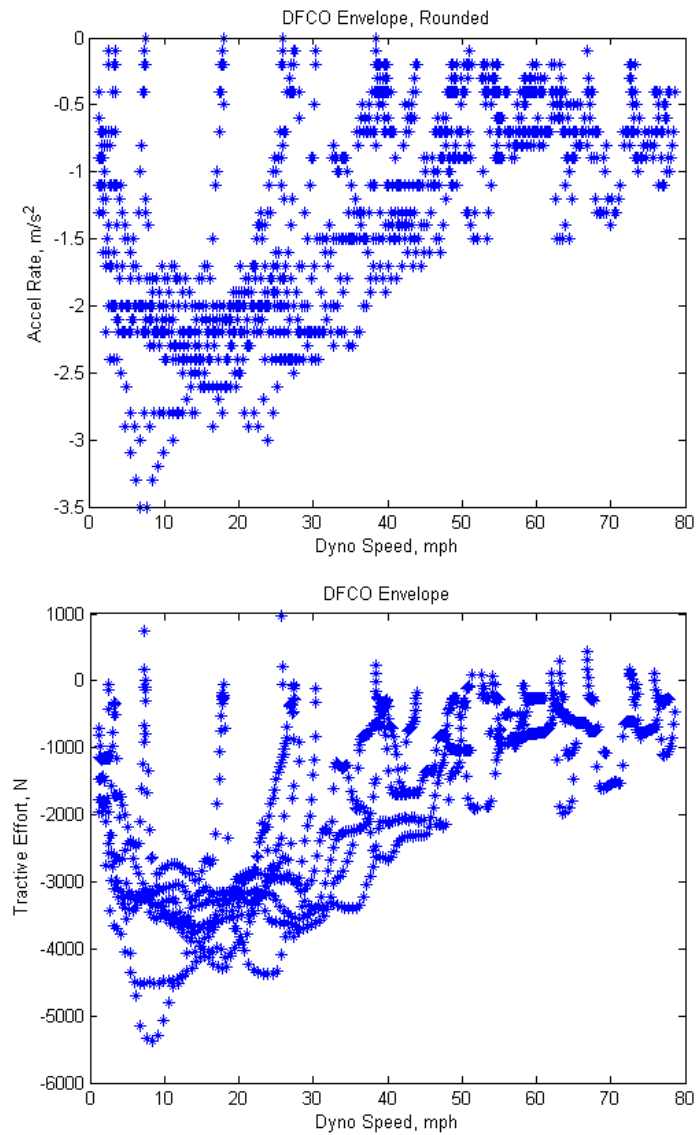
```









SS Map Plots

```
% figure (12)

% plot(SSMapPoints(:,5),SSMapPoints(:,4),'--rs','LineWidth',2,...

%           'MarkerEdgeColor','k',...

%           'MarkerFaceColor','g',...

%           'MarkerSize',10)
```

```

% xlabel('Engine Torque (Nm)')

% ylabel('Vehicle Efficiency (%)')

% title('Vehicle Efficiency vs. Estimated Engine Torque @ 40 mph')

%

% figure (13)

% plot(SSMapPoints(:,9),SSMapPoints(:,4),'--rs','LineWidth',2,...

%             'MarkerEdgeColor','k',...

%             'MarkerFaceColor','g',...

%             'MarkerSize',10)

% xlabel('Pedal Position (%)')

% ylabel('Vehicle Efficiency (%)')

% title('Vehicle Efficiency vs. Accelerator Pedal Position @ 40 mph')

%

% figure (14)

% plot(SSMapPoints(:,7)/1000,SSMapPoints(:,4),'--
rs','LineWidth',2,...

%             'MarkerEdgeColor','k',...

%             'MarkerFaceColor','g',...

%             'MarkerSize',10)

% xlabel('Engine Power (kW)')

% ylabel('Vehicle Efficiency (%)')

```

```

% title('Vehicle Efficiency vs. Indicated Engine Power @ 40 mph')

%

% figure (15)

%

% plot(SSMapPoints(:,7)/1000,SSMapPoints(:,8),'--
rs','LineWidth',2,...

%             'MarkerEdgeColor','k',...

%             'MarkerFaceColor','g',...

%             'MarkerSize',10)

% xlabel('Engine Power (kW)')

% ylabel('Indicated Fuel Conversion Efficiency (%)')

% title('Indicated Fuel Conversion Efficiency vs. Indicated Engine
Power @ 40 mph')

```

Published with MATLAB® R2012b

A.3 Permissions

Figure 6.1.1 was reprinted from SAE Technical Paper 2009-01-1061. Permission was granted for single use only. Further use or distribution is not permitted without permission from SAE. This technical paper is referenced in the bibliography of this document. The email granting this permission is copied below:

Terri Kelly [terri@sae.org]

In response to the message from Anderson, Jay, 8/16/2013

To:

Anderson, Jay

Tuesday, October 01, 2013 4:06 PM

Dear Jay,

Thank you for your correspondence requesting permission to reprint figure 1 from SAE paper 2009-01-1061 in your thesis for your MSME degree at Michigan Technological University.

Permission is hereby granted, and subject to the following conditions:

Permission is for this one time single use only. New requests are required for further use or distribution of the SAE material.

The following credit statement must appear below the figure: "Reprinted with permission from SAE Paper 2009-01-1061 © 2009 SAE International. Further use or distribution is not permitted without permission from SAE."

We also request that you credit the original source (author, paper number and SAE) in the reference section of your thesis.

Please feel free to contact me if you need further assistance.

Best regards,

Terri Kelly

Intellectual Property Rights Administrator

SAE INTERNATIONAL

400 Commonwealth Drive

Warrendale, PA 15096

o +1.724.772.4095

f +1.724-776-9765

e terri@sae.org

www.sae.org